UNIVERSIDADE FEDERAL DO PARÁ
INSTITUTO DE GEOCIÊNCIAS
PROGRAMA DE PÓS-GRADUAÇÃO EM GEOLOGIA E GEOQUÍMICA

TESE DE DOUTORADO N° 130

ESTUDOS ISOTÓPICOS DE U-Pb, Lu–Hf E $\delta^{18}O$ EM ZIRCÃO: IMPLICAÇÕES PARA A PETROGÊNESE DOS GRANITOS TIPO-A PALEOPROTEROZOICOS DA PROVÍNCIA CARAJÁS – CRÁTON AMAZÔNICO

Tese apresentada por:

MAYARA FRAEDA BARBOSA TEIXEIRA
Orientador: Roberto Dall'Agnol (UFPA)
Coorientador: João Orestes Schneider Santos(UWA)

Belém

2018

Dados Internacionais de Catalogação-na-Publicação (CIP)
Biblioteca do Instituto de Geociências/SIBI/UFPA

Teixeira, Mayara Fraeda Barbosa, 1986-

Estudos isotópicos de U-Pb, Lu–Hf e δ18O em zircão: implicações para a petrogênese dos granitos tipo-A paleoproterozóicos da Província Carajás – Cráton Amazônico / Mayara Fraeda Barbosa Teixeira. – 2018

xii, 203 f. ; 30 cm

Inclui bibliografias

Orientador: Roberto Dall'Agnol
Coorientador: João Orestes Schneider Santos

Tese (Doutorado) – Universidade Federal do Pará, Instituto de Geociências, Programa de Pós-Graduação em Geologia e Geoquímica, Belém, 2018.

1. Rochas ígneas. 2. Isótopos. 3. Geocronologia. 4. Crátons – Amazônia. I. Título.

CDD 22. ed.: 552.1

Elaborado por
Hélio Braga Martins
CRB-2/698

Universidade Federal do Pará
Instituto de Geociências
Programa de Pós-Graduação em Geologia e Geoquímica

ESTUDOS ISOTÓPICOS DE U-Pb, LU-Hf E $\delta^{18}O$ EM ZIRCÃO: IMPLICAÇÕES PARA A PETROGÊNESE DOS GRANITOS TIPO-A PALEOPROTEROZOICOS DA PROVÍNCIA CARAJÁS – CRÁTON AMAZÔNICO

TESE APRESENTADA POR:

MAYARA FRAEDA BARBOSA TEIXEIRA

Como requisito parcial à obtenção do Grau de Doutora em Ciências na Área de GEOQUÍMICA E PETROLOGIA

Data de Aprovação: 05 / 04 / 2018

Banca Examinadora:

Prof. Dr. Roberto Dall'Agnol
Orientador – UFPA

Prof. Dr. Wilson Teixeira
Membro – USP

Prof. Dr. Farid Chemale Júnior
Membro – UNISINOS

Prof. Dr. Moacir José Buenano Macambira
Membro – UFPA

Prof. Dr. Davis Carvalho de Oliveira
Membro – UFPA

Aos meus pais Maria das Graças Barbosa e Luis Augusto dos Santos Teixeira com todo meu amor e gratidão.

AGRADECIMENTOS

É difícil expressar os devidos agradecimentos a todas as pessoas e entidades que contribuíram para que este trabalho fosse desenvolvido ao longo desses 4 anos, em especial agradeço:

- Ao Programa de Pós-Graduação em Geociências da Universidade Federal do Pará (UFPA), pelo fornecimento de infra-estrutura;

- Ao CNPq pela concessão da bolsa de estudo de doutoramento e ao INCT de Geociências da Amazônia pelo suporte financeiro;

- Ao meu orientador e amigo prof. Roberto Dall'Agnol com quem tive a oportunidade de estar desenvolvendo pesquisas desde o mestrado. Por todo aprendizado, suporte, estimulo e força pra que eu pudesse terminar com êxito essa Tese. Obrigada também por acreditar na minha capacidade de desenvolver esse trabalho;

- Ao meu co-orientador João Orestes Schneider Santos que me auxiliou durante o estágio sanduiche no exterior, com a aquisição das análises, com todos os problemas que surgiram. Agradeço a todas as críticas e discussões durante o desenvolvimento dos artigos e finalização da Tese;

- A minha família, meus pais e irmãos Luis Augusto e Moreno Teixeira, e a minha tia Patricia Teixeira sempre presentes ao longo dessa jornada;

- Ao Grupo de Pesquisa Petrologia de Rochas Granitóides (GPPG) do Instituto de Geociências (IG) da UFPA, especialmente aos meus companheiros de sala, Caio Mesquita, Ingrid Cunha e Luan Alexandre pelos momentos de discussão e descontração, especialmente nas nossas horas de café.

- Ao Laboratório de Geologia Isotópica da UFPA pelo suporte na aquisição dos dados isotópicos;

- As funcionárias Cleida e Joelma, da UFPA, que estão sempre dispostas a auxiliar e ajudar no que for preciso;

- Ao meu namorado João Albuquerque por todo carinho, incentivo, paciência e apoio nos momentos mais difíceis, sempre me estimulando a fazer meu melhor;

- Agradeço imensamente a amiga Érika Santiago que me ajudou no Brasil e em Perth e esteve presente nos momentos de maior dificuldade;

- Aos amigos Aline Vieira, João Milhomen, Pablo Leite, Lilian Paula, Ana Flávia, pelos momentos de discussão e descontração, com muitas conversas de incentivo e apoio, sempre presentes ao longo desses anos;

Aos amigos da UWA Danilo Câmelo, Jéssica Bogossian, Sylvio Dutra e Sun Xiang que tanto me ajudaram durante meu período de estágio tornando minha estádia ainda mais agradável;

Aos amigos de Perth Hiromi Shidori e Felia com quem compartilhei momentos agradáveis em Perth.

“Inteligência é a
capacidade de se adaptar à
mudança” Stephen Hawking.

RESUMO

Em ~1880 Ma, um extenso evento magmático gerou granitos tipo-A com afinidade rapakivi no Cráton Amazônico, com destaque para a Província Carajás. Nesta província, esse magmatismo compreende batólitos e stocks anorogênicos agrupados em três suítes: (1) Suíte Jamon oxidada; (2) Suíte Velho Guilherme, ferrosa reduzida, com leucogranitos estaníferos associados; (3) Suíte Serra dos Carajás, constituída por plutons moderadamente reduzidos. Além dessas três suítes, também ocorrem nos diferentes domínios da província outros corpos graníticos tipo-A com características semelhantes aos das suítes mencionadas. Entre eles, dispõem-se de informações sobre os granitos Seringa, São João, Gogó da Onça, Rio Branco e Gradaús. O Granito Gogó da Onça Granite (GGO) compreende um stock localizado no sudeste de Canaã dos Carajás, composto por biotita-anfibólio granodiorios, biotita-anfibólio monzogranito e biotita-anfibólio sienogranito. Apresenta comportamento geoquímico similar aos granitos anorogênicos de Carajás. É um granito metaluminoso, ferroso do subtipo A2- com caráter reduzido. O comportamento dos elementos traços sugere que suas diferentes fácies são relacionadas por cristalização fracionada. Dados U-Pb SHRIMP em zircão e titanita mostraram que o GGO cristalizou entre ~ 1880 e 1870 Ma. Esse granito mostra contrastes significativos com as suítes Jamon e Velho Guilherme. O GGO é mais parecido com a Serra dos Carajás e com os granitos Seringa e São João, e aos granitos Sherman (mesoproterozóico) dos EUA e o Batólito Suomenniemi (paleoproterozóico) da Finlândia. Novos dados U-Pb SHRIMP para os granitos das suítes Jamon, Serra dos Carajás e Velho Guilherme, e para os granitos Seringa e São João mostraram que esses plutons cristalizaram entre 1880 Ma e 1857 Ma, situando-se o principal pico do magmatismo em cerca de 1880 Ma. As análises em zircão e titanita revelaram ainda idades de ~1900 Ma a ~1920 Ma nas suítes Velho Guilherme e Jamon e no Granito Seringa que representam possivelmente fases cristalizadas precocemente, incorporadas nos pulsos magmáticos dominantes, mais tardios. Também foram obtidas idades mais jovens (~1865 Ma a ~1857 Ma), comparadas aquelas obtidas para as fases menos evoluídas, para leucogranitos que formam stocks tardios nos corpos Bannach e Redenção. Esses dados sustentam a interpretação de que estes leucogranitos foram gerados por pulsos magmáticos independentes e tardios na evolução daqueles corpos, conforme já havia sido proposto por outros autores. Além das idades mencionadas, uma idade de 1732 ± 6 Ma foi obtida na facies de leucogranita do pluton Antônio Vicente da Suite Velho Guilherme, e poderia representar um evento magmático na região do Xingu ainda não relatado ou, eventualmente, poderia corresponder a um evento hidrotermal isolado que permitiu o crescimento de zircões. Além dos dados geocronológicos esses granitos foram analisados por

isótopos de Hf, O e alguns plutons por isótopos de Nd. Em geral, os zircões analisados desses granitos têm composição inicial $^{176}Hf/^{177}Hf$ razoavelmente restrita, variando entre 0,281156 e 0,281384, com valores fortemente negativos $\varepsilon_{Hf(t)}$ variando de -9 a -18 e $\delta^{18}O$ homogêneos variando de 5,50 ‰ a 7,00 ‰. Os valores obtidos para o $\varepsilon_{Hf(t)}$ nos diferentes granitos analisados são fortemente negativos e coerentes de modo geral com os dados isótopicos de Nd. Na Suíte Serra dos Carajás os valores de $\varepsilon_{Hf(t)}$ variam entre -14 a -15,5, na Suíte Jamon entre -9,5 a -15, e na Suíte Velho Guilherme entre -12 a -15, enquanto que os granitos São João, Seringa e Gogó da Onça tendem a apresentar valores mais acentuadamente negativos [$\varepsilon_{Hf(t)=}$ -12 a -18]. Apesar dos dados isotópicos serem homogêneos, pequenas variações foram observadas em diferentes plutons de uma mesma suíte e em diferentes fácies de um pluton. Com por exemplo na Suite Jamon, as composições isotópicas são mais variáveis, especialmente nos leucogranitos evoluídos dos plutons Bannach e Redenção, e fontes com contraste no grau de oxidação podem ser desenvolvidas na geração desses leucogranitos. Os dados isotópicos de Hf indicaram fontes crustais paleoarqueanas (3.3Ga 3.6 Ga) com menor contribuição mesoarquena (3,0 Ga a 3,2 Ga) como fontes desses granitos. Essas idades são mais antigas que as idades das rochas Arquenas encaixantes desses granitos, que estão expostas na Província Carajás, e é necessário investigar a presença de crosta arqueana mais antiga em Carajás. As composições de Nd, Hf e O dos granitos paleoprozozóicos da Província de Carajás atestam claramente fonte crustais ígnea arqueanas na origem de seus magmas. As diferenças observadas podem resultar em contrastes nos domínios crustais da Província Carajás que foram a fonte dos granitos ou por processos de contaminação local.

Palavras-chave: Granitos tipo-A. U-Pb-SHRIMP. Isótopos de Hf-O. Isotopos de Nd. Província Carajás. Cráton Amazônico.

ABSTRACT

In ca. 1880 Ma an extensive magmatic event generated A-type granites with rapakivi affinity in the Amazonian Craton, especially in the Carajás Province. In this Province these granites are grouped into three main suites according to mineralogy, geochemistry, and state of oxidation of their magmas – Jamon, Velho Guilherme, and Serra dos Carajás – and include also the Gogó da Onça, Seringa, São João, Gradaús, and Rio Branco plutons. The Gogó da Onça Granite (GOG) comprise a stock composed by biotite-amphibole granodiorite, biotite-amphibole monzogranite and amphibole-biotite syenogranite. The GGO crosscut discordantly the Archean country rocks and are not foliated. All Gogó da Onça Granite varieties are metaluminous, ferroan A2-subtype granites with reduced character. The major and trace element behavior suggests that its different facies are related by fractional crystallization. Zircon and titanite U–Pb SHRIMP ages show that the pluton crystallized at ~1880-1870 Ma. This is more akin to the Serra dos Carajás Suite and to the Seringa and São João granites of Carajás and to the Mesoproterozoic Sherman granite of USA and the Paleoproterozoic Suomenniemi Batholith of Finland. New U-Pb SHRIMP data for the Serra dos Carajás, Velho Guilherme and Jamon Suite and for Seringa and São João Granite show that these plutons crystallized between 1880 Ma to 1857 Ma. Some granites of the Velho Guilherme and Jamon suites and of the Seringa Granite presented 1920 to 1900 m. y. old zircon and titanite crystals interpreted here as antecrysts from an earlier pulse of magma that were incorporated in the main later pulse of 1880 Ma. We also obtained ages of 1865 Ma to 1857 Ma in the leucogranite facies of the Redenção and Bannach plutons, which indicate that the leucogranites of these plutons are younger than their ~1880 Ma old granites and were generated by independent magma pulses that are not cogenetic with the less evolved facies of the respective plutons. Besides it, an age of 1732 ± 6 Ma obtained in the leucogranite facies of the Antônio Vicente pluton of the Velho Guilherme Suite that could represent a magmatic event in the Xingu Region not yet reported or, eventually, could correspond to an isolate hydrothermal event that allowed the growth of zircons. This ranites have been also analysed by Lu–Hf and Oxygen isotopes and few granites also by Nd isotopes. Zircons from all the granites have remarkably restricted initial $^{176}Hf/^{177}Hf$ (0.281156 and 0.281384) and strongly negative εHf(t) values ranging from –9 to -18, and $\delta^{18}O$ fairly homogeneous varying from 5.50‰ to 7.00‰. Small differences were observed internally in the plutons or between them. The $\varepsilon_{Hf(t)}$ values of the analysed plutons are strongly negative and similar to Nd isotopic data. The Serra dos Carajás Suite has $\varepsilon_{Hf(t)}$ values of -14 to -15.5, the Jamon Suite of -9.5 to -15 and values of -12 to -15 for the Velho Guilherme Suite, while São João, Seringa and Gogó da

Onça granites have stronger negative values ($\varepsilon_{Hf(t)=}$ -12 to -18). Crustal model ages indicate a Paleoarchean source (3.3 Ga to 3.6 Ga) with a minor contribution from Mesoarchean (3.0 Ga to 3.2 Ga) melts for these granites. This model ages are older than the exposed Archean country rocks of the Orosirian granites of the Carajás Province and more investigation is needed to verify the real existence of that older Archean crust. The studied samples have Hf–O isotopic compositions that overlap within error, and evidence of contamination (crustal assimilation or mixing) of a mantle-derived magma cannot be seen. These plutons crystallized from magmas generated by melting of pre-existing igneous rocks with possibly in the Velho Guilherme Suite a minor contribution from a supracrustal (metasedimentary) component. The Nd, Hf, and O isotope compositions of the Paleoproterozoic granites of Carajás Province clearly attest to an igneous ancient crustal source in the origin of their magmas. The differences observed can result for contrasts in the crustal domains of the Carajás Province that were the source of the granites or of local contamination processes.

Keywords: A-type granites. U-Pb SHRIMP. Hf-O isotopes. Carajás Province. Amazon Craton.

Sumário

1. INTRODUÇÃO

1.1 APRESENTAÇÃO

Loiselle & Wones (1979) introduziram o termo granitos tipo-A para definir uma série de rochas graníticas colocadas em ambientes tectônicos extensionais, ao longo de riftes continentais ou em ambientes pós-colisionais. Comparados a outros tipos de granitos, os granitos tipo-A apresentam média a alta afinidade alcalina, altas razões Fe/Mg, (K+Na)/Al e K/Na, e altos conteúdos de elementos traços incompatíveis dos tipos LILE e HFSE. Um grande número de processos envolvendo cristalização fracionada de magmas basálticos derivados do manto, processos de assimilação e cristalização fracionada (AFC), fusão parcial do manto ou da crosta, e mistura de líquidos basálticos e crustais podem estar envolvidos na geração desses granitos.

O magmatismo tipo-A ocorre em diversos crátons com distribuição temporal desde o Noarqueano (~2,7 Ga; Cunha *et al.* 2016, Dall'Agnol *et al.* 2012, 2017) até o recente (Ali *et al.* 2015, Wu *et al.* 2002, Zhang *et al.* 2015), sendo mais abundantes no Paleoproterozoico e Mesoproterozoico (Anderson *et al.* 2004, Heinonen *et al.* 2010, Dall'Agnol *et al.* 1999a, b, c, 2005, 2012, Ramo & Haapala 1995, Goodge &Vervoort 2006).

Na Província Carajás, o magmatismo Orosiriano é constituido por três suítes anorogênicas e diversos outros pluton anorogênicos e diques máficos e félsicos relacionados, que seccionam os diferentes domínios que a constituem. As suítes Serra dos Carajás, Velho Guilherme e Jamon apresentam muitas similaridades, mas se diferenciam por mostrar alguns constrastes geoquímicos e pelas condições de fugacidade de oxigênio dominantes durante sua evolução magmática. Estudos anteriores de Nd, Sr, Pb e O em rocha total (Dall'Agnol *et al.* 2005) foram utilizados para discutir a natureza e a fonte desses granitos e são referência para a discussão da petrogêneses desse magmatismo.

Dall'Agnol et al. (2005), seguindo modelo de Hoffman (1989) e Windley (1993), propuseram que a origem dos granitos anorogênicos de Carajás seria relacionada ao início da quebra de um supercontinente Paleoproterozoico (~2,0 Ga) que propiciaria a fusão parcial do manto e geraria magmas máficos. Estes ascenderiam e se colocariam na base da crosta (*underplating;* Huppert & Sparks 1988) e o calor liberado por eles levaria à fusão da crosta inferior arqueana formando os magmas graníticos.

Portanto, a Província Carajás é uma área chave para o entendimento da influência de crosta arqueana na origem de granitos anorogênicos. Avanços na compreensão desses

processos também devem contribuir para esclarecer determinados aspectos da evolução do Cráton Amazônico. Além disso, embora a geração dos magmas graníticos paleoproterozoicos a partir da fusão parcial da crosta arqueana já esteja razoavelmente demonstrada (Dall'Agnol *et al*. 1999, 2005) e já tenham sido apresentadas hipóteses sobre a natureza das fontes, é indispensável aprofundar esta discussão.

Assim, o objetivo principal dessa Tese foi, através de novos métodos isotópicos, em particular de Lu-Hf e Oxigênio, e o aprimoramento dos dados geocronológicos, com datações de zircão por U-Pb em SHRIMP, estabelecer com maior rigor a idade do magmatismo e avaliar as hipóteses existentes sobre as fontes dos magmas paleoproterozoicos tipo-A.

Este documento foi elaborado seguindo o modelo de tese de integração de artigos. Desta forma, o corpo central da tese apresenta três artigos científicos que já foram ou serão submetidos a periódicos internacionais, sendo os mesmos apresentados na forma de capítulos (capítulos 2, 3 e 4). Os capítulos com os artigos são precedidos por um texto integrador, que é apresentado no presente capítulo de caráter introdutório (Capitulo 1) e que inclui a apresentação da pesquisa, contexto geológico e tectônico regional, as principais características do magmatismo granitóide da Província Carajás, bem como a apresentação do problema, os objetivos da tese e materiais e métodos usados para alcançar os objetivos. O capítulo final (capitulo 5), sumariza de forma integrada as discussões e as conclusões alcançadas nos três artigos científicos e no desenvolvimento da tese como um todo. Os artigos serão apresentados de acordo com a seguinte ordem:

Capítulo 2 – *Artigo 1:* **Geochemistry, geochronology and Nd isotopes of the Gogó da Onça Granite: A new Paleoproterozoic A-type granite of Carajás Province, Brazil.** Publicado na revista *Journal of South America Earth Sciences*. Este artigo apresenta os resultados obtidos apara o Granito Gogó da Onça recentemente mapeado a sudeste de Canaã dos Carajás, na Província Carajás. O artigo integra dados de petrografia, geoquímica e gecronologia U-Pb SHRIMP em zircão e titanita e isótopos de Nd. Os dados apresentados permitiram caracterizar, definir a natureza, idade do granito, estabelecer comparações entre ele e as Suites Paleoproterozoicas e demais granitos tipo-A da Província Carajás e de outros crátons, e discutir as possíveis fontes do magmatismo.

Capítulo 3 – *Artigo 2:* C**rystallization ages of Paleoproterozoic A-type granite Suites and Related granites of Carajás Province, Amazon Craton: constraints from U-Pb geochronology of zircon and titanite.** Submetido a revista *Precambrian Research.* Esse artigo apresenta novos dados geocronológicos U-Pb SHRIMP em zircão e titanita para os granitos que compõem as três suítes paleoproterozoicas de Carajás (Serra dos Carajás, Velho

Guilherme e Jamon), e para os granitos Seringa e São João. Destaca, ainda, a importância do episódio magmático de 1880 Ma no Cráton Amazônico, relacionado a SLIP Uatumã e também registrado em outros crátons do mundo, demonstrando a sua relevância na evolução tectônica de continentes proterozoicos.

Capítulo 4 – *Artigo 3:* P**etrogenesis of the Paleoproterozoic (Orosirian) A-type Magmatism of Carajas Province, Amazonian Craton, Brazil: combined *in situ* Hf–O isotopes of zircon.** A ser submetido a revista Lithos. Esse artigo apresenta as composições isotópicas de Hf e Oxigênio para os granitos tipo-A Paleoproterozoicos da Província Carjás, discutindo sobre os contrastes existentes entre os diferentes plutons estudados. Faz comparações entre os dados de Hf e Nd e entre os dados de Hf obtidos para os granitos estudados com outros granitos do Cráton Amazônicos, e de outros crátons do mundo. Discuti fontes geradoras dos granitos, e a influência de crosta arqueana na geração desses granitos.

1.2 JUSTIFICATIVA DA TESE

Granitos contém valiosas informações para evolução de crosta continental e têm sido tema de inúmeros trabalhos. Particularmente granitos tipo-A, também chamados de granitos ferrosos (Frost *et al.* 2001), são de considerável importância, uma vez que podem fornecer informações sobre ambientes e regimes tecônicos (Eby 1992, Whalen *et al.* 1987, Zhao *et al.* 2016) e são derivados de uma ampla variedade de rochas fontes e processos, o que implica significativos contrastes mineralógicos e geoquímicos. Uma intensa manifestação magmatica de granitos tipo-A com afinidade rapakivi ocorreu em diversos crátons do mundo desde o final do Paleoproterozoico até o início do Neoproterozoico, como por exemplo no crátons da China, Finlândia, Índia, além do Cráton Amazônico. Em diversas províncias deste último, em ~1880 Ma ocorreu expressivo magmatismo amplamente representado pelo vulcano-plutonismo Uatumã que constitui uma *Silicic Large Igneous Province* (SLIP; Klein *et al.* 2002, Fraga *et al.* 2017, Teixera *et al*. em impr.). O magmatismo tipo-A anorogênico orosiriano de Carajás faz parte, portanto, de um megaevento evento extensional paleoproterozoico (~1880) que gerou centenas de rochas graníticas e vulcânicas, cuja origem é relacionada à atividade de plumas mantélicas em escala global.

Por outro lado, apesar de existirem inquestionáveis semelhanças petrográficas, geoquímicas e isotópicas entre as suítes paleoproterozoicas de Carajás (Jamon, Velho Guilherme e Serra dos Carajás), há contrastes significativos entre as mesmas, que têm sido interpretados como indicativos de que esses granitos foram formados em condições algo contrastantes de temperatura, conteúdo de H_2O e fugacidade de oxigênio. Com base em

evidências petrológicas e geoquímicas, incluindo dados isotópicos de Nd e, subordinadamente, Pb e oxigênio em rocha-total, diferentes fontes e/ou graus de fusão foram propostos para os magmas formadores dos granitos anorogênicos da província (Dall'Agnol *et al*. 1999b, c, 2005, Dall'Agnol & Oliveira 2007, Scaillet *et al*. 1995, Rämö *et al.* 2002). Porém, quanto maior a diversidade das fontes que contribuíram para a formação do magma, menos esclarecedores sobre a natureza e grau de envolvimento das fontes envolvidas serão os dados de isótopos radiogênicos Sm-Nd e outros dados isotópicos devem permitir aprofundar esta discussão.

Os sistemas isotópicos radiogênicos (Sr, Nd, Pb, Hf) de intrusões graníticas retêm a memória da composição, idade e história petrogenética das fontes dos magmas graníticos situadas na crosta ou no manto superior (Andersen *et al.* 2009, Goodge & Vervoort 2006, Griffin *et al.* 2002, Kemp *et al.* 2007, Kurhila *et al.* 2010, Payne *et al.* 2016). Esses isótopos tendem a registrar as contribuições de fontes mantélicas e/ou crustais na gênese de rochas graníticas e podem ser usados como traçadores de ambientes tectônicos (Goodge & Vervoort 2006). Embora seja tradicional o uso de isótopos de estrôncio e neodímio em rocha total, os mesmos fornecem informações apenas sobre a composição média homogeneizada das rochas fontes e são, portanto, menos eficientes quando se trata de fontes heterogêneas, pois não levam em conta a possibilidade de processos de mistura ou contaminação.

Como em termos dos granitos paleoproterozoicos de Carajás, só se dispunha de dados isotópicos parciais, foi indispensável realizar estudos isotópicos complementares com métodos mais robustos para testar as hipóteses já formuladas.

A análise de Hf em zircão é uma poderosa ferramenta para se determinar as fontes envolvidas em processos magmáticos, uma vez que o zircão é um mineral estável, resistente a perturbações isotópicas, e que geralmente preserva a composição isotópica do háfnio do magma do qual este foi extraído (Amelin *et al.* 2000, Andersen *et al.* 2009, Belousova *et al.* 2010, Griffin *et al.* 2000, Griffin *et al.* 2002, Izuka *et al.* 2017, Kemp *et al*. 2007, Kemp and Hawkesworth 2007, Patchett *et al*. 1981). A baixa razão Lu/Hf no zircão, normalmente inferior a 0,0005, que torna a correção para o crescimento radiogênico *in situ* desprezível, aliada a alta concentração e a baixa mobilidade do Hf no zircão propiciam razões isotópicas bastante precisas, que podem permitir importantes inferências, não só quanto à idade de extração mantélica, mas também quanto à possível história evolutiva da rocha (Ali *et al.* 2015, Belousova *et al.* 2010, Izuka *et al.* 2017, Kemp *et al.* 2010, Payne *et al.* 2016). Além disso, a curta meia-vida do ^{176}Lu comparada com a do ^{147}Sm resulta em contrastes significativos nas razões iniciais de ^{176}Hf/^{177}Hf comparadas às razões ^{143}Nd/^{144}Nd. Assim, quando se trata do

sistema isotópico Lu-Hf em zircão, este apresenta vantagens significativas sobre o sistema Sm-Nd em rocha total, atuando como um importante traçador de fontes magmáticas e processos petrogenéticos.

Os isótopos de oxigênio em cristais de zircão de rochas ígneas refletem a composição do $\delta^{18}O_{Zr}$ da fonte magmática, e podem indicar a incorporação de materiais contaminantes dentro da fusão, quando estes têm valores de $\delta^{18}O_{Zr}$ maiores que o manto primitivo ($\delta^{18}O$ = 5,3 ± 3; Valley 2003). Assim, análises de oxigênio *in situ* em zircão permitem a determinação do $\delta^{18}O$ ígneo mesmo em rochas fortemente alteradas (Valley 2003). O zircão possui uma difusão de oxigênio extremamente lenta (Peck *et al.* 2003) e o fracionamento dos isótopos de oxigênio em zircão tem sido calibrado usando vários tipos de rochas diferentes (Valley *et al.* 2003, Valley *et al.* 2005). Como o fracionamento isotópico do oxigênio é baixo em altas temperaturas, a alta precisão analítica do $\delta^{18}O$ em zircão permite reconhecer e interpretar pequenas variações (décimo de permil) na composição isotópica, e assim avançar na interpretação da gênese e evolução magmática (Bindeman *et al.* 2008).

Adicionalmente, o mineral zircão tem a vantagem de poder ser datado também pelo método U-Pb em SHRIMP (*Sensitive High-Resolution Ion Microprobe*), técnica que possui alta resolução espacial, permite a seleção de domínios homogêneos em cristais com estrutura interna complexa resultante da superposição de várias fases de crescimento, e, ainda, possibilita a obtenção de análises pontuais com rapidez.

Sendo assim, a combinação de medidas isotópicas *in situ* de Hf por LA-ICP-MS (*Laser Ablation- Inductively Coupled Plasma - Massa Spectrometer*), $\delta^{18}O$ por microssonda iônica, e U-Pb no SHRIMP, em um mesmo cristal de zircão, permite gerar informações críticas para rastrear a evolução dos eventos magmáticos/pós-magmáticos e metamórficos que possam ter ocorrido na história de evolução magmática de uma rocha.

Portanto, apesar da quantidade relativamente expressiva de dados geoquímicos, isotópicos e geocronológicos disponíveis na literatura sobre os granitos paleoproterozoicos da Província Carajás, para avanços na compreensão da origem destes granitos mostraram-se essenciais estudos de Lu-Hf e O, em conjunto com novas datações U-Pb em zircão em SHRIMP, já que as idades disponíveis até o momento foram obtidas em sua maioria pelos métodos Pb-Pb e, subordinadamente, U-Pb por TIMS (*Thermal Ionization Mass Spectrometer*).

Deste modo, essa Tese integra os dados isotópicos obtidos de Hf, O e U-Pb, com alguns novos dados de Nd e aqueles disponíveis na literatura, buscando definir com maior rigor a idade do magmatismo anorogênico da Província Carajás e avançar nas discussões

sobre a natureza das fontes e processos responsáveis pela origem dos magmas formadores de granitos do tipo-A, e do magmatismo proterozoico de outras províncias do Cráton Amazônico e de outros crátons do mundo.

1.3 OBJETIVOS

Tendo em vista os problemas assinalados e discutidos no item anterior, essa Tese de Doutorado tem como objetivo principal, definir a composição isotópica dos magmas geradores e refinar as idades das diferentes suítes e demais granitos paleoproterozoicos da Província Carajás. Com base nestes dados pretende-se determinar a idade do magmatismo anorogênico e avaliar a origem dos granitos tipo-A e o papel da fonte na definição de suas caraterísticas petrológicas e geoquímicas.

Como objetivos específicos podem ser listados:

- Definir com maior precisão e acurácia, as idades de cristalização dos granitos paleoproterozoicos da Província Carajás;
- Definir as assinaturas isotópicas de Lu-Hf em zircão nos diferentes granitos;
- Definir a composição isotópica do $\delta^{18}O$ em zircão nos diferentes granitos;
- Estabelecer comparações entre as composições isotópicas de Hf e O;
- Estabelecer comparações entre os dados Lu-Hf em zircão (t_{DM} e ε_{Hf}) com as idades modelos t_{DM} e parâmetros ε_{Nd} dos granitos paleoproterozoicos de Carajás;
- Reavaliar as idades e natureza das fontes geradoras do magmatismo paleoproterozoico da Província Carajás, de modo a explicar os contrastes existentes entre as suítes;
- Avaliar possíveis processos de contaminação e mistura de magmas;
- Comparar os resultados obtidos com aqueles de outros granitos tipo-A do Cráton Amazônico e de outros crátons pré-cambrianos do mundo.

1.4 METODOLOGIA

1.4.1 Pesquisa Bibliográfica

A pesquisa bibliográfica foi centrada no tema granitos tipo-A e na fundamentação teórica das técnicas analíticas a serem utilizadas na pesquisa e nas suas aplicações. No tema granitos paleoproterozoicos, o foco foi em trabalhos relacionados com: (1) suítes graníticas paleoproterozoicas de Carajás e do Cráton Amazônico; (2) diferentes tipos de granitoides e

sequências arqueanas, fontes potenciais dos magmas graníticos paleoproterozoicos; (3) contexto geológico, distribuição, evolução, tipologia e petrogênese de granitos tipo-A em nível global; (4) magmatismo global de ~1880 Ma. No plano dos métodos, foi utilizada bibliografia voltada para conceitos básicos e aplicações dos diversos sistemas isotópicos, com ênfase nos métodos Lu-Hf, O e U-Pb em zircão, no estudo de processos petrogenéticos responsáveis pela geração de rochas afins as estudadas, no método Sm-Nd em rocha total e, especialmente, nas diferenças entre este e o método Lu-Hf em zircão.

1.4.2 *Amostragem dos corpos de granitos paleoproterozoicos*

O Grupo de Pesquisa Petrologia de Granitóides (GPPG) do Instituto de Geociências da UFPA possui em seu acervo amostras dos principais corpos das suítes graníticas de interesse para a pesquisa. Amostras representativas dos diferentes corpos graníticos foram submetidas a estudos petrográficos e geoquímicos detalhados em trabalhos anteriores de pesquisadores do referido grupo. Sendo assim, a primeira etapa do trabalho exigiu a integralização de todos os dados disponíveis na literatura sobre os granitos paleoproterozoicos de Carajás, com a criação de um banco de dados, dos granitos mais representativos de cada uma das três suítes, que possuíssem informações geológicas (dados de campo, coordenadas geográficas), petrográficas (análise modal), geoquímicas e isotópicas (Pb-Pb e/ou U-Pb em zircão, e Sm-Nd em rocha total). A partir desse banco de dados, foi feita uma seleção prévia das amostras que poderiam servir para o estudo. A etapa seguinte foi localizar as amostras consideradas mais adequadas para os estudos complementares que se pretende realizar no acervo do GPPG, na litoteca do Instituto de Geociências da UFPA, e verificar quais dispunham de material suficiente para geocronologia. Por fim, foram selecionadas amostras representativas das principais fácies dos corpos graníticos das suítes Serra dos Carajás, Velho Guilher e Jamon, e dos granitos Seringa, São João e Gogó da Onça, para estudos isotópicos. Além disso, foram selecionadas 14 amostras para estudos petrográficos e geoquímicos complementares.

Complementarmente, em agosto de 2015, foi realizada campanha de campo nas áreas de Bannach e Redenção, para re-amostragem dos granitos homônimos. Com base nas informações disponíveis, foram selecionados previamente pontos onde se dispunha de amostras estudadas em termos petrográficos e geoquímicos. Tais pontos foram re-amostrados para obtenção de quantidade maior de material. Esse trabalho de campo ocorreu em conjunto com o estudante de mestrado Caio Mesquita, o qual desenvolveu sua Dissertação de Mestrado no Granito Bannach, e contou com a colaboração dos professores José de Arimatéia Costa de Almeida, da Universidade Federal do Sul e Sudeste do Pará (UNIFESPA), e Davis Carvalho

de Oliveira da UFPA, os quais têm trabalhos desenvolvidos nesses granitos (Almeida *et al.* 2006, Oliveira *et al.* 2008, 2009, 2010) e foram de grande valia nessa etapa.

1.4.3 Mineralogia e Petrografia

De modo geral, os estudos petrográficos foram efetuados apenas para reconhecimento das principais fácies dos granitos estudados e envolveram: identificação da mineralogia da rocha (Deer *et al.* 1992, Kerr 1959), estudo das texturas magmáticas e de alteração (Bard 1980, Mackenzie *et al.* 1982), avaliação das composições modais, exame preliminar do zircão presente nos granitos. Em casos específicos, exemplificado pelo Granito Gogó da Onça, do qual não se dispunha de informações petrográficas, foi desenvolvido estudo clássico envolvendo descrições petrográficas em microscópio ótico, realização de análises modais, estudos complementares em microscopia eletrônica de varredura e medidas de suscetibilidade magnética. Em boa parte, tais estudos foram efetuados em colaboração com o estudante de graduação Luan Alexandre Martins de Sousa, tendo culminado na produção de seu Trabalho de Conclusão de Curso (TCC; Sousa, 2017).

1.4.4 Análises químicas

Foram realizadas análises químicas complementares, sobretudo no Granito Gogó da Onça do qual não se dispunha dessa informação.

As análises foram realizadas no laboratório comercial *Acme Analytical Laboratories Ltda* (Vancouver, Canadá), por ICP-ES, no caso de elementos maiores e menores (SiO_2, TiO_2, Al_2O_3, Fe_2O_3t, MgO, CaO, MnO, Na_2O, K_2O, P_2O_5), e por ICP-MS no caso dos elementos-traço (Rb, Sr, Ba, Ga, Y, Zr, Nb, U, Th, Cr, Ni, V), inclusive os elementos terras raras (La, Ce, Pr, Nd, Sm, Eu, Gd, Tb, Dy, Ho, Er, Tm, Yb e Lu).

A caracterização geoquímica destas rochas foi feita com base nos princípios gerais discutidos em Rollinson (1993). Ela consistiu em: determinação e representação dos *elementos maiores e menores* em diagramas de variação; definição das principais características geoquímicas (Dall'Agnol & Oliveira 2007, Debon & Le Fort 1983, Frost *et al.* 2001, Shand 1950, Sylvester 1989, Whalen *et al*. 1987), e estudo dos *elementos traços*, com destaque para os elementos terras raras (ETR).

1.4.5 Datações U-Pb em zircão e titanita por SHRIMP

Zircão ($ZrSiO_4$) e titanita ($CaTiSiO_5$) são minerais acessórios comuns que possuem concentrações de urânio (U) geralmente suficientes para seu uso como geocronômetros. O avanço das análises *in situ* por LA-ICP-MS (*Laser ablation inductively coupled plasm mass espectrometry*) e SHRIMP (*Sensitive High-Resolution Ion MicroProbe*) tem mostrado a complexidade de grãos de zircão e titanita que frequentemente apresentam mais de uma fase de cristalização. A determinação das idades de diferentes zonas desses minerais pode, assim, fornecer importantes informações petrogenéticas sobre a evolução das rochas que os contém.

Vinte e seis amostras selecionadas dos diferentes corpos graníticos paleoproterozoicos da Província Carajás foram datadas pelo método U-Pb em zircão e alguns granitos da Suite Jamon foram datados também pelo método U-Pb em titanita, utilizando a sonda iônica (SHRIMP) na *Curtin University*, em Perth, na Austrália. Os procedimentos metológicos na obtenção desses dados estão descritos nos capítulos 2 e 3.

1.4.6 Estudos isotópicos pelo método Lu-*Hf*

O sistema isotópico Lu-Hf em zircão se tornou uma importante ferramenta no estudo de fonte de rochas magmáticas e na proveniência de sedimentos. Diversos estudos têm definido assinaturas isotópicas do Hf de importantes reservatórios do manto superior e da crosta continental, e discutido sua evolução através do tempo geológico (Andersen *et al.* 2009, Belousova *et al.* 2010, Condie *et al.* 2011, Dhuime *et al.* 2012; Griffin *et al.* 2000, 2002, Hawkesworth & Kemp 2006, Iizuka *et al.* 2010). Esse sistema isotópico afirmou-se como um importante traçador da história de diferenciação da crosta e do manto.

As análises isotópicas Lu-Hf *in situ* em zircão por LA-ICP-MS dos granitos paleoproterozoicos da Província Carajás foram realizadas em duas sessões: a primeira sessão foi na *University of Western Australia*, onde foram analisados cristais de zircão das suítes Serra dos Carajás, Velho Guilherme e Jamon, e do Granito Gogó da Onça; a segunda sessão foi realizada na *Curtin University* onde foram analisados zircões dos granitos Seringa e São João. As condições analíticas utilizadas para obtenção dos resultados constam do capítulo 4.

1.4.7 Estudos Istópicos $\delta^{18}O$ em zircão

Análises de isótopos de oxigênio, em cristais de zircão ígneo cuja idade tenha sido determinada podem ser usadas como traçadores de evolução e reciclagem crustal e da interação manto-crosta (Payne *et al.* 2016). No estudo de suítes graníticas, o $\delta^{18}O_{Zr}$, em conjunto com as composições isotópicas do Hf, tem se mostrado uma importante ferramenta na determinação das fontes geradoras dos granitos, levando a importantes interpretações sobre

processos de contaminação e assimilação de material supracrustal, e no papel da crosta na geração de granitos do tipo-A (Andersen *et al.* 2004, Elliot *et al.* 2005, Goodge & Vervoort 2006, Heinonen *et al.* 2010, 2012).

Na presente Tese de Doutorado foram realizadas, em média, entre 10 e 15 análises de $\delta^{18}O$ em zircões das amostras selecionadas para estudo, sendo sido a maior parte das análises realizada em cristais preliminarmente datados. As análises foram realizadas em microssonda iônica CAMECA 1280, no CMCA (*Center for Microscopy, Characterization and Analyses*) na *University of Western Australia*. As condições analíticas utilizadas para obtenção dos resultados são descritas no capítulo 4.

1.4.8 Estudos isotópicos pelo método Sm-Nd (rocha total)

Esse sistema isotópico é amplamente utilizado na investigação de processos de formação e evolução de crosta continental. Na petrogênese de rochas graníticas, as idades modelo (t_{DM}), juntamente com o parâmetro ε_{Nd} auxiliam na discussão de fontes. Diversos trabalhos que envolvem sistemas isotópicos como traçadores se baseiam em análises em rocha total e, apesar das técnicas serem precisas em termos de acurácia analítica, oferecem limitada resolução espacial para registrar informações petrogenéticas contidas em populações heterogêneas de minerais. As incertezas analíticas podem ocorrer também devido a processos secundários que ocorrem em ambiente crustal, como a mistura de magmas.

Em razão disso, trabalhos que envolvem estudos de fontes têm integrado os dados isotópicos obtidos em rocha total (Nd, Sr), com análises isotópicas *in situ* como Hf e O. Na presente Tese de Doutorado, optou-se por realizar análises Sm-Nd em rocha total nos Granitos Seringa, São João e Gogó da Onça, afim de se estabelecer comparações preliminares com os dados de Nd já disponíveis na literatura para as suítes paleoporterozoicas de Carajás. As análises foram realizadas no Laboratório de Geologia isotópica Pará-Iso da Universidade Federal do Pará (UFPA). Nos Capítulos 2 e 4 são descritos os procedimentos para obtenção dos dados isotópicos de Nd.

1.5 CONTEXTO GEOLÓGICO REGIONAL

O Cráton Amazônico (CA) foi formado por sucessivos episódios de acresção crustal durante o Paleoproterozoico e Mesoproterozoico ao redor de um núcleo antigo estabilizado no final do Arqueano (Brito Neves & Cordani 1991, Cordani & Teixeira 2007, Santos *et al.* 2000; Teixeira *et al.* 1989, Tassinari & Macambira 1999). Dois modelos propostos para a divisão do cráton em províncias com base em dados geológicos e geocronológicos (U-Pb e

Sm-Nd) têm sido amplamente discutidos na literatura. Esses modelos são semelhantes em termos das grandes linhas de evolução do cráton, porém divergem em termos de idades, denominações e, principalmente, nos limites das diversas províncias (Tassinari & Macambira 2004, Santos *et al*. 2000).

Santos et al. (2000) propuseram a dividisão do cráton em sete províncias geocronológicas (Fig. 1a): Carajás (3100 – 2530 Ma), Transamazônica (2250 - 2000 Ma), Tapajós – Parima (2100 -1870 Ma), Amazônia Central (1880 – 1700 Ma), Rio Negro (1860 – 1520 Ma), Rondônia – Juruena (1760 – 1470 Ma), e Sunsás (1330 – 990 Ma). Tassinari & Macambira (2004; Fig. 1b) inserem a Província Carajás na Província Amazônia Central, considerada como a crosta continental mais antiga do cratón que não foi afetada pelo ciclo transamazônico, e definem as seguintes províncias: Maroni-Itacaiunas (2200-1950 Ma), Ventuari-Tapajós (1950-1800 Ma), Rio Negro-Juruena (1800-1550 Ma), Rondonia-San Ignácio (1550-1300 Ma) e Sunsás (1250-1000 Ma).

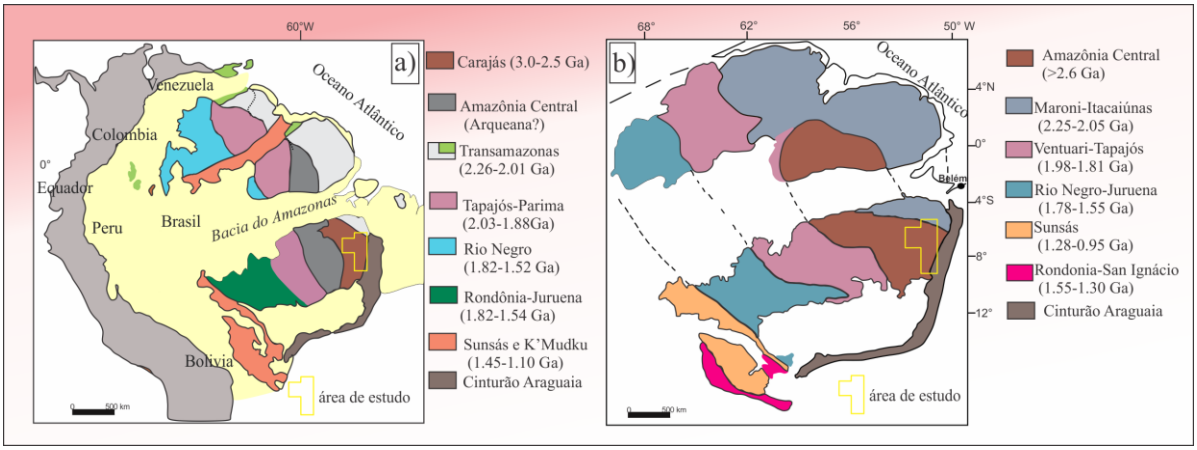

Figura 1- Províncias geocronológicas do Cráton Amazônico, com destaque para a região de Carajás representada na Figura 2.
Fonte dos dados: Segundo Santos et al. 2000 (a) e Tassinari & Macambira 2004 (b).

Diversos autores propõem que o Cratón Amazônico fez parte de um Supercontinente atualmente conhecido como Columbia (Meert *et al.* 2017, Zhao *et al.* 2011) que se aglutinou durante eventos colisionais no Paleoproterozoico (2,0 Ga a 1,8 Ga). Durante a Era Paleoproterozoica (Orosiriano), especialmente em ~1880 Ma um extensivo magmatismo orogênico e pós-colisional ocorreu formando centenas de *stocks*, batólitos e diques nas províncias Carajás, Tapajós-Parima, Amazônia Central e Rondônia-Juruena. Esse magmatismo é em grande parte representado pelas rochas vulcânicas e plutônicas do evento Uatumã, considerado como sendo uma Silicic Large Igneous Province (SLIP - Fraga *et al.* 2017, Teixeira, W. *et al.* submetido).

Na Província Carajás (PC; Fig 2) o evento de ~1880 Ma gerou diversos granitos anorogênicos com afinidade rapakivi e diques máficos e félsicos a eles correlacionados (Dall'Agnol *et al.* 1999 a, b, c, 2005, Silva *et al.* 2016, Oliveira & Dall'Agnol 2007, Teixeira *et al.* 2002). Esses granitos foram aglutinados em três suítes (Jamon, Serra dos Carajás e Velho Guilherme) que são o alvo principal desta Tese de Doutorado.

A Província Carajás está localizada na porção sul-oriental do CA (Fig. 1 e Fig 2a), no sudeste do estado do Pará. Foi redividida recentemente por Dall'Agnol et al. (2013) em três domínios distintos que serão apresentados abaixo:

1.5.1 Domínio Rio Maria

O Domínio Rio Maria ocorre na porção sul da Província Carajás (Fig. 2), apresenta idades variando entre 2,98 Ga e 2,86 Ga e é composto por: a) *greenstone belts do Supergrupo Andorinhas* (3,0 - 2,9 Ga), que consiste de rochas meta-ultramáficas (komatiitos), meta-básicas (basaltos e gabros), e subordinadamente rochas félsicas a intermediárias com intercalações de meta-grauvacas. b) *granitóides sódicos* que compreendem suítes tonalito-trondhjemito e suítes Leocogranito-granito (Almeida *et al.* 2017). As suítes tonalito-trondhjemito são representadas por Tonalito Arco Verde, Trondhjemito Mogno, Complexo Tonalítico Caracol, Tonalito Mariazinha e Trondhjemito Água Fria (Almeida *et al.* 2008, Almeida *et al*. 2011, Guimarães *et al.* 2010, Leite *et al.* 2001, Macambira & Lafon 1995, Rolando & Macambira 2003). A suíte leucogranito-granito (2,87 – 2,86 Ga) é composta pela Suíte Guarantã, Granodiorito Grotão e rochas similares (Almeida *et al.* 2010, 2013). c) *granitoides com alto Mg do tipo sanukitoide* (~2,87 Ga), representados pela Suíte Rio Maria composta pelo Granodiorito Rio Maria (Medeiros & Dall'Agnol 1988, Oliveira M.A *et al.* 2009) e rochas intermediárias a máficas associadas, o Granito Rancho de Deus (Dias 2009), e o Quartzo-diorito Parazônia (Guimarães *et al.* 2009). E, por fim, d) *leucogranitos potássicos* (2,87-2,86 Ga) representados pelos Granitos Xinguara e Mata Surrão e por pequenos *stocks* graníticos relacionados (Almeida *et al.* 2013, Althoff *et al*. 2000, Duarte & Dall'Agnol 1996).

1.5.2 Domínio Sapucaia

O Domínio Sapucaia (Fig. 2) apresenta fortes semelhanças com o Domínio Rio Maria em termos litológicos, porém as rochas que o constituem foram intensamente deformadas durante o Neoarqueano e seccionadas por granitóides subalcalinos neoarqueanos (suítes Planalto e Vila Jussara). Nesse domínio ocorrem: a) rochas tonalíticas distintas das associações TTG clássicas, as quais foram denominadas de Tonalito São Carlos (2,94 Ga;

Guimarães *et al.* 2012, Silva *et al.* 2014); b) clássicas suítes TTG arqueanas, denominadas Trondhjemito Colorado (~2,87 Ga; Santos *et al.* 2013, Silva *et al.* 2014,) e Trondhjemito Água Fria; c) granitoides mesoarqueanos de alto Mg denominados de Granodiorito Água Azul e Granodiorito Água Limpa (2,88 Ga - 2,87 Ga; Gabriel & Oliveira 2014); d) leucogranodioritos com alto Ba e Sr representados pelo Leucogranodiorito Pantanal (Teixeira *et al*. 2013) e Leucogranodiorito Nova Canadá (2,89 Ga; Leite-Santos *et al.* 2016, Oliveira *et al.* 2010); e) leucogranitos de alto K representados pelo Leucogranito Velha Canadá (2,74 Ga; Leite-Santos *et al.* 2016, Santos *et al.* 2010); finalmente, tem-se granitos subalcalinos noarqueanos agrupados nas suítes Planalto (~2,73 Ga; Feio *et al.* 2012, Cunha *et al.* 2016) e Vila Jussara (2,75 – 2,73 Ga; Dall'Agnol *et al.* 2017).

1.5.3 Domínio Canaã dos Carajás

O Domínio Canaã dos Carajás (Fig. 2) se distingue dos domínios Rio Maria e Sapucaia em termos de associações litológicas e também em assinaturas isotópicas de Nd em relação ao Domínio Rio Maria (Dall'Agnol *et al*. 2013, Feio *et al.* 2013). Feio et al. (2013) e Moreto et al. (2011, 2015) individualizaram naquele domínio diversos granitóides com assinaturas geoquímicas distintas e idades mesoarqueanas a neoarqueanas. São estes, em ordem de idades decrescentes: Tonalito Bacaba, Granito Canaã dos Carajás, Complexo Tonalítico Campina Verde, Trondhjemito Rio Verde, Granito Cruzadão, Granito Bom Jesus, Granito Serra Dourada (mesoarqueanos), granitos subalcalinos da Suíte Planalto, granitos sódicos da Suíte Pedra Branca, e rochas charnoquíticas associadas ao Diopsídio-Norito Pium (neoarqueanos). Esta última unidade era considerada como tendo idade mesoarqueana (Pidgeon *et al.* 2000), porém estudos geológicos, geoquímicos e geocronológicos demonstraram que a mesma possui idade neoarqueana e natureza charnockítica e não granulítica (Santos, R.D. *et al*. 2013).

1.5.4 Bacia Carajás

A principal unidade litoestratigráfica presente na Bacia Carajás (Fig. 2) é o Supergrupo Itacaiúnas (2,76 Ga; Gibbs *et al*. 1986, Machado *et al*. 1991) constituído principalmente por rochas máficas a intermediárias, metavulcânicas e formações ferríferas bandadas, que compreendem as rochas dos grupos Igarapé Salobo, Grão-Pará, Igarapé Bahia, Igarapé Pojuca e Rio Novo. Recentemente Martins et al. (2017) obteve idades mais jovens (~2,74 Ga) para os basaltos da Formação Parauapebas.

Ocorrem também neste domínio: a) rochas do Complexo Luanga (2,76 Ga; Machado *et al*. 1991), localizado nas proximidades de Serra Pelada, sendo constituído por rochas ultrabásicas e básicas acamadadas (Medeiros Filho & Meireles 1985); b) granitos subalcalinos foliados representados pelo Complexo Granítico Estrela (~2,75 Ga; Barros *et al.* 1991, Barros *et al*. 1997, Barros & Dall'Agnol 1994) e granitos Serra do Rabo (2,74 Ga, Sardinha *et al*. 2006), Igarapé Gelado e Velho Salobo. São dominantemente monzogranitos a álcali-feldspato granitos fortemente deformados, tendo sido admitida uma colocação sintectônica para o Complexo Granítico Estrela (Barros *et al*. 2009).

Sobreposta estratigraficamente as unidades arqueanas mencionadas tem-se a Formação Águas Claras, que constitui uma cobertura siliciclástica de possível idade paleoproterozoica (?), não metamorfisada, cortada por vários diques e *sills* de gabro e diabásio.

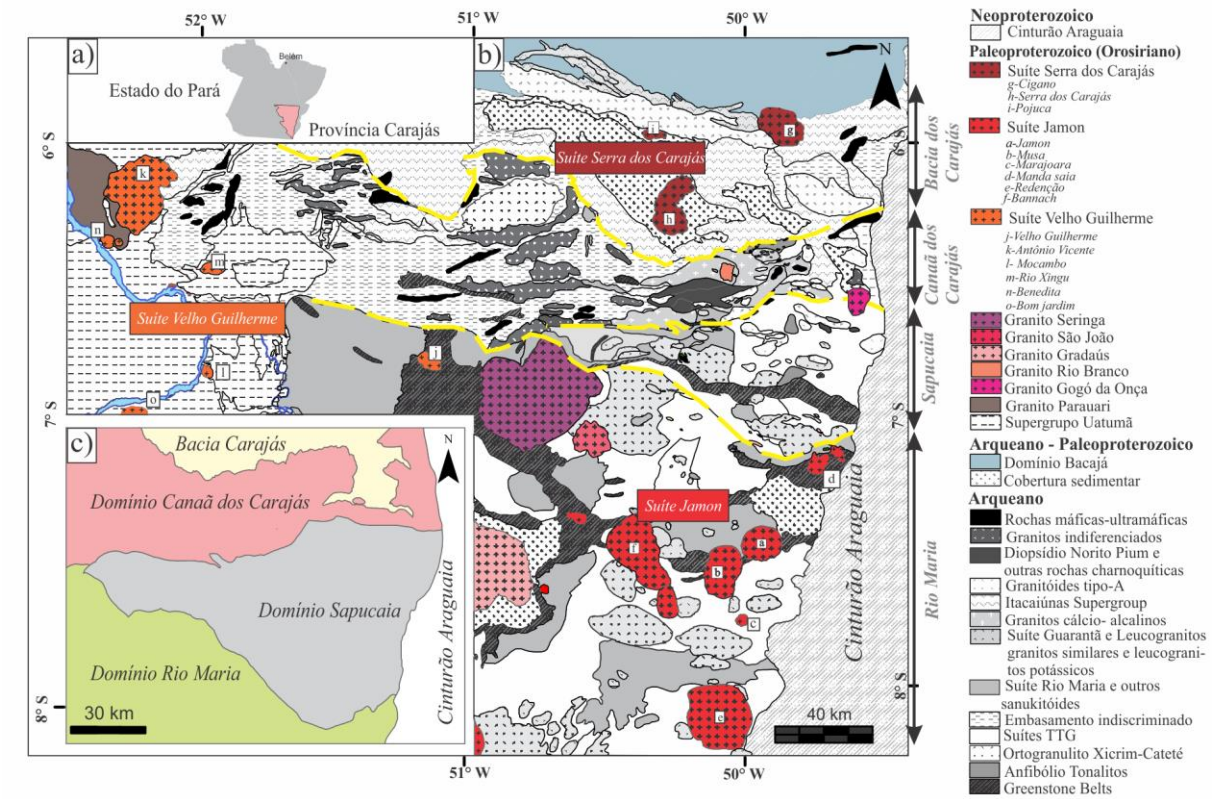

Figura 2 - a) Mapa do Estado do Pará mostrando a localização da Província Carajás; b) Mapa geológico de parte da Província Carajás destacando os granitos Paleoproterozoicos estudados. c) Mapa simplificado mostrando a compartimentação tectônica da Província Carajás.
Fonte dos dados: Almeida *et al.* 2011, Dall'Agnol et al. 2013, Feio *et al.* 2013, Gabriel & Oliveira 2014, Oliveira *et al.* 2010, Rodrigues *et al.* 2014, Santos, P.A. *et al.* 2013, Silva *et al.* 2014, Teixeira *et al.* 2013, Vasquez *et al.* 2008.

1.6 GRANITOS ANOROGÊNICOS DA PROVÍNCIA CARAJÁS

Os granitos tipo-A anorogênicos da Província Carajás formam uma série de corpos intrusivos que seccionam as unidades arqueanas dos seus diferentes domínios. Esses granitos se colocaram em ambiente extensional e são contemporâneos a diques de diabásio e dacitos/granitos pórfiros de direções WNW-ESE a NNW-SSE (Dall'Agnol *et al.* 2005, Oliveira *et al.* 2010, Silva *et al.* 2016).

São agrupados em três suítes (Fig. 2b), de acordo com suas características petrográficas e geoquímicas e estado de oxidação dos seus magmas. São estas: (1) Suíte Jamon, situada no Domínio Rio Maria, representada pelos granitos Jamon, Musa, Marajoara, Manda-Saia, Redenção e Bannach; (2) Suíte Velho Guilherme, formada por granitos estaníferos presentes na região do Xingu, os quais seccionam as rochas vulcânicas do Supergrupo Uatumã e o embasamento arqueano; compreende os granitos Velho Gilherme, Antônio Vicente, Mocambo, Benedita, Rio Xingu (Teixeira *et al.* 2002) e Bom Jardim (Lamarão *et al.* 2012); (3) Suíte Serra dos Carajás, situada no Domínio da Bacia Carajás, composta pelos granitos Serra dos Carajás, Cigano e Pojuca (Barros *et al.* 1995, Dall'Agnol *et al.* 2005, Javier-Rios *et al.* 1995, Teruya *et al*. 2008). Além das três suítes mencionadas, cabe destacar os granitos Gogó da Onça, Seringa, São João, Rio Branco e Gradaús (Fig. 2b), que não foram até o momento vinculados a nenhuma das três suítes.

Os plutons anorogênicos de Carajás foram colocados em niveis crustais rasos (~1-3 kbar), e comumente se observam enclaves angulares das rochas encaixantes nos granitos, indicando alto contraste de viscosidade entre os seus magmas e as rochas encaixantes arqueanas (Dall'Agnol *et al.* 2005). Diques félsicos e máficos seccionam as unidades arqueanas e, localmente, os corpos graníticos (Ferreira 2009, Gastal 1987, Huhn *et al*. 1988, Rivalenti *et al*. 1998, Silva et al. 2016, Silva Jr. *et al*. 1999, Souza *et al*. 1990).

Geoquímicamente, possuem características metaluminosas a peraluminosas e apresentam razões Na_2O/K_2O que variam entre 1,0 e 2,0 e aumentam da Suíte Jamon para as suítes Velho Guilherme e Serra dos Carajás. São granitos que exibem altas razões $FeO_t/(FeO_t + MgO)$ e são, portanto, ferrosos, segundo a terminologia de Frost et al. (2001). Possuem elevado conteúdo de HFSE e têm assinatura do tipo A (Dall'Agnol *et al*. 2005).

Datações pelos métodos U-Pb e/ou Pb-Pb em zircão (Avelar 1996, Dall'Agnol *et al.* 1999a, 2005, Lima 2011, Machado *et al.* 1991, Macambira & Lafon 1995, Paiva Jr. 2009) ou, menos comumente, Pb-Pb em rocha total (Barbosa *et al*. 1995), dessas suítes graníticas, forneceram idades de cristalização de ~1,88 Ga. Os dados isotópicos de Nd para estas rochas revelam idades t_{DM} arqueanas (~3,35 Ga a 2,60 Ga; Dall'Agnol *et al.* 2005, Rämö *et al.* 2002, Teixeira et al. 2002) e valores de ε_{Nd} (em 1,88 Ga) extremamente negativos (-12 a -8),

interpretados como indicativos de fontes arqueanas para os seus magmas. Uma síntese das princípais características petrográficas de cada uma das suítes e dos plutons Seringa, São João, Rio Branco e Gradaús é apresentada abaixo . O granito Gogó da Onça é apresentado em detalhe no capítulo 2. Os dados geocronológicos e isotópicos de Nd desses granitos estão sumarizados na Tabela 1.

1.6.1 Suíte Serra dos Carajás

Essa suíte é composta dominantemente por monzogranitos e sienogranitos; localmente ocorrem granitos hidrotermalizados, bolsões pegmatóides e greisens em zonas de fraturas (Barros *et al.* 1995, Javier Rios *et al.* 1995). Como minerais acessórios são descritos zircão, apatita, magnetita, ilmenita e allanita. Titanita primária é rara ou ausente, fluorita é comum, e a turmalina, por vezes, está presente (Barros *et al*. 1995, Rios *et al*. 1995). O conteúdo modal dos minerais óxidos de Fe e Ti é inferior a 1%, e é comum a ocorrência de magnetita, porém sem ilmenita associada. Os valores de suscetibilidade magnética (SM) da Suíte Serra dos Carajás são moderados, se comparados aos das suítes Jamon e Velho Guilherme. Seguindo a classificação de Ishihara (1981), os granitos da Suíte Serra dos Carajás pertenceriam a série magnetita, porém apresentam altas razões $FeO_t/(FeO_t + MgO)$ em rocha total e em biotita e anfibólio, o que sugere formação em condições relativamente redutoras (Dall'Agnol *et al.* 2005).

1.6.2 Suíte Velho Guilherme

É constituída predominantemente de sienogranitos e, subordinadamente, monzogranitos e álcali-feldspato granitos, sendo suas fácies mais evoluídas afetadas por intensa alteração hidrotermal pós-magmática. São comuns ocorrências de greisens que hospedam pequenas concentrações primárias de cassiterita (Teixeira & Bettencourt 2000; Teixeira *et al.* 2005). Como fases minerais acessórias ocorrem zircão, ilmenita, titanita, apatita e, nas fácies menos evoluídas, magnetita. Os minerais de alteração pós-magmática são sericita, fengita, clorita, fluorita, epidoto, topázio, esfalerita, microclina, albita, allanita e minerais argilosos. Cassiterita, calcopirita, estanita, fluocerita, esfalerita, xenotímio e monazita estão associados aos granitos mais intensamente alterados (Dall'Agnol *et al.* 1993; Teixeira *et al.* 2005).

No geral, os granitos desta suíte são mais pobres em máficos do que as rochas das outras suítes. As fácies dominantes não contém quantidades significativas de titanita e nem de magnetita e o conteúdo modal de minerais opacos é menor que 0,1%. Isto implica baixos

valores de suscetibilidade magnética e as características descritas fazem com que tais rochas sejam incluídas na série Ilmenita de Ishihara (1981).

1.6.3 Suíte Jamon

Os plútons dessa suíte são formados por monzogranitos e, subordinadamente, sienogranitos, com fases minerais acessórias que correspondem a zircão, apatita, magnetita, ilmenita, allanita, titanita e, somente em fácies mais evoluídas, fluorita (Almeida *et al.* 2006, Dall'Agnol *et al*. 1999a, c, Oliveira *et al.* 2009). Os conteúdos modais dos minerais óxidos de Fe e Ti variam geralmente de 0,5% a 0,2% e magnetita é dominante sobre ilmenita. Apresentam altos valores de suscetibilidade magnética (SM) e presença marcante da paragênese magnetita-titanita-quartzo, típica dos granitos da série magnetita (Ishirara 1981). A presença constante de magnetita e titanita primárias indica que essses granitos foram formados em condições oxidantes próximas ao tampão NNO (Dall'Agnol *et al.* 1997, 1999a, b). Texturas do tipo rapakivi são comumente observadas nos plutons Redenção e Bannach (Almeida *et al.* 2006, Oliveira, D.C *et al.* 2009).

A distribuição das fácies dentro dos plutons desta suíte é aproximadamente concêntrica com os granitos menos evoluídos ocupando as zonas externas e os mais evoluídos a porção central de cada corpo granítico. Nos pluton Jamon, Redenção e Bannach as principais fácies são relacionadas por cristalização fracionada (Dall'Agnol *et al.* 1999c). Contudo, na porção central dos granitos Bannach e Redenção ocorrem *stocks* de leucogranitos provavelmente derivados de um magma independente (Oliveira, D.C *et al.* 2009; Almeida *et al.* 2006; Mesquita *et al.* submetido).

1.6.4 Granito Seringa

Trata-se de um batólito com cerca de 2250 km^2 (Fig. 2b) formado por sienogranitos e monzogranitos, e, subordinadamente, leucogranitos. Os contatos entre o Granito Seringa e suas encaixantes são em geral bruscos e bem marcados, sendo comum nessas zonas a presença de enclaves angulosos englobados pelo Granito Seringa. Diques félsicos de orientação preferencial NE-SW e NW-SE cortam tanto as diferentes fácies do Granito Seringa quanto às unidades arqueanas.

Os minerais acessórios incluem zircão, magnetita, ilmenita, apatita e allanita. Apresenta conteúdos modais de opacos variando de 2,6% a 0,3% e valores moderados de SM, similares aos da Suíte Serra dos Carajás (Paiva Jr. 2009). A magnetita atinge proporções maiores que 1% nos monzogranitos e conteúdos de até 0,5% nas rochas mais evoluídas, sendo

mais frequente que a ilmenita (Paiva Jr. 2009; Paiva Jr. *et al.* 2011). Texturas rapakivis são observadas localmente nas facies monzograníticas. A distribuição espacial de suas fácies petrográficas mostra um zoneamento concêntrico, com as rochas mais ricas em máficos situadas predominantemente nas bordas do corpo e as fácies mais leucocráticas no centro (Paiva Jr. 2009).

Segundo Paiva Jr. (2009), o Granito Seringa pode ter sido formado por cristalização fracionada de um magma parental através de, pelo menos, três diferentes pulsos magmáticos. O primeiro estaria representado pelas rochas monzograníticas; o segundo teria formado as rochas sienograníticas; e o terceiro seria responsável pela formação de líquidos magmáticos mais evoluídos, geradores das rochas leucograníticas.

1.6.5 Granito São João

Esse granito possui dimensão de aproximadamente 160 km² e está localizado entre as cidades de Água Azul do Norte e Bannach (Fig. 2b). É formado por rochas monzo a sienograníticas, em geral com conteúdo de minerais máficos < 10% (leucocráticas). Zircão, apatita, allanita, magnetita e ilmenita são os minerais acessórios, sendo o conteúdo modal de opacos inferior a 1%. A ausência de titanita magmática é uma feição característica em todas as fácies desse pluton. Suas diversas variedades apresentam valores moderados de SM, similares aos dos granitos Seringa e Serra dos Carajás (Lima *et al*. 2014). Lima et al. (2014) considera que as diferentes facies deste pluton evoluíram por cristalização fracionada, diferentemente do que se oberva no Granito Seringa (Paiva Jr. et al. 2011).

1.6.6 Granito Rio Branco

O Granito Rio Branco (Santos *et al.* 2013) corresponde a um *stock* que aflora nas proximidades da mina de cobre do Sossego a NW de Canaã dos Carajás e secciona o Granito Cruzadão de idade arqueana (Fig. 2b). É composto por sienogranitos hololeucocráticos com textura equigranular. Fluorita, alanita e zircão são os minerais acessórios comuns, mas também ocorrem pitira e calcopitrita. São afetados por processos de alteração pós-magmatica, albitização e, subordinadamente, greisenização. A presença de hematita é comum nesse pluton e a magnetita é rara ou ausente. Santos et al. (2013) consideram que o Granito Rio Branco possui maior afinidade com aqueles da Suíte Velho Guilherme e, em menor grau, com os da Suíte Serra do Carajás, sendo claramente distinto dos granitos da Suíte Jamon.

1.6.7 Granito Gradaús

O Granito Gradaús foi recentemente estudado por Carvalho (2017). Trata-se de um batólito com formato subcircular e cerca de 800 km² de área aflorante. É intrusivo em metassedimentos do Grupo Rio Fresco no Domínio Rio Maria. Esse granito é contituído por dois conjuntos petrográficos distintos de rochas monzograníticas e sienograníticas. Os principais minerais acessórios são zircão, magnetita, ilmenita, allanita e apatita; subordinadamente ocorrem pirolusita, monazita e fluorita. Os valores de suscetibilidade magnética são moderados a baixos, o que permite classificá-lo como um granito moderadamente reduzido. Assim como os granitos Seringa e São João, o Granito Gradaús apresenta maior similaridade com os granitos da Suíte Serra dos Carajás (Carvalho 2017).

Tabela 1- Dados geocronológicos dos granitos paleoproterozoicos da Província Carajás

Pluton	material	Idade em Ma (Referências)	Método	Sm-Nd (rocha-total)	
				t_{DM}	ε_{Nd}
SUÍTE SERRA DOS CARAJÁS					
Cigano	zircão	1883 ± 2 (1)	U-Pb (TIMS)	2939	-9,7 (7)
				2668	-9,5 (7)
Serra dos Carajás	zircão	1880 ± 2 (1)	U-Pb (TIMS)	2611	-7,9 (7)
				2727	-9,2 (7)
Pojuca	zircão	1874 ± 2 (1)	U-Pb (TIMS)	3353	-9,7 (7)
SUÍTE VELHO GUILHERME					
Velho Guilherme	rocha-total	1873 ± 13 (2)	Pb-Pb		
Velho Guilherme	zircão	1853,7 ± 6,2 (13)	U-Pb (LA-ICP-MS)		
Antônio Vicente	zircão	1867 ± 5 (6)	evaporação do Pb	3254	-12,1(6)
Mocambo	zircão	1865 ± 2 (6)	evaporação do Pb	2976	-7,9 (6)
				3023	-12,2 (6)
Bom Jardim	zircão	1867 ± 1 Ma (11)	evaporação do Pb		
Serra Queimada	zircão	1882 ± 12 (11)	evaporação do Pb		
Rio Xingu	zircão	1866 ± 2 (6)	evaporação do Pb		
SUÍTE JAMON					
Musa	zircão	1883 ± 5 (1)	U-Pb (TIMS)	2821	-9,4 (5)
				2793	-9,3 (5)
	titanita	1884 ± 5 (1)		2596	-9,6 (5)
Jamon	zircão	1885 ± 32 (3)	evaporação do Pb	3024	-9,7 (5)
				2874	-9,5 (5)
Redenção	rocha-total	1870 ± 68 (4)	Pb-Pb	2785	-8,8 (14)
				2807	-10,5 (14)
				2789	-9,7 (14)
				2727	-9,6 (14)
Bannach				2844	-9,6 (14)
Diques félsicos (granito pórfiro)	zircão	1885 ± 2 (7)	evaporação do Pb	2830	-10 (14)
Diques félsicos (dacito pórfiro)	zircão	1886 ± 4 (7)	evaporação do Pb	2884	-9,4 (14)
OUTROS GRANITOS E DIQUES CORRELACIONADOS					
Seringa	zircão	1895 ± 1 (9)	evaporação do Pb		
		1892 ± 30 (2)			
São João	zircão	1890 ± 2 (10)	evaporação do Pb		
Diques félsicos	zircão	1880,9 ± 6,7 (14)	U-Pb (SHRIMP)		
Diques félsicos	zircão	1881,9 ± 8,8 (14)	U-Pb (SHRIMP)		

Fontes dos dados: (1) Machado et al. (1991); (2) Rodrigues et al. (1992); (3) Barbosa et al. (1995); (4) Avelar (1996); (5) Dall'Agnol et al. (1999a); (6) Teixeira et al. (2002); (7) Dall'Agnol et al. (2005); (8) Pinho et al. (2006); (9) Paiva Jr. (2009); (10) Lima (2011); (11) Lamarão et al. (2012); (12) Silva et al. (2016); (13) Antonio et al. (2017); (14) Rämö et al. (2002).

2. GEOCHEMISTRY, GEOCRONOLOGY AND Nd ISOTOPES OF THE GOGÓ DA ONÇA GRANITE: A NEW A-TYPE PALEOPROTEROZOIC GRANITE OF CARAJÁS PROVINCE, BRAZIL

Mayara Fraeda Barbosa Teixeira

Roberto Dall'Agnol

João Orestes Schneider Santos

Luan Alexandre Martins de Sousa

Jean-Michel Lafon

Publicado: Journal of South America Earth Sciences

Journal of South American Earth Sciences 80 (2017) 47–65

Contents lists available at ScienceDirect

Journal of South American Earth Sciences

journal homepage: www.elsevier.com/locate/jsames

Geochemistry, geochronology and Nd isotopes of the Gogó da Onça Granite: A new Paleoproterozoic A-type granite of Carajás Province, Brazil

Mayara Fraeda Barbosa Teixeira [a, *], Roberto Dall'Agnol [a, b], João Orestes Schneider Santos [c], Luan Alexandre Martins de Sousa [a], Jean-Michel Lafon [a]

[a] Graduate Course in Geology and Geochemistry, Geosciences Institute, Federal University of Pará (UFPA), INCT-GEOCIAM, Belém, PA, Brazil
[b] Instituto Tecnológico Vale (ITV), Belém, PA, Brazil
[c] University of Western Australia, Centre for Exploration Targeting, Crawley, WA, 6009, Australia

ARTICLE INFO

Article history:
Received 4 July 2017
Received in revised form
29 August 2017
Accepted 15 September 2017
Available online 21 September 2017

Keywords:
A-type granites
Paleoproterozoic
Geochemistry
Geochronology
Nd isotopes
Carajás Province

ABSTRACT

The Gogó da Onça Granite (GOG) comprise a stock located in the Carajás Province in the southeastern part of Amazonian Craton near its border with the Araguaia Belt. Three facies were identified in the pluton: biotite-amphibole granodiorite, biotite-amphibole monzogranite and amphibole-biotite syenogranite. The GGO crosscut discordantly the Archean country rocks and are not foliated. All Gogó da Onça Granite varieties are metaluminous, ferroan A2-subtype granites with reduced character. The major and trace element behavior suggests that its different facies are related by fractional crystallization. Zircon and titanite U–Pb SHRIMP ages show that the pluton crystallized at ~1880–1870 Ma and is related to the remarkable Paleoproterozoic magmatic event identified in the Carajás Province. Whole-rock Nd isotope data (T_{DM} ages 2.78 to 2.81, ε_{Nd} values of −9.07 to −9.48) indicate that the GOG magmas derived from an Archaean source compatible with that of some other Paleoproterozoic suites from Carajás Province. The GOG show significant contrasts with the Jamon and Velho Guilherme Paleoproterozoic suites from Carajás Province and the inclusion of the Gogó da Onça granite in any of these suites is not justified. The GOG is more akin to the Serra dos Carajás Suite and to the Seringa and São João granites of Carajás and to the Mesoproterozoic Sherman granite of USA and the Paleoproterozoic Suomenniemi Batholith of Finland. This study puts in evidence the relevance of precise geochronological data and estimation of magma oxidation state in the characterization and correlation of A-type granites.

1. Introduction

A-type granites have been recognized in different cratonic areas of the world and are widely distributed in time and space. At present, it is admitted that different sources and formation processes may be involved in the origin of these rocks. In the Amazonian Craton, as worldwide, the 1.88 to 1.0 Ga old, anorogenic or post-tectonic A-type magmatism is generally correlated with rapakivi granites (Teixeira et al., 1989; Machado et al., 1991; Dall'Agnol et al., 1999a,b, 2005; Bettencourt et al., 1999; Macambira and Lafon, 1995; Tassinari and Macambira, 1999; Santos et al., 2000). These Paleoproterozoic to Mesoproterozoic granites of the Amazonian Craton are often accompanied by felsic volcanism and plutonic mafic and charnockitics rocks as described in other Precambrian cratons. Tin mineralization, with subordinate W, F, Y, REE, Th, and Zr, occurs associated with evolved granites in the different provinces of the craton (Costi et al., 2009; Bettencourt et al., 2016).

In the Carajás Province (CP), the A-type granite magmatism is Paleoproterozoic (1.88–1.86 Ga; Table 1) and was subdivided into three suites: (1) the oxidized Jamon Suite which occurs in the Rio Maria Domain, in the southern part of the CP; (2) the reduced Velho Guilherme Suite with related tin-mineralized granites, found in the Xingu Region (western part of the CP); and (3) the moderately reduced Serra dos Carajás Suite from the Carajás Basin, in the northern domain of CP. Besides these three suites, the Seringa, São João, Rio Branco and Gradaús (the latter two undated) plutons also

* Corresponding author.
E-mail addresses: mayfraeda@gmail.com (M.F.B. Teixeira), robdal@ufpa.br, roberto.dallagnol@itv.org (R. Dall'Agnol), orestes.santos@bigpond.com (J.O.S. Santos), luansanmartins17@hotmail.com (L.A.M. de Sousa), lafonjm@ufpa.br (J.-M. Lafon).

http://dx.doi.org/10.1016/j.jsames.2017.09.017
0895-9811/

Table 1
Geochronology and Nd isotope data of the Paleoproterozoic A-type granites from Carajás province.

Tectonic blocks	Plutons	Analysed material	U-Pb (TIMS) AGE (Ma)	Pb Evaporation age (Ma) or Pb-Pb isochron	Sm-Nd (Whole-rock)	
					T_{DM} (Ma)	ε_{Nd} (T)
	SERRA DOS CARAJÁS SUITE					
CARAJÁS BASIN	CIGANO	zircon	1883 ± 2 (1)		2939	−9.7 (8)
					2668	−9.5(8)
	SERRA DOS CARAJÁS	zircon	1880 ± 2 (1)		2611	−7.9(8)
					2727	−9.2(8)
	POJUCA	zircon	1874 ± 2 (1)		3353	−9.7(8)
	VELHO GUILHERME SUITE					
XINGU REGION	VELHO GUILHERME	whole-rock		1873 ± 13 (5)		
	ANTÔNIO VICENTE	zircon		1867 ± 5 (7)	3254	−12.1(7)
	MOCAMBO	zircon		1865 ± 2 (7)	2976	−7.9 (7)
	RIO XINGU	zircon		1866 ± 2 (7)	3023	−12.2 (7)
	JAMON SUITE					
RIO MARIA DOMAIN (*Jamon Suite)	MUSA*	zircon	1883 + 5/- 2 Ma (1)		2821	−9.4 (3, 6)
					2793	−9.3 (3, 6)
					2596	−9.6 (3, 6)
	JAMON*	zircon		1885 ± 32 (3)	3024	−9.7 (3, 6)
					2874	−9.5 (3, 6)
	REDENÇÃO*	whole-rock		1870 ± 68 Ma (4)	2785	−8.8 (6)
					2807	−10.5 (6)
					2789	−9.7 (6)
					2727	−9.6 (6)
	FELSIC DIKES*	zircon		1885 ± 2 (3)	2830	−10 (3)
					2884	−9.4 (3)
	BANNACH*				2844	−9.6 (6)
	SERINGA	zircon		1895 ± 1 (9)		
				1892 ± 30 (2)		
	SÃO JOÃO	zircon		1890 ± 2 (10)		

*Granites from the Jamon Suite.
Data sources: (1) Machado et al. (1991); (2) Avelar (1996); (3) Dall'Agnol et al. (1999b); (4) Barbosa et al. (1995); (5) Macambira and Lafon (1995); (6) Rämö et al. (2002); (7) Teixeira et al. (2002); (8) Dall'Agnol et al. (2005); (9) Paiva Jr. (2009); (10) Lima (2011)

occur in the province.

The Gogó da Onça pluton is a new stock recently identified in the Sapucaia Domain of CP and tentatively correlated with its Paleoproterozoic suites. The present paper is the first study of the Gogó da Onça granite and the results reported here intend to define its main petrographical and geochemical characteristics, as well as its age and Nd isotope signature. These data are employed to evaluate its origin and affinities with the three Paleoproterozoic suites and similar granites of the CP. The study represents a contribution to the understanding of the Paleoproterozoic A-type magmatism of the southeastern Amazonian craton. It shows also the relevance of precise zircon and titanite SHRIMP dating and the estimation of redox conditions in A-type granite studies.

2. Geological setting

The Carajás Province is the main Archean domain of the Amazonian Craton (Fig. 1b). It is considered as an independent tectonic province (Santos et al., 2000) or included into the Central Amazonian Province (Tassinari and Macambira, 2004). It contains large mineral deposits of iron, manganese, copper-gold, nickel, tin, and gold-PGE (Tallarico et al., 2005; Bettencourt et al., 2016; Moreto et al., 2015). It has been divided into the Rio Maria, Sapucaia, and Canaã dos Carajás domains and Carajás Basin (Fig. 1c; Dall'Agnol et al., 2013).

Situated in the southern part of the Carajas Province, the Rio Maria Domain (Fig. 1c; ca. 3.0 to 2.86 Ga; Machado et al., 1991; Macambira and Lafon, 1995; Almeida et al., 2011) is composed of greenstone belts grouped in the Andorinhas Supergroup (Souza et al., 2001) and a variety of Archean granitoids (Dall'Agnol et al., 2006) that comprises tonalitic-trondhjemitic series (TTG - 2.98–2.92 Ga; Almeida et al., 2011), sanukitoids (2.87 Ga; Oliveira et al., 2009a,b, 2011; Santos and Oliveira, 2014) and granite to leucogranodiorite suites (ca. 2.87–2.86 Ga; Almeida et al., 2013).

The Sapucaia Domain shows strong similarity with the Rio Maria Domain in terms of dominant lithologies (Fig. 1c). It includes TTGs (ca. 2.93 to 2.87 Ga; P.A. Santos et al., 2013a,b; Silva et al., 2014), sanukitoids (ca. 2.87 Ga; Gabriel and Oliveira, 2014; Gabriel et al., 2014), high Ba- and Sr leucogranodiorites and potassic leucogranites (Teixeira et al., 2013; Leite-Santos and Oliveira, 2016). However, contrarily to Rio Maria, besides Mesoarchean granitoids Neoarchean A-type like granites also occur in that domain (Vila Jussara suite, ca. 2.75–2.73 Ga; Oliveira et al., 2010; Silva et al., 2014; Dall'Agnol et al., 2017).

In the Canaã dos Carajás domain (Fig. 1c), it was reported a variety of Mesoarchean granitoids with different ages and geochemical signatures: Bacaba Tonalite (ca. 3.0 Ga; Moreto et al., 2011); Canaã dos Carajás Granite and Rio Verde Trondhjemite (2.96–2.93 Ga; Feio et al., 2013); Campina Verde Tonalitic Complex, Rio Verde Trondhjemite, Cruzadão, Bom Jesus, Boa Sorte, and Serra Dourada granites (2.87–2.83 Ga; Feio et al., 2013; Rodrigues et al., 2014). In that domain, Neoarchean A-type like granites also occur (Planalto suite, ca 2.75–2.73 Ga; Feio et al., 2012, 2013; Huhn et al., 1999), and charnockitic plutons (Pium Diopside Norite; R.D. Santos et al., 2013a,b; Feio et al., 2012).

The Neoarchean Carajás Basin is composed dominantly of volcano-sedimentary units of the Itacaiúnas Supergroup (Fig. 1c; ca. 2.76 Ga; Hirata et al., 1982; DOCEGEO, 1988; Gibbs et al., 1986; Machado et al., 1991; Tallarico et al., 2005) and Rio Novo Group (Hirata et al., 1982). Mesoarchean granitoids are the local basement and they are similar to those found in the Canaã dos Carajás and Sapucaia domains. Neoarchean granites are also common and crosscut the Itacaiúnas supergroup (ca. 2.76 to 2.74 Ga; Igarapé Gelado and Serra do Rabo granites, and Estrela complex; Barros

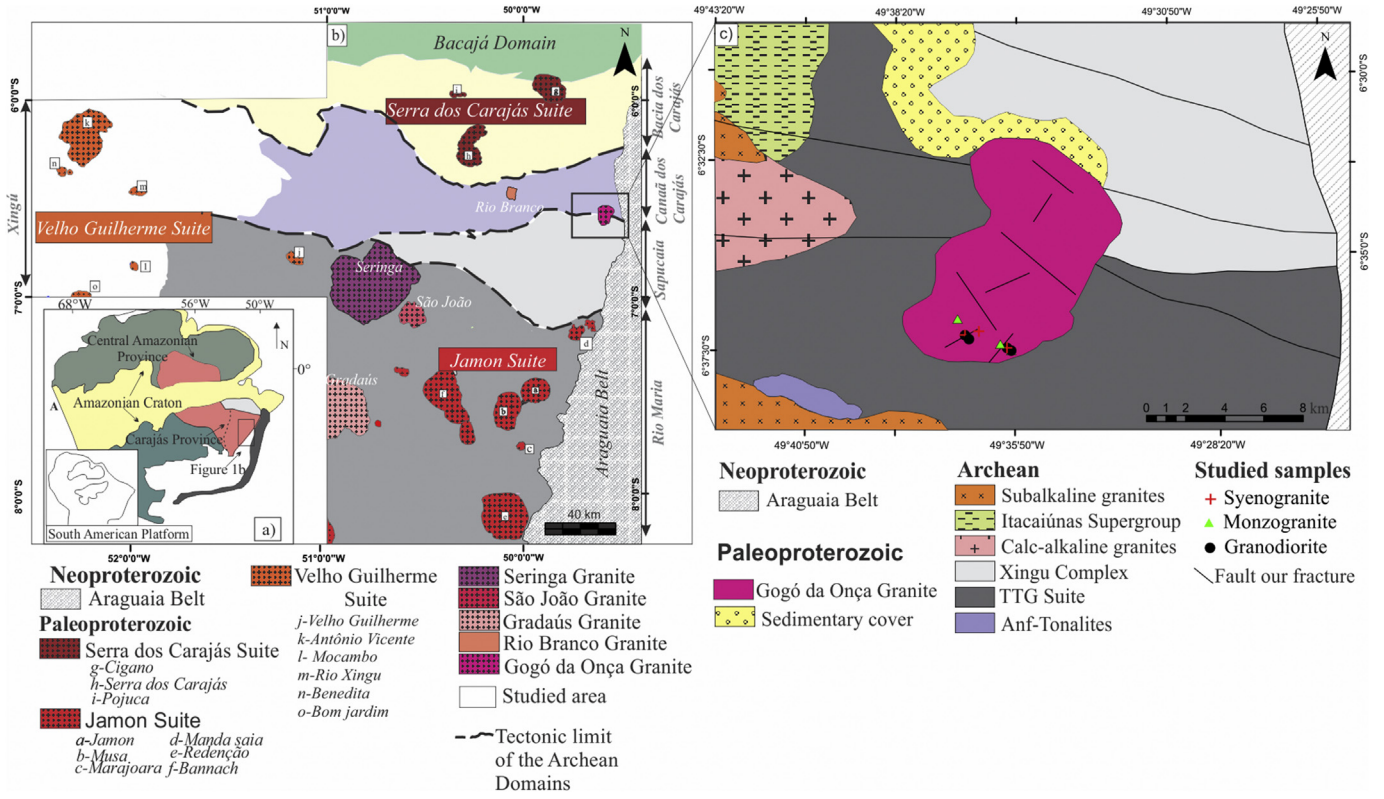

Fig. 1. (a) Location of the Carajás Province in the Amazonian Craton; (b) Simplified geologic map of the Carajás Province highlighting the A-type Paleoproterozoic granites; the rectangle corresponds to the studied area detailed in Fig. 1c. (c) Geological map of the Gogó da Onça Granite showing the location of studied samples.

et al., 1997, 2009; Sardinha et al., 2006).

The cratonization of the province occurred at the end of the Archean and it was later affected in its different domains by the intrusion of Paleoproterozoic A-type granites (Fig. 1c; Dall'Agnol et al., 2005).

3. A-type Paleoproterozoic granites of Carajás Province

The anorogenic granites form plutons and batholiths that are widespread in all the domains of CP and also in the Carajás Basin. Based on geologic, petrographic and geochemical characteristics and the oxidation state of their magmas, three suites were distinguished (Dall'Agnol et al., 2005; Dall'Agnol and Oliveira, 2007).

The oxidized Jamon Suite intruded the Archaean rocks of the Rio Maria Domain and is represented by the Jamon, Musa, Marajoara, Manda Saia, Redenção, and Bannach plutons (Fig. 1c; Gastal, 1987; Dall'Agnol et al., 1999a,b; 2005; Almeida et al., 2006; Dall'Agnol and Oliveira, 2007; D. C. Oliveira et al., 2008a,b, 2009a,b, 2010).

The moderately reduced A-type granites are located in the Carajás Basin and they were grouped in the Serra dos Carajás Suite composed of Serra dos Carajás, Pojuca and Cigano plutons (DOCEGEO, 1988; Machado et al., 1991; Dall'Agnol et al., 2005).

The reduced granites of the Velho Guilherme Suite occur in the Xingu region (Fig. 1c). Its plutons cut the Xingu complex, the intermediate to felsic volcanic rocks of the Uatumã group and the Paleoproterozoic Parauari granite. The more evolved granites are commonly tin-mineralized with local occurrence of wolframite and tantalite. The suite is composed of the Velho Guilherme, Antônio Vicente, Mocambo, Rio Xingu, and Bom Jardim granites (Teixeira, 1999; Teixeira et al., 2002; Dall'Agnol et al., 2005; Lamarão et al., 2012).

Mafic and felsic dikes, locally forming composite dikes, are associated with Jamon Suite granites. The felsic dikes display geochemical and petrological affinities with the granites and yielded Pb-Pb zircon ages of ca. 1.88 Ga similar to those of the Jamon, Serra dos Carajas and Velho Guilherme suites.

In addition to these three suites, the Seringa (Paiva Jr., 2009; Paiva Jr. et al., 2011), São João (Lima, 2011; Lima et al., 2014), Gradaús (Carvalho, in prep.), and Rio Branco granites (Santos P.A et al., 2013) were also described in the CP (Fig. 1c). All these granites and the Gogó da Onça granite (this paper) are anorogenic granites but it is not defined yet if they can be included in any one of those suites or if they should be seen as new and independent units.

All granites display characteristics of A-type granites and show within-plate signature. They are composed essentially of granites *stricto sensu* (monzogranite to syenogranite with rare alkali feldspar granite). They occur as shallow level sheeted-like batholiths and stocks (D. C Oliveira et al., 2008a,b, 2010), emplaced at pressures of ca. 1 to 3 kbar. Near the contacts, the granites commonly include angular enclaves of the Archean country rocks and the Archean rocks show clear imprints of low-pressure contact metamorphism.

4. Geologic and petrographic aspects of the Gogó da Onça Granite

The GOG is exposed in the border between Sapucaia and Canaã dos Carajás domains as a stock with an approximate area of 48 km^2. It forms hills of moderate altitude that contrast with the dominant flat relief of the Archean country rocks (Fig. 2a). The pluton cross-cuts the Colorado Trondhjemite, a 2.87 Ga old tonalite-trondhjemite-granodiorite suite (P. A. Santos et al., 2013a,b; Silva et al., 2014), the Xingu Complex (~2.97 Ga; Avelar et al., 1999) undifferentiated Mesoarchean granitoids and Paleoproterozoic

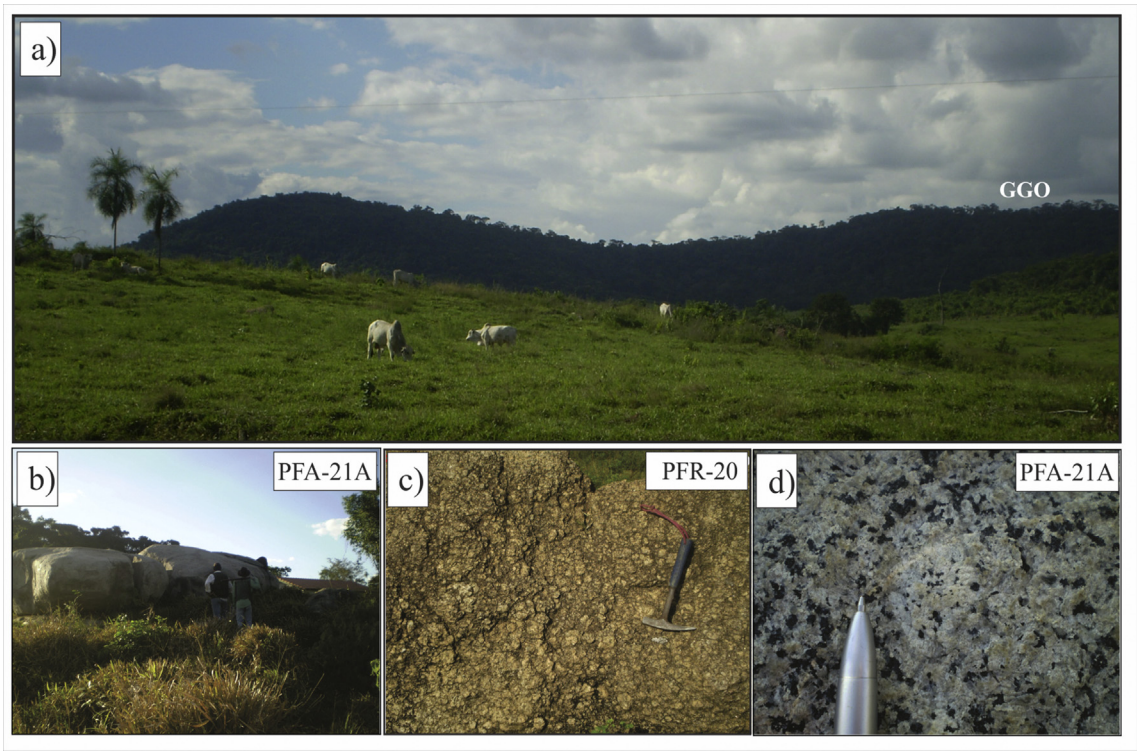

Fig. 2. (a) Geomorphologic contrast between the Gogó da Onça Granite (GOG) and the Archean rocks; (b) Representative outcrop of the GOG; (c) altered biotite-amphibole monzogranite of GOG showing ovoidal alkali feldspar phenocrysts with rapakivi texture (biotite-amphibole monzogranite); (d) Coarse ovoidal megacryst of alkali feldspar with plagioclase mantle in a medium-grained matrix rich in amphibole and biotite (biotite-amphibole granodiorite).

sedimentary covers (Fig. 1d). The granite outcrops as meter-sized blocks and boulders (Fig. 2b). Its contacts with the country rocks were not observed in the field and the limits of the intrusion were defined employing radar images and radiometric surveys. The rocks of GOG are not foliated and cross-cut the NW–SE to E-W structural trend of the host Archean rocks. Geological mapping and sampling were limited to the southern part of the intrusion due to the restricted access to the northern area of the granite.

The GOG comprise porphyritic coarse-grained biotite-amphibole granodiorite (BAGrd), porphyritic coarse-grained to even medium-grained biotite-amphibole monzogranite (BAMzg) and, subordinate, coarse-to fine-grained seriated amphibole-biotite syenogranite (ABSG). The BAMzg and BAGrd exhibit local development of rapakivi texture (Fig. 2c and d).

4.1. Modal composition and classification

Modal compositions of the Gogó da Onça granite are presented in Table 2 and QAP and Q-(A + P)-M′ diagrams are shown in Fig. 3. All analyzed rocks are leucocratic, but the granodiorite and monzogranite varieties have similar mafic mineral contents ranging from 10.8% to 13.2% and 12.2% to 15.4%, respectively, and in both amphibole is dominant over biotite. On the other hand, in the syenogranite facies, biotite is more abundant than amphibole and its mafic mineral contents are significantly lower than in the other varieties (up to 7.2%).

4.1.1. Biotite-amphibole granodiorite (BAGrd)

The biotite-amphibole granodiorite display porphyritic or granular hypidiomorphic texture. Besides quartz, plagioclase and subordinate perthitic alkali-feldspar, they have significant modal proportions of amphibole and biotite (Table 2). Zircon, titanite, apatite, allanite, ilmenite, and magnetite are the primary accessory phases and chlorite, clay minerals, sericite, epidote, and carbonate the secondary ones. Quartz occurs as medium-grained subhedral to anhedral crystals (Fig. 4a and b) or as fine grains forming granophyric intergrowths with alkali feldspar. Plagioclase is subhedral and show intense alteration to white micas, especially in the crystal cores (Fig. 4a). The alkali feldspar is subhedral and displays modified perthite exsolution textures (Smith and Brown, 1988). It also occurs as phenocrysts (~15 mm) rimmed by plagioclase. Amphibole is represented by medium-to fine-grained subhedral hornblende, with inclusions of zircon, apatite, allanite, and Fe-Ti oxides. Biotite

Table 2
Modal compositions of the Gogó da Onça Granite.

Mineralogy	BAGrd				BAMzg			ABSG		
	PFR	PFA	PFA	PFR	PFR	PFR	PFR	PFA	PFR	PFR
	18B	21A	22	19A	18A	22	20	21B	19B	21
Quartz	23.9	23.4	20.2	24.2	30.3	31.9	30.6	21.9	21.2	21.1
Plagioclase	48.8	49.6	49.1	44.8	28.6	27.9	23.6	21.7	20.3	20.7
Alkali-feldspar	14.8	15.7	18.6	19.2	29.0	28.4	29.1	49.9	49.1	52.1
Amphibole	8.1	7.2	6.9	7.1	6.7	6.2	8.1	0.3	3.4	1.6
Biotite	3.1	3.6	3.4	5.1	4.6	5.1	6.5	4.1	4.8	3.3
Apatite	X	0.1	0.1	X	X	X	X	X	X	X
Allanite	0.6	X	X	0.4	X	0.1	0.2	0.6	0.9	1.0
Titanite	X	0.1	X	0.1	X	X	0.1	–	–	–
Zircon	X	0.1	0.6	X	X	0.1	X	X	X	X
Opaques	0.6	0.8	0.8	0.6	0.9	0.4	0.6	0.2	X	X
∑ Mafic = M′	11.2	10.8	11.7	13.2	12.2	11.9	15.4	5.2	7.2	5.9

X: mineral observed in thin section but not registered in the modal counting; -: absent mineral. Abbreviations: BAGrd: biotite-amphibole granodiorite; BAMzg: biotite-amphibole monzogranite; ABSG: amphibole-biotite syenogranite.

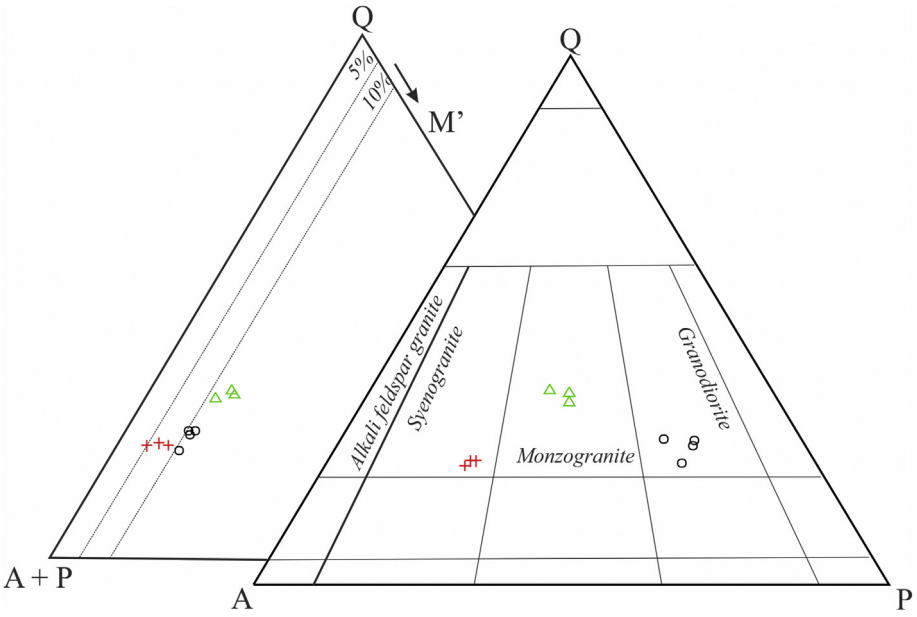

Fig. 3. Q-A-P (fields according to Streckeisen, 1976) and Q-(A + P)-M′ modal diagrams for the Gogó da Onça Granite. BAGrd: biotite-amphibole granodiorite; BAMzg: biotite-amphibole monzogranite; ABSG: amphibole-biotite syenogranite.

is subhedral, medium-to fine-grained and partially altered to chlorite and epidote (Fig. 4b). In the granodiorite and monzogranite facies, hornblende and biotite appears as interstitial crystals denoting later crystallization (Fig. 4a, b, d).

4.1.2. Biotite-amphibole monzogranite (BAMzg)

The biotite-amphibole monzogranite has porphyritic or equigranular hypidiomorphic texture and quartz modal contents are higher compared to the granodiorite (Table 2). Quartz occurs mostly as subhedral to anhedral medium-grained crystals (Fig. 4c and d), but fine-grains are included in biotite and amphibole; it forms symplectites with amphibole and granophyric intergrowths with alkali-feldspar. Alkali feldspar crystals are subhedral and perthitic (Fig. 4c and d), locally forming phenocrysts (~15 mm). Plagioclase is subhedral and shows moderate sericitization, especially in the crystal cores. Amphibole is medium-to fine-grained subhedral hornblende, has zoned allanite inclusions, and is sometimes associated with titanite. The biotite is subhedral to anhedral, medium-to fine-grained, and is partially altered to chlorite.

4.1.3. Amphibole-biotite syenogranite (ABSG)

The amphibole-biotite syenogranites display seriated texture and differ from the other varieties by dominance of biotite over amphibole (Table 2). The primary and secondary accessory minerals are similar to those of the other facies except for the absence of magnetite and titanite. Quartz occurs mostly as subhedral, medium-grained crystals, but anhedral fine-grained crystals are included in alkali feldspar (Fig. 4e) and plagioclase, and form granophyric intergrowths. K-feldspar crystals are subhedral and perthitic (Fig. 4a). Poorly developed intergranular albite is observed along the K-feldspar contacts of its crystals. Biotite is subhedral to anhedral, medium-to fine-grained and contains inclusions of zircon. Allanite is the most representative accessory phase in this facies. It occurs as subhedral to euhedral fine crystals (Fig. 4f), displaying irregular zoning and inclusions of zircon.

5. Analytical procedures

5.1. Whole-rock geochemistry

Whole-rock chemical analyses of 10 samples from Gogó da Onça Granite were performed at the ACME Analytical Laboratories Ltd in Vancouver, Canada. The analytical package includes analysis of major oxides by inductively coupled plasma atomic emission spectrometry (ICP-ES) and trace elements, including rare earth elements (REE), by inductively coupled plasma atomic mass spectrometry (ICP-MS). The geochemical results were processed by GeoChemical Data Toolkit 3.0 software (available at http://www.gcdkit.org/download) and plotted in several classificatory diagrams. The detailed analytical procedures performed by ACME labs are available on http://acmelab.com.

5.2. U–Pb SHRIMP

A representative sample of each facies (BAGdr, BAMzg, and ABSG) of the GOG was selected for U-Pb SHRIMP analysis. The samples were crushed and milled for zircon and titanite separation, and then sieved at 60 mesh. The obtained concentrates were washed and decanted with water. The heavy minerals were separated using heavy liquids (LST) and magnetic separation was made using a Frantz separator. Mineral separation was done by hand picking under a binocular microscope. Selected grains were mounted on adhesive tape and enclosed in epoxy resin together with fragments of the standards. The mountings were ground up to attain the crystal cores and then polished with diamond paste (P4000-2400) until nearly half of each grain.

Backscattered electrons (BSE) images of the crystals were made to obtain information about their inner structures and to select the best areas for isotopic analyses. Then the mounts were cleaned and gold coated for SHRIMP analysis.

In situ U-Pb zircon and titanite isotopic compositions were determined by SHRIMP II at Curtin University of Technology (Perth, Western Australia) using methods based on those of Compston et al. (1992). Spot analyses about 25 μm on selected zircon and

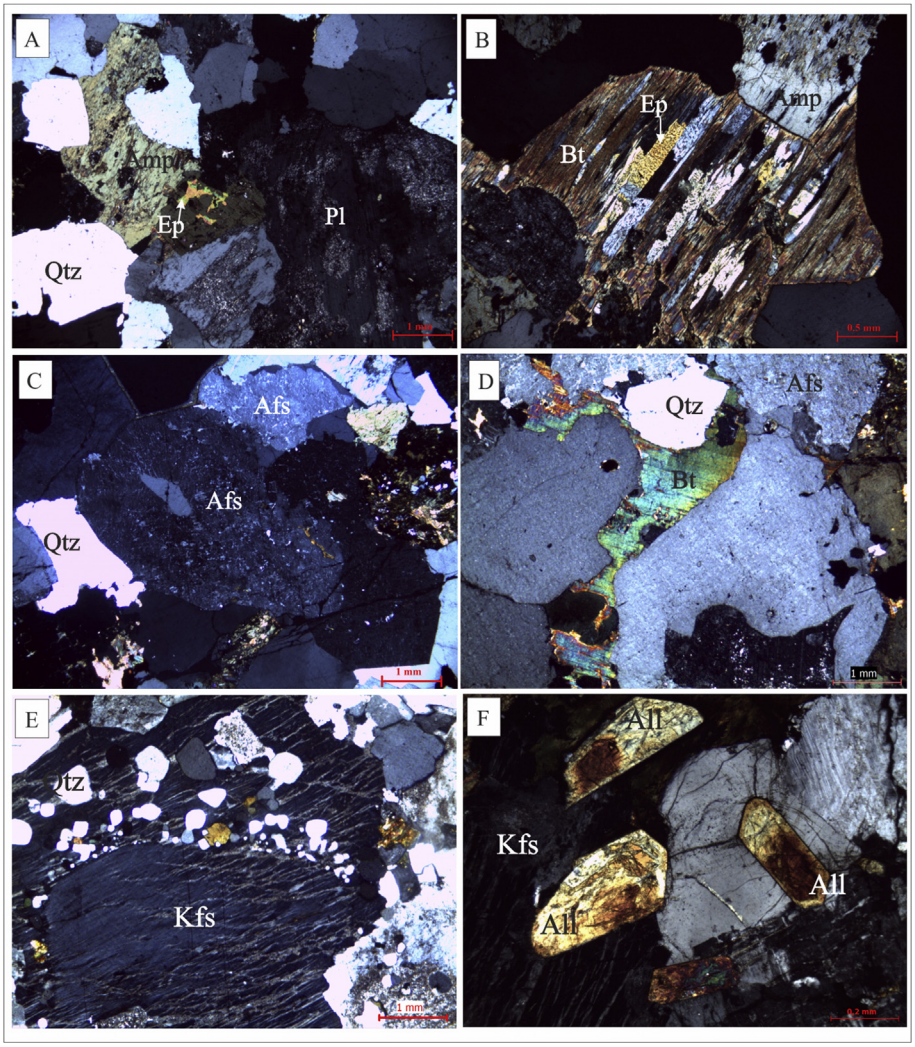

Fig. 4. Photomicrographies of the Gogó da Onça Granite taken with crossed nicols. (A) Textural aspects of plagioclase, quartz, and interstitial amphibole crystals in the granodiorite; (B) Biotite altered to epidote and chlorite in the BAGdr; (C) Textural aspect of alkali feldspar and quartz in the BAMzg; (d) interstitial biotite crystals in the monzogranite; (E) Perthitic alkali feldspar with aligned quartz inclusions, a common feature in the syenogranite; (F) Subhedral to euhedral allanite crystals in the ABSG. Abbreviations of mineral names follow Whitney and Evans (2010).

titanite crystals were made to determine U–Th–Pb concentrations and Pb isotope composition. BR266 (559 Ma, 903 ppm U; Stern, 2001) and M257 (522.2 Ma, 680 ppm U) were used as zircon standards and KHAN (518 Ma, 220 ppm U; Heaman, 2009) as titanite standard. Data reduction of measured ratios for zircon and titanite was performed using the software SQUID (Ludwig, 2009), and results were plotted on concordia diagrams using ISOPLOT/3.70 software (Ludwig, 2008).

5.3. Sm-Nd analysis

Nd isotopic compositions were determined in three samples of the GOG using an LA-ICP-MS (Laser Ablation- Inductively Coupled Plasma- Massa Spectrometer) at the Isotope Geology Laboratory of the Federal University of Pará (Pará-Iso) using analytical procedures described by Gioia and Pimentel (2000) and Oliveira et al. (2008a, 2008b). Whole-rock samples weighing up about 100 mg, were spiked by a mixture of ^{149}Sm and ^{146}Nd for isotope dilution measurements. Samples were dissolved using a mixture of HF and $HClO_4$ in tightly closed teflon. The accuracy and reproducibility of results were controlled according to the BCR-1 and La Jolla reference material (Oliveira et al., 2008a,b). The decay constant used was 6.54 × 10-12 year-1 (Lugmair and Harti, 1978) and the Nd model ages were calculated according to the model of depleted mantle evolution (T_{DM}) from DePaolo (1981).

6. Results

6.1. Elemental geochemistry

Major and trace element compositions of the Gogó da Onça Granite are listed in Table 3. The GOG analyzed samples contain SiO_2 ranging from 64.20 to 73.50 wt %, K_2O from 3.14 to 5.20 wt %, and K_2O/Na_2O ratios from 0.84 to 1.87, all of them increasing from the granodiorite to the syenogranite facies. In the Harker type diagrams, the GOG analyzed samples show negative correlations with Al_2O_3, TiO_2, FeO_t, MgO, CaO, Na_2O and P_2O_5 and positive correlation with K_2O (Fig. 5). The Al_2O_3 contents are relatively high in the granodiorite and monzogranite facies, a feature not commonly observed in most A-type granites (Dall'Agnol and Oliveira, 2007; Dall'Agnol et al., 2012). The general trends defined by the different facies are compatible with a fractional

Table 3
Chemical compositions of the Gogó da Onça Granite.

Gogó da Onça Granite										
Facies	BAGrd				BAMzG			ABSG		
Samples	PFA-22	PFR-18B	PFA-21A	PFR-19A	PFR-18A	PFR-22	PFR-20	PFA-21B	PFR-19B	PFR-21
SiO_2 (%)	64.20	64.22	64.59	64.85	67.04	68.06	68.93	71.57	72.75	73.50
TiO_2	0.76	0.68	0.72	0.69	0.69	0.51	0.51	0.23	0.27	0.17
Al_2O_3	15.36	15.81	15.33	14.68	14.14	14.06	13.63	12.34	12.18	12.14
Fe_2O_{3t}	6.16	5.78	6.12	6.32	5.78	4.82	4.99	4.37	3.94	3.42
MnO	0.09	0.08	0.08	0.09	0.08	0.07	0.06	0.06	0.05	0.04
MgO	0.66	0.59	0.65	0.61	0.52	0.43	0.38	0.13	0.19	0.09
CaO	4.01	4.19	4.29	3.73	3.34	3.1	2.7	1.46	1.43	1.23
Na_2O	3.6	3.76	3.55	3.37	3.19	3.27	3.14	2.78	2.73	2.74
K_2O	3.22	3.14	3.29	3.64	3.9	3.81	4.26	5.2	5.03	5.08
P_2O_5	0.27	0.26	0.27	0.26	0.23	0.16	0.15	0.03	0.05	0.02
LOI	1.2	1.1	0.7	1.4	1.3	0.6	1.3	0.8	1.0	1.2
Total	99.54	99.59	99.57	99.59	99.51	99.53	99.56	99.54	99.65	99.61
Ba (ppm)	2070	1830	1942	2182	2092	2090	1985	764	1133	711
Rb	93.5	91.3	87.7	114.9	109.7	105	117.9	187.5	186.4	210.9
Sr	380.7	358.2	351.9	288.7	284.4	259.1	211.3	104.4	116.3	93.7
Zr	577	509.6	559	752.1	765.9	562.6	658.2	437.4	496.2	350
Hf	12.9	11.9	13.2	17.2	17.8	13.1	16.7	14.2	14.9	11.0
Nb	23.6	21.6	23	27.9	30	22.5	30.8	43.4	39.7	43.2
Y	62.4	52.2	54.1	67.7	60.6	54.1	70.5	110	85.5	118.2
Ga	23	22.6	21.9	21.8	21.1	20	19.4	22.5	20.3	21.3
Sn	2	2	2	4	3	3	2	2	2	2
U	2.9	2.3	2.5	2.6	2.1	2.9	3.1	10.6	6.4	7.7
Th	20.3	14.9	16.4	19.7	15.5	23	25.4	77.8	45.8	79.2
La (ppm)	116.9	102.4	102.6	114.8	111.7	99.6	132.5	476.6	215.7	418.6
Ce	221.1	209.5	204.7	237.9	233.8	210.7	265.6	863.4	409	782.6
Pr	24.91	23.62	23.47	26.98	26.71	22.37	27.78	86	43.86	81.56
Nd	86.8	82.1	86	99.7	97.8	82.4	105.9	260	149.6	254.4
Sm	14.47	13.43	14.07	16.44	16.13	13.3	17.73	33.63	23.02	35.01
Eu	3.7	3.28	3.28	3.3	2.96	2.92	2.92	1.84	2.04	1.82
Gd	12.09	11.31	12.15	14.05	13.55	11.53	14.86	25.22	18.81	26.84
Tb	1.8	1.68	1.79	2.11	2	1.73	2.28	3.69	2.74	3.86
Dy	9.91	9.34	10.02	12.03	11.1	9.99	12.58	20.41	15.6	21.05
Ho	1.97	1.8	1.93	2.3	2.16	1.9	2.55	3.93	3.03	4.01
Er	5.73	5.36	5.49	6.5	6.24	5.45	7.42	11.82	8.82	11.99
Tm	0.8	0.76	0.83	0.99	0.9	0.83	1.11	1.76	1.37	1.75
Yb	5.06	4.75	5.42	6.37	5.79	5.46	7.06	11.39	8.84	11.02
Lu	0.77	0.72	0.77	1.0	0.9	0.78	1.06	1.73	1.36	1.65
K_2O/Na_2O	0.89	0.84	0.93	1.08	1.22	1.17	1.36	1.87	1.84	1.85
$FeO_t/(MgO + FeO_t)$	0.89	0.9	0.89	0.9	0.91	0.91	0.92	0.97	0.95	0.97
(La/Yb)n	15.59	14.55	12.78	12.16	13.02	12.31	12.67	28.24	16.47	25.64
Eu/Eu*	0.83	0.79	0.75	0.65	0.6	0.7	0.54	0.19	0.29	0.17

LOI: loss on ignition; BAGrd: biotite-amphibole granodiorite; BAMzG: biotite-amphibole monzogranite; ABSG: amphibole-biotite syenogranite.

crystallization process but there are compositional gaps between them, possibly a reflex of the limited number of analyzed samples.

The GOG granites have high $FeO_t/(FeO_t + MgO)$ ratios and plot in the fields of ferroan (Frost et al., 2001) and reduced A-type (Dall'Agnol and Oliveira, 2007) granites (Fig. 6a and b). According to Shand's index (classification diagram of Manilar and Piccoli, 1989), the three varieties of the Gogó da Onça granite are metaluminous (Fig. 6c). In the MALI vs. SiO_2 diagram (Fig. 6d; fields of Frost et al., 2001), the studied granites plot in the calc-alkalic field. The $FeO_t/(FeO_t + MgO)$ ratios vary between 0.89 and 0.97, increase from the granodiorite to the monzogranite and attain the highest values in the syenogranite (Table 3).

The contents of large ion lithophile elements (LILE) in the GOG are variable (Table 3, Fig. 7, high for Ba (2092-711 ppm), moderate for Sr (381-94 ppm), and relatively low for Rb (88–211 ppm). On the other hand, contents of high field strength elements (HFSE) are generally high, especially those of Zr (766-350 ppm) and Y (52–118 ppm). Nb, Y, U, and Th contents are higher in the syenogranite facies (Table 3). Ba and Zr show similar values in the granodiorites and monzogranites and decrease notably in the syenogranites (Table 5; Fig. 7a, d). Nb, Y, U, and Th contents are higher in the syenogranite facies (Table 5). Sr decreases from the granodiorite to the syenogranite and shows a clear negative correlation with SiO_2 (Fig. 7b), whereas Rb show positive correlation with SiO_2 and increases in the reverse sense (Fig. 7c).

In the Zr + Nb + Ce + Y vs FeO_t/MgO diagram (fields of Whalen et al., 1987), all analyzed samples of the GOG plot in the field of A-type granites (Fig. 8a). The ferroan and reduced A-type character of the granite discussed above, added to this additional geochemical evidence, demonstrates that the GOG can be classified as A-type granite. Besides, the Nb-Y-Zr/4 triangular plot (fields of Eby, 1992) indicate that it has affinity with the A2-subtype granites (Fig. 8b).

The GOG has high contents of rare earth elements (REE contents are higher than 1000 ppm in some syenogranite samples; Table 3), exhibit enrichment in light REE (LREE) and sub horizontalized heavy REE (HREE) patterns indicative of absent or limited fractionation of the HREE during the origin or differentiation of its magma [(La/Yb)n varying from 12.16 to 28.24; Table 3]. The BAGrd and BAMzG have similar and slightly negative Eu anomalies (0.83–0.54), whereas the ABSG show strong negative Eu anomalies

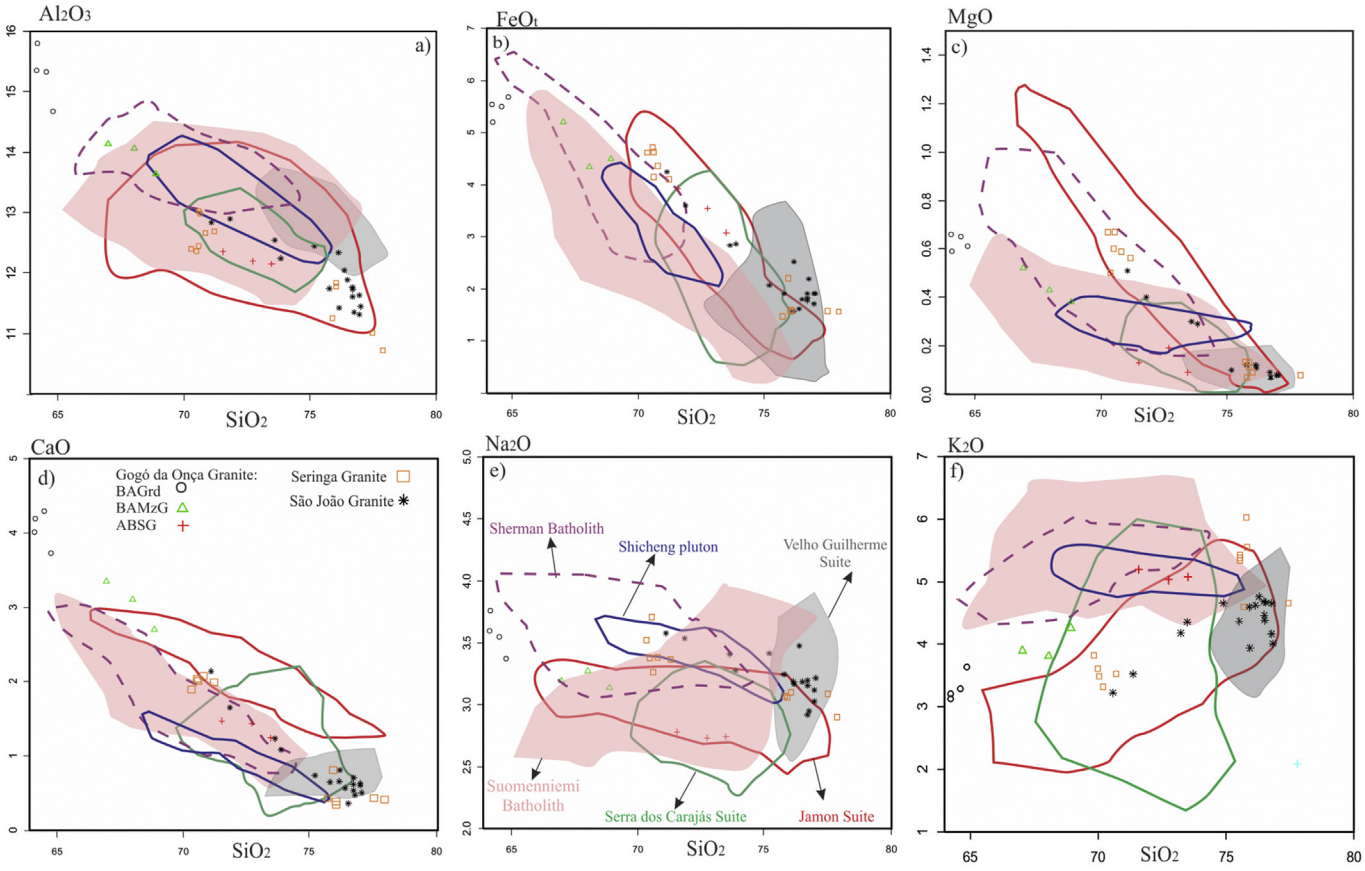

Fig. 5. Major elements Harker diagrams (oxides in wt.%) for the Gogó da Onça Granite. The fields of A-type Paleoproterozoic granites from the Carajás Province are plotted for comparison. Data source: Jamon Suite (Dall'Agnol et al., 1999a,b, Dall'Agnol and Oliveira, 2007; Almeida et al., 2006); Velho Guilherme Suite (Dall'Agnol et al., 1994; Teixeira, 1999; Teixeira et al., 2005); Serra dos Carajás Suite (Barros et al., 1995; Javier Rios et al., 1995; Dall'Agnol et al., 2005); Seringa Granite (Paiva Júnior et al., 2011); São João Granite (Lima et al., 2014). The Suomenniemi Batholith from southeastern Finland (Rämö, 1991), the Sherman Batholith from SE Wyoming, USA (Frost et al., 1999) and the Shicheng pluton of the North China Craton (Zhao and Zhou, 2009) are also plotted for comparison.

(0.29–0.17) (Table 3; Fig. 9a). In the primitive mantle normalized (Sun and Mcdonough, 1989) trace element diagram, the GOG show negative Nb, Sr, P, and Ti anomalies. In the ABSG, there are additionally negative Ba and Zr anomalies, while the BAGrd and BAMzG display positive anomalies of those elements (Fig. 9b).

6.2. Geochronology

Analytical results for the different facies of the Gogó da Onça Granite are presented in Table 4.

6.2.1. Biotite-amphibole granodiorite

The zircon grains are subhedral transparent and colorless with 100–250 μm in length, fractured and with common internal oscillatory zoning. No inherited zircon cores were observed (Fig. 10a). Eight analysis from sample PFR-18B of 8 crystals were obtained in sets of six scans during a single analytical session. U and Th concentrations are 168–412 ppm and 112–363 ppm, respectively, except for the spot I.9–2 that has a low concentration of U (70 ppm) and Th (86 ppm). The Th/U ratios vary between 0.69 and 0.97, and the spot I.9-2 has 1.26 of U/Th ratio. The obtained data define a concordia age of 1877 ± 9 Ma and MSWD of 0.8 (Fig. 11a). This age is interpreted as the crystallization age of the sample.

Titanite crystals are subhedral and brown with 100–200 μm in length. BSE images show dark-gray and light-gray zones in titanite (Fig. 10b), and no overgrowths were observed. Analyses of 5 crystals from sample PFR-18B were obtained in sets of five scans during a single analytical session. U–Pb age data from titanite are plotted in Fig. 11b. The titanite shows two age groups: the oldest ages are from two crystals that yielded a composite weighted average age of 1924 ± 20 Ma and MSWD of 0.28 (Fig. 11b); the other crystals have a younger composite weighted average age of 1879 ± 15Ma and MSWD of 0.39 (Fig. 11b). The latter is similar to the zircon age obtained for this granite and interpreted as its crystallization age. The locations of analysed spots are in both dark and light-gray zones and core and rim but the different ages do not follow a pattern.

6.2.2. Biotite-amphibole monzogranite

The analyzed zircon grains are subhedral to euhedral mostly transparent with 100–250 μm in length, with common internal oscillatory zoning. No inherited zircon cores were observed. BSE images show dark-gray rim and bright cores in some crystals (Fig. 10c). Analyses of 7 crystals from sample PFR-22 were obtained in sets of six scans during a single analytical session. U and Th concentrations are 176–297 ppm and 157–284 ppm, respectively. The Th/U ratios vary between 0.73 and 1.05. The obtained data define a concordia age of 1866 ± 10 Ma and MSWD of 1.7 (Fig. 11c), interpreted as the crystallization age of the monzogranite.

The titanite crystals of this sample are subhedral and brown with 100–200 μm in length and very similar to those of the granodiorite (PFR-18b, Fig. 10b), showing dark-gray and light-gray zones as well (Fig. 10d). Analyses of 8 crystals from sample PFR-22 were obtained in sets of five scans during a single analytical session. U–Pb age data from titanite are plotted in Fig. 11d. Likewise

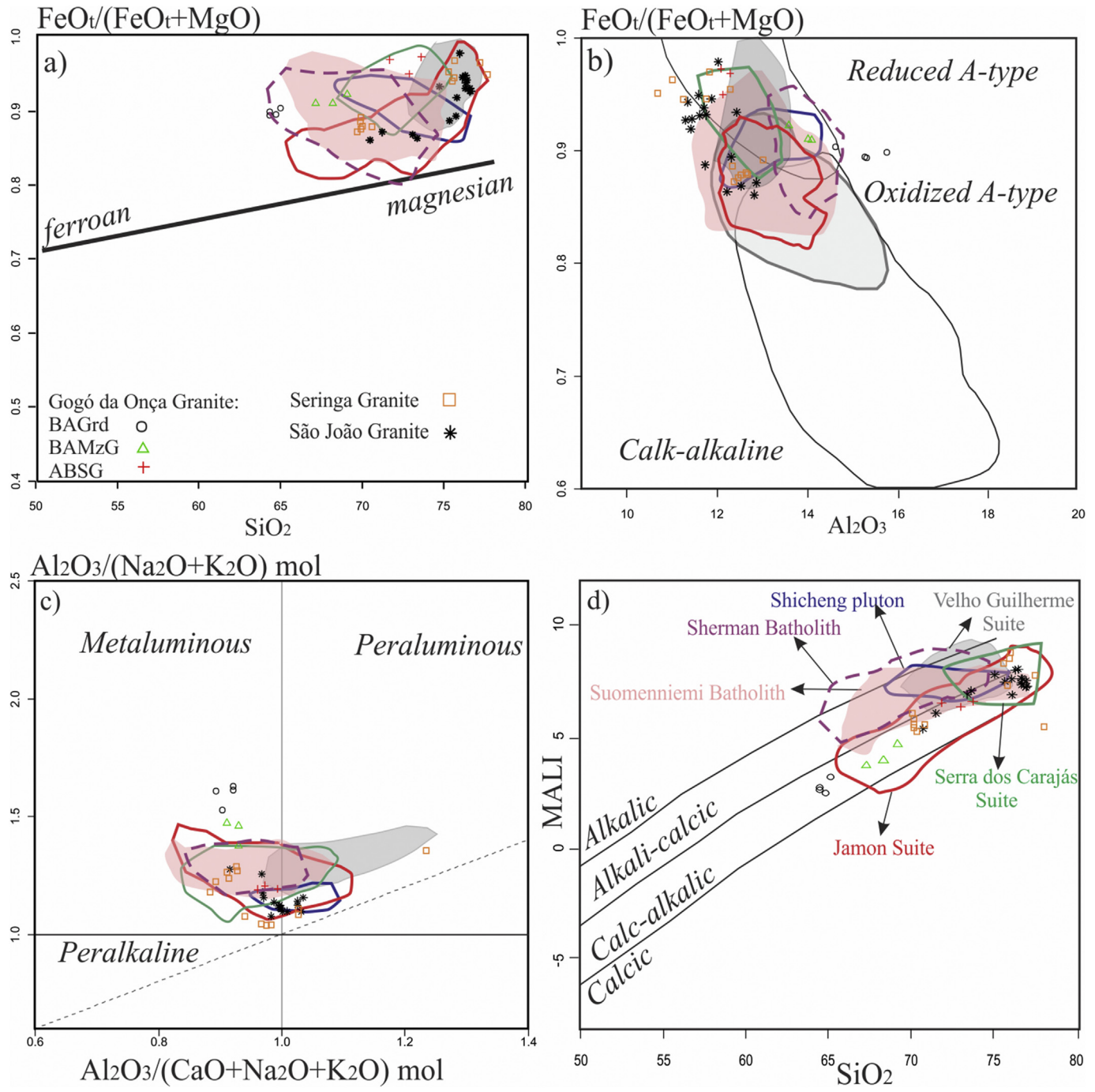

Fig. 6. Geochemical classification diagrams for the GOG. (a) ($FeO_t/FeO_t + MgO$) vs SiO_2 diagram (Frost and Frost, 1997); (b) $FeO_t/(FeO_t + MgO)$ vs. Al_2O_3 diagram (fields of calc-alkaline and reduced and oxidized A-type granites of Dall'Agnol and Oliveira, 2007); (c) ANK vs. A/CNK plot showing the metaluminous nature of the GOG (fields of Manilar and Piccoli, 1989); (d) $Na_2O + K_2O - CaO$ vs SiO_2 (alkalic, alkalic-calcic, calc-alkalic, and calcic fields from Frost et al., 2001). The fields of A-type Paleoproterozoic granites from the Carajás Province: Jamon Suite (Dall'Agnol et al., 1999a,b, Dall'Agnol and Oliveira, 2007; Almeida et al., 2006); Velho Guilherme Suite (Dall'Agnol et al., 1994; Teixeira, 1999; Teixeira et al., 2005); Serra dos Carajás Suite (Barros et al., 1995; Javier Rios et al., 1995; Dall'Agnol et al., 2005); Seringa Granite (Paiva Júnior et al., 2011); São João Granite (Lima et al., 2014). The Suomenniemi Batholith from southeastern Finland (Rämö, 1991), the Sherman Batholith from SE Wyoming, USA (Frost et al., 1999) and the Shicheng pluton of the North China Craton (Zhao and Zhou, 2009) are also plotted for comparison.

to the results obtained for PFR-18B sample, the titanites from the monzogranite also contains two age groups. The oldest age is from two crystals that yielded a composite weighted average age of 1923 ± 12 Ma and MSWD of 0.13 (Fig. 11d). The youngest age is from six crystals that yield a composite weighted average age of 1872 ± 13 Ma and MSWD of 2.3 (Fig. 11d).

6.2.3. Amphibole-biotite syenogranite

The analyzed zircon grains are subhedral to euhedral mostly transparent and colorless with 100–250 μm, with common internal oscillatory zoning. No inherited zircon cores were observed. Eight crystals from sample PFR-19B were analysed in sets of six scans during two analytical sessions. U and Th concentrations are

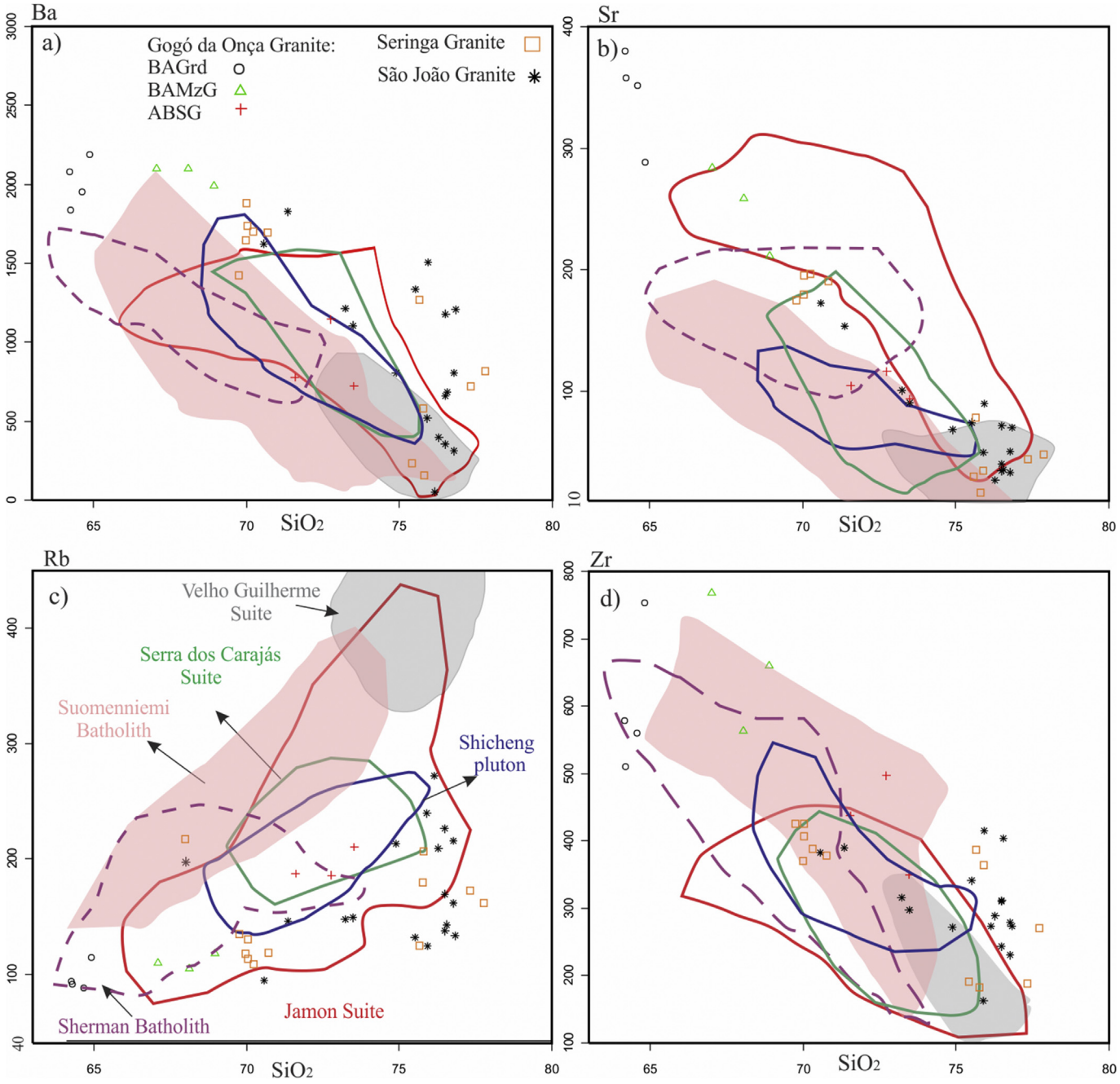

Fig. 7. Trace elements Harker diagrams for the Gogó da Onça Granite. The fields of A-type Paleoproterozoic granites from the Carajás Province are plotted for comparison: Data source: Jamon Suite (Dall'Agnol et al., 1999a,b, Dall'Agnol and Oliveira, 2007; Almeida et al., 2006); Velho Guilherme Suite (Dall'Agnol et al., 1994; Teixeira, 1999; Teixeira et al., 2005); Serra dos Carajás Suite (Barros et al., 1995; Javier Rios et al., 1995; Dall'Agnol et al., 2005); Seringa Granite (Paiva Júnior et al., 2011); São João Granite (Lima et al., 2014). The Suomenniemi Batholith from southeastern Finland (Rämö, 1991), the Sherman Batholith from SE Wyoming, USA (Frost et al., 1999) and the Shicheng pluton of the North China Craton (Zhao and Zhou, 2009) are also plotted for comparison.

281–387 ppm and 188–340 ppm, respectively, except for the spot C.4–5 that has a low concentration of U (75 ppm) and Th (78 ppm). The Th/U ratios vary between 0.59 and 0.96. They define a concordia age of 1869 ± 4 Ma and MSWD of 1.9 (Fig. 11e). This age is interpreted as the crystallization age of the sample.

6.3. Whole-rock Nd composition

The Sm–Nd isotope data for three samples of GOG, two of granodiorite and one of monzogranite facies, are listed in Table 5 and plotted in Fig. 8. The GOG has Nd concentration varying between 84.86 and 106.79 ppm, and Sm contents of 13.72–17.76 ppm. It shows little variation in $^{147}Sm/^{144}Nd$ (0.0982–0.1006). The *T*DM ages and εNd values are quite uniform, T_{DM} model ages varying from 2.78 to 2.81 Ga, and ε_{Ndt} (at 1870 Ma) shows negative values varying from −9.07 to −9.48.

7. Discussion

7.1. Comparison with similar A-type Proterozoic granites

The granites selected for comparison are: the three

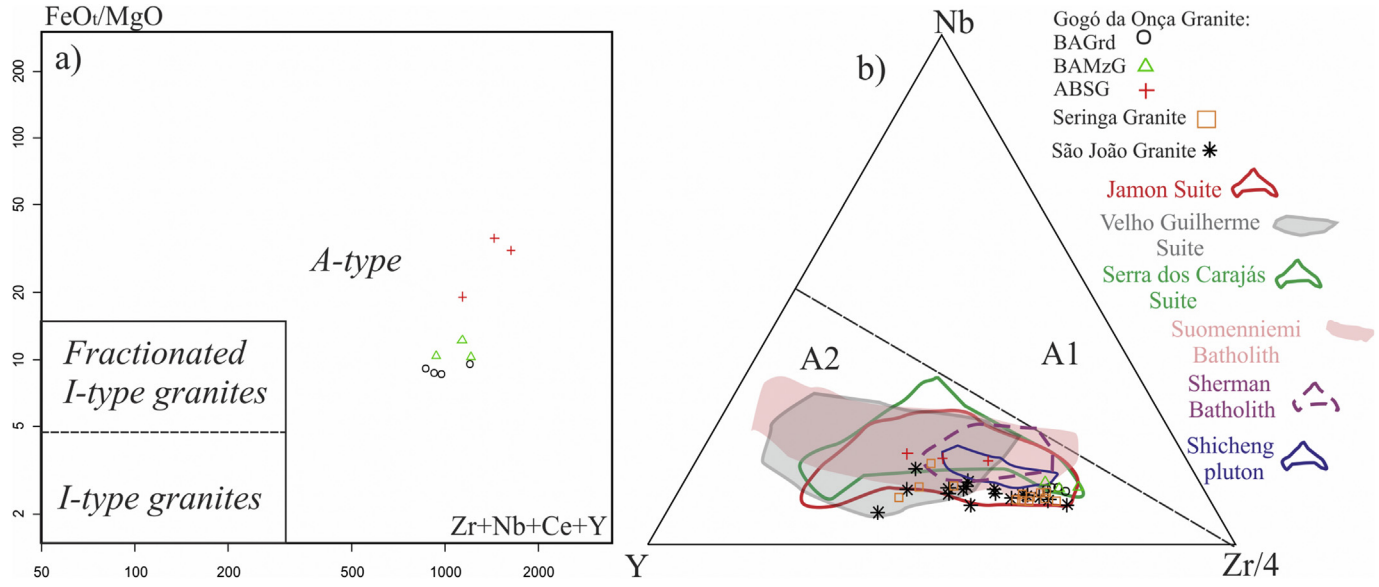

Fig. 8. (a) FeOt + MgO vs (Zr + Nb + Ce + Y) discrimination diagram of Whalen et al. (1987); (b) diagrama Y-Nb-Zr/4 (Eby, 1992). The fields of A-type Paleoproterozoic granites from the Carajás Province are plotted for comparison: Data source: Jamon Suite (Dall'Agnol et al., 1999a,b, Dall'Agnol and Oliveira, 2007; Almeida et al., 2006); Velho Guilherme Suite (Dall'Agnol et al., 1994; Teixeira, 1999; Teixeira et al., 2005); Serra dos Carajás Suite (Barros et al., 1995; Javier Rios et al., 1995; Dall'Agnol et al., 2005); Seringa Granite (Paiva Júnior et al., 2011); São João Granite (Lima et al., 2014). The Suomenniemi Batholith from southeastern Finland (Rämö, 1991), the Sherman Batholith from SE Wyoming, USA (Frost et al., 1999) and the Shicheng pluton of the North China Craton (Zhao and Zhou, 2009) are also plotted for comparison.

Paleoproterozoic suites (Jamon, Serra dos Carajás, and Velho Guilherme suites; Dall'Agnol et al., 2005), and the Seringa (Paiva Júnior et al., 2011) and São João (Lima et al., 2014) granites of the Carajás Province; the Suomenniemi batholith (1.64Ga) a rapakivi granite complex exposed in southeastern Finland (Rämö, 1991; Rämö and Mänttäri, 2015), the Sherman Granite (1.43Ga), a Mid-Proterozoic granite of North America (Frost et al., 1999), and the Shicheng pluton (1.74Ga), a Paleoproterozoic granite of the North China Craton (Zhao and Zhou, 2009).

Despite the limitations of our sampling, it is clear the presence in the Gogó da Onça pluton of a significant number of granodioritic rocks, whereas only *stricto sensu* granitic modal compositions, varying from monzogranite to syenogranite and alkali feldspar granite, are observed in the Paleoproterozoic A-type granites of the Carajás province (Dall'Agnol et al., 1994, 2005; Dall'Agnol and Oliveira, 2007). The Shicheng pluton has a marginal phase of aphyric granodiorite rocks that become porphyritic in the center of the body (Zhao and Zhou, 2009).

In the granodiorite and monzogranite facies of GOG, titanite and magnetite associated with ilmenite are the accessory minerals. A similar mineral assemblage was described especially in Jamon Suite; titanite and magnetite also occur in the Serra dos Carajás Suite but they are rare or absent in the Velho Guilherme Suite (Dall'Agnol et al., 2005). Moreover, in the Serra dos Carajás Suite, magnetite is found as homogeneous grains without associated ilmenite (Dall'Agnol et al., 2005). In the Seringa and São João granites, the presence of magnetite and ilmenite was also registered. On the other hand, titanite is absent and opaque modal contents are very low in the syenogranites of GOG (Table 2). In addition, it is known that the FeOt/(FeOt + MgO) ratios in whole rock are strongly dependent of the oxygen fugacity prevalent during rock evolution (Dall'Agnol et al., 2005, 2017). All varieties of the Gogó da Onça pluton have a quite uniform $FeO_t/(FeO_t + MgO)$ ratio varying from 0.89 in the granodiorites to 0.97 in the syenogranites, and they plot in the field of reduced A-type granites in the $FeO_t/(FeO_t + MgO)$ vs. Al_2O_3 diagram (Fig. 6b). On the other hand, the crystallization in the magmatic stage of titanite and magnetite in the granodiorite and monzogranite facies of GOG suggests that these facies could be possibly oxidized. However, although some authors consider that magnetite-bearing granites are necessarily oxidized, generally based on the classification of Ishihara (1981), the presence of magnetite in granites is not incompatible with a reduced character (Anderson et al., 2008; Dall'Agnol et al., 2005; Dall'Agnol and Oliveira, 2007; Cunha et al., 2016). Therefore, we conclude that the monzogranitic variety is moderately reduced compared to the syenogranitic rocks that are truly reduced and that GOG is a moderately reduced to reduced A-type granite, similar in this respect to the granites of the Serra dos Carajás suite, and Seringa, São João, Suomenniemi batholith and Sherman granite.

The analysed GOG samples plot exclusively in the calc-alkalic fields in the MALI vs. SiO_2 diagram (Fig. 6d). The Serra dos Carajás Suite, Jamon Suite, Seringa and São João granites are transitional between alkali-calcic and calc-alkalic fields while Velho Guilherme Suite, Suomenniemi batholith, Sherman Batholith and Shicheng pluton plot between alkalic and alkalic-calcic fields.

A comparison based in Harker diagrams for major elements (Fig. 5) is limited for the graniodiorite of GOG because of its contrast in silica with the different granites chosen for comparison. Only the granites of Sherman have silica contents similar to those of the Gogó da Onça granodiorite. Nevertheless, the available data indicate some relevant aspects: 1) There is a net contrast in MgO contents between the oxidized granites of the Jamon Suite and the GOG (Fig. 5c), the latter approaches in this regard the moderately reduced granites of the Serra dos Carajás Suite and the Suomenniemi, Sherman and Shicheng granites, and this is also clearly indicated by the variations in FeOt/(FeOt + MgO) in these granites (Fig. 6a); 2) The GOG facies are enriched in Al_2O_3 and CaO compared to the other granites and impoverished in K_2O and Na_2O compared to the Sherman and Shicheng granites.

Ba and Zr contents of the granodiorite and monzogranite facies of GOG are higher and those of Rb tend to be lower than in the other granites of the Carajás Province (Fig. 7). Compared to the Sherman granites, the different varieties of GOG have similar Rb and Zr contents and higher Ba and Sr contents.

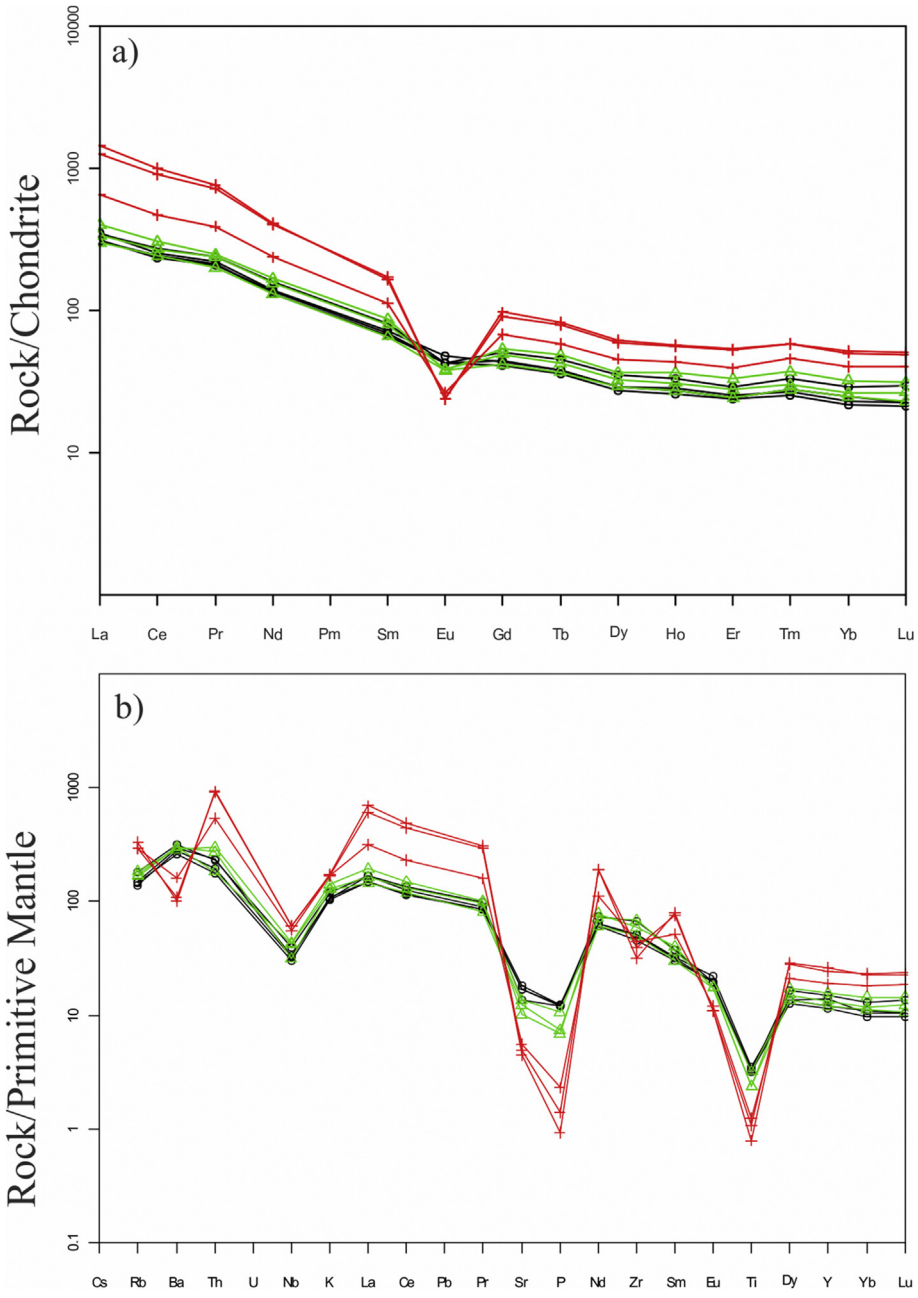

Fig. 9. (a) Rare earth element patterns normalized to chondrite (Nakamura, 1974); (b) Multi-element plots normalized to primitive mantle (Sun and Mcdonough, 1989) for the Gogó da Onça Granite.

Eby (1992) subdivided A-type granites into two groups A_1 and A_2. The A_2 group would be formed by melting of continental crust or underplated mafic crust and can be emplace in a variety of tectonic settings. According with the geochemical discrimination diagram of Eby (1992), the GOG as well the other granites presented here fall into the A_2 group (Fig. 8b). That author suggested a post-orogenic tectonic setting for the A_2 granites, but they have been described also in post-collisional settings (Nardi, 2016; Mesquita et al., 2017) and an anorogenic setting is admitted for the Paleoproterozoic A2 granites of the Carajás Province (Dall'Agnol et al., 2005).

The relative enrichment in yttrium in the syenogranite facies from GOG was also observed in the more evolved facies of the Serra dos Carajás and Jamon Suites (Dall'Agnol et al., 1999b).

The data presented in this work indicate that there are significant differences between the Gogó da Onça Granite and the Jamon and Velho Guilherme suites, and strong geochemical affinities with the Serra dos Carajás Suite and Seringa and São João granites of the Carajás Province. The GOG approaches also the rapakivi rocks of Suomenniemi Batholith and Sherman granite in several

Table 4
SHRIMP U-Pb zircon and titanite isotopic data for the Gogó da Onça Granite.

spot no.	U	Th	Th	^{206}Pb	4f^{206}	isotopic ratios									Ages (Ma)				Disc.
						^{207}Pb		^{207}Pb		^{206}Pb		error	^{208}Pb		^{206}Pb		^{207}Pb		
	ppm	ppm	U	ppm	%	^{206}Pb		^{235}U		^{238}U		correl.	^{232}Th		^{238}U		^{206}Pb		%
PFR-18B (BAGrd). Zircon																			
N1619I.1-1-1	168	112	0.69	49	0.031	0.11326	±0.93	5.3034	±1.80	0.3396	±1.54	0.857	0.0943	±2.01	1885	±25	1852	±17	−2.0
N1619I.2-1	227	201	0.92	65	0.000	0.11535	±0.71	5.2759	±1.50	0.3317	±1.19	0.881	0.0929	±1.58	1847	±21	1885	±13	+2.4
N1619I.5-1	214	201	0.97	62	0.118	0.11402	±0.82	5.2620	±1.59	0.3347	±1.36	0.856	0.0928	±1.67	1861	±22	1864	±15	+0.2
N1619I.7-1	205	191	0.96	59	0.020	0.11600	±0.75	5.3945	±1.55	0.3373	±1.35	0.875	0.0940	±1.63	1874	±22	1895	±13	+1.3
N1619I.7-2	412	363	0.91	118	0.030	0.11497	±0.53	5.3071	±1.29	0.3348	±1.18	0.911	0.0933	±1.35	1862	±19	1879	±10	+1.1
N1619I.8-1	306	239	0.81	87	0.055	0.11489	±0.65	5.2345	±1.39	0.3304	±1.23	0.883	0.0932	±1.58	1840	±20	1878	±12	+2.3
N1619I.9-1	380	264	0.72	105	0.119	0.11465	±0.64	5.0647	±1.35	0.3204	±1.19	0.881	0.0893	±1.48	1792	±19	1874	±12	+5.1
N1619I.9-2	70	86	1.26	20	0.000	0.11570	±1.25	5.3501	±2.27	0.3354	±1.89	0.834	0.0948	±2.33	1864	±31	1891	±23	+1.6
PFR-22 (BAMzg). Zircon																			
N1619B.4-1	223	157	0.73	65	0.133	0.11348	±0.73	5.2784	±1.52	0.3374	±1.33	0.878	0.0925	±1.66	1874	±22	1856	±13	−1.1
N1619B.4-2	292	275	0.97	84	0.027	0.11473	±0.62	5.3188	±1.87	0.3362	±1.77	0.943	0.0944	±1.92	1868	±29	1876	±11	+0.4
N1619B.5-1	176	179	1.05	51	−0.044	0.11436	±2.12	5.3251	±2.56	0.3377	±1.44	0.562	0.0939	±1.72	1876	±23	1870	±38	−0.4
N1619B.5-2	210	186	0.91	59	0.147	0.11510	±0.87	5.1674	±1.62	0.3256	±1.36	0.843	0.0889	±1.73	1817	±22	1881	±16	+3.9
N1619B.5-3	273	262	0.99	77	−0.042	0.11434	±0.64	5.1814	±1.43	0.3287	±1.28	0.894	0.0918	±1.49	1832	±20	1869	±12	+2.3
N1619B.5-4	297	284	0.99	86	−0.026	0.11429	±0.60	5.3162	±1.39	0.3374	±1.25	0.901	0.0941	±1.45	1874	±20	1869	±11	−0.3
N1619B.9-1	268	232	0.90	76	0.015	0.11512	±0.64	5.2623	±1.44	0.3315	±1.29	0.896	0.0919	±1.82	1846	±21	1882	±12	+2.2
PFR-19B (ABSG). Zircon																			
1634C.5-1	307	282	0.95	84	−0.019	0.11424	±0.94	5.0467	±1.68	0.3204	±1.39	0.829	0.0910	±1.68	1792	±22	1868	±17	+4.7
1634C.5-2	331	188	0.59	87	0.094	0.11408	±0.51	4.8316	±1.47	0.3072	±1.38	0.938	0.0864	±2.10	1727	±21	1865	±9	+8.5
N1634C.4-5	75	78	1.08	21	0.152	0.11373	±1.18	5.1640	±2.09	0.3293	±1.72	0.824	0.0936	±2.15	1835	±27	1860	±21	+1.5
N1634C.4-4	335	287	0.89	95	0.086	0.11355	±0.54	5.1795	±1.86	0.3308	±1.78	0.957	0.0959	±1.90	1842	±28	1857	±10	+0.9
N1634C.4-2	371	318	0.89	105	0.079	0.11470	±0.53	5.2002	±2.37	0.3288	±2.31	0.974	0.0938	±2.40	1833	±37	1875	±10	+2.6
N1634C.3-4	281	262	0.96	81	−0.010	0.11487	±0.54	5.3051	±1.29	0.3349	±1.17	0.908	0.0971	±1.37	1862	±19	1878	±10	+1.0
N1634C.3-1	387	318	0.85	103	0.201	0.11451	±0.63	4.8982	±1.61	0.3102	±1.48	0.921	0.0951	±1.66	1742	±23	1872	±11	+7.9
N1634C.3-5	380	340	0.92	108	0.070	0.11451	±0.53	5.2235	±1.99	0.3308	±1.92	0.964	0.0957	±2.16	1842	±31	1872	±10	+1.8
PFR-18B (cBAGrd). titanite																			
N1619H.1-1	258	83	0.33	100	0.080	0.11819	±0.80	5.4019	±2.08	0.3315	±1.92	0.924	0.0978	±2.65	1846	±31	1929	±14	+5.0
N1619H.1-1B	240	73	0.32	60	0.154	0.11731	±0.83	5.5433	±2.11	0.3427	±1.94	0.920	0.1056	±2.71	1900	±32	1916	±15	+1.0
N1619H.2-1	216	126	0.60	73	0.000	0.11497	±0.77	5.4360	±2.07	0.3429	±1.92	0.928	0.0999	±2.38	1901	±32	1879	±14	−1.3
N1619H.3-1	344	198	0.60	71	0.000	0.11412	±0.65	5.3098	±1.94	0.3374	±1.83	0.942	0.0991	±2.15	1874	±30	1866	±12	−0.5
N1619H.3-2	205	131	0.66	64	0.000	0.11581	±0.83	5.4581	±2.06	0.3418	±1.88	0.914	0.1005	±2.34	1895	±31	1892	±15	−0.2
PFR-22 (mBAMzg). titanite																			
N1619A.1-1	194	111	0.59	56	0.000	0.11379	±0.79	5.3012	±2.07	0.3379	±1.91	0.923	0.1000	±2.38	1876	±31	1861	±14	−1.0
N1619A.1-2	204	114	0.58	60	0.000	0.11554	±0.76	5.4861	±2.04	0.3444	±1.90	0.928	0.1031	±2.81	1908	±31	1888	±14	−1.2
N1619A.1−2b	181	101	0.58	52	0.000	0.11369	±1.09	5.2806	±2.36	0.3369	±2.09	0.887	0.0975	±2.91	1872	±34	1859	±20	−0.8
N1619A.2-1	193	81	0.43	55	0.000	0.11474	±0.87	5.2374	±2.13	0.3310	±1.94	0.913	0.0984	±2.61	1843	±30	1876	±16	+2.0
N1619A.2-2	184	114	0.64	53	0.224	0.11474	±0.95	5.3483	±2.12	0.3381	±1.90	0.894	0.1019	±2.46	1877	±31	1876	±17	−0.1
N1619A.2-3	93	45	0.50	27	0.000	0.11800	±1.13	5.5617	±2.43	0.3418	±2.15	0.884	0.1006	±3.12	1895	±35	1926	±20	+1.8
N1619A.3-1	214	128	0.61	61	0.000	0.11665	±0.71	5.3374	±2.01	0.3318	±1.88	0.934	0.1014	±2.27	1847	±31	1906	±13	+3.5
N1619A.3-1b	269	163	0.63	70	0.410	0.11377	±1.18	4.7732	±2.26	0.3043	±1.94	0.853	0.0882	±2.76	1713	±29	1860	±21	+9.0

Notes: Isotopic ratios errors in %.
All Pb in ratios are radiogenic component. all corrected for 204 Pb.
disc. = discordance. as 100 - 100{t[206 Pb/238U]/t[207Pb/206 Pb]}.
4f206 = (common ^{206}Pb)/(total measured ^{206}Pb) based on measured ^{204}Pb.
Uncertainties are 1s.

characteristics. Hence, it is concluded that there is significant evidence indicating that the GOG can be associated with the Serra dos Carajás Suite.

7.2. Magmatic evolution of the Gogó da Onça Granite

The sampling of the GOG was limited and only a preliminary discussion of its magmatic evolution can be done. Rb and Sr behavior can be used to monitor fractional crystallization or melting partial process (Hanson, 1978, 1989; Halliday et al., 1991; Frost et al., 2016). Sr is compatible in plagioclase and K-feldspar and Rb is incompatible in plagioclase and slightly compatible to incompatible in alkali feldspar (Nash and Crecraft, 1985; Frost et al., 2016).

In spite of the compositional gap between different facies, some geochemical diagrams suggest that the different facies of the Gogó da Onça granite could possibly be related by fractional crystallization. In particular, Sr and Rb behavior are compatible with a fractional crystallization process (Fig. 7b and c). This is reinforced by the Sr vs. Eu/Eu* diagram (Fig. 12a) where the GOG display a positive correlation trend which suggest that K-feldspar and plagioclase were important fractionating phases. This is also confirmed by negative correlation trend between Rb and Eu/Eu* (Fig. 12b). On the other hand, the decrease of Sr from the granodiorite to the monzogranite facies is not accompanied by Ba (Fig. 7a; Table 3). If a fractional crystallization process controlled the evolution from the granodiorite to the monzogranite in the Gogó da Onça granites, this indicates that at this stage the plagioclase fractionation was the main responsible for the evolution of the magma and the role of K-feldspar was subordinate. In a next stage, corresponding to the differentiation of the monzogranite to the syenogranite, Sr and Ba decrease and Rb continues to increase suggesting that plagioclase and K-feldspar where main fractionating phases, probably accompanied by

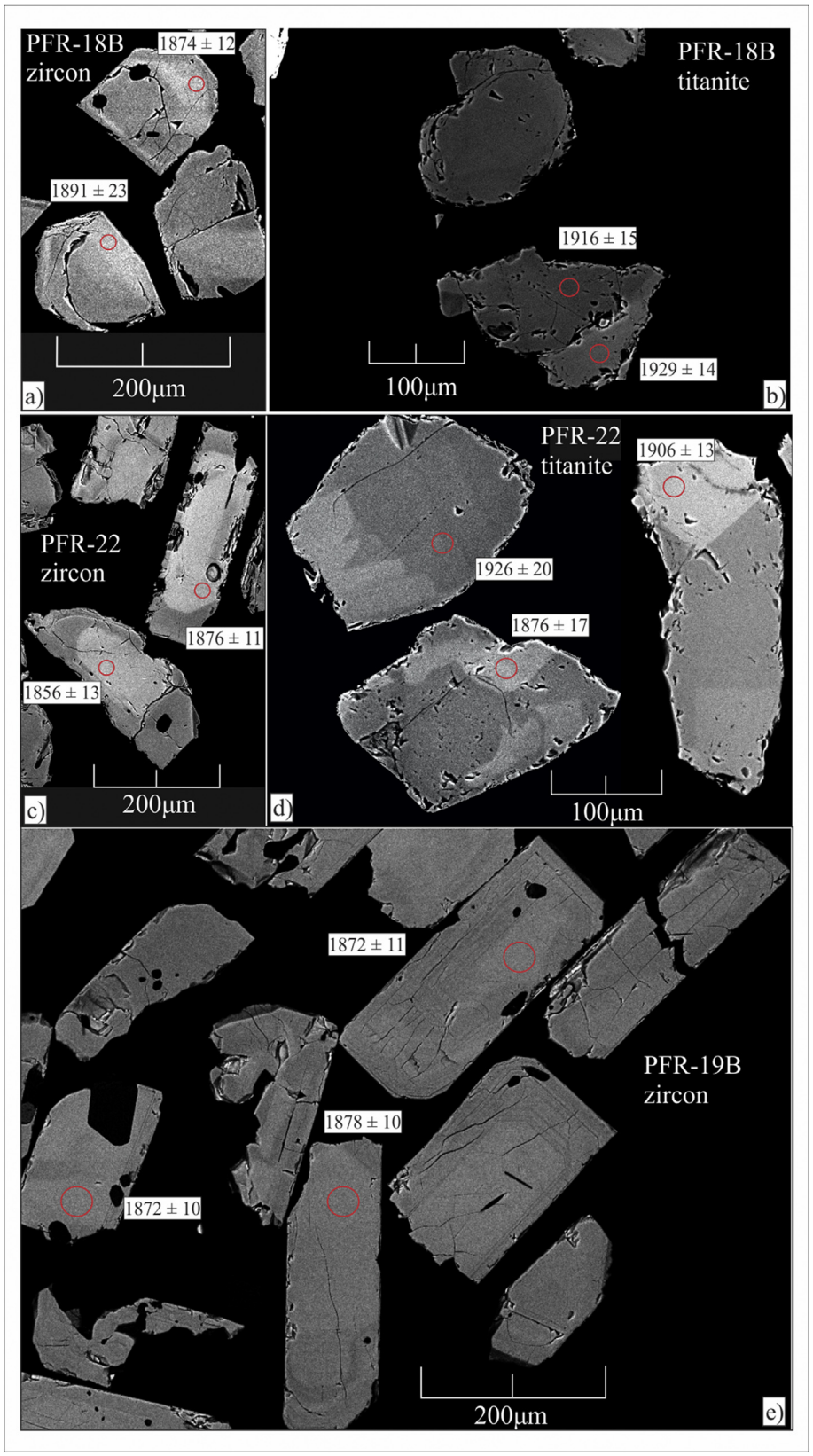

Fig. 10. Backscattered electrons (BSE) images of zircon and titanite of the GOG. Red circles (about 25 µm in diameter) indicate locations of SHRIMP analyses. (For interpretation of the references to colour in this figure legend, the reader is referred to the web version of this article.)

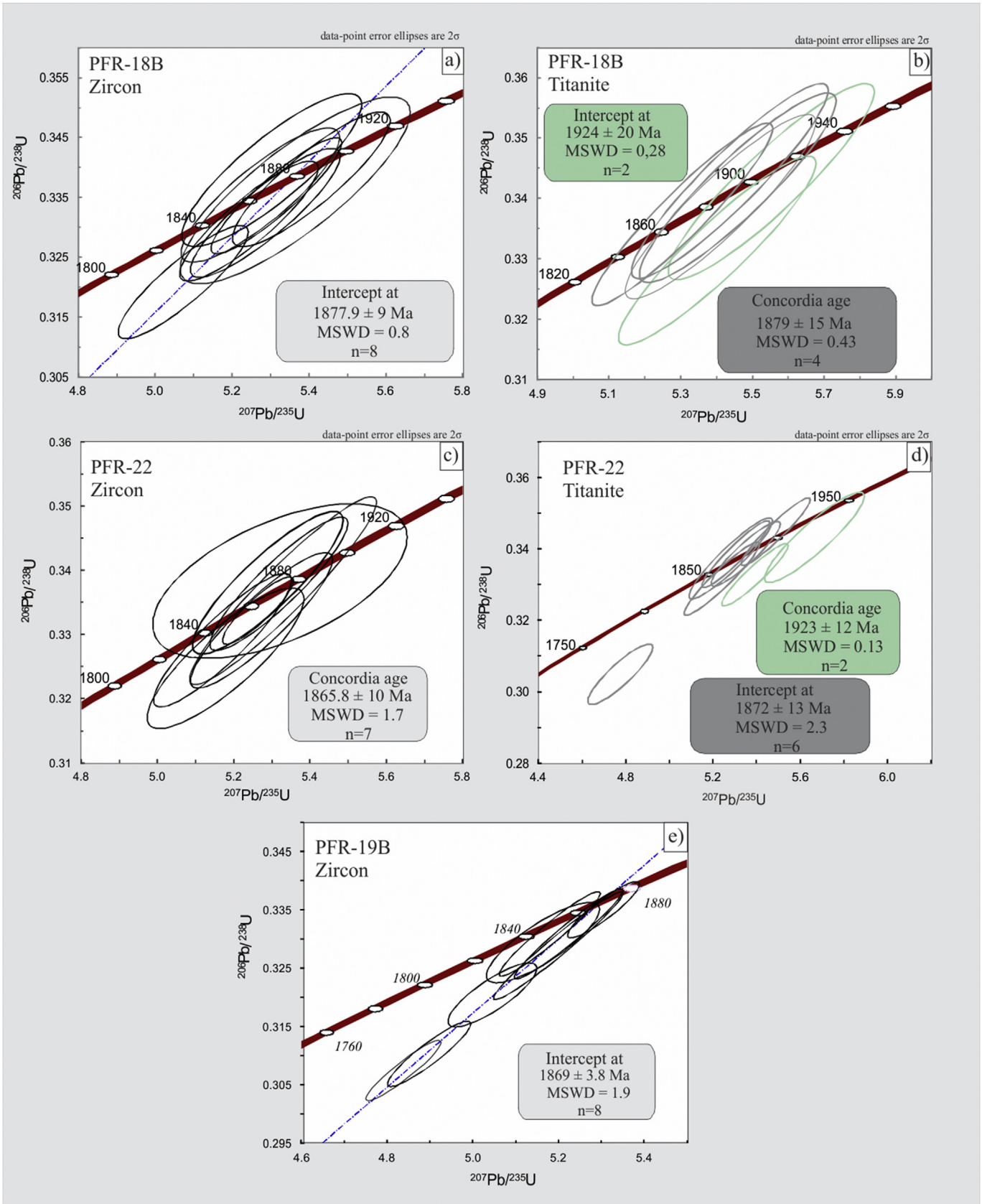

Fig. 11. Concordia diagrams showing SHRIMP U-Pb zircon and titanite data of three dated samples of GOG. U–Pb concordia plot of zircon (a) and titanite (b) of sample PFR-18B of the granodiorite facies; U–Pb concordia plot of zircon (c) and titanite (d) of sample PFR-22 of the monzogranite facies; (e) U–Pb concordia plot of zircon from sample PFR-19B of the syenogranite facies.

Table 5
Whole-Rock Sm-Nd isotopic composition of the Gogó da Onça Granite.

Amostra	Sm(ppm)	Nd(ppm)	147Sm/144Nd	2σ	143Nd/144Nd	2σ	f (Sm/Nd)	Age(Ga) U-Pb	$T_{(DM)}$	eNd(t)
PFA-22 (BAGrd)	13.83	85.10	0.0982	0.0003	0.510936	0.000004	−0.501	1.87	2.81	−9.48
PFR-18B (BAGrd)	13.72	84.86	0.0977	0.0004	0.510945	0.000005	−0.503	1.87	2.78	−9.18
PFR-20 (BAMzg)	17.76	106.79	0.1006	0.0003	0.510986	0.000001	−0.489	1.87	2.80	−9.07

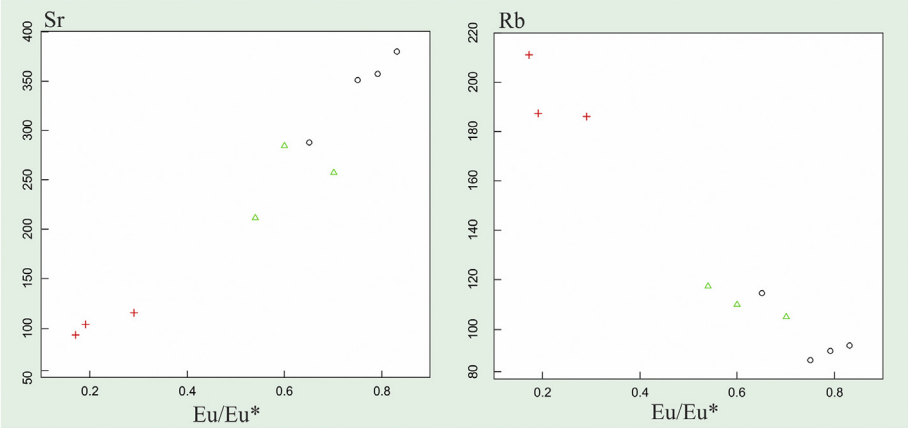

Fig. 12. Diagrams of (a) Sr vs Eu/Eu* (b) Rb vs Eu/Eu* for the Gogó da Onça samples.

amphibole and apatite (Fig. 7a, b, c).

7.3. Age, Nd isotopic signature and origin of the Gogó da Onça Granite

In this work, new U-Pb SHRIMP in zircon and titanite data for the different facies of the Gogó da Onça pluton were obtained: granodiorite (1877± 9Ma zircon, 1879 ± 15Ma titanite); monzogranite (1865 ± 10Ma zircon, 1872 ± 13Ma titanite) and syenogranite (1869 ± 4Ma zircon). These ages are very close and overlap on the analytical error. According to these data, the crystallization age for GOG is from 1866 ± 10 Ma to 1879 ± 15 Ma, and similar to the ~1.88 Ga age of the Paleoproterozoic granites from the Carajás Province. Along with field and geochemical evidence, these data allow to conclude that GOG is a member of the Paleoproterozoic A-type granite association of the Carajás Province. Besides, the coincidence between the zircon and titanite ages indicates that the studied granites were not submitted to metamorphic events after their crystallization. This confirms that the Carajás Province remained tectonically stable probably after the final of the Archean and certainly after the final of the Paleoproterozoic.

Additionally, ages of ~1920 Ma were obtained in titanite of the granodiorite and monzogranite facies of GOG. At our knowledge, other titanite ages in Paleoproterozoic granites of the Carajás Province were not reported so far. The meaning of these comparatively older ages is not evident. They could hypothetically represent the initial crystallization of the rocks of GOG. However, all the information available in the literature indicates a crystallization age near 1880–1870 Ma for the Paleoproterozoic anorogenic granites (cf. Table 1). Another possibility is to infer that these older ages correspond to inheritance in the analyzed titanites crystals. Inheritance in titanite is considered as relatively uncommon, but it was demonstrated by Zhang and Scharer (1996) that the closure temperature for the U–Pb system in titanite is about 700 °C. Thus titanite crystals extracted from felsic igneous rock could preserve the initial in print of an older crystallization event. However, the absence of oldest zircons in the studied rocks weakens this hypothesis that needs to be better evaluated and tested.

The analysed samples of the GOG show strongly unradiogenic initial Nd isotopic compositions indicating a long period of crustal residence time for its magma sources. The Nd isotopic composition of the three facies of the GOG fall along the evolution path of Nd isotopes of the Canaã dos Carajás crust (2.8–3.2 Ga; Fig. 13) and also along that of the Rio Maria crust because both partially overlap. However, the existence of a distinct and significantly older crust for the Canaã domain was assumed by Feio et al. (2013). The model ages (T_{DM}) for the GOG, range from 2.78 to 2.81 Ga, suggesting that the source rocks have ages and Nd isotopes similar to those of the Mesoarchean basement rocks of the Carajás Province. This isotopic behavior is in general compatible with those of other Paleoproterozoic suites from Carajás (T_{DM} model ages 3.35 to 2.60 Ga; ε_{Nd} values −12 to −8 at 1880 Ma). A more specific comparison with the Serra dos Carajás granites, geochemically akin to the GOG, indicates similar ε_{Nd} values (−9.7 to −7.9 at 1880 Ma) and T_{DM} model ages (2611–2939 Ma, except for the Pojuca Granite; data from Dall'Agnol et al., 2005).

A-type granites can be formed by partial melting of mafic rocks or by fractional crystallization of mantle-derived mafic magmas (Frost and Frost, 1997; Bonin, 2007). Anderson (1983) and Dall'Agnol et al. (1999b) suggested that their magmas can be derived by partial melting of quartz diorite, tonalite, and granodiorite rocks. Patiño Douce (1997) and Frost and Frost (2011) suggest that partial melting of tonalitic to granodioritic crust produces alkali-calcic to calc-alkalic granitoids that are metaluminous at low pressures and peraluminous at high pressures. Poitrasson et al. (1995) and Nardi and Bitencourt (2009) argue that mantle-derived magmas may also assimilate crustal material during their ascent or residency time in the crust to produce 'mixed' source characteristics.

The origin of the anorogenic granites from Carajás is probably related to a mantle superswell beneath the Trans-Amazonian supercontinent (Dall'Agnol et al., 2005; following the model proposed

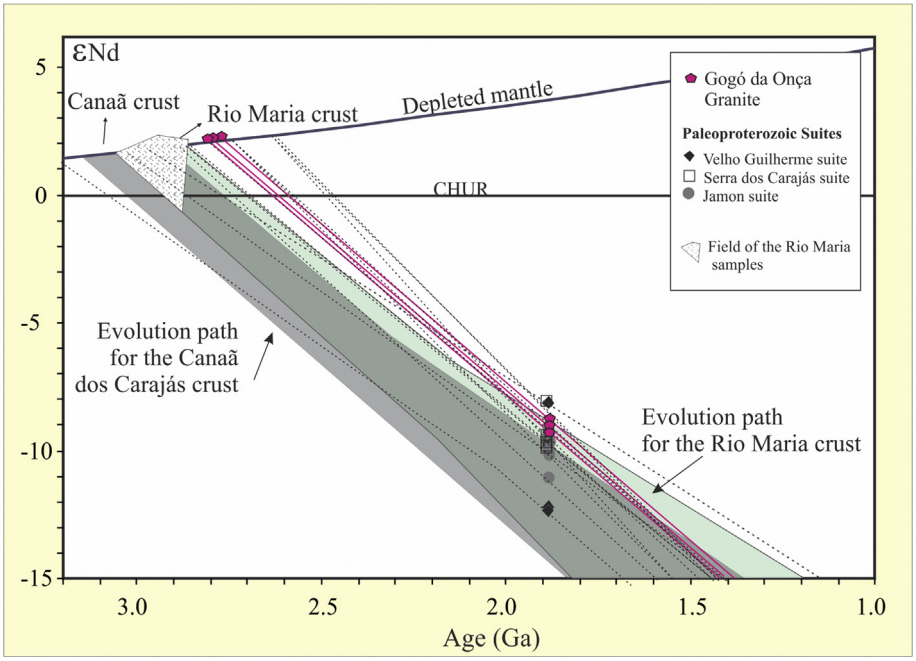

Fig. 13. εNd versus age diagram showing initial Nd isotopic composition of Gogó da Onça Granite. The three Paleoproterozoic suites from Carajás Province and the fields of the Archean rocks of the Rio Maria (Rämö et al., 2002) and Canaã dos Carajás Domain (Feio et al., 2013) are also plotted for comparison.

by Hoffman, 1989). This caused the breakup of the continent and was associated with magmatic underplating of mantle mafic magmas that induced crustal melting and generation of A-type granite magmas (Dall'Agnol et al., 2005). The Jamon granites may have been derived from a quartz dioritic source, the Velho Guilherme granites from K-feldspar-bearing granitoid rocks with some sedimentary input, and the Serra dos Carajás granites from a more mafic source than Velho Guilherme or resulted of a larger degree of melting (Dall'Agnol et al., 2005).

The ε_{Nd} values (−9.07 to −9.48) are quite uniform in the different facies of GOG and compatible with a comagmatic origin of the analyzed varieties. The GOG is intrusive in a ~2.87 Ga old TTG association (Colorado Trondhjemite). This age is similar to the TDM ages (2.78–2.81 Ga) obtained but more detailed studies are required to further constrain the origin of the GOG.

8. Conclusions

On the basis of the obtained geochemical, geochronological, and Nd isotope data, the following conclusions can be made:

- The Gogó da Onça granite is a stock with an approximate area of 48 km^2. Three facies, varying from biotite-amphibole granodiorite to biotite-amphibole monzogranite and amphibole-biotite syenogranite were identified in the geological mapping. The stock is intrusive in the Colorado Trondhjemite and located in the border between the Sapucaia and Canaã dos Carajás domains of the Carajás Province;
- U-Pb SHRIMP ages in zircon and titanite indicate that the GOG was emplaced at ~1880–1870 Ma, and has an age similar to that of the A-type Paleoproterozoic magmatism of the Carajás Province;
- Whole-rock Nd isotope data (T_{DM} ages 2.78 to 2.81, ε_{Nd} values of −9.07 to −9.48) indicate that the GOG magma derived from a Mesoarchaean source compatible with those of other Paleoproterozoic suites from Carajás (T_{DM} ages 3.35 to 2.60 Ga; ε_{Nd} values −12 to −8 at 1880 Ma);
- Geochemical features classify the GOG as A-type reduced granite of A2-subtype. It is metaluminous and enriched in HFSE, and have high K_2O/Na_2O and Y/Nb (2.15–2.54) ratios;
- The geochemical data of the Gogó da Onça granite also suggest that the different facies of this granite are possibly related by fractional crystallization;
- The obtained data suggest that the GOG has strong affinity with the granites of the Serra dos Carajás Suite from Carajás Province and could be possibly included in that suite. The GOG is also similar in several aspects to the Sherman Granite of USA and Suomenniemi Batholith of Finland.

Acknowledgements

We are grateful to the colleagues of the Group of Granite Petrology (UFPA), and to P.J. Leite-Santos and J.M. Milhomem-Neto for scientific discussions; to the Isotope Geology Laboratory of the Federal University of Pará (Pará-Iso) and to J.M. Lafon for the support for Sm-Nd analysis; part of the study was conducted under a sandwich Ph.D. fellowship awarded by CAPES (Coordenação de Aperfeiçoamento de Pessoal de Nível Superior) in the context of the National Program of Strategic Areas (INCT-GEOCIAM; Bex 0201/16-2); to the John De Laetter Centre for Mass Spectrometry at Curtin University of Technology in Perth, Western Australia where the SHRIMP U-Pb analyses were performed; to the Center for Microscopy, Characterization and Analysis (CMCA) of the University of Western Australia; to the CNPq for doctor thesis scholarship to MFBT. This research received financial support from the INCT program (CNPq/FAPESPA/CAPES/PETROBRAS; Proc. 573733/2008-2) and the Federal University of Pará (UFPA). This paper is a contribution to the Brazilian Institute of Amazonian Geosciences (INCT GEOCIAM).

References

Almeida, J.A.C., Dall'Agnol, R., Oliveira, D.C., 2006. Geologia, petrografia e geoquímica do granito anorogênico Bannach, Terreno granito-greenstone de Rio

Maria, Pará. Rev. Bras. Geociências 36, 282–295 (in Portuguese).
Almeida, J.A.C., Dall'Agnol, R., Oliveira, M.A., Macambira, M.J.B., Pimentel, M.M., Rämö, O.T., Guimarães, F.V., Leite, A.A.S., 2011. Zircon geochronology and geochemistry of the TTG suites of the Rio Maria granite-greenstone terrane: implications for the growth of the Archean crust of Carajás Province, Brazil. Precambrian Res. 187, 201–221.
Almeida, J.A.C., Dall'agnol, R., Leite, A.A.S., 2013. Geochemistry and zircon geochronology of the Archean granite suites of the Rio Maria granite-greenstone terrane, Carajás Province, Brazil. J. S. Am. Earth Sci. 42, 103–126.
Anderson, J.L., 1983. Proterozoic anorogenic granite plutonism of North America. Geol. Soc. Am. Mem. 161, 133–154.
Anderson, J.L., Barth, A.P., Mazdab, J.L.W.F., 2008. Thermometers and thermobarometers in granitic systems. Rev. Mineralogy Geochem. 69, 121–142.
Avelar, V.G., 1996. Geocronologia Pb-Pb por evaporação em monocristal de zircão, do magmatismo da região de Tucumã, SE do Estado do Pará. Amazônia oriental. Federal University of Para. Dissertation. Graduated Program on Geology and Geochemistry, Institute of Geosciences, p. 199 (in Portuguese).
Avelar, V.G., Lafon, J.M., Correia Jr., F.C., Macambira, E.M.B., 1999. O Magmatismo arqueano da região de Tucumã-Província Mineral de Carajás: novos resultados geocronológicos. Rev. Bras. Geociências 29 (2), 454–460 (in Portuguese).
Barbosa, A.A., Lafon, J.M., Neves, A.P., Vale, A.G., 1995. Geocronologia Rb–Sr e Pb–Pb do Granito Redencão, SE do Pará: implicações para a evolução do magmatismo proterozóico da região de Redenção. Boletim do Museu Paraense Emílio Goeldi. Ciências Terra 7, 147–164 (in Portuguese).
Barros, C.E.M., Dall'Agnol, R., Vieira, E.A.P., Magalhães, M.S., 1995. Granito Central da Serra dos Carajás: avaliação do potential metalogenético para estanho com base em estudos da borda oeste do corpo. Bol. do Mus. Para. Emílio Goeldi. Série Ciências Terra 7, 93–123 (in Portuguese).
Barros, C.E.M., Dall'Agnol, R., Barbey, P., Boullier, A.M., 1997. Geochemistry of the Estrela granite complex, Carajás region, Brazil: an example of an archean A-type granitoid. J. S. Am. Earth Sci. 10, 321–330.
Barros, C.E.M., Sardinha, A.S., Barbosa, J.P.O., Macambira, M.J.B., 2009. Structure, petrology, geochemistry and zircon U/Pb and Pb/Pb geochronology of the synkinematic Archean (2.7 Ga) A-type granites from the Carajás Metallogenic Province, northern Brazil. Can. Mineralogist 47, 1423–1440.
Bettencourt, J.S., Tosdal, R.M., Leite Júnior, W.B., Payolla, B.L., 1999. Mesoproterozoic rapakivi granites of the Rondonia Tin Province, southwestern border of the Amazonian craton, Brazil - I. Reconnaissance U-Pb geochronology and regional implications. Precambrian Res. 95, 41–67.
Bettencourt, J.S., Juliani, Xavier, R.P., Monteiro, L.V.s., Neto, A.C.B., Klein, E.L., Assis, R.R., Leite Jr., W.P., Moreto, C.P.N., Fernandes, C.M.D., Pereira, V.P., 2016. Metallogenetic systems associated with granitoid magmatism in the Amazonian Craton: an overview of the present level of understanding and exploration significance. J. S. Am. Earth Sci. 68, 22–49.
Bonin, B., 2007. A-type granites and related rocks: evolution of a concept, problems and prospects. Lithos 97, 1–2.
Compston, W., Williams, I.S., Kirschvink, J.L., Zichao, Z., Guogan, M.A., 1992. Zircon U-Pb agesfor the early cambrian time-scale. J. Geol. Soc. Lond. 149, 171–184.
Costi, H.T., Dall'Agnol, R., Pichavant, M., Ramo, O.T., 2009. The peralkaline tin-mineralized Madeira cryolite albite-rich granite of Pitinga, Amazonian Craton, Brazil: petrography, mineralogy and crystallization processes. Can. Mineral. 47, 1301–1327.
Cunha, I.R.V., Dall'Agnol, R., Feio, G.R.L., 2016. Mineral chemistry and magnetic petrology of the archean planalto suite, Carajás province – amazonian craton: implications for the evolution of ferroan archean granites. J. S. Am. Earth Sci. 67, 100–121.
Dall'Agnol, R., Lafon, J.M., Macambira, M.J.B., 1994. Proterozoic anorogenic magmatism in the Central Amazonian Province: geochronological, petrological and geochemical aspects. Mineralogy Petrology 50, 113–138.
Dall'Agnol, R., Rämö, O.T., Magalhães, M.S., Macambira, M.J.B., 1999a. Petrology of the anorogenic, oxidised Jamon and Musa granites, Amazonian Craton: implications for the genesis of Proterozoic A-type granites. Lithos 46, 431–462.
Dall'Agnol, R., Scaillet, B., Pichavant, M., 1999b. An experimental study of a lower Proterozoic A-type granite from the eastern Amazonian craton, Brazil. J. Petrology 40, 1673–1698.
Dall'Agnol, R., Teixeira, N.P., Rämö, O.T., Moura, C.A.V., Macambira, M.J.B., Oliveira, D.C., 2005. Petrogenesis of the paleoproterozoic, rapakivi, a-type granites of the ArcheanCarajás metallogenic province, Brazil. Lithos 80, 101–129.
Dall'Agnol, R., Oliveira, M.A., Almeida, J.A.C., Althoff, F.J., Leite, A.A.S., Oliveira, D.C., Barros, C.E.M., 2006. Archean and paleoproterozoic granitoids of the Carajás metallogenetic province, eastern amazonian craton. In: Dall'Agnol, R., Rosa-Costa, L.T., Klein, E.L. (Eds.), Symposium on Magmatism, Crustal Evolution, and Metallogenesis of the Amazonian Craton. Abstracts Volume and Field Trips Guide. PRONEX-UFPA/SBG-NO, Belém, pp. 99–150.
Dall'Agnol, R., Oliveira, D.C., 2007. Oxidized, magnetite-series, rapakivi-type granites of Carajás, Brazil: implications for classification and petrogenesis of A-type granites. Lithos 93, 215–233.
Dall'Agnol, R., Frost, C.D., Rämö, O.T., 2012. IGCP Project 510 "A-type granites and related rocks through time": project vita, results, and contribution to granite research. Lithos 151, 1–16.
Dall'Agnol, R., Oliveira, D.C., Guimarães, F.V., Gabriel, E.O., Feio, G.R.L., Lamarão, C.N., Althoff, F.J., Santos, P.A., Teixeira, M.F.B., Silva, A.C., Rodrigues, D.S., Santos, M.J.P., Silva, C.R.P., Santos, R.D., Santos, P.J.L., 2013. Geologia do Subdomínio de Transição do Domínio Carajás – implicações para a evolução arqueana da Província Carajás - pará. In: SBG, Simpósio de Geologia da Amazônia 13. CDrom, Anais, Belém (in Portuguese).
Dall'Agnol, R., Cunha, I.R.V., Guimarães, F.V., Oliveira, D.C., Teixeira, F.B.T., Feio, G.R., Lamarão, C.N., 2017. Mineralogy, geochemistry, and petrology of Neoarchean ferroan to magnesian granites of Carajás Province, Amazonian Craton: the origin of hydrated granites associated with charnockites. Lithos 277, 3–32.
DePaolo, D.J., 1981. A neodymium and strontium isotopic study of the Mesozoic calc-alkaline granitic batholiths of the Sierra Nevada and Peninsular Ranges, California. J. Geophys. Res. Solid Earth 86, 10470–10488.
DOCEGEO (Rio Doce Geologia e Mineração - Distrito Amazônia), 1988. Revisão litoestratigráfica da Província Mineral de Carajás e Litoestratigrafia e principais depósitos minerais. In: 35th Congresso Brasileiro de Geologia, Belém (in Portuguese).
Eby, G.N., 1992. Chemical subdivision of the A-type granitoids: petrogenesis and tectonic implications. Geology 20, 641–644.
Feio, G.R.L., Dall'Agnol, R., Dantas, E., Macambira, M.J.B., Gomes, A.C.B., Sardinha, A.S., Santos, P., 2012. Geochemistry, geochronology, and origin of the Planalto granite suite and associated rocks: implications for the Neoarchean evolution of the Carajás Province. Lithos 151, 57–73.
Feio, G.R.L., Dall'Agnol, R., Dantas, E.L., Macambira, M.J.B., Santos, J.O.S., Althoff, F.J., Soares, J.E.B., 2013. Archean granitoid magmatism in the Canaã dos Carajás area: implications for crustal evolution of the Carajás province, Amazonian craton. Braz. Precambrian Res. 227, 157–185.
Frost, B.R., Barnes, C.G., Collins, W.J., Arculus, R.J., Ellis, D.J., Frost, C.D., 2001. A geochemical classification for granitic rocks. J. Petrology 42, 2033–2048.
Frost, C.D., Frost, B.R., 1997. Reduced rapakivi type granites: the tholeiitic connection. Geology 25, 647–650.
Frost, C.D., Frost, B.R., Chamberlain, K.R., Edwards, B., 1999. Petrogenesis of the 1.43 Ga Sherman batholith, SE Wyoming, USA: a reduced, rapakivi-type anorogenic granite. J. Petrology 40, 1771–1802.
Frost, C.D., Frost, B.R., 2011. On ferroan (A-type) granitoids: their compositional variability and modes of origin. J. Petrology 52, 39–55.
Frost, D.C., Frost, B.R., Beard, J.S., 2016. On silica-rich granitoids and their eruptive equivalents. Am. Mineralogist 101, 1268–1284.
Gabriel, E.O., Oliveira, D.C., 2014. Geologia, petrografia e geoquímica dos granitoides arqueanos de alto magnésio da região de Água Azul do Norte, porção sul do Domínio Carajás, Pará. Bol. do Mus. Para. Emílio Goeldi Ciências Nat. Belém 9, 533–564 (in Portuguese).
Gabriel, E.O., Oliveira, D.C., Santos, M.S., 2014. Sanukitoides mesoarqueanos de Água Azul do Norte, Sul do Domínio Carajás: novos dados e perspectivas. In: SBG, Congresso Brasileiro de Geologia 47. CDrom, Anais, Salvador (in Portuguese).
Gastal, M.C.P., 1987. Mapeamento e petrologia do maciço granítico Musa. Rio Maria, Sudeste do Para. Unpublished M.Sc. Thesis. Univ. Federal do Para, Belem.
Gibbs, A.K., Wirth, K.R., Hirata, W.K., Olszewski, W.J., 1986. Age and composition of the grão Pará group volcanics, Serra dos Carajás. Rev. Bras. Geociências 16, 201–211 (in Portuguese).
Gioia, S.M.C.L., Pimentel, M.M., 2000. The Sm-Nd isotopic method in the geochronology laboratory of the University of Brasília. An. Acad. Bras. Ciências 72, 220–245. http://dx.doi.org/10.1590/S0001-37652000000200009.
Halliday, A.N., Davidson, J.P., Hildreth, W., Holden, P., 1991. Modelling the petrogenesis of high Rb/Sr silicic magmas. Chem. Geol. 92, 107–114.
Hanson, G.N., 1978. The application of trace elements to the petrogenesis of igneous rocks of granitic composition. Earth Planet. Sci. Lett. 38, 26–43.
Hanson, G.N., 1989. An approach to trace element modeling using a simple igneous system as an example. In: Lipin, B.R., McKay, G.A. (Eds.), Geochemistry and Mineralogy of Rare Earth Elements, Reviews in Mineralogy, vol. 21, pp. 79–97.
Heaman, L., 2009. The application of U-Pb geochronology to mafic, ultramafic and alkaline rocks: an evaluation of three mineral standards. Chem. Geol. 261, 42–51.
Hirata, W.K., Rigon, J.C., Kadekaru, K., Cordeiro, A.A.C., Meireles, E.A., 1982. Geologia Regional da Província Mineral de Carajas. In: 1st Simpósio de Geologia da Amazonia, Belém (in Portuguese).
Hoffman, P., 1989. Speculations on Laurentia's first gigayear (2.0 to 1.0 Ga). Geology 17, 135–138.
Huhn, S.B., Macambira, M.J.B., Dall'Agnol, R., 1999. Geologia e geocronologia Pb/Pb do granito alcalino arqueano Planalto, região da Serra do Rabo, Carajás-PA. Simpósio Geol. Amazônia 6, 463–466 (in Portuguese).
Ishihara, S., 1981. The granitoid series and mineralization. Econ. Geol. 75, 458–484.
Javier Rios, F., Villas, R.N., Dall'Agnol, R., 1995. O Granito Serra dos Carajás: fácies petrográficas e avaliação do potential metalogenético para estanho no setor norte. Rev. Bras. Geociências 25, 20–31 (in Portuguese).
Lamarão, C.N., Pinho, S.C.C., Paiva Junior, A.L., Toro, M.A.G., 2012. Mineralogy and geochemistry of the Paleoproterozoic, tin mineralized Bom Jardim Granite of the Velho Guilherme Suite, eastern Amazonian Craton. J. S. Am. Earth Sci. 38, 159–173.
Leite-Santos, P.J., Oliveira, D.C., 2016. Geologia, petrografia e geoquímica das associações leucograníticas arqueanas da área de Nova Canadá e Domínio Carajás. Bol. IG-USP - Série Científica 16 (2), 37–66.
Lima, P.H.A., 2011. Geologia, petrografia e geocronologia do Granito São João, Província Carajás. In: SSE do Pará. Trabalho de Conclusão de Curso – Federal University of Pará, Belém, pp. 1–47 (in Portuguese).
Lima, P.H.A., Lamarão, C.N., Santo, M.J.P., 2014. Petrografia, geoquímica e suscetibilidade magnética do Granito Paleoproterozoico São João, sudeste do Cráton Amazônico, Província Carajás. Bol. do Mus. Para. Emilio Goeldi 9, 47–72 (in Portuguese).

Ludwig, K.R., 2008. Using ISOPLOT/Ex, Version 2: a Geochronological Toolkit for Microsoft Excel, vol. 4. Berkeley Geochronological Center Special Publication, p. 76.
Ludwig, K.R., 2009. Squid 2.5, a Geochronological Toolkit for Microsoft Excel, vol. 5. Berkeley Geochronological Center Special Publication, Berkeley, California, USA, p. 110.
Lugmair, G.W., Harti, K., 1978. Lunar initial 143Nd/144Nd: differential evolution of the lunar crust and mantle. Earth Planet. Sci. Lett. 39, 349–357.
Machado, N., Lindenmayer, Z., Krogh, T.E., Lindenmayer, D., 1991. U/Pb geochronology of Archean magmatism and basement reactivation in the Carajás Área, Amazon Shield, Brazil. Precambrian Res. 49, 329–354.
Macambira, M.J.B., Lafon, J.M., 1995. Geocronologia da Província Mineral de Carajás; Síntese dos dados e novos desafios. Bol. do Mus. Para. Emílio Goeldi 7, 263–287 (in Portuguese).
Manilar, P.D., Piccoli, P.M., 1989. Tectonic discrimination of granitoids. Geol. Soc. Am. Bull. 101, 635–643.
Mesquita, R.B.D., Jordt-Evangelista, H., Queiroga, G.N., Medeiros Júnior, E.B.D., Dussin, I.A., 2017. Petrogenesis and age of skarns associated with felsic and metamafic dykes from the Paraíba do Sul Complex, southern Espírito Santo State. Braz. J. Geol. 47 (2), 301–325.
Moreto, C.P.N., Monteiro, L.V.S., Xavier, R.P., Amaral, W.S., Santos, T.J.S., Juliani, C., Souza Filho, C.R., 2011. Mesoarchean (3.0 and 2.86 Ga) host rocks of the iron oxide–Cu–Au Bacaba deposit, Carajás Mineral Province: U–Pb geochronology and metallogenetic implications. Miner. Deposita 46, 789–811.
Moreto, C.P.N., Monteiro, L.V.S., Xavier, R.P., Creaser, R.A., DuFrane, A., Melo, G.H.C., Silva, M.A.D., Tassinari, C.C.G., Sato, K., 2015. Timing of multiple hydrothermal events in the iron oxide-copper-gold deposits of the Southern Copper Belt, Carajas Province, Brazil. Miner. Deposita 50, 517–546.
Nardi, L.V.S., 2016. Granitoides e séries magmáticas: o estudo contextualizado dos granitoides. Pesqui. em Geociências 43 (1), 85–99 (in portugese).
Nardi, L.V.S., Bitencourt, M.F., 2009. A-type granitic rocks in post-collisional settings in southernmost Brazil: their classification and relationship with tectonics and magmatic series. Can. Mineral. 47, 1493–1503.
Nash, W.P., Crecraft, H.R., 1985. Partition coefficients for trace elements in silicic magmas. Geochimica Cosmochimica Acta 49, 2309–2322.
Nakamura, N., 1974. Determination of REE, Ba, Fe, Mg, Na and K in carbonaceous and ordinary chondrites. Geochimica Cosmochimica Acta 38, 757–775.
Oliveira, D.C., Dall'Agnol, R., Silva, J.B.C., Almeida, J.A.C., 2008a. Gravimetric, radiometric, and magnetic susceptibility study of the Paleoproterozoic Redenção and Bannach plutons: implications for architecture and zoning of A-type granites. J. S. Am. Earth Sci. 25, 100–115.
Oliveira, D.C., Dall'Agnol, R., Barros, C.E.M., Oliveira, M.A., 2009a. Geology, geochemistry and magmatic evolution of the Paleoproterozoic, anorogenic oxidized A-type Redenção granite of the Jamon Suite, eastern Amazon Craton, Brazil. Can. Mineral. 47, 1441–1468.
Oliveira, D.C., Santos, P.J.L., Gabriel, E.O., Rodrigues, D.S., Faresin, A.C., Silva, M.L.T., Sousa, S.D., Santos, R.V., Silva, A.C., Souza, M.C., Santos, R.D., Macambira, M.J.B., 2010. Aspectos geológicos e geocronológicos das rochas magmáticas e metamórficas da região entre os municípios de Água Azul do Norte e Canaã dos Carajás – Província Mineral de Carajás. In: Congresso Brasileiro de Geologia 45. CDrom, Belém (in Portuguese).
Oliveira, E.C., Lafon, J.M., Gioia, S.M.C.L., Pimentel, M.M., 2008b. Datação Sm-Nd em rocha total e granada do metamorfismo granulítico da região de Tartarugal Grande, Amapá Central. Rev. Bras. Geociências 38,116–38,129 (in Portuguese).
Oliveira, M.A., Dall'Agnol, R., Althoff, F.J., Leite, A.A.S., 2009b. Mesoarchean sanukitoid rocks of the Rio Maria Granite-Greenstone Terrane, Amazonian craton, Brazil. J. S. Am. Earth Sci. 27, 146–160.
Oliveira, M.A., Dall'Agnol, R., Almeida, J.A.C., 2011. Petrology of the Mesoarchean Rio Maria suite: implications for the genesis of sanukitoid rocks. J. Petrology 51, 2121–2148.
Paiva Júnior, A.L., 2009. Geologia, petrografia, geocronologia e geoquímica do Granito anorogênico Seringa, Província Mineral de Carajás, SSE do Pará. Federal University of Para. Dissertation. Graduated Program on Geology and Geochemistry, Institute of Geosciences, p. 158 (in Portuguese).
Paiva Júnior, A.L., Lamarão, C.N., Lima, P.H.A., 2011. Geologia, Petrografia e Geoquímica do Batólito Seringa, Província Carajás, SSE do Pará. Rev. Bras. Geociências 41, 185–202 (in Portuguese).
Patiño Douce, A., 1997. Generation of metaluminous A-type granites by low pressure melting of calc-alkaline granitoids. Geology 25, 743–747.
Poitrasson, F., Duthou, J.L., Pin, C., 1995. The relationship between petrology and Nd isotopes as evidences for contrasting anorogenic granite genesis: example of the Corsican Province (SE France). J. Petrology 36, 1251–1274.
Rämö, O.T., 1991. Petrogenesis of the Proterozoic rapakivi granites and related basic rocks of southeastern Fennoscandia: Nd and Pb isotopic and general geochemical constraints. Geol. Surv. Finl. Bull. 355, 161.
Rämö, O.T., Dall'AGnol, R., Macambira, M.J.B., Leite, A.A.S., Oliveira, D.C., 2002. 1.88 Ga oxidized A-type granites of the Rio Maria region, eastern Amazonian craton, Brazil: positively anorogenic! J. Geol. 110, 603–610.
Rämö, O.T., Mänttäri, I., 2015. Geochronology of the Suomenniemi rapakivi granite complex revisited: Implications of point-specific errors on zircon U-Pb and refined λ_{87} on whole-rock Rb-Sr. Bull. Geol. Soc. Finl. 87, 25–45. http://dx.doi.org/10.17741/bgsf/87.1.002.
Rodrigues, D.S., Oliveira, D.C., Macambira, M.J.B., 2014. Geologia, geoquímica egeocronologia do Granito Mesoarqueano Boa Sorte, município de Água Azul doNorte, Pará – Província Carajás. Bol. do Mus. Para. Emílio Goeldi. SérieCiências Terra 9, 597–633 (in Portuguese).
Santos, J.O.S., Hartmann, L.A., Gaudette, H.E., Groves, D.I., McNaugthon, N.J., Fletcher, L.R.A., 2000. New understanting of the Provinces of Amazon Craton based on Integration of Field Mapping and U-Pb and Sm-Nd geochronology. Gondwana Res. 3, 453–488.
Santos, P.A., Teixeira, M.F.B., Dall'Agnoll, R., Guimaraes, A.V., 2013a. Geologia, petrografia e geoquímica da associação Tonalito-Trondhjemito-Granodiorito (TTG) do extremo leste do Subdomínio de Transição, Província Carajás, Pará. Bol. do Mus. Para. Emílio Goeldi. Ciências Nat. 8, 257–290 (in Portuguese).
Santos, P.J.L., Oliveira, D.C., 2014. Trondhjemitos da área de Nova Canadá: novas ocorrências de associações magmáticas tipo TTG no Domínio Carajás. Boletim do Museu Paraense Emílio Goeldi. Ser. Ciências Terra 9, 635–659 (in Portuguese).
Santos, R.D., Galarza, M.A., Oliveira, D.C., 2013b. Geologia, geoquímica e geocronologia do Diopsídio-Norito Pium, Província Carajás. Bol. do Mus. Para. Emílio Goeldi, Série Ciências Terra 8, 355–382 (in Portuguese).
Sardinha, A.S., Barros, C.E.M., Krymsky, R., 2006. Geology, geochemistry, and U-Pb geochronology of the Archean (2.74 Ga) Serra do Rabo granite stocks, Carajás Province, northern Brazil. J. S. Am. Earth Sci. 20, 327–339.
Silva, A.C., Dall'Agnol, R., Guimaraes, F.V., Oliveira, D.C., 2014. Geologia, petrografia e geoquímica de Associaçoes Tonalíticas e Trondhjemíticas Arqueanas de Vila Jussara, Província Carajás, Pará. Bol. do Mus. Para. Emílio Goeldi. Ser. Ciencias Nat. 9, 13–45 (in Portuguese).
Smith, J.V., Brown, W.L., 1988. Feldspar Minerals, 2. ed. Springer-Verlag, Berlin, p. 828.
Souza, Z.S., Potrel, H., Lafon, J.M., Althoff, F.J., Pimentel, M.M., Dall'Agnol, R., Oliveira, C.G., 2001. Nd, Pb and Sr isotopes of the Identidade Belt, an Archaean greenstone belt of the Rio Maria region (Carajas Province, Brazil): implications for the Archaean geodynamic evolution of the Amazonian Craton. Precambrian Res. 109, 293–315.
Stern, R.A., 2001. A New Isotopic and Trace Element Standard for the Ion Microprobe: Preliminary TIMS U-pb and Electron Microprobe Data, Current Research. Radiogenic Age and Isotopic Studies: Report 14. Geological Survey of Canada, Ottawa, Canada.
Streckeisen, A., 1976. To each plutonic rock its proper name. Earth-Sci. Rev. 12, 1–33.
Sun, S.S., Mcdonough, W.F., 1989. Chemical and isotopic systematics of oceanic basalts: implications for mantle composition and processes. In: Saunders, A.D., Norry, M.J. (Eds.), Magmatism in the Ocean Basins. Geological Society of London Special Publication 42, pp. 313–345.
Tallarico, F.H.B., Figueiredo, B.R., Groves, D.I., Kositcin, N., McNaughton, N.J., Fletcher, I.R., Rego, J.L., 2005. Geology and SHRIMP U-Pb geochronology of the Igarape Bahia deposit, Carajás copper - gold belt, Brazil: an Archean (2.57 Ga) example of iron-oxide Cu-Au-(U-REE) mineralization. Econ. Geol. 100, 7–28.
Tassinari, C.C.G., Macambira, M.J.B., 1999. Geochronological provinces of the Amazonian craton. Episodes 22, 174–182.
Tassinari, C.C.G., Macambira, M.J.B., 2004. A evolução tectonica do craton Amazônico. In: Matesso-Neto, V., Bartorelli, A., Carneiro, C.D.R., Britto-Neves, B.B. (Eds.), Geologia Do Continente Sul-americano. Sao Paulo, SP, Brazil, pp. 471–485 (in Portuguese).
Teixeira, M.F.B., Dall'Agnol, R., Silva, A.C., Santos, P.A., 2013. Geologia, petrografia e geoquímica do Leucogranodiorito Pantanal e dos leucogranitos arqueanos da área de Sapucaia, Província Carajás, PA: implicações petrogenéticas. Bol. do Mus. Para. Emílio Goeldi, Série Ciências Nat. 8, 291–323 (in Portuguese).
Teixeira, N.P., Bettencourt, J.S., Dall'Agnol, R., Moura, C.A.V., Fernandes, C.M.D., Pinho, S.C.C., 2005. Geoquímica dos granitos paleoproterozóicos da Suíte Granítica Velho Guilherme, Província Estanífera do Sul do Pará. Rev. Bras. Geociências 35 (2), 217–226.
Teixeira, N.P., 1999. Contribuição ao estudo das rochas granitóides e mineralizações associadas da Suíte Intrusiva Velho Guilherme, Província Estanífera do Sul do Pará. State University of Campinas. Ph.D. Thesis. Institute of Geosciences, p. 217 (in Portuguese).
Teixeira, N.P., Bettencourt, J.S., Moura, C.A.V., Dall'Agnol, R., Macambira, E.M.B., 2002. Archean crustal sources for Paleoproterozoic tin-mineralized granites in the Carajás Province, SSE Pará, Brazil: Pb–Pb geochronology and Nd isotope geochemistry. Precambrian Res. 119, 257–275.
Teixeira, W., Tassinari, C.C.G., Cordani, U.G., Kawashita, K., 1989. A review of the geochronology of the Amazonian Craton: tectonic implication. Precambian Res. 42, 213–227.
Whalen, J.B., Currie, K.L., Chappell, B.W., 1987. A-type granite: geochemical characteristics, discrimination and petrogenesis. Contributions Mineralogy Petrology 95, 407–419.
Whitney, D.L., Evans, B.W., 2010. Abbreviations for names of rock-forming minerals. Am. mineralogista 95 (1), 185.
Zhang, L.S., Scharer, U., 1996. Inherited Pb components in magmatic titanite and their consequence for the interpretation of U-Pb ages. Earth Planet. Sci. Lett. 138, 57–65.
Zhao, T.P., Zhou, M.F., 2009. Geochemical constraints on the tectonic setting of Paleoproterozoic A-type granites in the southern margin of the North China Craton. J. Asian Earth Sci. 36, 183–195.

3 GEOCHEMISTRY, GEOCRONOLOGY AND Nd ISOTOPES OF THE GOGÓ DA ONÇA GRANITE: A NEW A-TYPE PALEOPROTEROZOIC GRANITE OF CARAJÁS PROVINCE, BRAZIL

Mayara Fraeda Barbosa Teixeira

Roberto Dall'Agnol

João Orestes Schneider Santos

Luan Alexandre Martins de Sousa

Jean-Michel Lafon

Submetido: *Precambrian Research*

Dear Ms. Barbosa Teixeira,

Thank you for submitting your manuscript for consideration for publication in Precambrian Research. Your submission was received in good order.

To track the status of your manuscript, please log into EVISE® at: http://www.evise.com/evise/faces/pages/navigation/NavController.jspx?JRNL_ACR=PRECAM and locate your submission under the header 'My Submissions with Journal' on your 'My Author Tasks' view.

Thank you for submitting your work to this journal.

Kind regards,

Precambrian Research

CRYSTALLIZATION AGES OF PALEOPROTEROZOIC A-TYPE GRANITE SUITES AND RELATED GRANITES OF CARAJÁS PROVINCE, AMAZON CRATON: CONSTRAINTS FROM U-Pb GEOCHRONOLOGY OF ZIRCON AND TITANITE

Mayara Fraeda Barbosa Teixeira[1]*, Roberto Dall'Agnol[1,3], João Orestes Schneider Santos[2], Davis Carvalho de Oliveira[1], Claudio Nery Lamarão[1], Neal J. McNaughton[4]

[1]Graduate Course in Geology and Geochemistry, Geosciences Institute, Federal University of Pará (UFPA), Belém, PA, Brazil. E-mails: mayfraeda@gmail.com; robdal@ufpa.br;
[2]University of Western Australia, Centre for Exploration Targeting, Crawley, WA, 6009, Australia. E-mail: orestes.santos@bigpond.com
[3]Vale Institute of Technology (ITV), Belém, PA, Brazil. E-mail: roberto.dallagnol@itv.org.
[4] John de Laeter Centre for Isotope Research, Curtin University, Kent Street, Bentley, WA 6102, Australia. E-mail: N.McNaughton@curtin.edu.au
*corresponding author

Abstract

New U-Pb SHRIMP dating in zircon and titanite showed that the three large Paleoproterozoic A-type granite Suites and related granites from Carajás Province of the Amazon Craton (Brazil) were emplaced between 1880 Ma and 1857 Ma, with the main magmatic peak at 1880 Ma. We have identified also some particular ages not reported before: (i) Some granites of the Velho Guilherme and Jamon suites and of the Seringa Granite presented 1920 to 1900 m. y. old zircon and titanite crystals interpreted here as antecrysts from an earlier pulse of magma that were incorporated in the main later pulse of 1880 Ma; (ii) ages of 1865 Ma to 1857 Ma in the leucogranite facies of the Redenção and Bannach plutons, which indicate that the leucogranites of these plutons are younger than their ~1880 Ma old granites and were generated by independent magma pulses that are not cogenetic with the less evolved facies of the respective plutons; (iii) an age of 1732 ± 6 Ma obtained in the leucogranite facies of the Antônio Vicente pluton of the Velho Guilherme Suite that could represent a magmatic event in the Xingu Region not yet reported or, eventually, could correspond to an isolate hydrothermal event that allowed the growth of zircons. The more precise and detailed geochronological data obtained in the Paleoproteozoic A-type granites of Carajás Province, added to the information available in the literature, demonstrate the relevance of that magmatic event and indicate that the emplacement of those granites was done in about ~20 m.y., that means in a relatively short geological time. This 1880 Ma magmatic episode was also intense in other provinces of the Amazon Craton, where it is linked mostly to the formation of the Uatumã Silicic Large Igneous Province. This event was mostly extensional and is also registered in several cratons worldwide demonstrating its relevance in the tectonic evolution of Proterozoic continents.

Keywords: A-type magmatism, Paleoproterozoic, Orosirian, Carajás Province, Amazon Craton, U-Pb SHRIMP.

1. Introduction

The Amazon Craton (AC) is the largest stable tectonic unit of the South American Platform (Almeida et al., 1981). The craton has more than 5,000,000 km^2 and is composed of several geological provinces generated by accretional, arc-related processes and by recycling of continental crust (Santos et al., 2000; Tassinari and Macambira, 2004). According to Santos et al. (2000), it is formed by an Archean province (Carajás), followed along time by dominant Paleoproterozoic provinces (Transamazonic; Central Amazonian; Tapajós-Parima; Rondônia-Juruena and Rio Negro provinces) and locally by Mesoproterozoic provinces (Sunsás and K'Mudku provinces)– Fig. 1. Extensive anorogenic and post-tectonic magmatism occurred during Paleoproterozoic (Orosirian) forming widesppread batholiths and stocks concentrated in the Tapajós-Parima, Central Amazonian, and Carajás provinces.

A-type granites are present in different cratons of the world and different sources and formation processes were proposed to explain the origin of these rocks. A-type granites can be formed in extensional environment, either in tardi- to post-orogenic or anorogenic settings (Collins et al., 1982; Whalen et al., 1987; Sylvester, 1989; Eby, 1992; Bonin, 2007).

A large number of petrological, geochemical and geochronological (Rb-Sr whole-rock; Pb-Pb evaporation in zircon; U-Pb in zircon by TIMS-multigrain) analyses have been performed on the Paleoproterozoic (Orosirian) A-type suites from Carajás Province in the past decades. However, advances in geochronology permit to obtain in situ U-Pb analyses in zircon by SHRIMP (Sensitive High-Mass Resolution Ion Microprobe). This method provides higher spacial resolution and accuracy of the resulting ages and was not employed so far in the Orosirian A-type granites of Carajás Province. It can also provide information of the time duration of the magmatic evolution of different suites or intrusions.

Most anorogenic granite bodies (1880-1860 Ma) of Carajás Province are grouped into three main suites according to their mineralogical composition, geochemical characteristics, and the oxidation state of their magmas (Dall'Agnol et al., 2005, Dall'Agnol and Oliveira, 2007): a) oxidized granites represented by Jamon Suite (Dall'Agnol et al., 1999a; Oliveira, D.C. et al., 2009); b) moderately reduced A-type granites included in the Serra dos Carajás Suite (Machado et al., 1991), and c) reduced granites of Velho Guilherme Suite (Teixeira, 1999, Teixeira et al., 2002). However, there are other anorogenic, Paleoproterozoic A-type granites that constitute independent bodies

and have not been included in any of the three above suites: Seringa (Paiva Júnior et al., 2011), São João (Lima et al., 2014), Gogó-da-Onça (Teixeira et al., 2017), Gradaús (Carvalho, 2017) and Rio Branco (Santos P.A. et al., 2013) granites.

Nd isotope compositions of these Orosirian suites (T_{DM} model ages 3.35 to 2.60 Ga; ε_{Nd} values -12 to -8 at 1880 Ma; Dall'Agnol et al., 1999a, 2005; Rämö et al., 2002; Teixeira et al., 2002) constitute evidence that they are derived from the melt of Archean protoliths, possibly equivalent to units of the Carajás Province in depth. It was proposed that the origin of these suites is linked to the asthenospheric upwelling and magma production in the mantle. The underplating of mafic mantle magmas in the lower continental crust provided heat and induced its partial melting (Dall'Agnol et al., 2005).

In this paper, we report new high-precision zircon and titanite U–Pb ages for the A-type Orosirian granites of the Carajás Province of the Amazon Craton and combine then with previous data in order to discuss their crystallization ages, emplacement time and petrogenetic characteristics. The detailed geochronological data obtained by us demonstrate the relevance of the Paleoproteozoic magmatic event in the Carajás Province. The presence of this mostly extensional event in other provinces of the Amazon Craton and in several cratons worldwide is also discussed, as well as its relationship with the tectonic evolution of Proterozoic continents.

2. Geological setting

The Carajás Province (Figure 1) is located in the southeastern part of the Amazon Craton (Almeida et al., 1981) and hosts world-class mineral deposits of iron and iron oxide-copper-gold (IOCG), besides manganese, nickel, tungsten, tin, and gold-PGE deposits (Tallarico et al., 2005; Moreto et al., 2015; Bettencourt et al., 2016). The Carajás province is considered as the eastern domain of the Central Amazon Province (Tassinari and Macambira, 1999, 2004) or seen as an independent tectonic province (Santos et al., 2000). It is limited to the west by Proterozoic granitoids and volcano-pyroclastic assemblages mostly included in the Uatumã Supergroup (Juliani and Fernasdes 2010; Fernandes et al., 2011; Ferreira and Lamarão, 2013) of the Central Amazon Province, as proposed by Santos et al. (2000); to the east, by the Neoproterozoic-Cambrian Araguaia belt; to the north by the Bacajás Domain (Santos, 2003), that has Archean remnants but was mostly formed during the 2.2-2.06 Ga Trans-Amazonian orogen (Vasquez et al., 2008b); and to the south by the Santana do Araguaia Domain of Archean age but

reworked during the Paleoproterozoic (Vasquez et al., 2008; Corrêa and Macambira, 2014). The Carajás Province was divided initially into the Carajás and Rio Maria domains (Santos, 2003) and more recently into the Rio Maria, Sapucaia, and Canaã dos Carajás domains, and the Carajás Basin (Dall'Agnol et al., 2013).

In the southern part of the province, it occurs the Mesoarchean Rio Maria Domain composed of greenstone belts (3.0–2.90 Ga; Macambira and Lafon, 1995; Souza et al., 2001), and several Archean granitoids that comprises tonalitic-trondhjemitic series (TTG - 2.98 - 2.92 Ga; Almeida et al., 2011, 2017), sanukitoids (2.87 Ga; Althoff et al., 2000; Oliveira M.A. et al., 2009, 2011) and potassic leucogranite and leucogranodiorite-granite suites (ca. 2.87-2.86 Ga; Almeida et al., 2011, 2013).

The Sapucaia Domain is formed by strongly deformed Mesoarchean to Neoarchean units, including TTG (ca. 2.87 Ga; Santos, P.A. et al., 2013; Leite-Santos and Oliveira, 2014; Silva et al., 2014), sanukitoids (ca. 2.87 Ga; Gabriel and Oliveira, 2014; Gabriel et al., 2014), undated leucogranodiorites with high Ba and Sr (Teixeira et al., 2013) and A-type-like granitoids (Vila Jussara Suite; ca. 2.75 - 2.73 Ga; Oliveira, D.C. et al., 2010; Dall'Agnol et al., 2017).

The Canaã dos Carajás Domain encompasses several granitoids with different geochemical signatures. It includes: remnants of greenstone belts; the Bacaba Tonalite (ca. 3.0 Ga; Moreto et al., 2011); Canaã dos Carajás Granite and Rio Verde Trondhjemite (2.96 – 2.93 Ga; Feio et al., 2013); Late Mesoarchean granitoids, represented by the Campina Verde Tonalitic Complex, and Cruzadão, Bom Jesus, Boa Sorte, and Serra Dourada granites (2.87 – 2.83 Ga; Feio et al., 2013; Rodrigues et al., 2014; Moreto et al., 2015); and, finally, Neoarchean granites of the Planalto suite (ca 2.75 to 2.73 Ga; Feio and Dall'Agnol., 2012; Huhn et al., 1999; Cunha et al., 2016), and associated charnockitic plutons (Pium Diopside Norite; Santos, R.D. et al., 2013; Feio et al., 2012, 2013).

The Neoarchean Carajás Basin is composed dominantly of volcano-sedimentary sequences included in the Itacaiúnas Supergroup (Hirata et al., 1982; DOCEGEO 1988; Machado et al., 1991; Tallarico et al., 2005), which is formed by mafic to intermediate metavolcanic rocks and banded iron formations aged of ca. 2.76 Ga (Gibbs et al., 1986; Machado et al., 1991) or a little younger (2749 ± 6.5 and 2745 ± 5 Ma, SHRIMP U-Pb ages obtained in mafic metavolcanic rocks of the Parauapebas Formation; Martins et al., 2017). The rocks of the Itacaiúnas Supergroup are cross-cut by the Estrela Suite, Igarapé Gelado and Serra do Rabo Neoarchean granites (Barros et al., 1997, 2009; Sardinha et al., 2006).

These tectonic domains were stabilized at the end of the Archean and remained stable until ca. 1880-1860 Ma when occurred the generation and emplacement of A-type granites (Dall'Agnol et al., 1994, 1999b, 2005).

3. Geological background of the A-type Orosirian granites of the Carajás Province

The anorogenic granites are widespread in the Rio Maria, Sapucaia, and Canaã dos Carajás domains and also in the Carajás basin (Fig. 1). These plutons were emplaced in an extensional tectonic setting and are coeval with WNW–ESE to NNW–SSE striking diabase and granite porphyry dikes (Dall'Agnol et al., 2005; Oliveira, D.C. et al., 2010; Silva et al., 2016). These three suites are composed of 1.89 Ma to 1.86 Ma (Table 1) undeformed granites forming stocks and batholiths with geochemical and petrological affinities with Mesoproterozoic rapakivi granite suites of Laurentia-Baltica (Anderson and Smith, 1995; Anderson and Morrison, 2005; Emslie, 1991; Rämö and Haapala, 2005; Heinonen et al., 2012), and also with similar granites of the Amazon Craton such as those of Rondônia Suite, Surucucus Suite, Mucajaí Complex and Parguaza Granite (Dall'Agnol et al., 1994; Fraga et al., 2009; Bettencourt et al., 2016; Sidder and Mendoza, 1991).

A synthesis about the main geologic features of the Jamon, Velho Guilherme, and Serra dos Carajás suites, as well as of the Seringa, São João, and Gogó-da-Onça independent plutons is given in the following.

3.1 Jamon Suite

The plutons of the Jamon Suite and associated coeval mafic and felsic dikes intruded Archaean rocks (TTG, greenstone belts, sanukitoids) of the Rio Maria Domain (Figure 1c). This suite is represented by the Jamon, Musa, Marajoara, Manda-Saia, Redenção, and Bannach intrusions (Gastal, 1987; Dall'Agnol et al., 1999a, b, 2005; Almeida et al., 2006; Dall'Agnol and Oliveira 2007; Oliveira, D.C. et al., 2008, 2009). Pedra Preta wolframite deposits are related to the Musa granite (Javier-Rios et al., 2003).

Except for a local magmatic foliation observed near the border of the Redenção and Bannach plutons (Oliveira, D.C., 2008), the plutons of the Jamon Suite are unfoliated. The Archean country rocks were affected by hornblende hornfels contact metamorphism and contact aureoles were identified around the Jamon and Musa plutons (Dall'Agnol et al., 1994, 1999a, b). Angular xenoliths and enclaves of the Archean rocks are commonly observed near the border of the Jamon, Musa, Redenção, and Bannach plutons

(Dall'Agnol et al., 1999a; Gastal, 1987; Oliveira D.C. et al., 2009; Almeida et al., 2006). Local mingling features involving distinct granite facies were observed in the Redenção and Bannach plutons (Oliveira, D.C. et al., 2009). The granites of the Jamon Suite contain magnetite and titanite as primary accessory minerals and were formed in moderately oxidizing conditions around the nickel/nickel oxide (NNO) oxygen buffer (Dall'Agnol et al., 1997, 1999a, b).

Swarms of mafic and felsic dikes, including locally composite dikes, are associated with the Jamon Suite (Dall'Agnol et al., 2005; Oliveira, D.C. et al., 2009). The felsic rock in the composite dike (1885 ± 4 Ma; Pb-Pb zircon age; Table 1) shows evidence of mingling with the associated mafic dike indicating that they are contemporaneous.

The plutons of the Jamon Suite are composed of monzogranite and subordinate syenogranite with biotite or, in the less evolved facies, biotite-amphibole ± clinopyroxene. The accessory minerals are zircon, apatite, magnetite, ilmenite, allanite, and titanite (Dall'Agnol et al., 1999a, b; Oliveira, D. C. et al., 2009). Rapakivi textures are more common in Redenção and Bannach plutons (Oliveira, D.C. et al., 2009; Almeida et al., 2006).

The facies distribution within most of the plutons of the suite is approximately concentric with the less evolved granites occupying the outer zones and the more evolved in the central area of each body. In the Jamon, Redenção, and Bannach plutons the main facies are related by fractional crystallization (Dall'Agnol et al., 1999c). However, in the central portions of the Redenção and Bannach plutons, there are small stocks of leucogranites which probably were derived from an independent magma (Oliveira, D.C. et al., 2009; Almeida et al., 2006; Mesquita et al., submitted).

Based in gravimetric and magnetic anisotropy geophysical studies, Oliveira, D.C. et al. (2008, 2010) concluded that the Bannach and Redenção plutons are sheeted-like intrusions and proposed for those plutons an intrusion model in which the magmas ascended through dikes and were amalgamated in sheeted or tabular bodies.

3.2 Serra dos Carajás Suite

The Serra dos Carajás, Cigano, and Pojuca plutons constitute the Serra dos Carajás Suite (Dall'Agnol et al., 2005). The ages of these granites were determined by Machado et al. (1991; cf. Table 1). They are located in the Carajás Basin, in the northern part of the

Carajás Province (Figure 1). These granites contain magnetite but they show high FeOt/(FeOt+MgO) in whole rock and mafic minerals and are classified as moderately reduced A-type granites (Dall'Agnol et al., 2005). Chalcopyrite, molybdenite, and Sn mineralization are spatially associated with hydrothermally altered zones within Serra dos Carajás granite cupola (Javier-Rios et al., 1995; Bettencourt et al., 2016).

The sedimentary rocks of the Águas Claras Formation were affected by the emplacement of the Serra dos Carajás pluton and show recrystallization and neoformed tourmaline crystals (Javier-Rios et al., 1995). Fracture plans without preferential orientation were developed in the contact zone and should result in hydraulic fracturing under weak or nonexistent tectonic tension. The magma emplacement has taken place under high liquid/crystal ratio, implying high viscosity contrast between the magma and the country rocks (Javier-Rios et al., 1995). Sparse rapakivi textures are common in this granite (Dall'Agnol et al., 1994). Decimeter-sized enclaves were observed in the Cigano pluton, which is composed of (amphibole)-biotite monzogranite with subordinate syenogranite. Disseminated molybdenite was observed in quarries of the altered biotite monzogranite.

The accessory minerals of Serra dos Carajás Suite are zircon, apatite, magnetite, ilmenite, and allanite. Primary titanite is rare or absent, fluorite is common, and tourmaline is sometimes present, possibly related to exchanges with sedimentary country rocks (Javier-Rios et al., 1995; Barros et al., 1995; Dall'Agnol et al., 2005).

The absence of lineation and foliation in the plutons of the Serra dos Carajás Suite, as well as the sharp contacts and overall discordant character of the plutons, all indicate relatively low pressure for their emplacement, probably on the order of 2.0 ± 1.0 kbar (Dall'Agnol et al., 2005).

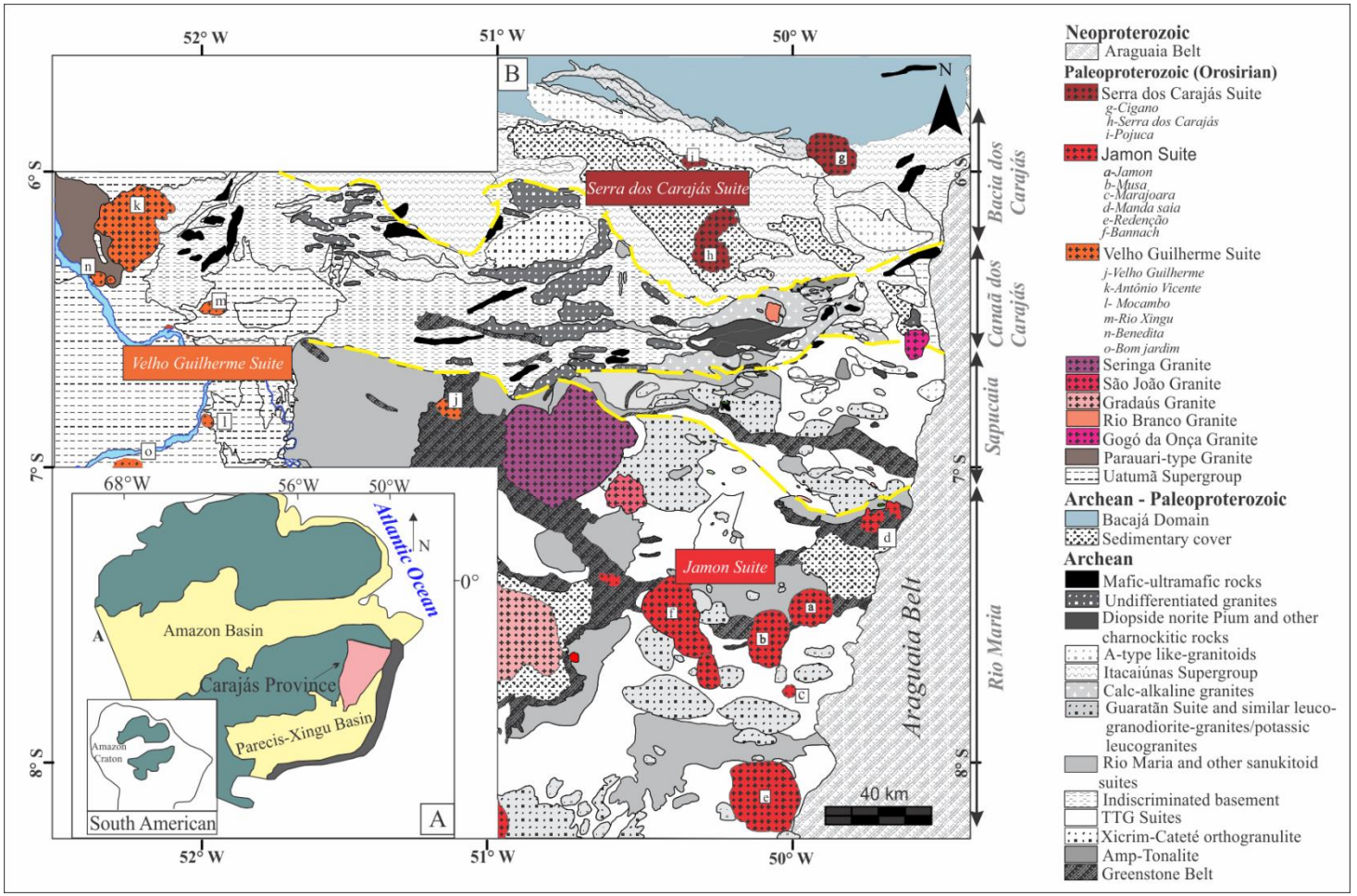

Fig.1. (A) Location of the Carajás Province in the Amazon Craton; (B) Simplified geologic map of Carajás Province highlighting the A-type Paleoproterozoic Granites of the Province (Dall'Agnol et al., 2005; Vasquez et al., 2008; Almeida et al., 2011; Oliveira et al., 2010; Feio et al., 2013; Silva et al., 2014; Teixeira et al., 2013; Santos, P.A. et al., 2013; Gabriel and Oliveira, 2014; Rodrigues et al., 2014, modified), and the approximate limits of the tectonic Archean domains of Carajás Province (dashed yellow lines; Dall'Agnol et al., 2013).

3.3 Velho Guilherme Suite

The Velho Guilherme Suite is composed of the Velho Guilherme, Antônio Vicente, Mocambo, Rio Xingu, Benedita, and Bom Jardim granites (Teixeira 1999; Teixeira et al., 2002; Lamarão et al., 2012). These rocks outcrop in the Xingu region and cut undifferentiated Archean rocks, intermediate to felsic volcanic rocks of the Uatumã group and the Orosirian Parauari granite. There are tin and subordinate wolframite and tantalite-columbite mineralization associated with the plutons of the suite.

The plutons of Velho Guilherme Suite are composed of syenogranite, monzogranite, and subordinated alkali-feldspar granite. The more evolved leucogranitic facies are intensely affected by late to postmagmatic hydrothermal alteration. Primary concentrations of cassiterite are associated with greisen zones and albitized granites (Dall'Agnol et al., 1993; Teixeira, 1999).

The dominant syenogranite does not contain titanite or significant magnetite and display low magnetic susceptibility values which indicate crystallization under reducing conditions on or below those of the FMQ (fayalite-magnetite-quartz) buffer. Fluorite, topaz monazite, thorite, xenotime, and columbite are common accessory minerals (Dall'Agnol et al., 1993; Teixeira et al., 2002; Lamarão et al., 2012).

The country rocks are affected by contact metamorphism and the contact aureoles grade outward from hornblende hornfels to albite/epidote hornfels facies (Dall'Agnol, 1980; Teixeira, 1999). The absence of foliated structures in the interior of the plutons, their discordant character and the presence of micrographic intergrowths suggest a shallow level of emplacement.

The different facies of the plutons of the Velho Guilherme Suite are related by fractional crystallization. The more evolved facies associated with tin mineralization are the product of fractionation crystallization and interaction with late- to post-magmatic fluids (Dall'Agnol et al., 1993; Teixeira et al., 2005).

3.4 Seringa, São João, Rio Branco, and Gogó-da-Onça granites

The Seringa (Paiva Jr. et al., 2011) and São João (Lima et al., 2014) granites outcrops in the northern part of the Rio Maria Domain (Fig. 1b). They are essentially composed of moderately reduced monzogranite to reduced syenogranite, with biotite and amphibole as mean mafic minerals and zircon, apatite, magnetite, ilmenite, and allanite as the accessory phases. Primary titanite is rare or absent. The Seringa Granite includes

angular enclaves of the country rocks, which indicates a high viscosity contrast between the Seringa magma and Archean rocks similar to that observed in the three Paleoproterozoic suites. Felsic dikes cut the Seringa Granite but were not observed in the São João Pluton (Lima et al., 2014).

The Rio Branco Granite (Santos, P.A. et al., 2013) intrudes the Mesoarchean Cruzadão Granite. It is located in the Canaã dos Carajás Domain nearby the Sossego copper mine (Fig. 1b). It is constituted by syenogranites containing commonly chloritized biotite and fluorite, allanite, and zircon as accessory minerals. Albitization and subordinate greisenization are the main alteration processes that affected locally the granite. Albite, fluorite, topaz, chlorite, muscovite, siderophyllite, and iron oxides are the secondary phases.

The Gogó-da-Onça Granite (GOG; Teixeira et al., 2017) is a stock located in the northeast of Carajás Province, in the border between the Sapucaia and Canaã dos Carajás domains (Fig. 1). The granitic pluton is comprised of reduced granodiorite, monzogranite, and syenogranite. Amphibole is the mean mafic mineral followed by biotite. Accessory minerals are zircon, titanite, allanite, apatite, magnetite, and ilmenite. Titanite is absent in the syenogranite facies.

Paiva Jr. et al. (2011) and Lima et al. (2014) argue that Seringa and São João granites display strong similarities with the granites of the Serra dos Carajás Suite, and should be included in that suite. Teixeira et al. (2017) also consider that the GOG has a strong affinity with the granites of the Serra dos Carajás Suite, whereas Santos, P.A. et al. (2013) identified in the Rio Branco Granite strong similarities with the Velho Guilherme Suite and, subordinately, with the Serra dos Carajás Suite.

Table 1 – Selected geochronology data of the Paleoproterozoic (Orosirian) A-type granites from Carajás Province

Pluton	material	Age in Ma (Reference)	Method
SERRA DOS CARAJÁS SUITE			
Cigano	zircon	1883 ± 2 (1)	U-Pb (TIMS)
Serra dos Carajás	zircon	1880 ± 2 (1)	U-Pb (TIMS)
Pojuca	zircon	1874 ± 2 (1)	U-Pb (TIMS)
VELHO GUILHERME SUITE			
Velho Guilherme	whole-rock	1873 ± 13 (2)	Pb-Pb isochron
Velho Guilherme	zircon	1853.7 ± 6.2 (13)	U-Pb (LA-ICP-MS)
Antônio Vicente	zircon	1867 ± 5 (6)	Pb evaporation
Mocambo	zircon	1865 ± 2 (6)	Pb evaporation
Bom Jardim	zircon	1867 ± 1 Ma (11)	Pb evaporation
Serra Queimada	zircon	1882 ± 12 (8)	Pb evaporation
Rio Xingu	zircon	1866 ± 2 (6)	Pb evaporation
JAMON SUITE			
Musa	zircon	1883 ± 5 (1)	U-Pb (TIMS)
Musa	titanite	1884 ± 5 (1)	U-Pb (TIMS)
Jamon	zircon	1885 ± 32 (5)	Pb evaporation
Redenção	whole-rock	1870 ± 68 (3)	Pb-Pb isochron
Felsic dikes	zircon	1885 ± 2 (7)	Pb evaporation
Felsic dikes	zircon	1886 ± 4 (7)	Pb evaporation
OTHER OROSIRIAN GRANITES AND DIKES			
Seringa	zircon	1895 ± 1 (9)	Pb evaporation
		1892± 30 (4)	
São João	zircon	1890 ± 2 (10)	Pb evaporation
Gogó-da-Onça	zircon	1869 ± 4 (14)	U-Pb SHRIMP
		1866 ± 10 (14)	
		1878 ± 9 (14)	
	titanite	1879 ± 15 (14)	
		1872 ± 13 (14)	
Felsic dikes	zircon	1880.9 ± 6.7 (12)	U-Pb (SHRIMP)
Felsic dikes	zircon	1881.9 ± 8.8 (12)	U-Pb (SHRIMP)

Data sources: (1) Machado et al., (1991); (2) Rodrigues et al., (1992); (3) Barbosa et al., (1995); (4) Avelar (1996); (5) Dall'Agnol et al., (1999a); (6) Teixeira et al., (2002); (7) Dall'Agnol et al., (2005); (8) Pinho et al., (2006); (9) Paiva Jr., (2009); (10) Lima (2011); (11) Lamarão et al., (2012); (12) Silva et al., (2016); (13) Antonio et al., (2017); (14) Teixeira et al., (2017).

4. Geochemistry

Whole rock geochemical data of the Orosirian granites from Carajás Province have been previously discussed (Jamon and Musa: Gastal, 1987; Dall'Agnol et al., 1999a, 2005; Redenção: Oliveira, D.C. et al., 2009; Bannach: Almeida et al., 2006; Velho Guilherme: Dall'Agnol et al., 1993, 1994; Teixeira et al., 2002, 2005; Serra dos Carajás: Barros et al., 1995; Javier-Rios et al., 1995; Seringa: Paiva Jr. et al., 2011; São João: Lima

et al., 2014; Rio Branco: P.A. Santos et al., 2013; Gogó-da-Onça: Teixeira et al., 2017) and they will be just sumarized here.

All granites display the general characteristics of A-type granites (see Dall'Agnol et al., 2012). They plot in the A-type field in the Zr+Nb+Ce+Y vs FeO_t/MgO diagram of Whalen et al. (1987) (Fig.2a) and show geochemical affinities with within-plate granites (Fig. 2b). The $FeO_t/(FeO_t+MgO)$ ratios normally are higher than 0.8 placing the granites in the ferroan A-type granite field of Frost et al. (2001) (Fig.2c). The Jamon Suite granites plot in the oxidized A-type field whereas the other granites plot mostly in the reduced A-type field as shown in $FeO_t/(FeO_t+MgO)$ vs. Al_2O_3 diagram (fields from Dall'Agnol and Oliveira, 2007) (Fig. 2d). According to the discrimination diagrams of Eby (1992), they have also a geochemical affinity with the A_2-subtype granites (Fig. 2e).

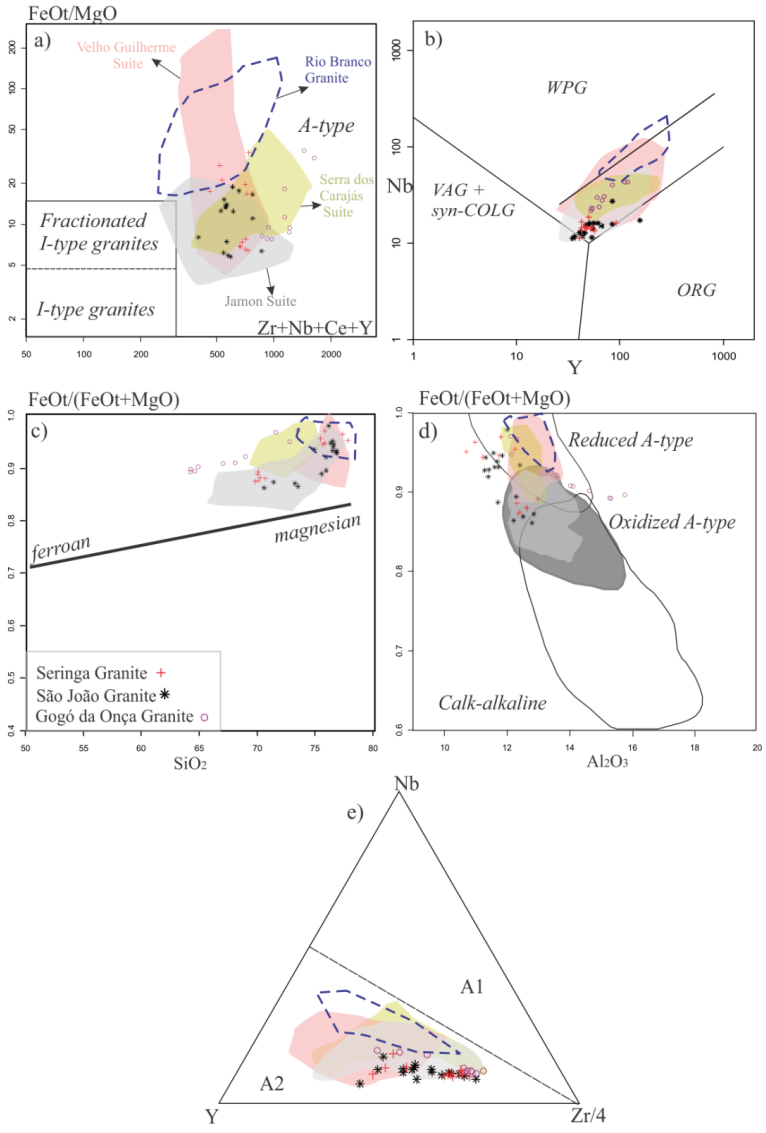

Fig. 2. Geochemical classification diagrams for Paleoproterozoic granites of Carajás Province. (a) FeO_t+MgO vs (Zr+Nb+Ce+Y) discrimination diagram with fields of Whalen et al. (1987); (b) Nb-Y discrimination diagram (fields of Pearce et al., 1984); (c) (FeO_t/FeO_t+MgO) vs SiO_2 diagram (Frost et al., 2001); (d) $FeO_t/(FeO_t$+MgO) vs. Al_2O_3

diagram (fields of calc-alkaline, reduced, and oxidized A-type granites of Dall'Agnol and Oliveira, 2007); (e) Y-Nb-Zr/4 plot (A1 and A2 fields of Eby, 1992). Data sources: Jamon Suite [Dall'Agnol et al. (1999c), Dall'Agnol and Oliveira (2007); Almeida et al. (2006)]; Velho Guilherme Suite [Dall'Agnol et al. (1993); Teixeira (1999); Teixeira et al. (2005)]; Serra dos Carajás Suite [Barros et al. (1995), Javier-Rios et al. (1995)]; Seringa Granite (Paiva Júnior et al., 2011); São João Granite (Lima et al., 2014); Rio Branco Granite (P.A. Santos et al., 2013); Gogó-da-Onça Granite (Teixeira et al., 2017).

5. Analytical procedures for U–Pb isotopic analyzes by Sensitive High-Resolution Ion Microprobe (SHRIMP)

Zircon and titanite were extracted from 1–4 kg of whole-rock of selected samples using standard crushing, sieving (60 mesh), heavy liquid (LST), and magnetic separation (Frantz) techniques. The mineral selection was made by hand picking using a binocular microscope. The selected grains were mounted on double-sided sticky tape, cast in epoxy resin together with fragments of standards, and polished to expose surfaces suitable for in situ isotopic analysis.

Back-scattered electrons (BSE) images of the grains were obtained in Tescan Vega3 at the Centre for Microscopy, Characterization, and Analysis (CMCA) of the University of Western Australia. Images were made to obtain information about the internal structure of the grains and to select the best locations for isotopic analysis. The epoxy mounts were then cleaned and gold coated for SHRIMP sessions.

U-Pb zircon and titanite isotopic ratios were determined in situ by SHRIMP II (De Laeter and Kennedy, 1998) at Curtin University (Perth, Western Australia), and the isotopic compositions of the minerals were determined using methods based on those of Compston et al. (1992).

Circular spot analyses of 10 to 25 μm in diameter were performed on selected zircon and titanite grains to determine U–Th–Pb concentrations and Pb isotope composition. Zircons standards were BR266 (559 Ma, 903 ppm U; Stern, 2001) and M257 (561 Ma, 840 ppm U; Nasdala et al., 2008). Titanite standard was Khan (522.2 Ma, 680 ppm U; Heaman, 2009). For each spot analysis, initial 60–90s were used for pre-sputtering to remove the gold and avoid common Pb contamination from the coat.

The analytical results are reported with 1σ error. Data reduction of measured ratios for zircon and titanite was performed using the software SQUID 2.5 (Ludwig, 2009), and results were plotted on concordia diagrams using ISOPLOT 3.70 software (Ludwig, 2003). Error ellipses on concordia plots are shown at the 95% confidence level (2σ).

6. Geochronological results

Twenty three samples of ten distinct Paleoproterozoic plutons of the Carajás Province were investigated by U-Pb SHRIMP geochronology using zircon and, for the granites of the Jamon Suite, also titanite (Table 2). The selected samples are representative of the three suites and most independent plutons of the A-type anorogenic magmatism of Carajás. Analytical data are given in Supplementary tables 1 to 5. Recent results obtained in the Gogó da Onça Granite (Teixeira et al., 2017) using the same methods are also presented.

6.1 Serra dos Carajás Suite

Samples of biotite-hornblende syenogranite of Serra dos Carajás Granite (ECR-SC-01), biotite-hornblende monzogranite and biotite-monzogranite of Cigano Granite (ECR-CG-14A and CIG-1, respectively) were selected as representative for U-Pb analyses of this suite. All zircon grains are subhedral to euhedral and form transparent and colorless short to long prisms, with 100-250 μm; they are strongly to moderately fractured or without significant fracture; internal oscillatory zoning and irregular metamict areas are observed in some grains but there is no evidence of older cores (Fig. 3a, b, c). Monazite inclusions were observed in zircon of sample CIG-1, but not large enough to be analysed by SHRIMP.

The U–Pb isotope data of zircon of the selected granites of this suite are listed in Supplementary Table 1 and graphically displayed in concordia diagram (Fig. 4).

Serra do Carajás Granite

Eight grains of zircon of biotite-hornblende syenogranite (ECR-SC-01) were analysed in sets of six scans during one analytical session. They show concentration ranges of U from 189 to 687 ppm (except for one spot with 1315 ppm U), and 66 to 395 ppm of Th with Th/U ratios of 0.21 to 0.64. Individual spot ages range from 1869 ± 9 Ma to 1898 ± 17 Ma (Supplementary Table 1). The upper concordia intercept age is 1882 ± 10 Ma with MSWD of 0.96 (Fig. 4a). Most zircons have less than 10% discordance, except two spots that were excluded from the age calculation but are presented in the analytical results: the analysis N1619D.2-1, which has a very high U content (1315 ppm), is very discordant and yielded a significantly younger $^{207}Pb/^{206}Pb$ age of 893 ± 21 Ma (Supplementary Table 1), and the spot N1619D.7-1 that is 33% discordant despite showing a coherent age.

The zircons do not show any evidence of metamorphic or hydrothermal alteration (Fig. 3 a) and the age of 1882 ± 10 Ma (Fig. 4a) is interpreted as the time of zircon crystallization.

Cigano Granite

Six grains of zircon (Fig. 3b) of biotite-hornblende monzogranite (ECR-ECG-14) were analyzed in sets of six scans during one analytical session, and results are presented in Supplementary Table 1 and in the concordia plot of Fig. 4b. Uranium contents vary from 242 to 799 and those of Th from 81 to 500 ppm resulting Th/U ratios of 0.11 to 0.77. Individual spot ages range from 1863 ± 8 Ma to 1892 ± 8 Ma. The upper concordia intercept age for this sample is 1884 ± 4 Ma with MSWD of 2.0 (Fig. 4b). Most zircons have less than 10% discordance.

Five spot analyses on zircon (Fig. 3c) of biotite monzogranite (CIG-1) were performed in sets of six scans during two analytical sessions, and results are presented in Supplementary Table 1 and in the concordia plot of Fig. 4c. They show uranium contents between 430 to 759 (except for one spot with 1092 ppm U). Th contents vary from 308 to 600 ppm and Th/U ratios between 0.57 and 0.77. Individual spot ages range from 1878 ± 8 Ma to 1888 ± 9 Ma. The upper concordia intercept age for this analysis is 1884 ± 3 Ma with MSWD of 1.3 (Fig. 4c). All zircons are less than 10% discordant.

The magmatic ages obtained for the above three samples of Serra dos Carajás Suite are quite similar and overlap on the analytical error, and we interpret these as reflecting the crystallization age of this suite.

6.2 *Velho Guilherme Suite*

Three different varieties of rocks of this suite were investigated by U-Pb SHRIMP: albitized leucogranite (L-42) from the Velho Guilherme pluton and hornblende-biotite syenogranite (R-10) and leucogranite (R-05) both of the Antônio Vicente Granite.

Table 2 - Summary of the rock samples of the Paleoproterozoic granites of the Carajás Province dated in this work

Sample	Rock	Unit	Northing	Easting	References
ECR-SC-01	biotite-hornblende syenogranite	*Serra dos Carajás Granite*			Javier-Rios et al. (1995)
ECR-CG-14A	biotite-hornblende monzogranite	*Cigano Granite*			Teruiya et al. (2008)
CIG-1	biotite monzogranite	*Cigano Granite*			Teruiya et al. (2008)
L-42	albitized leucogranite	*Velho Guilherme Granite*			Dall'Agnol et al. (1993)
R-10	hornblende-biotite syenogranite	*Antônio Vicente Granite*			Dall'Agnol et al. (1993)
R-5	leucogranite	*Antônio Vicente Granite*			Dall'Agnol et al. (1993)
PROA-11	biotite-hornblende monzogranite	*Jamon Granite*			Dall'Agnol et al. (1999a)
KM-144B	biotite-hornblende monzogranite	*Musa Granite*	-7.6697	-50.0370	Dall'Agnol et al. (1999a)
CREMU-37A	biotite monzogranite	*Musa Granite*	-7.5091	-50.0443	Dall'Agnol et al. (1999a)
KM-77A	hornblende-biotite monzogranite	*Musa Granite*	-7.5378	-50.0874	Dall'Agnol et al. (1999a)
DC-111	even-grained biotite monzogranite	*Redenção Granite*	-8.0351	-50.1765	Oliveira D.C et al. (2009)
DC-120	seriate leucomonzogranite	*Redenção Granite*	-8.1013	-50.0601	Oliveira D.C et al. (2009)
DCR-42A	medium even-grained leucomonzogranite	*Redenção Granite*	-8.1402	-50.1408	Oliveira D.C et al. (2009)
ADR-136I	cumulate granite	*Bannach Granite*	-7.4142	-50.3516	Almeida et al. (2006)
ADR-35A	fine-grained leucomonzogranite	*Bannach Granite*	-7.4761	-50.4469	Almeida et al. (2006)
AC-45	heterogranular leucosyenogranite	*Seringa Granite*	-6.5278	-50.4389	Paiva Jr. et al. (2011)
AC-59	coarse-grained biotite-hornblende monzogranite	*Seringa Granite*	-6.5077	-50.5401	Paiva Jr. et al. (2011)
AC-85	coarse-grained hornblende-biotite monzogranite	*Seringa Granite*	-6.5162	-50.5021	Paiva Jr. et al. (2011)
AC-42	heterogranular hornblende-biotite syenogranite	*Seringa Granite*	-6.5475	-50.4446	Paiva Jr. et al. (2011)
PC-03B	hornblende-biotite syenogranite	*São João Granite*	-7.0485	-50.5177	Lima et al. (2014)
PC-21	biotite monzogranite	*São João Granite*	-7.0612	-50.5891	Lima et al. (2014)
PCM-10	biotite-hornblende monzogranite	*São João Granite*	-7.0600	-50.5198	Lima et al. (2014)
PCM-13	biotite-hornblende syenogranite	*São João Granite*	-7.0858	-50.5244	Lima et al. (2014)
PFR-18B	biotite-hornblende granodiorite	*Gogó-da-Onça Granite*	-6.3741	-49.3507	Teixeira et al. (2017)
PFR-22	biotite-hornblende monzogranite	*Gogó-da-Onça Granite*	-6.3653	-49.3636	Teixeira et al. (2017)
PFR-19B	hornblende-biotite syenogranite	*Gogó-da-Onça Granite*	-6.3735	-49.3514	Teixeira et al. (2017)

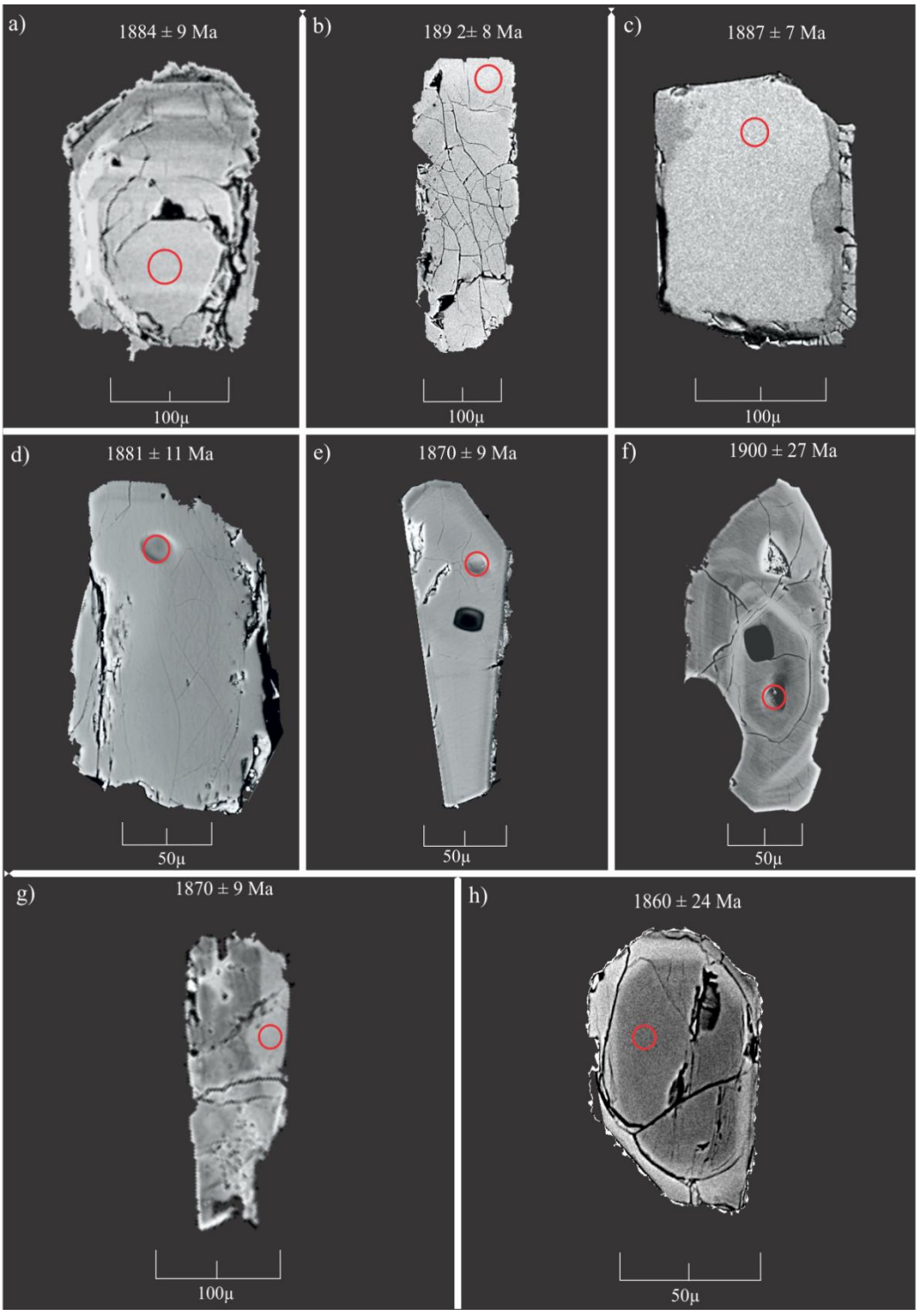

Fig. 3. BSE images showing the analytical pits on zircons of the: Serra dos Carajás Suite - (a) ECR-SC-01 (Serra dos Carajás pluton), (b) ECR-CG-14A, (c) CIG1 (Cigano pluton); Velho Guilherme Suite: (d) L-42 (Velho Guilherme pluton), (e, f), R-10, (g) R-5 (Antonio Vicente pluton); Jamon Suite (h) PROA-11 (Jamon pluton).

Most zircons of the three samples (L-42, R-10, and R-5) are subhedral to euhedral, and form short to long prisms, with lengths of 100-250 µm, fractured, with common internal oscillatory zoning, and no evidence of older cores (Fig. 3d, e, f, g). They are transparent and light yellow and they have apatite and less often xenotime and monazite inclusions. Zircons from the leucogranite (R-5) are sometimes corroded with irregular

metamict areas and recrystallized zones (Fig. 3g) indicating that the crystals were affected by hydrothermal processes.

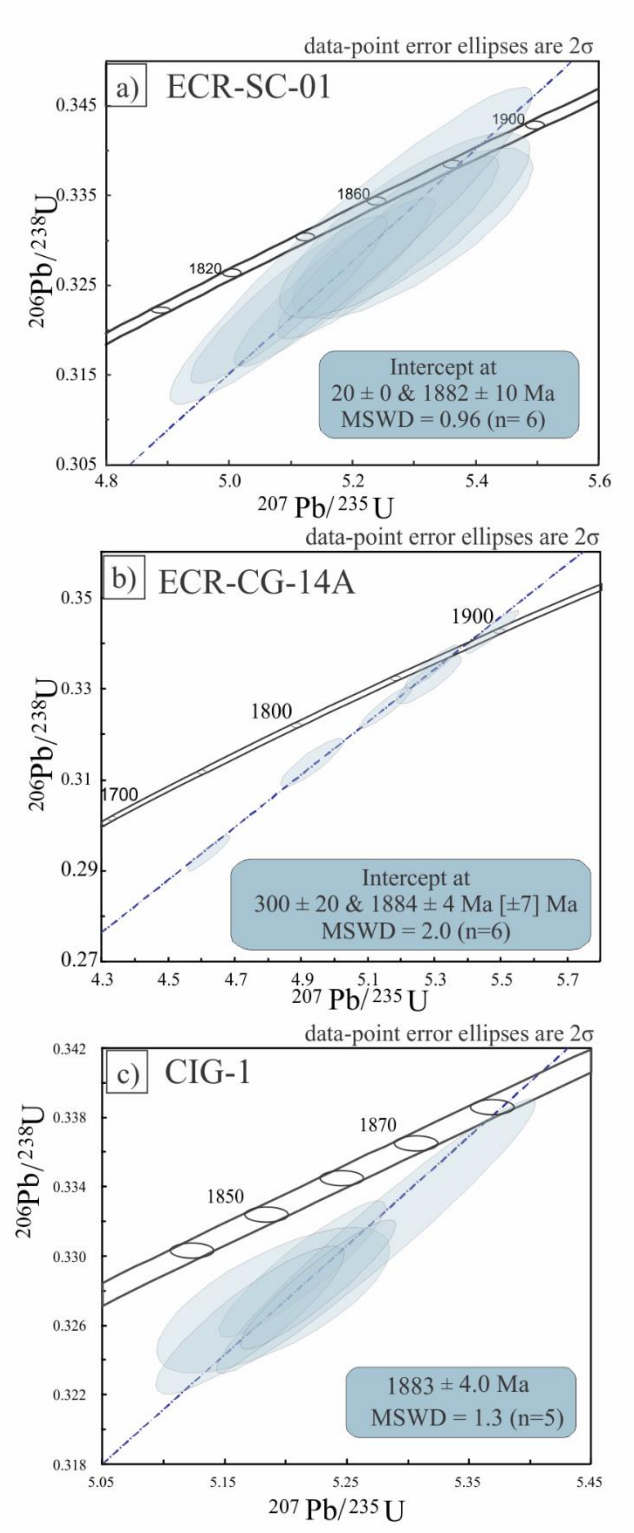

Fig. 4. Concordia diagrams showing U-Pb zircon SHRIMP ages of three samples of Serra dos Carajás Suite [a) of the Serra dos Carajás pluton; b) and c) of the Cigano pluton]: (a) U–Pb concordia plot of biotite-hornblende syenogranite (ECR-SC-01); (b) U–Pb concordia plot of biotite-hornblende monzogranite (ECR-SC-14A); (c) U–Pb concordia plot of biotite monzogranite (CIG-1).

The U–Pb isotope data of zircon for this Suite are listed in Supplementary Table 2 and graphically displayed in concordia diagrams (Fig. 5).

Velho Guilherme Granite

Nine grains of the albitized leucogranite (L-42) were analyzed in sets of six scans during two analytical sessions. The uranium and Th contents are, respectively, between 93 to 387, and 55 to 283 ppm with resulting Th/U ratios of 0.52 to 0.76. Individual spot ages range from 1867 ± 16 Ma to 1891 ± 7 Ma. The upper concordia intercept age for this sample is 1882 ± 6 Ma with MSWD of 2.1 (Fig. 5a) which is interpreted as the crystallization age of the sample. All zircons are less than 10% discordant.

Antônio Vicente Granite

Ten grains of zircon of hornblende-biotite syenogranite (R-10) were analyzed in sets of six scans during one analytical session. Zircon shows high uranium and Th content varying, respectively, between 409 to 781 ppm, and 189 to 563 ppm, except for 3 zircon grains (N1634A.6-2, N1634A.6-5, N1634A.2-2) that have low contents of those elements (Supplementary Table 2). Th/U ratios are between 0.29 and 1.30. Most analyzed zircon grains have less than 10% discordance but show two age groups: Two crystals define an upper intercept age of 1900 ± 19 Ma and MSWD of 0.0024 (Fig. 5b); the other eight crystals have a younger upper intercept age of 1878 ±3 Ma and MSWD of 1.4 (Fig. 5c). The latter age is similar to the zircon ages obtained for most anorogenic granites of the Carajás Province (Table 1) and it is interpreted as the crystallization age of the Antônio Vicente pluton. The age of 1900 ± 19 Ma is comparatively older. Its meaning is not evident and it will be discussed in the next session.

Zircons from R-5 leucogranite were analyzed in sets of six scans during two analytical sessions. They have uranium contents between 133 and 598 (except the grains N1635F.6-1 and N1635F.6-2, with 2210 and 1679 ppm, respectively). Th vary between 79 to 453 ppm and Th/U ratios are between 0.62 to 0.81, with low ratios for the grains with highest U (Supplementary Table 2). Most zircons have less than 10% discordance, except one spot (N1635F.4-1; Supplementary Table 2 of the Appendix) that was excluded from the zircon age calculation because the grain presented a high grade of discordance. The eight remainder spot analysis of zircons yielded two age populations: four grains define a concordia age of 1724 ± 14 Ma with MSWD of 1.8 (Fig. 5c), and four other crystals yield an upper intercept age of 1882 ± 15 Ma with MSWD of 0.36 (Fig. 5c).

The age of 1882 ± 15 Ma is similar and overlap to the zircon age obtained for the other facies of this granite and it is the best estimate of the crystallization age of the rock. The younger age of 1724 ± 14 Ma was not reported so far in the Orosirian granites of the Carajás Province and will be discussed in the next session. It is important to emphasize that there is no detectable difference in age between cores and rims zones in the analyzed zircons.

6.3 *Jamon Suite*

To constrain the age of the Jamon Suite, we dated zircon and titanite of the Jamon, Musa, Redenção, and Bannach Granites. As representative of the Jamon pluton we selected a biotite-hornblende monzogranite (PROA-11); for the Musa Granite different facies were analysed: hornblende-biotite monzogranite (KM-144B), biotite-hornblende monzogranite (KM-77), and biotite monzogranite (CRE-MU-37A); Three facies of Redenção pluton were dated: coarse even-grained biotite monzogranite (DC-111), seriate leucomonzogranite (DC-120), and a medium even-grained leucomonzogranite (DCR-42). Two facies were selected in Bannach pluton: cumulate granite (ADR-136I), and a fine-grained leucomonzogranite (ADR-35A).

The U–Pb isotope data of zircon for this suite are listed in Supplementary Table 3.

Jamon Granite (PROA11)

Zircons from the biotite-hornblende monzogranite of the Jamon Pluton are transparent to light brown, subhedral, and form long prisms with lengths of 100-300 μm, strongly fractured, with common internal oscillatory zoning and no evidence of older cores (Fig. 3h). Eight zircon grains of the selected sample were analyzed in sets of six scans during one analytical session. The results show uranium and Th contents between 47 and 58 ppm and 23 and 52 ppm, respectively, and Th/U ratios between 0.62 and 0.98. Individual spots range from 1842 ± 23 Ma to 1864 ± 24 Ma, except for one zircon that yielded an age of 1915 ± 32 Ma (Supplementary Table 3; N17-26E.5-1). The zircons yielded an upper concordia intercept age of 1864 ± 8 Ma with MSWD of 2.3 (Fig. 6). Most zircons have less than 10% discordance. No age difference was detected between core (N17-26E.8-1) and rim (N17-26E.3-2) analyses and the age of 1864 ± 8 Ma is accepted as crystallization age of the pluton.

Musa Granite (KM-144B, CREMU-37A, KM-77)

Zircons from the different monzogranites of the Musa pluton are transparent to light brown, subhedral, long prisms with lengths of 200-300 µm, fractured, with common internal oscillatory zoning and no evidence of older cores (Fig 7a, b, c). Titanite crystals are anhedral to subhedral and brown with 100-200 µm in length. BSE images show dark-gray and light-gray zones in titanite, and no overgrowths were observed (8a, b). Titanite of biotite-hornblende monzogranite (KM-77) shows corroded rims and metamictic areas (Fig 8c).

Seven zircon grains of the hornblende-biotite monzogranite (KM-144B) were analyzed in sets of six scans during one analytical session. The results show uranium contents between 154 and 588 ppm; Th 110 and 418 ppm and Th/U ratios between 0.46 and 1.13. Individual spots range from 1864 ± 8 Ma to 1880 ± 9 Ma. Zircons have less than 10% discordance, except one spot (N1620B.7-1; Suplementary Table 3) that was excluded from the zircon age calculation. Six zircon grains yielded an upper concordia intercept age of 1871 ± 4 Ma with MSWD of 2.2 (Fig. 9a). Analyses of eight titanites of the same sample (KM-144B) were collected in sets of five scans during a single analytical session. U–Pb age data from titanite are plotted in Fig. 9b. The results of titanite scatter between 1842 ± 33 Ma and 1892 ± 30 Ma. The plotted spots analysis define a reversely discordant intercept age of 1875 ± 14 Ma with MSWD of 1.7 (Fig. 9b). Within errors, this titanite age agrees with the date of the zircons (1871 ± 4 Ma; Fig 9a) that is considered as the crystallization age of this granite variety. No age difference was detected between core and rim analyses.

Eight zircon grains of biotite monzogranite (CREMU-37A) were analyzed in sets of six scans during a single analytical session. The results show U and Th contents between 53 to 406, and 43 to 211 ppm, respectively, and Th/U ratios between 0.53 to 0.97. Individual spots range from 1861 ± 10 Ma to 1898 ± 13 Ma. Most zircons have less than 10% discordance, except one spot (N1620E.7-2; Suplementary Table 3) that was excluded from the zircon age calculation. Seven out of eight zircon analyses yielded an upper concordia intercept age of 1876 ± 13 Ma with MSWD of 0.35 (Fig 9c). Analyses of six titanites crystals of the same sample (CREMU-37A) were obtained in sets of five scans during a single analytical session. U–Pb age data from titanite are plotted in Fig. 9d. The titanite data produced two groups of ages: two crystals show an upper concordia intercept age of 1926 ± 17 Ma and MSWD of 0.48 (Fig. 9d); the other four crystals define a younger upper concordia intercept age of 1871 ± 22 Ma and MSWD of 0.093 (Fig. 9d).

The latter is similar to the zircon age obtained for this granite and interpreted as its crystallization age. No age difference was detected between core (spots N1620E.2-1) and rim analyses (spots N1620E.3-1).

Eight zircons of biotite-hornblende monzogranite facies (KM-77) were analysed in sets of six scans during a single analytical session. Zircons have variable contents of U (197 – 863 ppm) and Th (156 -824 ppm). Th/U ratios are normal for magmatic zircon (0.63 to 0.99). Four of the analyzed zircons have more than 10% discordance and were excluded from the age calculation. Individual spots considered for age calculation range from 1856 ± 12 Ma to 1894 ± 16 Ma. Four out of eight zircon analyses yielded an upper concordia intercept age of 1882 ± 4 Ma with MSWD of 1.2 (Fig 9e). Analyses of titanite in this sample (KM-77) were obtained in sets of five scans during a single analytical session. U–Pb age data from titanite are plotted in Fig. 9f. The results of titanite scatter between 1840 ± 33 Ma and 1883 ± 54 Ma (within error). The plotted spot analyses define a reversely discordant intercept age of 1878 ± 9 Ma with MSWD of 1.3 (Fig. 9f). The analytical data have some degree of discordance, however, the titanite age is in the same error range of the zircon age (1882 ± 4 Ma) which is considered as the best estimate for the crystallization age. Likewise to other facies no age difference was detected between core and rim analyses.

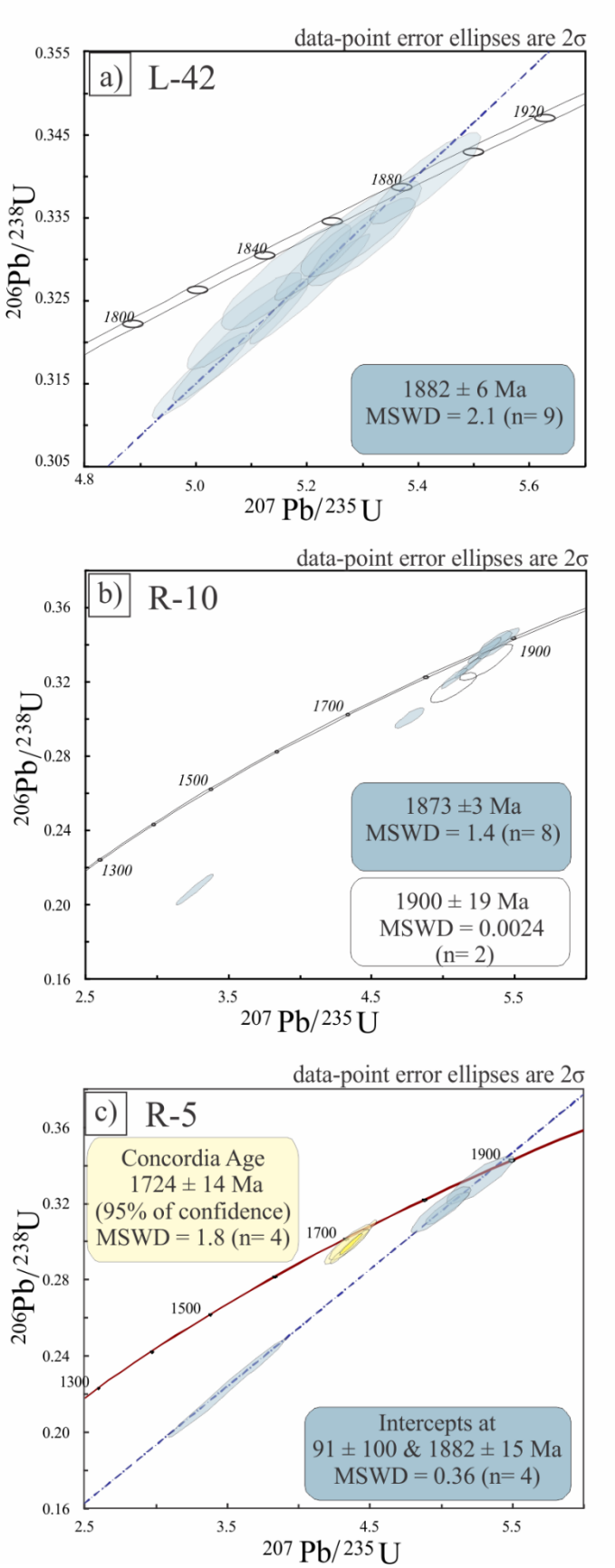

Fig. 5. Concordia diagrams showing U-Pb zircon SHRIMP ages of three samples of Velho Guilherme Suite: a) U–Pb concordia plot of albitized leucogranite (L-42; Velho Guilherme pluton); b) U–Pb concordia plot of hornblende-biotite syenogranite (R-10); c) U–Pb concordia plot of leucogranite (R-5); b and c of the Antônio Vicente pluton.

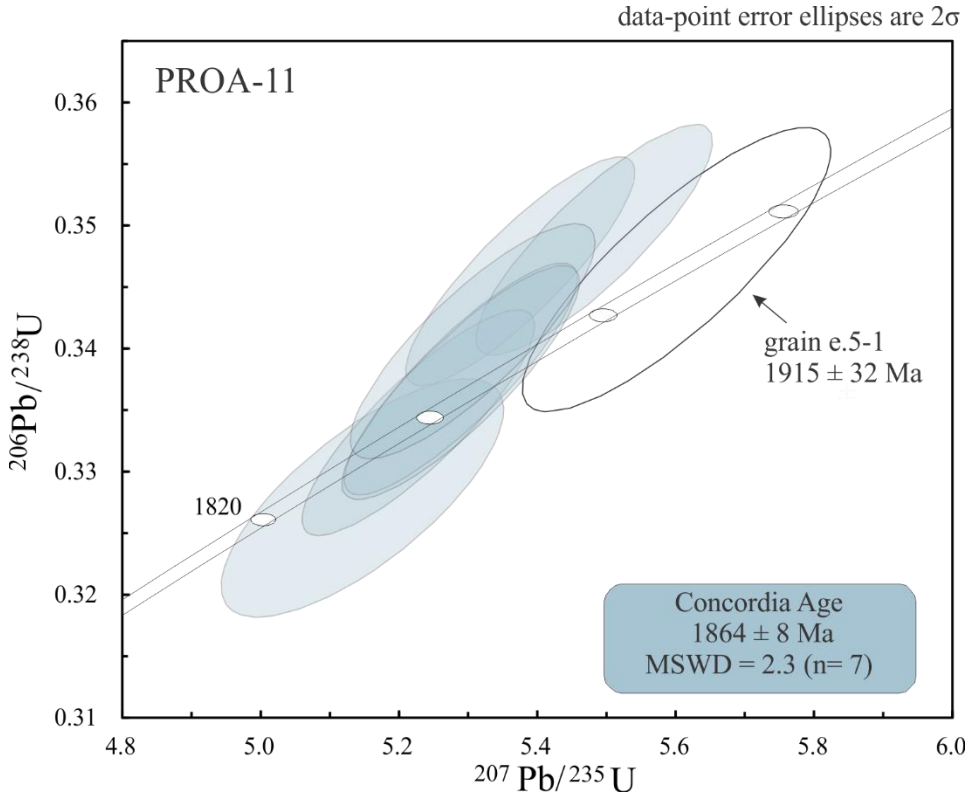

Fig. 6. Concordia diagrams showing U-Pb zircon SHRIMP ages of Jamon pluton.

Redenção Granite (DC-111, DC-120, DCR-42A)

Zircons from the analyzed facies of the Redenção Granite are transparent to light pink, subhedral to euhedral, long prisms with lengths of 100-350 µm, fractured, with common internal oscillatory zoning, no evidence of older cores and sometimes with metamictic zones, especially in the core of the crystals (Fig 7d, e, f, g). Titanite is anhedral to subhedral and brown with 100-200 µm in length. BSE images show dark-gray and light-gray zones in titanite, and no overgrowths or metamictic processes were observed (Fig. 8d).

Zircons from the biotite monzogranite (DC-111) were analyzed in sets of six scans during a single analytical session. They have high uranium and Th contents, between 449 to 560 and 234 to 551 ppm, respectively. Th/U ratios are between 0.47 and 1.02. Six spot analyses of zircons yielded two age populations: four grains define an upper intercept age of 1867 ± 5 Ma with MSWD of 0.34 (Fig. 10a); two other crystals yields an upper intercept age of 1890 ± 6 Ma with MSWD of 0.0097 (Fig. 10a). Most zircons have less than 10% discordance. Analyses of six titanite crystals of the same sample (DC-111) were obtained in sets of five scans during a single analytical session. U–Pb age data from

titanite are plotted in Fig. 10b. Titanite also yielded two age groups: three grains show an upper concordia intercept age of 1935 ± 21 Ma and MSWD of 0.10 (Fig. 10b), and the other two crystals have a younger upper concordia intercept age of 1881 ± 52 Ma (Fig. 10b). The analytical error of the youngest age (1881 ± 52; Fig. 10b) is very high, but the obtained age is similar to those of the other dated Paleoproterozoic granites of Carajás and will be considered. One spot (N1619G.2-2; Suplementary Table 3) was excluded from the titanite age calculation because the grain presented a high grade of discordance.

Analyses of zircon from seriate leucomonzogranite (DC-120) were obtained in sets of six scans during a single analytical session. They have high and variable uranium and Th contents, respectively, between 160 and 638 ppm and 85 and 482 ppm, with Th/U ratios between 0.48 and 0.91. Individual spots range from 1836 ± 8 Ma to 1871 ± 14 Ma. One of the zircons have more than 10% discordance and was excluded from the age calculation. Six out of seven zircon analyses yielded an upper concordia intercept age of 1865 ± 6 Ma with MSWD of 2.0 (Fig. 10c), which is interpreted as the crystallization age of the sample.

Zircons from the medium even-grained leucomonzogranite (DCR-42) were analysed in sets of six scans during two analytical sessions. They have moderate uranium contents between 60 and 329 ppm; Th between 44 and 294 ppm, and Th/U ratios between 0.76 and 1.09. Individual spots range from 1820 ± 30 Ma to 1876 ± 23 Ma. One of the zircons is more than 10% discordant and was excluded from the age calculation. Four out of five zircons analysis yielded an upper concordia intercept age of 1871 ± 5 Ma with MSWD of 0.98 (Fig. 10d). This age is within error superposed with the age of the leucomonzogranite (1865 ± 6 Ma; DC-120) and is interpreted as the crystallization age of the rock. No age difference was detected between core and rim analyses in any of the studied facies of the Redenção Granite.

Bannach Granite (ADR-136I, ADR-35A)

Studied zircons from the two dated facies of the Bannach Granite (cumulate granite -ADR-136I; fine-grained leucomonzogranite - ADR-35A) are transparent to light pink, subhedral to euhedral, long prisms with lengths of 100-400 µm in the cumulate granite (ADR-136I) (Fig 7h, i) and lengths of 100-250 µm in the leucomonzogranite ADR-35A (Fig. 11a, b), fractured, with common internal oscillatory zoning, no evidence of older cores and sometimes with apatite inclusions.

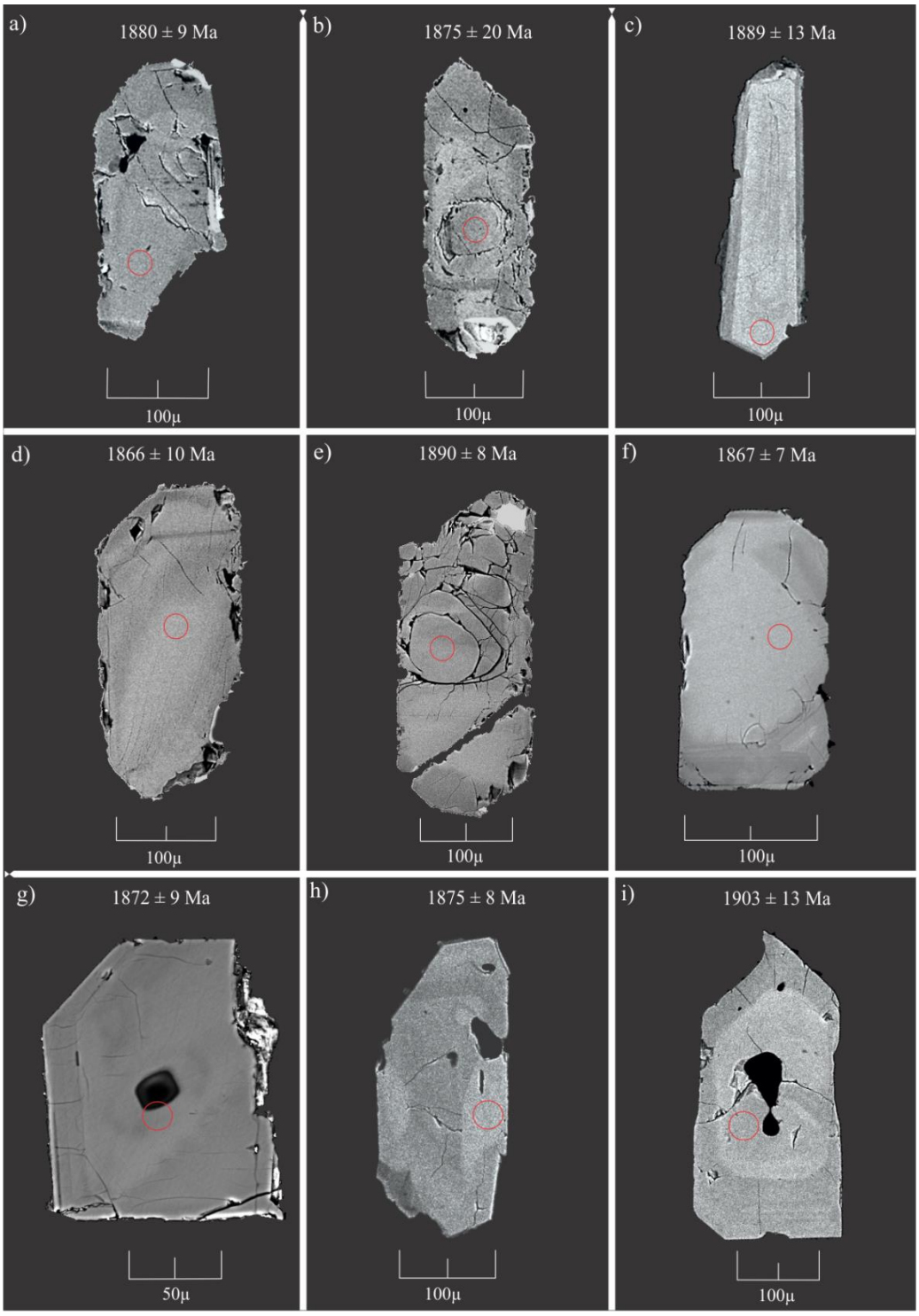

Fig. 7. BSE images showing the analytical pits on zircons of the Jamon Suite: Musa Granite - (a) KM-144B; (b) CRE-MU-37A, (c) KM-77; Redenção Granite - (d, e) DC-111, (f) DC-120, (g) DCR-42A; Bannach Granite - (h, i) ADR-136I.

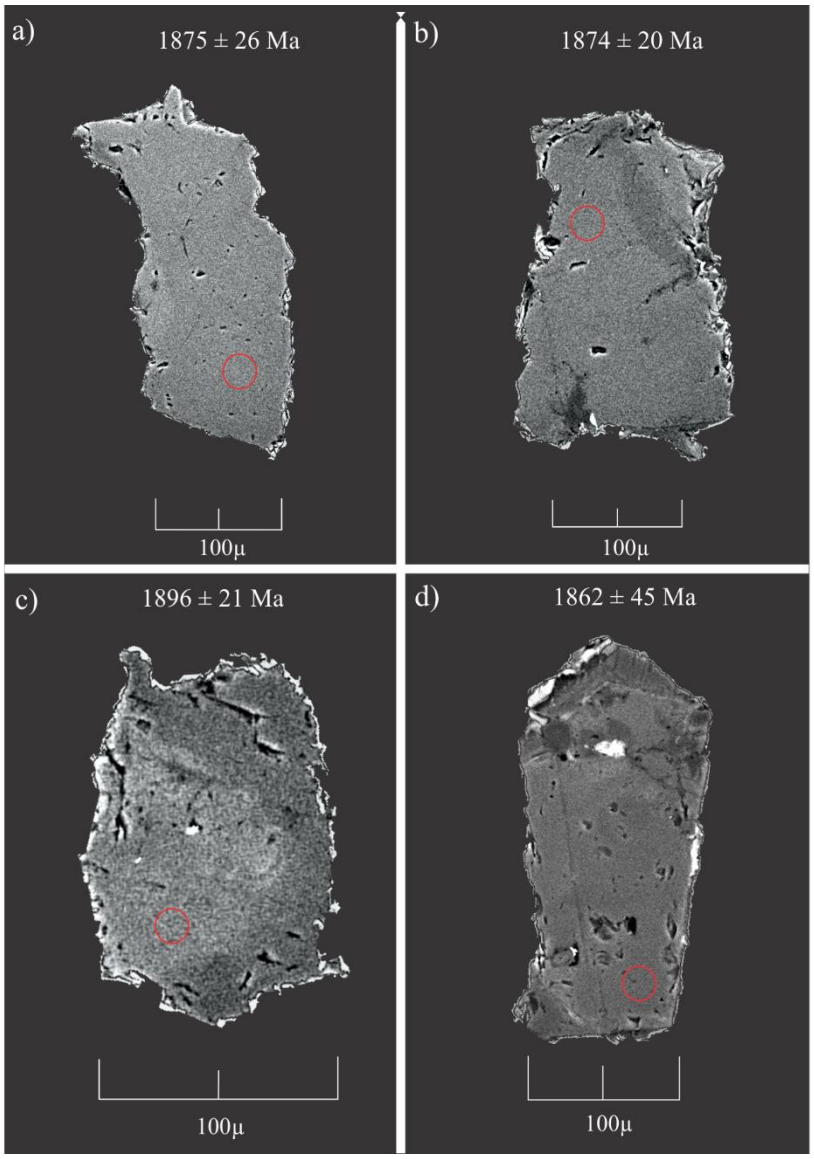

Fig. 8. BSE images showing the analytical pits on titanite of the: Musa Granite - (a) KM-144B, (b) CREMU-37A, (c) KM-77; Redenção Granite: (d) DC-111.

Zircons from the cumulate granite (ADR-136I) were analyzed in sets of six scans during two analytical sessions. They have moderate U and Th contents between 71 to 347 and 57 to 202 ppm, respectively, with Th/U ratios between 0.27 and 0.98. Individual spots range from 1859 ± 10 Ma to 1911 ± 10 Ma. Most zircons have less than 10% discordance and eleven out of thirteen zircons analyses yielded two age populations: two crystals yielded an upper intercept age of 1908 ± 8 Ma with MSWD of 0.74 (Fig. 10e); nine grains define an upper intercept age of 1874 ± 6 Ma with MSWD of 2.5 (Fig. 10e).

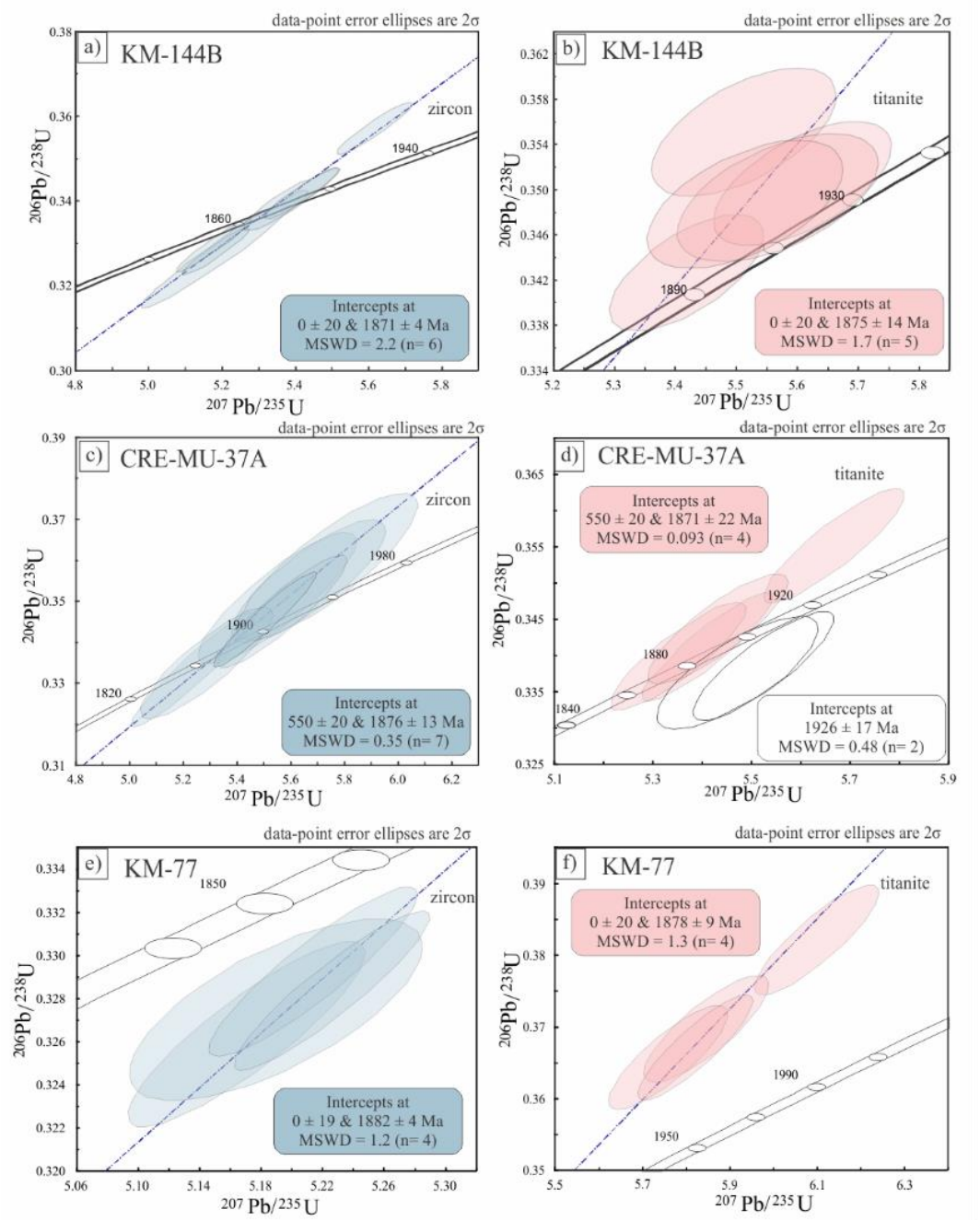

Fig. 9. Concordia diagrams showing U-Pb zircon and titanite SHRIMP ages of three samples of the Musa Granite: a), c), and e) U–Pb concordia plot of zircon of, respectively, KM-144B, CRE-MU-37A, and KM-77; b), d) and f) U–Pb concordia plot of titanite of, respectively, KM-144B, CRE-MU-37A, and KM-77.

Zircons from the leucomonzogranite (ADR-35A) were analysed in sets of six scans during two analytical sessions. They have low to moderate uranium and Th contents between 24 and 297 and 36 to 397 ppm, respectively, with Th/U ratios between 0.24 and 2.02. Individual spots range from 1826 ± 33 Ma to 1916 ± 32 Ma. Most zircons are concordant to subconcordant and ten out of eleven zircons analyses yielded two age populations: Three grains yield an upper intercept age of 1897 ± 13 Ma (MSWD = 0.94;

Fig. 10f), and seven grains define an upper intercept age of 1857 ± 5 Ma (MSWD = 0.38; Fig. 10f).

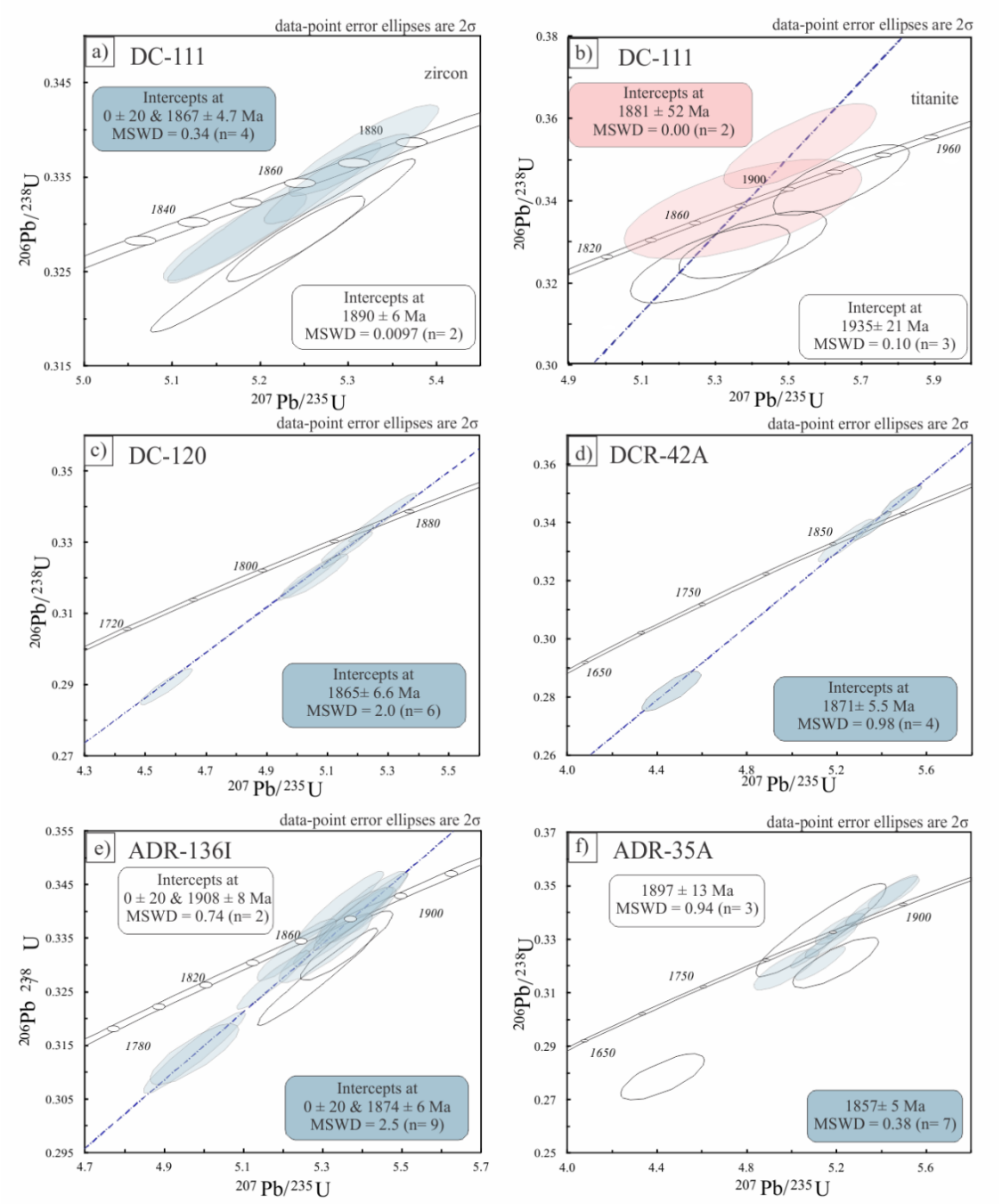

Fig. 10. Concordia diagrams showing U-Pb zircon and titanite SHRIMP ages of Redenção and Bannach Granites: a) zircon and b) titanite of DC-111 (Redenção Granite); c) zircon of DC-120 (Redenção Granite); d) zircon of DCR-42A (Redenção Granite); e) zircon of ADR-136I (Bannach Granite); and f) zircon of ADR-35A (Bannach Granite).

6.4 Seringa Granite

Zircons of four different facies of the Seringa Batholith were dated: heterogranular leucosyenogranite (AC-45); coarse-grained biotite-hornblende monzogranite (AC-59); coarse-grained hornblende-biotite monzogranite (AC-85); and heterogranular hornblende-biotite syenogranite (AC-42).

Most zircon grains are subhedral to euhedral, short to long prisms, with lengths of 100-250 µm, fractured, with common internal oscillatory zoning and no evidence of older cores. They are transparent, have apatite inclusions and sometimes metamictic cores are observed (Fig 11c, d, e, f, g, h).

The U–Pb isotope data of zircon for the Seringa Granite are listed in Supplementary Table 4 and graphically displayed in concordia diagrams (Fig. 12).

Eleven zircon grains of leucosyenogranite (AC-45) were analyzed in sets of six scans during two analytical sessions. Zircon shows high and variable uranium and Th contents between 40 and 1176 and 43 and 571 ppm, respectively. Th/U ratios are from 0.31 to 0.80. Zircon has two age groups: three grains define an upper intercept age of 1919 ± 13 Ma and MSWD of 0.91 (Fig. 12a), and eight grains define an upper intercept younger age of 1879 ± 5 Ma and MSWD of 2.6 (Fig. 12b). All zircons are less than 10% discordant.

Zircons from biotite-hornblende monzogranite (AC-59) were analyzed in sets of six scans during one analytical session. Nine spot analyses show high and variable uranium (between 76 and 747 ppm) and Th (from 33 to 621 ppm) contents. Th/U ratios are between 0.43 and 0.86. Similar to the leucosyenogranite sample (AC-45), the zircons of this facies also show two groups of ages: three grains define an upper intercept age of 1898 ± 8 Ma (MSWD of 0.21, Fig. 12b); seven grains have an upper intercept younger age of 1870 ± 3 Ma (MSWD of 1.7, Fig. 12b). All zircons are concordant to subconcordant.

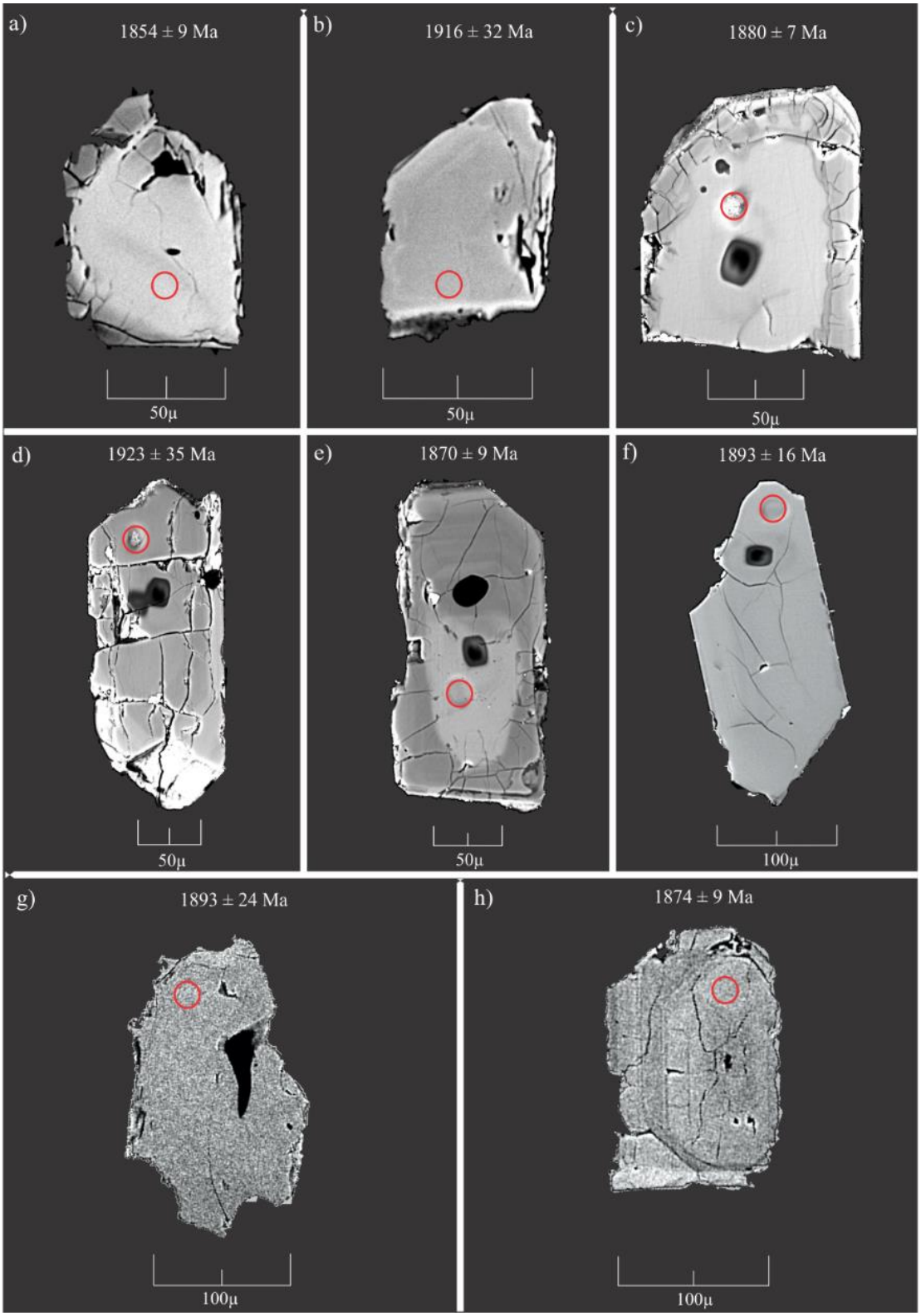

Fig. 11 BSE images showing the analytical pits on zircons of the: Bannach Granite (Jamon Suite) - (a, b) ADR-35A; Seringa Granite - (c, d) AC-45, (e, f) AC-59, (g) AC-85, (h) AC-42.

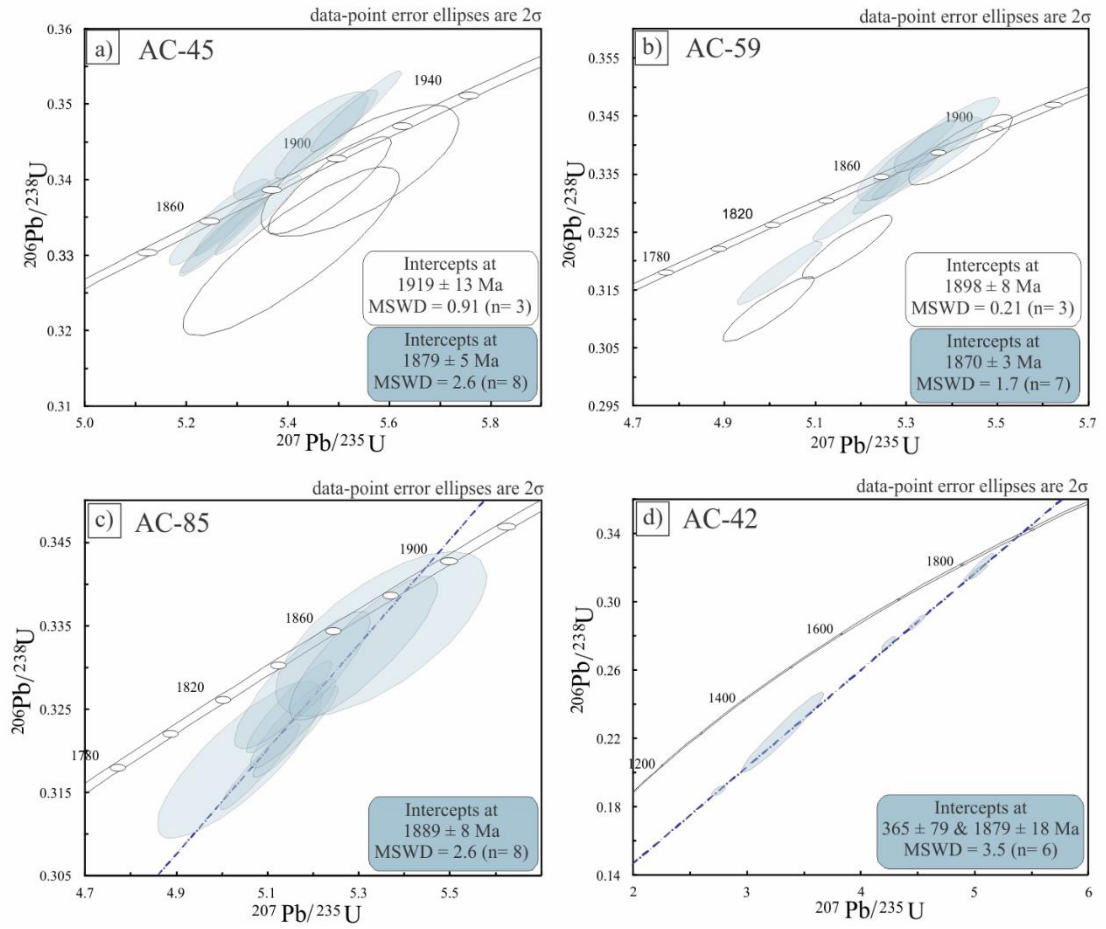

Fig. 12. Concordia diagrams showing U-Pb zircon SHRIMP ages of samples of four different varieties of Seringa Granite: a) sample AC-45; b) sample AC-59; c) sample AC-85; d) sample AC-42.

Zircons from hornblende-biotite monzogranite (AC-85) were analyzed in sets of six scans during one analytical session. Eight spot analysis show uranium and Th contents between 34 and 589 and 16 to 610 ppm, respectively. Th/U ratios are between 0.47 and 1.07. Individual analysis range from 1868 ± 21 Ma to 1898 ± 46 Ma. The analyses yielded a single upper concordia intercept of 1889 ± 8 Ma with MSWD of 2.6 (Fig. 12c). All zircons are concordant to subconcordant.

Zircons from heterogranular hornblende-biotite syenogranite (AC-42) were analyzed in sets of six scans during one analytical session. The analyses show high uranium contents between 453 and 1110 ppm. Th contents vary between 208 and 487 ppm, and Th/U ratios from 0.39 to 0.75. Six out of two zircons analyses yielded an upper concordia intercept of 1879 ± 18 Ma with MSWD of 3.5 (Fig. 12d). Most results are discordant and the elevated MSWD of 3.5 could indicate that the ages are not equivalent. However, the obtained age is similar and overlap in the analytical error with those of the

other facies of the Seringa Granite and is the best estimate for the crystallization of the sample AC-42.

6.5 *São João Granite*

Samples of zircon from four facies of São João Granite were investigated: hornblende-biotite syenogranite (PC-03B); biotite monzogranite (PC-21); biotite-hornblende monzogranite (PCM-10); biotite-hornblende syenogranite (PCM-13).

Most zircon grains are subhedral to euhedral, short to long prisms, with lengths of 100-250 µm, fractured, with common internal oscillatory zoning and no evidence of older cores (Fig. 13a). They are light yellow, have apatite inclusions and sometimes metamictic cores. Xenotime inclusions were detected in zircon of sample PC-21.

The zircon U–Pb isotope data of São João Granite are listed in Supplementary Table 5 and graphically displayed in concordia diagrams (Fig. 14).

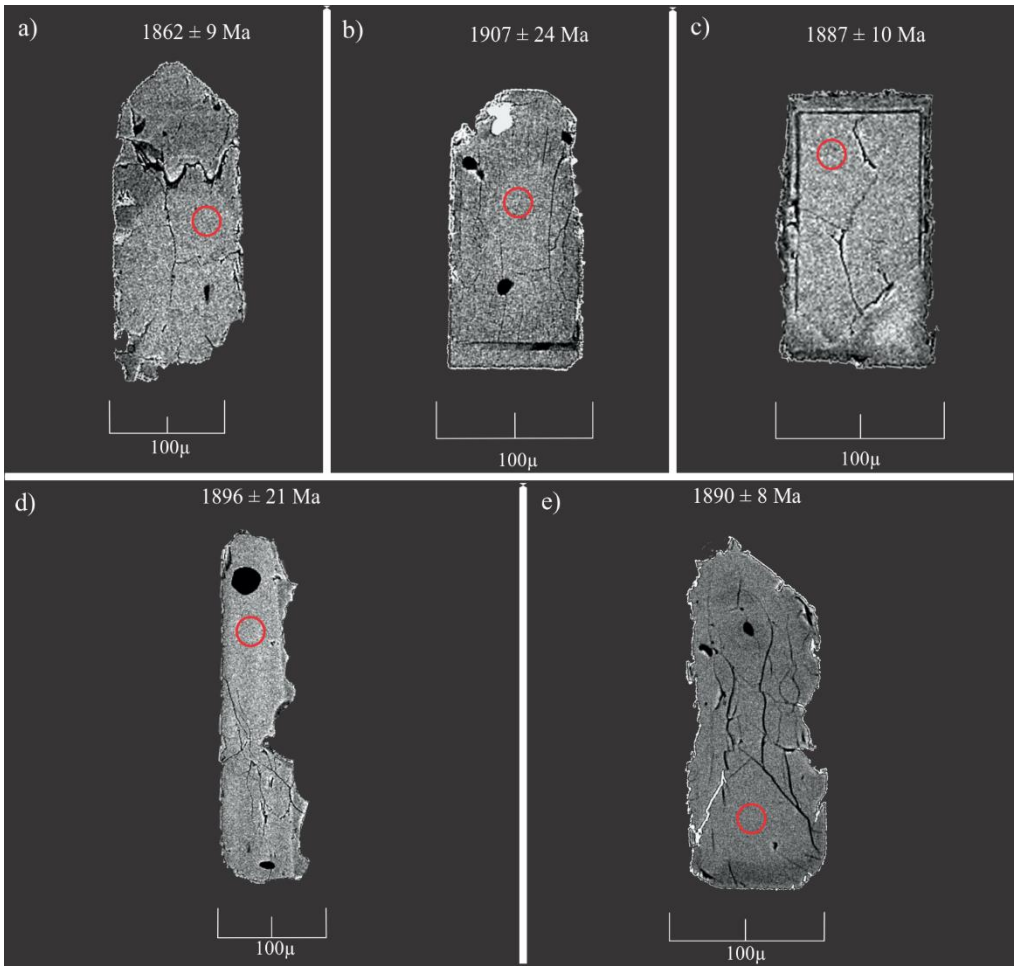

Fig. 13. BSE images showing the analytical pits on zircons of the São João Granite: (a, b) PC-03B; (c) PC-21; (d) PCM-10; (e) PCM-13.

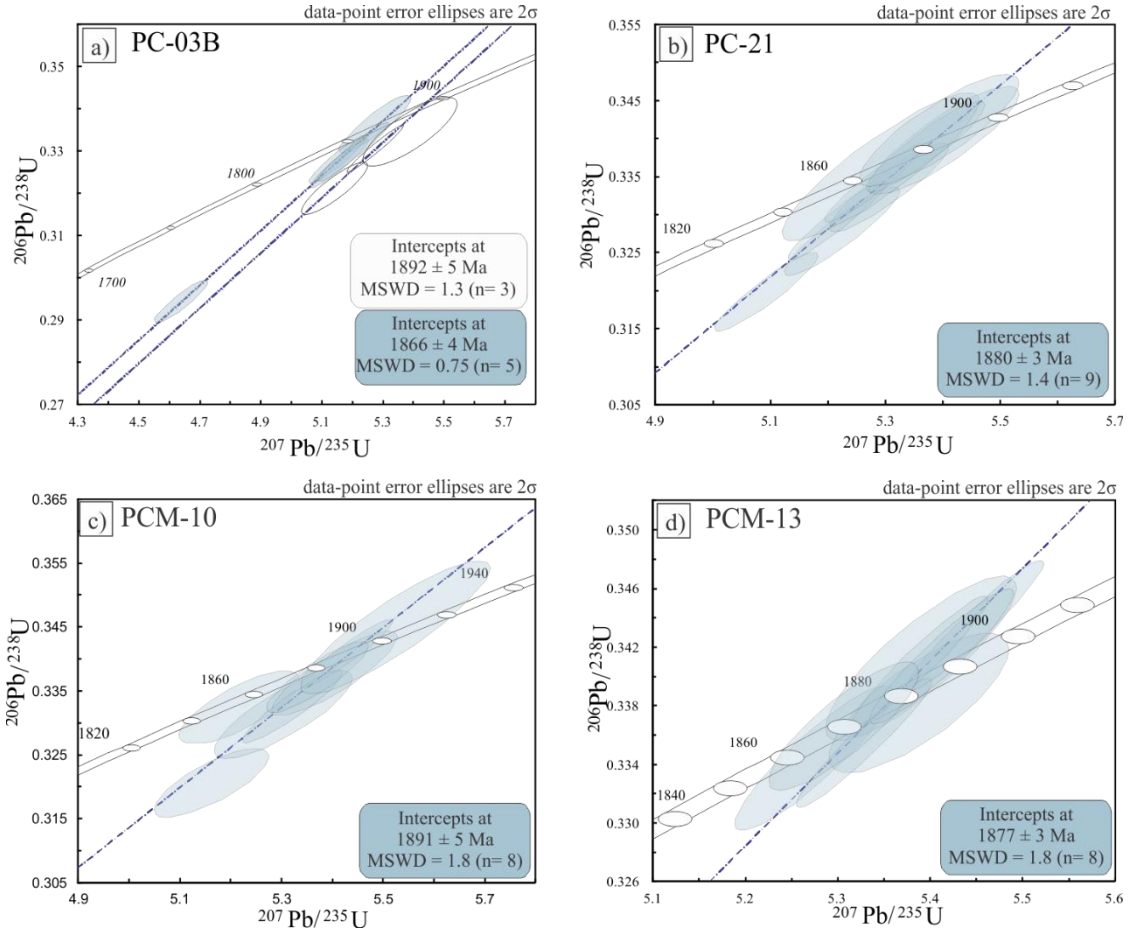

Fig. 14. Concordia diagrams with U-Pb SHRIMP data of zircon of four different varieties of São João Granite: a) sample PC-03B; b) sample PC-21; c) sample PCM-10; d) sample PCM-13.

Eight grains of the hornblende-biotite syenogranite (PC-03B) were analyzed in sets of six scans during one analytical session. Zircons show high uranium and Th contents, between 123 and 658 ppm and between 99 and 404 ppm, respectively. Th/U ratios vary from 0.43 to 0.74. The zircons show two age groups: three crystals define an upper intercept age of 1892 ± 5 Ma and MSWD of 1.3 (Fig. 14a); the other five grains have an upper intercept younger age of 1866 ± 4 Ma (MSWD = 0.75; Fig. 14a).

Fourteen zircon grains of biotite-monzogranite (PC-21) were analyzed in sets of six scans during two analytical sessions. They show uranium contents between 73 and 1962 ppm; Th between 42 and 1002 ppm and 0.29 to 0.7 Th/U ratios. The analysis (N16-26C.6-2-1) is 34% discordant and was not included in the age calculation. Nine zircons define an upper concordia intercept age of 1880 ± 3 Ma with MSWD of 1.4 (Fig. 14b). This age is interpreted as the crystallization age of the sample. Four grains yielded significantly younger $^{206}Pb/^{238}U$ ages in the 623-532 Ma interval (Supplementary Table 5). All four ages are discordant (15% to 36 %) and are not grouping in a defined age. These data would require further investigation but they give an indication of

Neoproterozoic activity in the area possibly related to the Brasiliano (Pan-African) cycle that was active in the Araguaia Belt to the east of the craton.

Zircon of biotite-hornblende monzogranite (PCM-10) was analyzed in sets of six scans during one analytical session, and results are presented in Supplementary Table 5 and in the concordia plot of Fig. 14c. The analyzed zircon grains show uranium contents between 80 and 818 ppm, Th between 39 and 605 ppm, and Th/U ratios from 0.47 to 0.93. All eight analyses are concordant and define an upper concordia intercept age of 1891 ± 5 Ma (MSWD = 1.8; Fig. 14c). This age is older than that of the biotite monzogranite (1880 ± 3 Ma) and is interpreted as the crystallization age of the biotite-hornblende facies.

Zircon grains of the biotite-hornblende syenogranite (PCM-13) were analyzed in sets of six scans during two analytical sessions. They show uranium contents between 237 and 1097 ppm; Th between 156 and 787 ppm, and Th/U ratios varying from 0.45 to 0.79. All eight analyses are concordant and define an upper concordia intercept age of 1878 ± 3 Ma (MSWD = 1.8; Fig. 14d). This age overlaps in the analytical errors with the age of biotite monzogranite (1880 ± 3 Ma) and is interpreted as the crystallization age of the biotite-hornblende syenogranite facies.

7. Discussion

7.1 Meaning of zircon and titanite ages

7.1.1 Zircon ages

Single analyses by SIMS of zircon from magmatic rocks can reveal information on when zircons grew, and precise zircon ages can define the crystallization ages of the studied rocks and constrain the emplacement time of individual plutons or complex suites. The analytical methods employed in our study allow high spatial resolution and accuracy, besides the possibility of analysis of distinct stages of crystallization that are eventually present in a single grain of zircon.

Backscattered electron imaging is often used to visualize textural aspects including old cores and growth processes in zircons (Corfu et al., 2003). The zircon grains in all the studied granites (Fig. 3, 7, 8, 11, 13) show clear magmatic features including euhedral to subeuhedral prismatic form, oscillatory zoning, and high Th/U values. Some of them display metamictic areas, fractures, and inclusions that were avoided for the SHRIMP analysis. The spots used for age calculation are from rims and cores of zircon

grains. Despite this, no clear dependence between the analyzed zircon zone or external morphology and apparent $^{207}Pb/^{206}U$ age could be recognized. The majority of zircon grains yielded upper intercepts very close to the concordia. The analyzed samples showed scatter of single zircon analyses along concordia and only a few percent are discordant. Almost all of our U–Pb analyses are less than 10% discordant. No inheritance in the analyzed zircon grains was observed, but the presence of Archean inherited zircons was registered in previous works (Jamon Granite, Dall'Agnol et al., 1999a; Musa Granite, Machado et al., 1991). Scatter in the data is usually attributed to some combination of Pb loss and/or inheritance. However, there is no evidence of metamorphic imprint in the studied granites (Dall'Agnol et al., 1999a, 2005; Teixeira et al., 2002; Machado et al., 1991; Javier-Rios et al., 1995; Teruiya et al., 2008; Vasquez et al., 2008) and Pb loss in unmetamorphosed rocks should be low. Besides, it is unlikely that the individual grains analyzed by SIMS, which have variable size and U content, will exhibit identical inheritance or Pb loss. Consequently, we interpret that most of the zircon ages of these samples as representative of their crystallization ages. A possible exception are evolved leucogranites strongly affected by hydrothermal processes like the tin-mineralized facies of the Velho Guilherme Suite because these specialized granites can have their U-Pb system in zircon disturbed (Costi et al., 2000, 2009).

The new geochronological data cover the majority of the A-type anorogenic granites of the Carajás Province. All the results obtained here combined with those from previous works are represented in an age diagram (Fig.15) in order to show the distribution of the ages of each granite and allow a comparison between them.

Considering the whole available data, the anorogenic magmatism of the Carajás Province, represented by the Serra dos Carajás, Velho Guilherme, and Jamon Suites, and the Seringa, São João, and Gogó-da-Onça plutons, occurred mainly at the age of ~1880 Ma as shown in figure 15. These results are in agreement with the strong evidences that at 1880 Ma the Amazon Craton underwent a major period of crustal extension (Dall'Agnol et al., 2005; Lamarão et al., 2002, 2005; Oliveira et al., 2008, 2010) that favored the emplacement of A-type anorogenic or post-tectonic plutons.

The dominant zircon ages acquired by U-Pb SHRIMP in zircon do not show great contrasts with the ages obtained by other methods (Fig. 15). However, analyzing the U-Pb data presented in this work and the data synthesis (Fig. 15), we can identify some particular ages not reported before: (a) older zircon ages of 1900 Ma to 1920 Ma in the granites of the Velho Guilherme and Jamon suites and in the Seringa Granite; (b) younger

ages of 1857 Ma to 1865 Ma in the leucogranite facies of the Redenção (DC-120, DCR-42; Fig. 10c, d) and Bannach (ADR 35A; Fig. 10f) plutons, and in the biotite-hornblende monzogranite of the Jamon Pluton (PROA11; Fig. 6); (c) an age of 1732 ± 6 Ma (Fig. 5c) obtained in the leucogranite facies (R-05) of the Antônio Vicente pluton of the Velho Guilherme Suite. All these particular ages will be discussed in the following sessions.

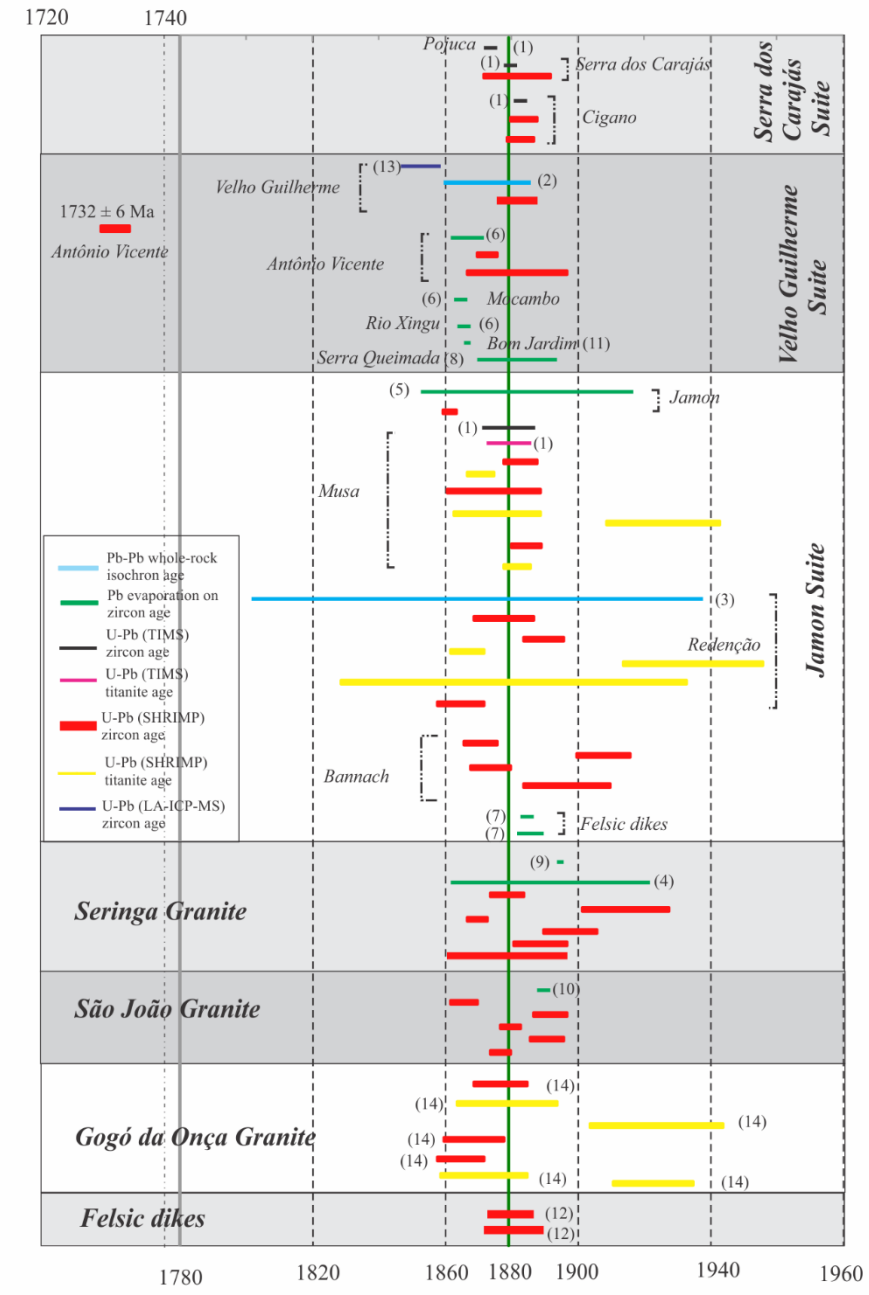

Fig. 15. Age diagram of the previously available data and new data obtained in this work of the Paleoproterozoic granites of the Carajás Province. Data source: (1) Machado et al. (1991); (2) Rodrigues et al. (1992); (3) Barbosa et al. (1995); (4) Avelar (1996); (5) Dall'Agnol et al. (1999a); (6) Teixeira et al. (2002); (7) Dall'Agnol et al. (2005); (8) Pinho et al. (2006); (9) Paiva Jr. (2009); (10) Lima (2011); (11) Lamarão et al. (2012); (12) Silva et al. (2016); (13) Antonio et al. (2017); (14) Teixeira et al. (2017). U-Pb SHRIMP ages represented by red and yellow bars without references are from this work.

7.1.2 Titanite ages

Titanite is stable over a large range of P–T conditions and has a relatively high closure temperature for the U–Pb system [~750 °C or higher; Pidgeon et al. (1996); Zhang and Scharer (1996); Spencer et al. (2013); Stearns et al. (2015)]. It is admitted that in situ microanalyses of titanite can provide new information about the timing and rates of igneous processes (Aleinikoff et al., 2002). Several authors have employed titanite isotopic studies to determine multiple age components of magmatic complexes and constrain chronologic episodes of igneous crystallization and metamorphic growth (Schaltegger et al., 2009; Aleinikoff et al., 2002; Corfu, 1996).

Titanite is considered a magmatic phase in the granites of the Jamon Suite and, when present, also in the Serra dos Carajás Suite (Dall'Agnol et al., 1999a, b; 2005). A phase diagram obtained in oxidizing conditions in experiments on the Jamon hornblende-biotite monzogranite indicate that titanite initiated to crystallize at temperatures a little higher than 750ºC (Dall'Agnol et al., 1999b, their Fig. 3a).

Investigation of titanite using BSE imaging reveals that most crystals are homogenous, free of inclusions and no overgrowths were observed. Irregular zones with contrasting BSE intensity (Fig. 8) were recognized. However, the isotopic compositions of distinct zones are similar and do not indicate different ages. Th/U ratios of the titanites from the Jamon Suite are generally much higher than the unit suggesting its magmatic origin (Supplementary Table 3). Some titanite grains show reversely discordant $^{207}Pb/^{206}Pb$ ages. However, those titanite ages are similar to the zircon ages in the same samples, suggesting that the discrepancy may be due to an unknown error in the determination of the Pb/U ratios.

The titanite results for the Musa Granite (KM-144B, CRE-MU-37A, and KM-77 from this work; MU-4 from Machado et al., 1991), and the Redenção Granite (DC-111) are plotted in the integrated age diagram as well as the data of the titanite from the Gogó-da-Onça Granite previously obtained by Teixeira et al. 2017 (Fig.15). The U–Pb dates from titanites of those granites are similar in ages with the zircons of the same samples confirming that the studied titanites are of igneous origin. On the other hand, alike zircon, titanite ages show also a bimodal distribution. Most ages are concentrated around 1880 Ma, the age of dominant granite crystallization. However, there is a significant number of older titanite ages varying from 1900 to 1940 Ma that are similar within analytical error with old zircon ages obtained in the Musa and Redenção granites (Fig. 15). In the anorogenic Gogó da Onça Granite (GGO), Teixeira et al. (2017) also obtained in titanite

of different facies two different age populations (Fig. 15). A first population corresponds to ages of 1879 ± 15 Ma and 1872 ± 13 which are similar to the zircon ages of the same samples (1878 ± 8 Ma and 1865 ± 10 Ma), interpreted as the crystallization age of the granitic body. A second population was defined by titanite ages of 1924 ± 20 Ma and 1923 ± 12 Ma and it was not registered in zircons. Teixeira et al. (2017) argue that these older ages could represent the initial crystallization of the rocks of GOG or eventually correspond to inheritance in the analyzed titanites since in felsic igneous rocks titanite may preserve the initial imprint of an older crystallization event.

7.1.3 Interpretation of the older ages (1900 to 1920 Ma)

Apart from the dominant age population around 1880 Ma, the obtained data revealed an older age population in zircon and titanite (1900 to 1920 Ma), that was registered in the Velho Guilherme and Jamon suites and in the Seringa Granite. As discussed before, the analyzed zircon and titanite crystals of this population are clearly of igneous origin. Among the hypotheses able to explain these contrasting ages, it should be considered: (a) inheritance in the analyzed zircon and titanite crystals; (b) prolonged growth of autocrystic zircon and titanite crystals in the same magma batch; (c) incorporation of older antecrystic zircon and titanite crystals from different magma batches of the same magma system.

Inheritance in zircon crystals of magmatic rocks are very common and the grains showing such features are usually distinguished by being appreciably older than most of zircon crystals of the rock. Following this reasoning, the older zircon and titanite ages of the studied granites could represent inheritance of older country rocks. However, even though the presence of inherited zircon from immediately older magmatism is an extremely common fact, it is important to emphasize that contrasts between core and rim of zircons and titanites were not observed. Besides, this hypothesis is also weakened due to the lack of 1900-1920 Ma older exposed rocks in the Carajás Province.

On the other hand, differences in crystallization age between zircons of a same rock sample with dispersions of up to 50 m. y. may indicate prolonged growth of zircon in the same magma batch (Schaltegger et al., 2009). However, the time of emplacement and crystallization of the anorogenic granites of Carajás Province must have been almost coincident, because those granites were emplaced at low crustal depth as indicated by their discordant character with common presence of angular enclaves of the Archean

country rocks in the borders of the plutons (Dall'Agnol et al., 2005), This imply high temperature and viscosity contrasts with the country rocks and rapid cooling. Besides it, if crystallization showed prolonged continuity, it should be expected a continuous range of ages from 1920 Ma to 1860 Ma in the suites and this is not observed.

It is accepted that all zircon crystals in a particular rock do not need to have crystallized from the same pulse or increment of melt and to share the same history despite occurring within the same rock. Zircons present in a magmatic rock can be inherited either from the country rocks (xenocrysts) or from earlier phases of magmatism or eventually can be related to older phases of similar magmatism which could be sourced from the magmatic plumbing system (antecrysts) (Siégel et al., 2018; Miller et al., 2007; Schaltegger et al., 2009). The age differences between antecrysts and autocrysts in the same rock can be as little as 10–100's years or up to several million years (Siégel et al., 2018). Thus, the 1900 to 1920 m. y. old zircon and titanite crystals could hypothetically represent antecrysts from an earlier pulse of magma that was incorporated in the later pulse of 1880 Ma. The U–Pb dating of magmatic titanites from Musa (Fig. 9b, d, f) and Redenção granites (Fig. 10b) of the Jamon Suite and Gogó da Onça Granite (Fig.15; Teixeira et al., 2017) are compatible with this hypothesis once titanite can be preserved at high temperatures. Howsoever, it is not possible to distinguish antecrysts from autocrysts based only on U-Pb ages and the integration of different techniques is necessary to confirm this hypothesis.

7.1.4 Leucogranites of 1857 Ma to 1865 Ma

As mentioned before and displayed in the U-Pb concordia age diagrams (Fig. 10c, d, f) and in Figure 15, the leucomonzogranite facies of the Bannach and Redenção pluton yield ages of 1857 Ma to 1865 Ma, interpreted as being the crystallization ages of the corresponding samples. These ages are significantly younger in comparison with the ages of the less evolved facies of the same granites (Fig. 15).

Several authors have performed studies on the different facies of the studied granites to investigate the mechanisms involved in the generation of these Paleoproterozoic suites and to understand the evolution of their magmas. In general, it is admitted that the different magmas derived dominantly by crustal melting of Archean sources and evolved mostly by fractional crystallization (Dall'Agnol et al., 1999a, b; 2005; Dall'Agnol and Oliveira, 2007; Teixeira et al., 2002; Oliveira, D.C. et al., 2009).

However, geochemical and mineralogical characteristics indicated that the later leucogranite facies of the Redenção and Bannach granites are not derived by fractional crystallization of the less evolved facies of the same plutons (Oliveira, D.C. et al., 2009; Almeida et al., 2006; Mesquita et al., submitted). Oliveira, D.C. et al. (2008, 2009) admitted that the Redenção and Bannach plutons were formed by two magma pulses: the first magma pulse ascended by dikes, formed sheeted-like bodies and was fractionated in situ after emplacement. It generated the less evolved granite facies, including coarse, even-grained monzogranite with variable modal proportions of biotite and hornblende and biotite monzogranites; a second magma pulse, composed of a more evolved liquid, was emplaced towards the center of the plutons and originate the leucogranites. That hypothesis of evolution in two independent magma pulses was reinforced by recent mineralogical study (Mesquita et al., submitted) showing that the less evolved dominant facies of the Bannach pluton crystallized under moderately oxidizing conditions, while its late leucomonzogranite facies shows high Fe/(Fe+Mg) ratio in whole rock and biotite and should have crystallized under comparatively lower oxygen fugacity.

The U-Pb SHRIMP younger ages of 1857 Ma to 1865 Ma of zircons of the leucomonzogranites of Redenção (DC-120, DCR-42; Fig 10b, d) and Bannach plutons (ADR 35A; Fig 10f) support the interpretation that the younger leucogranites of these plutons were generated by independent magma pulses that were late in their magmatic evolution and reinforce the hypothesis of a distinct origin for those leucogranites, implying that they should not be related to the dominant less evolved facies of the respective plutons by fractional crystallization.

In addition, the biotite monzogranite of the Redenção pluton (DC-111; Fig. 10a), and the biotite-amphibole monzogranite of Jamon Pluton (PROA-11) also presented similar younger ages. However, the coarse even-grained biotite monzogranite (DC-111; Fig. 10a) of Redenção Pluton presents also an age of 1890 ± 6 Ma in zircon and an age of 1881 ± 52 Ma in titanite that approach the dominant crystallization age admitted for the studied granites. Hence, the meaning of the age of 1867 ± 5 Ma of DC-111 sample needs to be better investigated. In the same way, the age obtained for the PROA-11 sample of the Jamon Granite is distinct of those of similar facies of the other plutons of the Jamon Suite and complementary studies are also recommended for that granite.

The Pb-evaporation on zircon ages of the Antônio Vicente, Rio Xingu and Mocambo granites (Teixeira et al., 2002) are also situated around 1.86 to 1.87 Ga (Fig. 15). Although, the fact that the analyzed zircons of those granites are mostly metamictic

and the obtained ages less precise, it is possible that the tin-specialized reduced leucogranites of the Velho Guilherme Suite could also have a little younger age compared to the remainder studied granites.

7.1.5 Age of 1732 Ma

The leucogranite R-05 of the Antônio Vicente pluton of the Velho Guilherme Suite displayed two very distinct zircon age populations. Four grains yielded an upper intercept age of 1882 ± 15 Ma, similar to those of the other two samples of the same suite (Fig. 5c) and Paleoproterozoic A-type granites of Carajás in general; other four crystals defined a concordia age of 1732 ± 6 Ma (Fig. 5c).

As shown in the BSE images (Fig. 3g), the zircons of R-5 leucogranite display zones with sieve texture indicating that the crystals were affected by intense hydrothermal processes. There is no register of any magmatic or hydrothermal event at 1720 Ma in the Carajás Province so far and the obtained age of 1732 ± 8 Ma is difficult to explain. It is known that zircons of tin-specialized A-type granites of the Amazon craton are affected by F-rich late- to post-magmatic fluids and commonly they are altered and present porous aspect and sieved textures (Costi et al., 2009; Nardi et al., 2012; Lamarão et al., 2014). A similar aspect is presented by the zircon of R-05 leucogranite (Fig. 3g). The isotopic system of some of these altered zircon grains is disturbed and they are not able to give confident ages (e.g, the Pitinga albite granite, Costi et al., 2000, 2009). We can wonder if the younger age obtained in the R-05 sample is not a consequence of disequilibrium in the isotopic system. However, the fact that the younger age is concordant (Fig. 5c) do not favor the mentioned hypothesis. Alternatively, we can suppose that such age represent a not yet reported magmatic event in the Xingu Region or could correspond to an isolate hydrothermal event that allowed the growth of zircons.

7.2 Relevance of the 1.88 Ga magmatic event in the Amazon Craton

The relevance of the 1.88 Ga granite magmatic event in the Carajás Province of the Amazon Craton is clearly demonstrated by the data presented in this work. However, magmatic events with that age are not restricted to that province. The 1.88 Ga Orosirian magmatism is also widespread in other provinces of the Amazon Craton (Supplementary Table 6; Fig. 16a), as put in evidence by Dall'Agnol et al. (1994, 1999c), Lamarão et al. (2002, 2005), Santos et al. (2000, 2004), Vasquez et al. (2008), where it is mostly represented by the Uatumã volcano-plutonism that constitute a Silicic Large Igneous

Province (SLIP; Klein et al., 2012; Fraga et al., 2017). This SLIP covers large areas of the Central Amazonian (Iriri-Xingu and Erepecuru-Trombetas domains) and Tapajós-Parima provinces and is also locally represented in the Rondônia-Juruena province (Dall'Agnol et al., 1994, 1999c; Santos et al., 2001, 2004; Bettencourt et al., 2016; Antonio et al., 2017).

Controversial issues still exist about the meaning and tectonic setting of the Uatumã volcano-plutonic magmatism (cf. Fraga et al., 2017; Santos et al., 2004; Lamarão et al., 2005) and the definition of the Iriri Group (cf. Semblano et al., 2016). However, it is unquestionable that there is a large igneous province in the Amazon craton aged of ca. 1.88 Ga, and that this province is related to the Uatumã magmatism.

Geochronological data about the Uatumã vulcanism in the Iriri-Xingu Domain, located in the southern part of the Central Amazonian Province, is presented in Supplementary Table 6, and the petrographic, geological and metallogenetic aspects of the volcanic associations were discussed by Juliani and Fernandes (2010), Fernandes et al. (2011), Roverato et al. (2017), and Cruz et al. (2016). ~1.88 Ga old plutonic rocks with A-type alkaline affinity, represented by the Rio Dourado Suite, were described in the extreme south of the domain and in the Santana do Araguaia Domain (Barros et al., 2006, 2011).

In the northern Erepecuru-Trombetas domain of the Central Amazonian Province and in the Tapajós-Parima Province, near its border with the Central Amazonian Province, in the southern part of the Guyana Shield, Orosirian units are abundant and mainly represented by the A-type Iricoumé-Mapuera volcano-plutonic rocks related to the Uatumã Supergroup (~1.88 Ga; Ferron et al., 2010; Barreto et al., 2013, 2014). The ~1.88 Ga São Gabriel AMCG association (Anauá-Uatumã Domain; Valerio et al., 2018), and the ~1.90-1.89 Ga calc-alkaline rocks of the Água Branca Suite, not related and a little older than the Uatumã units also occur in those provinces (Suppl. Table 6). Finally, in the Pitinga Tin Province, occur the Madeira Suite (~1.83-1.82 Ga; Costi et al., 2000, 2009; Lenharo et al., 2003; Bastos et al., 2014), that succeed the Uatumã volcano-plutonism.

The Tapajós Domain corresponds to the southern part of the Tapajós-Parima Province and it includes one of the main gold provinces of Brazil. The ~1.88-1.87 Ga Orosirian magmatism in this domain is largely represented by the Iriri group, including A-type ignimbrites and rhyolites of the Moraes Almeida Formation and similar units and plutons of the Maloquinha Intrusive Suite (Suppl. Table 6). However, in that area, it

occurs also a remarkable Orosirian magmatism with calc-alkaline affinity corresponding to the granitic Parauari Suite (~1.89-1.88 Ga) and Tropas tonalite (~1.90-1.89 Ga). The dominantly mafic rocks of the Ingarana Suite are also 1.88 Ga old (Santos et al., 2004).

The geochronological data of the ca. 1.88 Ga magmatic units of the Amazon craton were listed (Supplementary Table 6) and presented in a probability density plot (Fig. 16b, c, d). It can be seen, a clear concentration of ages and an age peak of all the selected magmatic rocks at ~1880 Ma. This confirms the relevance and the large spatial distribution of the 1880 Ma magmatic episode in the Amazon Craton. However, the geochemical signature and the tectonic setting of the different provinces where these magmatic rocks occur are quite distinct, as well the dominant ages of their crystalline basement. The Carajás Province differ of the other provinces because it was stabilized tectonically at the end of the Archean. The 1.88 Ga Orosirian granitic suites of that province were formed 1000 to 700 m. y. after the final Archean events, are anorogenic and the Uatumã volcanism is not significant in it. On the other hand, in the Central Amazonian and Tapajós-Parima provinces, the 1.88 Ga units were formed short after a complex Paleoproterozoic evolution and are mostly related to the Uatumã volcano-plutonic units. The tectonic settings of these domains are still controversial (cf. Santos et al., 2004; Lamarão et al., 2002, 2005; Juliani and Fernandes, 2010; Fraga et al., 2017), however, we consider that the 1.88 Ga event in the Amazon craton is dominantly distensional and marks a period of intracontinental magmatism related to the beginning of the taphrogenesis that affected the Paleoproterozoic supercontinent and would continue throughout the Mesoproterozoic (Brito Neves, 1999; Lamarão et al., 2005; Fraga et al., 2017).

It is concluded that an Orosirian 1.88 Ga old magmatic event was remarkable in the Amazon craton, particularly in the provinces located to the south of the Rhyacian Transamazonas Province. In the Archean Carajás Province, the Orosirian magmatism is composed of A-type granites, derived from the partial melting of Archean sources, whereas in other comparatively younger provinces it has volcanic-plutonic character and its geochemical signature is variable from calc-alkaline, I-type-like to A-type. According to Dall'Agnol et al. (2005), there is no geological or geochronological evidence for the Carajás Granites being related to remote subduction processes. This implies emplacement of these granites in non-compressional anorogenic settings.

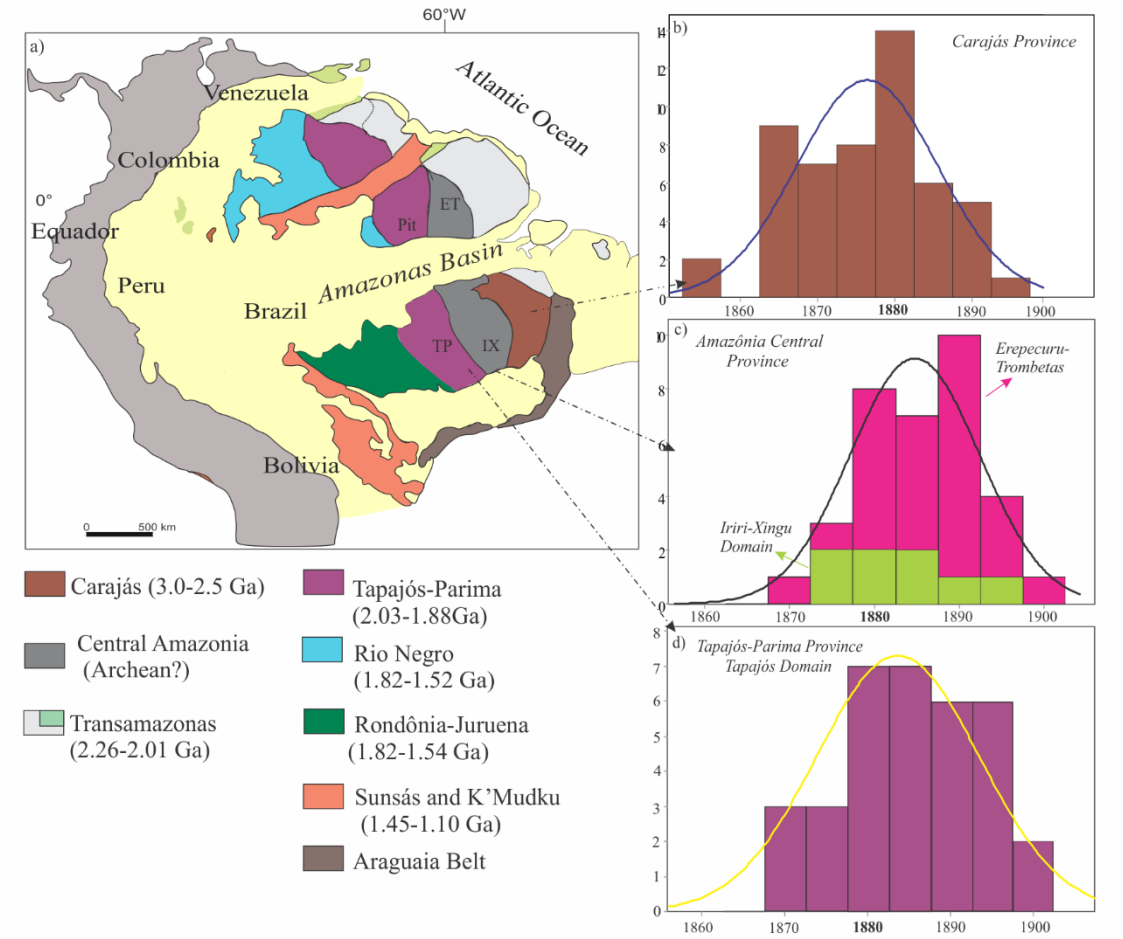

Fig. 16. a) Geologic map showing the location of the Amazon Craton in South America and its different provinces (Santos et al. 2004). Probability density plots of geochronologic data on the ~1.88 Ga Orosirian magmatism of the craton: b) Carajás Province; c) Iriri-Xingu, Erepecuru-Trombetas and Anauá-Uatumã domains and Pitinga Tin Province of the Central Amazonian and Tapajós-Parima provinces; d) Tapajós Domain of the Tapajós-Parima Province. TP= Tapajós Domain; IX= Iriri-Xingu; ET=Erepecuru-Trombetas; Pit=Pitinga.

7.3 Global magmatism at 1900-1880 Ma

The Paleoproterozoic Era (2500 to 1600 Ma) corresponds to ~20 % of the Earth's History. During the period between 2300 Ma and 1500 Ma, it occurred an intense granitoid activity and three major episodes of granitoid magmatism were identified in different cratons around the World (Condie et al., 2009). The first, between about 2150 and 2000 Ma, the second between 1950 to 1850 Ma (with a peak at ~1900 Ma) and the third from 1800 to 1550 Ma. The 1900 Ma episode was identified in primary magmatic zircons and also in detrital zircons. It is one of the more significant events of granitic magmatism and is represented in several continents, including South America, and in different cratons (Condie et al., 2009).

Dall'Agnol et al. (2005), following Hoffman (1989) and Windley (1993) models, proposed that the 1.88 Ga granite magmatic event in the Carajás Province was related to the beginning of the breakup of a Paleoproterozoic supercontinent (~2.0 Ga). The upwelling of a mantle superswell developed beneath the stationary supercontinent induced the uplift of the Amazon craton and was followed by magmatic underplating that was responsible for melting of the Archean crust and resulting A-type magmas. The extensional setting is demonstrated by the occurrence of dike swarms contemporaneous of the granitic magmatism (Dall'Agnol et al., 2005; Silva et al., 2016).

Evidences of mantle plumes active at 1.88 Ga have been found also in other continents. The Circum-Superior Large Igneous Province of North America, that consists predominantly of ultramafic-mafic lavas, dikes and sills with minor carbonatite complexes and felsic components, was interpreted to have formed from a single mantle plume and the upper mantle was the source of the magmas (Ciborowski et al., 2017). On the other hand, NW trending tholeiitic dykes in the Bhanupratappur region in the NE region of the Bastar Craton are 1.88 Ga and contemporaneous and compositionally correlative with dykes in the southern Bastar Craton and the Dharwar Craton (Shellnutt et al., in press). Dykes from the Yilgarn Craton (1888 ± 9) of Western Australia are also coeval and it was concluded that the Bastar, Dharwar and Yilgarn Cratons were linked before 1.88 Ga Craton (Shellnutt et al., in press). Those authors argue that a mantle plume model for the emplacement of the radiating mafic dyke swarms dykes throughout those cratons is plausible and admit that the dikes where emplaced during continental break-up.

In their synthesis about the intraplate Proterozoic mafic magmatism in the Amazon craton, Teixeira et al. (submitted) admitted an interaction between subduction related processes and mantle plumes with synchronous lithosphere extension during the formation of the Uatumã SLIP.

It is concluded that a major extensional event related to mantle plume activity was active in a World scale at 1.88 Ga. This event generate distinct magmatic rocks in different areas. In the Amazon Craton it was responsible for the origin of the A-type Orosirian granites of the Carajás Province and for the intermediate to felsic vulcano-plutonic rocks of the Uatumã SLIP.

8. Conclusions

- The Paleoproterozoic A-type granites of Carajás were emplaced between 1880 to 1860 Ma, with the main peak of this magmatism at 1880 Ma. At that time, the Amazon Craton underwent a major period of crustal extension.
- A little older ages (1900 -1920 Ma) obtained in zircon and titanite crystals may represent antecrysts from an earlier pulse of magma that were incorporated in the later pulse of 1880 Ma.
- The leucogranite facies of Redenção and Bannach plutons of the Jamon Suite are younger (1857 to 1865 Ma) than the less evolved facies of the same plutons(1880 Ma) and represent independent magma pulses that were later in their magmatic evolution.
- The age of 1732 ± 6 Ma of the leucogranite facies of the Antonio Vicente pluton could represent a magmatic event in the Xingu Region not yet reported or an isolate hydrothermal event that allowed the growth of zircons.
- The 1880 Ma magmatic event is remarkable also in other provinces of the Amazon Craton where it is mostly represented by the Uatumã SLIP.
- The 1880 Ma event corresponds to a peak in granitic magmatism in the World and is coincident in time with several plume related events found in other continents and cratons.

ACKNOWLEDGEMENTS

We thank the colleagues of the Group of Granite Petrology (UFPA) for discussions and to José de Arimatéia Costa de Almeida for support in complementary field work. This study was conducted under a sandwich Ph.D. fellowship awarded to MFBT by CAPES (Coordenação de Aperfeiçoamento de Pessoal de Nível Superior) in the context of the National Program of Strategic Areas (INCT-GEOCIAM; Bex 0201/16-2). Zircon and titanite analyses were carried out on the Sensitive High Resolution Ion Micro Probe mass spectrometer (SHRIMP II) at the John de Laeter Centre, Curtin University, with the financial support of the Australian Research Council and Auscope NCRIS. Mineral images and compositional tests by EDS were performed at the Center for Microscopy, Characterization, and Analysis (CMCA) of the University of Western Australia. We are grateful to the CNPq (Conselho Nacional de Desenvolvimento Cientifico e Tecnológico) for doctoral thesis scholarship to MFBT, and research grants to R. Dall'Agnol (Proc. 306108/2014-3), C.N. Lamarão (Proc. 305701/2014-2) and D.C. Oliveira (Proc. 485806/2013-4). This research received financial support of the INCT GEOCIAM (CNPq/FAPESPA/CAPES/PETROBRAS; Proc. 573733/2008-2) and of the Federal University of Pará (UFPA). This paper is a contribution to the Brazilian Institute of Amazonian Geosciences (INCT GEOCIAM).

REFERENCES

Aleinikoff, J.N., Wintsch, R.P., Fanning, C.M., Dorais, M.J., 2002. U–Pb geochronology of zircon and polygenetic titanite from the Glastonbury Complex, Connecticut, USA an integrated SEM, EMPA, TIMS, and SHRIMP study. Chemical Geology 188, 125-147.

Almeida F.F.M. de, Hasui Y, Poncano W.L., Dantas A.S.L., Carneiro C.D.R., Melo M.S. de, Bistrichi C.A. 1981. Mapa Geológico do Estado de São Paulo, escala 1:500.000 - Nota Explicativa. Institute de Pesquisas Tecnológicas do Estado de São Paulo, 126p.

Almeida, J.A.C., Dall'Agnol, R., Rocha, M.C., 2017. Tonalite–Trondhjemite and Leucogranodiorite–Granite Suites from the Rio Maria Domain, Carajás Province, Brazil: implications for discrimination and origin of the Archean Na-granitoids. The Canadian Mineralogist 55, 437-456.

Almeida, J.A.C., Dall'Agnol, R., Oliveira, D.C., 2006. Geologia, petrografia e geoquímica do granito anorogênico Bannach, Terreno granito-greenstone de Rio Maria, Pará. Revista Brasileira de Geociências 36, 282-295 (in Portuguese).

Almeida, J.A.C., Dall'Agnol, R., Oliveira, M.A., Macambira, M.J.B., Pimentel, M.M., Rämö, O.T., Guimarães, F.V., Leite, A.A.S., 2011. Zircon geochronology and geochemistry of the TTG suites of the Rio Maria granite-greenstone terrane: Implications for the growth of the Archean crust of Carajás Province, Brazil. Precambrian Research 187, 201-221.

Almeida, J.A.C, Dall'Agnol R., Leite A.A.S., 2013. Geochemistry and zircon geochronology of the Archean granite suites of the Rio Maria granite-greenstone terrane, Carajás Province, Brazil. Journal of South American Earth Sciences 42, 103-126.

Almeida, M.E., Macambira, M.J.B., Oliveira, E.C., 2007. Geochemistry and zircon geochronology of the I-type high-K calc-alkaline and S-type granitoid rocks from southeastern Roraima, Brazil: Orosirian collisional magmatism evidence (1.97–1.96 Ga) in central portion of Guyana Shield. Precambrian Research 155, 69–97.

Altoff F. J., Barbey P., Boullier A. M. 2000. 2.8-3.0 Ga plutonism and deformation in the SE Amazonian craton: the Archean granitoids of Marajoara (Carajás Mineral Province, Brazil). Precambrian Research 104, 187-206.

Anderson, J.L., 1983. Proterozoic anorogenic granite plutonism of North America. Geological Society of America, Memoir 161, 133–154.

Anderson, J.L., Barth, A.P., Mazdab, J.L.W.F., 2008. Thermometers and thermobarometers in granitic systems. Reviews in Mineralogy and Geochemistry 69, 121–142.

Anderson, J.L., Morrison, J., 2005. Ilmenite, magnetite, and peraluminous Mesoproterozoic anorogenic granites of Laurentia and Baltica, Lithos 80, 45–60.

Anderson, J.L., Smith, D.R., 1995. The effects of temperature and fO_2 on the Al-in-hornblende barometer. American Mineralogist 80, 549–559.

Antonio, P.Y.J., D'Agrella-Filho, M.S., Trindade, R.I.F, Nédélec, A., Oliveira, D.C., Silva, F.F., Roverato, M., Lana, C., 2017. Turmoil before the boring billion: Paleomagnetism of the 1880–1860 Ma Uatumã event in the Amazonian craton. Gondwana Research 49, 106-129.

Avelar, V.G. 1996. Geocronologia Pb-Pb por evaporação em monocristal de zircão, do magmatismo da região de Tucumã, SE do Estado do Pará, Amazônia oriental. Federal University of Pará. Dissertation. Graduated Program on Geology and Geochemistry, Institute of Geosciences, 199 pp. (in Portuguese).

Avelar, V.G., Lafon, J.M., Correia Jr, F.C., Macambira E.M B., 1999. O Magmatismo arqueano da região de Tucumã-Província Mineral de Carajás: novos resultados geocronológicos. Revista Brasileira de Geociências 29(2), 454-460 (in Portuguese).

Barbosa, A.A., Lafon, J.M., Neves, A.P., Vale, A.G., 1995. Geocronologia Rb–Sr e Pb–Pb do Granito Redenção, SE do Pará: implicações para a evolução do magmatismo proterozóico da região de Redenção. Boletim do Museu Paraense Emílio Goeldi. Ciências da Terra 7, 147–164 (in Portuguese).

Barreto, C.J.S., Lafon, J.M., Costa, L.T.R., Lima, E.F., 2013. Vulcanismo félsico paleoproterozoico do Grupo Iricoumé, Domínio Erepecuru-Trombetas, Província Amazônia Central: dados de campo, caracterização petrográfica e geocronologia Pb-Pb em zircão. Geologia-USP, Série Científica 13, 47-71. (In Portuguese).

Barreto, C.J.S., Lafon, J.M., Costa, L.T.R., Lima, E.F., 2014. Palaeoproterozoic (~1.89 Ga) felsic volcanism of the Iricoumé Group, Guyana Shield, South America: geochemical and Sm-Nd isotopic constraints on sources and tectonic environment. International Geology Review. http://dx.doi.org/10.1080/00206814.2014.930800.

Barros, C.E.M., Dall'Agnol, R., Vieira, E.A.P., Magalhães, M.S., 1995. Granito Central da Serra dos Carajás: avaliação do potencial metalogenético para estanho com base em estudos da borda oeste do corpo. Boletim do Museu Paraense Emílio Goeldi. Série Ciências da Terra 7, 93–123 (in Portuguese).

Barros, C.E.M., Dall'Agnol, R., Barbey, P., Boullier, A.M., 1997. Geochemistry of the Estrela Granite Complex, Carajás region, Brazil: an example of an Archean A-type granitoid. Journal of South American Earth Sciences 10, 321–330.

Barros, C.E.M., Sardinha, A.S., Barbosa, J.P.O., Macambira, M.J.B., 2009. Structure, petrology, geochemistry and zircon U/Pb and Pb/Pb geochronology of the synkinematic Archean (2.7 Ga) A-type granites from the Carajás Metallogenic Province, northern Brazil. The Canadian Mineralogist 47, 1423–1440.

Barros M.A.S., Padilha R.A., Rubert R.R., Pimentel M.M., ChemaleJr. F. 2006. Iriri volcanism and Rio Dourado Granite: A-Type Paleoproterozoic Magmatism in northeastern Mato Grosso – Brazil. In: Symposium on magmatism, crustal evolution, and metallogenesis of the Amazonian Craton/workshop on A-Type granites and related rocks through time (IGCP 510), 2006, Belém. Abstract volume and Field Trips Guide… Belém: PRONEX-UFPA/ SBG-NO, p.39-39.

Barros, M.A.S., Pimentel ,M.M., Silva F.R., Dantas, E.L., 2011. A Suíte Intrusiva Rio Dourado – um granito tipo A de 1,88 Ga – sudeste do Cráton Amazônico – Mato Grosso – Brasil. Geologia USP, Série Científica 11(1), 75-93.

Bastos Neto, A.C., Ferron, J.T.M.M., Chauvet, A., Chemale Jr, F., Lima, E.F., Barbanson, L., Costa, C.F.M., 2014. U–Pb dating of the Madeira Suite and structural control of the albite-enriched granite at Pitinga (Amazonia, Brazil): Evolution of the A-type magmatism and implications for the genesis of the Madeira Sn–Ta–Nb (REE, cryolite) world-class deposit. Precambrian Research 243, 181-196.

Bettencourt, J.S., Juliani., Xavier, R.P., Monteiro, L.V.S., Bastos-Neto, A.C., Klein, E.L., Assis, R.R., Leite-Jr., W.P., Moreto, C.P.N., Fernandes, C.M.D., Pereira, V.P., 2016. Metallogenetic systems associated with granitoid magmatism in the Amazon Craton: An overview of the present level of understanding and exploration significance. Journal of South American Earth Sciences 68, 22-49.

Brito-Neves, M.F.L., Almeida, M.E., Macambira, M.J.B., 1999. $^{207}Pb/^{206}Pb$ age of calc-alkaline rapakivi granite in Tapajós Gold Province, Amazon Craton, Brazil. In: South American Symposium on Isotope Geology, 2. Actas, 40-43.

Bonin, B., 2007. A-type granites and related rocks: evolution of a concept, problems and prospects. Lithos 97, 1–29.

Carvalho T. A. Petrografia, Geoquímica e Suscetibilidade Magnética do Granito Gradaús, Província Carajás, SE do Pará. Federal University of Pará. Dissertation. Graduated Program on Geology and Geochemistry, Institute of Geosciences, Belém 58pp. (in Portuguese).

Ciborowski, T.J.R., Minifie, M.J., Kerr, A.C., Ernst, R.E., Baragar, B., Millar, I.L., 2017. A mantle plume origin for the Palaeoproterozoic Circum-Superior Large Igneous Province. Precambrian Research 249, 189-2013.

Compston, W., Williams, I.S., Kirschvink, J.L., Zichao, Z., Guogan, M.A., 1992. Zircon U-Pb ages for the Early Cambrian time-scale. Journal of the Geological Society, London 149, 171 - 184.

Condie, K.C., 2002. Continental growth during a 1.9-Ga superplume event. Journal of Geodynamics 34, 249–264.

Condie, K.C., Belousova, E., Griffin, W.L. and Sircombe, K.N., 2009. Granitoid events in space and time: Constraints from igneous and detrital zircon age spectra. Gondwana Research 15, 228-242.

Corfu, F., 1996. Multistage zircon and titanite growth and inheritance in an Archean gneiss complex, Winnipeg River Subprovince, Ontario. Earth Planet. Sci. Lett. 141, 175– 186.

Corfu, F., Hanchar, J.M., Hoskin, P.W.O., and Kinny, P., 2003, Atlas of zircon textures, in: Hanchar, J.M., and Hoskins, P.W.O. (eds.), Zircon: Reviews in Mineralogy and Geochemistry 53, 468–500.

Corrêa, L.W.C., Macambira, M.J.B. 2014. Evolução da região de Santana do Araguaia (PA) com base na geologia e geocronologia Pb-Pb em zircão de granitoides. Geologia USP - Serie Científica 14 (2), 45-66. (in Portuguese).

Costi, H.T., Dall'Agnol, R., Moura, C.A.V., 2000. Geology and Pb/Pb geochronology of Paleoproterozoic volcanic and granitic rocks of the Pitinga Province, Amazonian craton, northern Brazil. International Geology Review 42, 832–849.

Costi, H.T., Dall'Agnol, R., Pichavant, M., Ramo, O.T., 2009. The peralkaline tin-mineralized Madeira cryolite albite-rich granite of Pitinga, Amazonian Craton, Brazil: petrography, mineralogy and crystallization processes. Canadian Mineralogist 47, 1301-1327.

Cruz, D. R.S., Fernandes, C.M.D., Villas, R.N.N., Juliani, C., Monteiro, L.V.S., Lagler, B., Misas, C.M.E., 2016. Paleoproterozoic volcanic centers of the São Félix do Xingu

region, Amazonian Craton, Brazil: hydrothermal alteration and metallogenetic potential. Journal of Volcanology and Geothermal Research 320, 75-87.

Cunha, I.R.V., Dall'Agnol, R., Feio, G.R.L., 2016. Mineral chemistry and magnetic petrology of the Archean Planalto Suite, Carajás Province – Amazonian Craton: implications for the evolution of ferroan Archean granites. Journal of South American Earth Sciences 67, 100–121.

Dall'Agnol, R., Teixeira, N.P., Magalhães, M.S., 1993. Diagnostic features of the Tin-specialized anorogenic granites of the Eastern Amazonian region. Anais da Academia Brasileira de Ciências 65 (Suppl. 1), 33-50.

Dall'Agnol, R., Lafon, J.M., Macambira, M.J.B., 1994. Proterozoic anorogenic magmatism in the Central Amazonian Province: geochronological, petrological and geochemical aspects. Mineralogy and Petrology 50, 113–138.

Dall'Agnol, R., Rämö, O.T., Magalhães, M.S., Macambira, M.J.B., 1999a. Petrology of the anorogenic, oxidised Jamon and Musa granites, Amazonian Craton: implications for the genesis of Proterozoic A-type granites. Lithos 46, 431–462.

Dall'Agnol, R., Scaillet, B., Pichavant, M., 1999b. An experimental study of a lower Proterozoic A-type granite from the eastern Amazonian craton, Brazil. Journal of Petrology 40, 1673–1698.

Dall'Agnol, R., Costi I.T, Leite A.A. da S., Magalhaes M.S. de, Teixeira N.P. 1999c. Rapakivi granites from Brazil and adjacent areas. Precambrian Research 95, 9-39.

Dall'Agnol, R., Silva Jr, R.O., Oliveira, E. P., 1999d. Geologia, petrografia e geoquímica dos diques proterozóicos da região de Rio Maria, Sudeste do Pará. Geochimica Brasiliensis 13, 163-18. (in Portuguese).

Dall'Agnol, R., Teixeira, N.P., Rämö, O.T., Moura, C.A.V., Macambira, M.J.B., Oliveira, D.C., 2005. Petrogenesis of the Paleoproterozoic, rapakivi, A-Type granites of the Archean Carajás Metallogenic Province, Brazil. Lithos 80, 101–129.

Dall'Agnol, R., Oliveira, M.A., Almeida, J.A.C., Althoff, F.J., Leite, A.A.S., Oliveira, D.C., Barros, C.E.M., 2006. Archean and Paleoproterozoic granitoids of the Carajás Metallogenetic Province, eastern Amazonian craton. In: Dall'Agnol, R., Rosa-Costa, L.T., Klein, E.L. (Eds.), Symposium on Magmatism, Crustal Evolution, and Metallogenesis of the Amazon Craton. Abstracts volume and field trips guide. Belém, PRONEX-UFPA/SBG-NO, pp. 99–150.

Dall'Agnol, R., Oliveira, D.C., 2007. Oxidized, magnetite-series, rapakivi-type granites of Carajás, Brazil: implications for classification and petrogenesis of A-type granites. Lithos 93, 215 - 233.

Dall'Agnol, R., Frost, C.D., Rämö, O.T., 2012. IGCP Project 510 "A-type granites and related rocks through time": project vita, results, and contribution to granite research. Lithos 151, 1–16.

Dall'Agnol, R., Oliveira, D.C., Guimarães, F.V., Gabriel, E.O., Feio, G.R.L., Lamarão, C.N., Althoff, F.J., Santos, P.A., Teixeira, M.F.B., Silva, A.C., Rodrigues, D.S., Santos, M.J.P., Silva, C.R.P., Santos, R.D., Santos, P.J.L., 2013. Geologia do Subdomínio de Transição do Domínio Carajás – Implicações para a evolução arqueana da Província Carajás - Pará. SBG, Simpósio de Geologia da Amazônia 13. CD-ROM, Anais, Belém (in Portuguese).

Dall'Agnol, R., Cunha, I.R.V., Guimarães, F.V., Oliveira, D.C., Teixeira, F.B.T., Feio, G.R., Lamarão, C.N., 2017. Mineralogy, geochemistry, and petrology of Neoarchean ferroan to magnesian granites of Carajás Province, Amazonian Craton: The origin of hydrated granites associated with charnockites. Lithos 277, 3 - 32.

DePaolo, D.J., 1981. A neodymium and strontium isotopic study of the Mesozoic calc-alkaline granitic batholiths of the Sierra Nevada and Peninsular Ranges, California. J. Geophys. Res.: Solid Earth 86, 10470–10488.

DOCEGEO, 1988. Revisão litoestratigráfica da Província Mineral de Carajás e Litoestratigrafia e principais depósitos minerais. In: 35th Congresso Brasileiro de Geologia, Belém (in Portuguese).

Eby, G.N., 1992. Chemical subdivision of the A-type granitoids: petrogenesis and tectonic implications. Geology 20, 641–644.

Emslie, R.F., 1991. Granitoids of rapakivi granite–anorthosite and related associations. Precambrian Research 51, 173–192.

Feio, G.R.L., Dall'Agnol, R., 2012. Geochemistry and petrogenesis of the Mesoarchean granites from the Canaã dos Carajás Area, Carajás Province, Brazil: implications for the origin of Archean granites. Lithos 154, 33–52.

Feio, G.R.L., Dall'Agnol, R., Dantas, E., Macambira, M.J.B., Gomes, A.C.B., Sardinha, A.S., Santos, P., 2012. Geochemistry, geochronology, and origin of the Planalto granite suite and associated rocks: implications for the Neoarchean evolution of the Carajás Province. Lithos 151, 57–73.

Feio, G.R.L., Dall'Agnol, R., Dantas, E.L., Macambira, M.J.B., Santos, J.O.S., Althoff, F.J., Soares, J.E.B., 2013. Archean granitoid magmatism in the Canaã dos Carajás area: implications for crustal evolution of the Carajás province, Amazonian craton, Brazil. Precambrian Research 227, 157–185.

Fernandes C.M.D., Juliani C., Monteiro L.V.S., Lagler B., Misas C.M.E. 2011. High-K calc-alkaline to A-type fissure-controlled volcanoplutonism of the São Félix do Xingu region, Amazonian craton, Brazil: Exclusively crustal sources or only mixed Nd model ages? Journal of South American Earth Sciences 32(4), 351-368.

Ferreira, A.T.R., Lamarão, C.N., 2013. Geologia, petrografia e geoquímica das rochas vulcânicas Uatumã na área sul de São Félix do Xingu (PA), Província Carajás. Brazilian Journal of Geology 43 (1), 152-167.

Ferron, J.M.T.M., Bastos Neto, A.C., Lima, E.F., Costi, H.T., Moura, C., Prado, M., Galarza, M., 2006. Geologia e geocronologia Pb-Pb de rochas graníticas e vulcânicas ácidas a intermediárias Paleoproterozóicas da Província Pitinga, Craton Amazônico. Revista Brasileira de Geociências 36 (3), 499–512. (in Portuguese).

Ferron, J.M.T.M., Bastos Neto, A.C., Lima, E.F., Nardi, L.V.S., Costi, H.T., Pierosan, R., Prado, M. 2010. Petrology, geochemistry, and geochronology of Paleoproterozoic volcanic and granitic rocks (1.89–1.88 Ga) of the Pitinga Province, Amazonian Craton, Brazil. Journal of South American Earth Sciences 29, 483-449.

Fraga, L.M.B., Dall'Agnol, R., Costa, J.B.S., Macambira, M.J.B., 2009. The Mesoproterozoic Mucajaí anorthosite–mangerite–rapakivi granite complex, Amazonian craton, Brazil. The Canadian Mineralogist 47, 1469–1492.

Fraga, L.M., Vasquez, M.L., Almeida, M., Dreher, A.M., Reis, N. 2017. A influência da orogenia eo-orosiriana na formação da SLIP Uatumã, parte central do Craton

Amazônico. Anais do 15º Simpósio de Geologia da Amazônia, Belém. (in Portuguese).

Frost, B.R., Barnes, C.G., Collins, W.J., Arculus, R.J., Ellis, D.J, Frost, C.D., 2001. A geochemical classification for granitic rocks. Journal of Petrology 42, 2033–2048.

Fuck, H.A., Pimentel, M.M., Daoud, W.E.K., 1993. Idade U-Pb do Granito Madeira, Pitinga (AM). 4°Congresso Brasileiro de Geoquímica, Anais 246-249, Brasília. (in Portuguese).

Gabriel, E.O., Oliveira, D.C., 2014. Geologia, petrografia e geoquímica dos granitoides arqueanos de alto magnésio da região de Água Azul do Norte, porção sul do Domínio Carajás, Pará. Boletim do Museu Paraense Emílio Goeldi, Ciências Naturais 9 (3), 533–564 (in Portuguese).

Gabriel, E.O., Oliveira, D.C., Santos, M.S., 2014. Sanukitoides mesoarqueanos de Água Azul do Norte, Sul do Domínio Carajás: Novos dados e perspectivas. SBG, Congresso Brasileiro de Geologia 47. CD-ROM, Anais, Salvador (in Portuguese).

Gastal, M.C.P., 1987. Mapeamento e petrologia do maciço granítico Musa. Rio Maria, Sudeste do Pará. Unpublished M.Sc. Thesis, Universidade Federal do Pará, Belem.

Gibbs, A.K., Wirth, K.R., Hirata, W.K., Olszewski, W.J., 1986. Age and composition of the Grão Pará Group Volcanics, Serra dos Carajás. Revista Brasileira de Geociências 16, 201–211 (in Portuguese).

Gioia, S.M.C.L., Pimentel M.M. 2000. The Sm-Nd isotopic method in the geochronology laboratory of the University of Brasília. Anais da Academia Brasileira de Ciências 72, 220-245. doi:10.1590/S0001-37652000000200009.

Goodge, J.W., Vervoort, J.D., 2006. Origin of Mesoproterozoic A-type granites in Laurentia: Hf isotope evidence. Earth and Planetary Science Letters 243, 711-731.

Haapala, I., Rämö, O.T. Frindt, S., 2005. Comparison of Proterozoic and Phanerozoic rift-related basaltic–granitic magmatism. Lithos 80, 1–32.

Heaman, L. M. (2009). The application of U-Pb geochronology to mafic, ultramafic and alkaline rocks: an evolution of the three mineral standards. Chemical Geology, 261, 43-52.

Heilimo, E., Halla, J., Lauri, L.S., Rämö, O.T., Huhma, H., Kurhila, M.I., Front, K., 2009. The Paleoproterozoic Nattanen-type granites in northern Finland and vicinity post-collisional oxidized A-type suite. Bulletin of the Geological Society of Finland 81, 7–38.

Heinonen, A., Fraga, L., Rämö, O.T., Dall'Agnol, R., Mänttäri, I. & Andersen, T. 2012. Petrogenesis of the igneous Mucajaí AMG complex, northern Amazonian craton: Geochemical, U–Pb geochronological, and Nd–Hf–O isotopic constraints. Lithos 151, 17–34

Hirata, W.K., Rigon, J.C., Kadekaru, K., Cordeiro, A.A.C., Meireles, E.A., 1982. Geologia Regional da Província Mineral de Carajás. In: 1st Simpósio de Geologia da Amazonia, Belém (in Portuguese).

Hoffman, P.F., 1988. United Plates of America, the birth of a craton-Early Proterozoic assembly and growth of Laurentia. Annual Review of Earth and Planetary Sciences 16, 543–603.

Huhn, S.B., Macambira, M.J.B., Dall'Agnol, R., 1999. Geologia e geocronologia Pb-Pb do granito alcalino arqueano Planalto, região da Serra do Rabo, Carajás-PA. Simpósio de Geologia da Amazônia 6, 463–466 (in Portuguese).

Ishihara, S., 1981. The granitoid series and mineralization. Economic Geology 75, 458–484.

Javier-Rios, F., Villas, R.N., Dall'Agnol, R., 1995. O Granito Serra dos Carajás: fácies petrográficas e avaliação do potencial metalogenético para estanho no setor norte. Revista Brasileira de Geociências 25, 20–31 (in Portuguese).

Juliani, C., Fernandez, C.M.D., 2010. Well-preserved Late Paleoproterozoic volcanic centers in the São Félix do Xingu region, Amazonian craton, Brazil. J. Volcanol. Geotherm. Res. 191, 167–179.

Kaur, P., Zeh, A., Chaudhri, N., Eliyas, N., 2017. Two distinct sources of 1.73–1.70 Ga A-type granites from the northern Aravalli orogen, NW India: Constraints from in situ zircon U-Pb ages and Lu-Hf isotopes. Gondwana Research 49, 164-181.

Klein E., Almeida M., Rosa-Costa L.T., 2012. The 1.89-1.87 Ga Uatumã Silicic Large Igneous Province, northern South America. Large Igneous Provinces Commission. (http://www.largeigneousprovinces.org), November 2012 LIP of the Month.

Klein, E.L., Vasquez, M.L. 2000. Projeto Especial Província Mineral do Tapajós. Geologia e recursos minerais da Folha Vila Riozinho (SB.21-Z-A). Estado do Pará. Escala 1:250.000. CPRM-Serviço Geológico do Brasil, (Nota explicativa CD-ROM). (in Portuguese).

Lamarão C.N., Dall'Agnol R., Pimentel, M.M., 2005. Nd Isotopic composition of Paleoproterozoic volcanic and granitoid rocks of Vila Riozinho: Implications for the crustal evolution of the Tapajós Gold Province, Amazon craton. Journal of South American Earth Sciences 18, 277-292.

Lamarão, C.N., Pinho, S.C.C., Paiva Junior, A.L., Galarza-Toro, M.A., 2012. Mineralogy and geochemistry of the Paleoproterozoic, tin mineralized Bom Jardim Granite of the Velho Guilherme Suite, eastern Amazonian Craton. Journal of South American Earth Sciences 38, 159-173.

Lamarão C.N., Dall'Agnol R., Lafon J.M., Lima E.F. 2002. Geology, geochemistry, and Pb-Pb zircon geochronology of the Paleoproterozoic magmatism of Vila Riozinho, Tapajós Gold Province, Amazonian craton, Brazil. Precambrian Research 119 (1-4), 189-223

Lamarão, C.N., Silva, J.S., Borges, R.M., Dall'Agnol, R., 2014. Morphological and compositional variations of zircon and their metallogenetic implications: the example of the Jamon, Serra dos Carajás and Velho Guilherme suites, Amazonian Craton. Brazilian Journal of Geology 44(1), 105-120.

Lenharo, S.L., 1998. Evolução magmática e modelo metalogenético dos granitos mineralizados da região de Pitinga, Amazonas, Brasil, São Paulo. Doctoral thesis. University of São Paulo, São Paulo, Brazil, 290 pp. (In Portuguese).

Lenharo, S.L., Pollard, P.J., Born, H., 2003. Petrology and textural evolution of granites associated with tin and rare-metals mineralization at the Pitinga mine, Amazonas, Brazil. Lithos 66, 37–61.

Leite-Santos, P.J., Oliveira, D.C., 2014. Trondhjemitos da área de Nova Canadá: novas ocorrências de associações magmáticas tipo TTG no Domínio Carajás. Boletim do Museu Paraense Emílio Goeldi. Serie Ciências Terra 9, 635-659 (in Portuguese).

Lima, P.H.A., 2011. Geologia, petrografia e geocronologia do Granito São João, Província Carajás, SSE do Pará. Trabalho de Conclusão de Curso – Federal University of Pará, Belém, pp. 1-47. (in Portuguese).

Lima, P.H.A., Lamarão, C.N., Santo, M.J.P., 2014 Petrografia, geoquímica e suscetibilidade magnética do Granito Paleoproterozóico São João, sudeste do Cráton Amazônico, Província Carajás. Boletim do Museu Paraense Emílio Goeldi 9, 47-72 (in Portuguese).

Ludwig, K.R., 2003. Isoplot 3.00, a geochronological took-kit for Excel: Berkeley Geochronology Center Special Publication 4, 67 p.

Ludwig, K.R., 2009. SQUID 2: A User's Manual, rev. 2.50, 12 Apr, 2009. Berkeley Geochronology Centre Special Publication 5, 110 p.

Machado, N., Lindenmayer, Z., Krogh, T.E., Lindenmayer, D., 1991. U-Pb geochronology of Archean magmatism and basement reactivation in the Carajás area, Amazon Shield, Brazil. Precambrian Research 49, 329–354.

Macambira, M.J.B., Lafon, J.M., 1995. Geocronologia da Província Mineral de Carajás; Síntese dos dados e novos desafios. Boletim do Museu Paraense Emílio Goeldi 7, 263–287 (in Portuguese).

Macambira, M.J.B., Almeida, M.E., Santos, L.J., 2002. Idade zircão de vulcânicas Iricoumé do sudeste de Roraima: Contribuição para a redefinição do Supergrupo Uatumã. Boletim do II Simpósio sobre Vulcanismo e Ambientes Associados. SBG/NO, Belém - PA, p. 22. (In Portuguese).

Martins, P.L.G., Toledo, C.L.B., Silva, A.M., Chemale Jr, F., Santos, J.O.S., Assis, L.M., 2017. Neoarchean magmatism in the southeastern Amazonian Craton, Brazil: Petrography, geochemistry and tectonic significance of basalts from the Carajás Basin. Precambrian Research 302, 340-357.

Marques, S.N.S., Souza, V.S., Dantas, E.L., Valério, C.S., Nascimento, R.S.C., 2014. Contributions to the petrography, geochemistry and geochronology (U-Pb and Sm-Nd) of the Paleoproterozoic effusive rocks from Iricoumé Group, Amazonian Craton, Brazil. Brazilian Journal of Geology 44 (1), 121–138.

Mesquita, C.J., Dall'Agnol, R., Almeida, J.A.C., Mineral chemistry and crystallization parameters of the A-type Paleoproterozoic Bannach Granite, Carajás Province – Pará. Brazillian Journal of Geology (Submitted).

Miller, J.S., Matzel, J.E.P., Miller, C.F., Burgess, S.D., Miller, R.B., 2007. Zircon growth and recycling during the assembly of large, composite arc plutons. Journal of Volcanology and Geothermal Research 167, 282–299.

Moreto, C.P.N., Monteiro, L.V.S., Xavier, R.P., Amaral, W.S., Santos, T.J.S., Juliani, C., Souza Filho, C.R., 2011. Mesoarchean (3.0 and 2.86 Ga) host rocks of the iron oxide–Cu–Au Bacaba deposit, Carajás Mineral Province: U–Pb geochronology and metallogenetic implications. Mineralium Deposita 46, 789–811.

Moreto, C.P.N., Monteiro, L.V.S., Xavier, R.P., Creaser, R.A., DuFrane, S.A., Melo, G.H.C., Silva, M.A.D., Tassinari, C.C.G., Sato, K., 2015. Timing of multiple

hydrothermal events in the iron oxide-copper-gold deposits of the Southern Copper Belt, Carajás Province, Brazil. Mineralium Deposita 50, 517-546.

Moura C.A.V., Gorayeb P.S.S., Matsuda N.S. 1999. Geocronologia Pb-Pb em zircão do riolito Vila Raiol, Formação Iriri – sudoeste do Pará. In: Simpósio de Geologia da Amazônia, 6. Manaus. Resumos expandidos... Manaus: SBG p.475-477. (In Portuguese)

Nardi, L.V.S., Formoso, M.L L., Jarvis, K., Oliveira, L., Bastos Neto, A.C., 2012. REE, Y, Nb, U, and Th contents and tetrad effect in zircon from a magmatic-hydrothermal F-rich system of Sn-rare metal-cryolite mineralized granites from the Pitinga Mine, Amazonia, Brazil. Journal of South American Earth Sciences 33, 34-42.

Nasdala, L., Hofmeister, W., Norberg, N., Valley, J.W., 2008. Zircon M257 - a Homogeneous Natural Reference Material for the Ion Microprobe U-Pb Analysis of Zircon. Geostandards and Geoanalytical Research 32(3), 247 – 265.

Oliveira, D.C., Dall'Agnol, R., Silva, J.B.C., Almeida, J.A.C., 2008. Gravimetric, radiometric, and magnetic susceptibility study of the Paleoproterozoic Redenção and Bannach plutons: implications for architecture and zoning of A-type granites. Journal of South American Earth Sciences 25, 100–115.

Oliveira, D.C., Dall'Agnol, R., Barros, C.E.M., Oliveira, M.A., 2009. Geology, geochemistry and magmatic evolution of the Paleoproterozoic, anorogenic oxidized A-type Redenção granite of the Jamon Suite, eastern Amazon Craton, Brazil. Canadian Mineralogist 47 (6), 1441–1468.

Oliveira, D.C., Neves, S.P., Trindade, R.I.F., Dall'Agnol, R., Mariano, G., Correia, P.B., 2010. Magnetic anisotropy of the Redenção granite, eastern Amazonian craton (Brazil): Implications for the emplacement of A-type plutons. Tectonophysics 493, 27 - 41.

Oliveira, D.C., Santos, P.J.L., Gabriel, E.O., Rodrigues, D.S., Faresin, A.C., Silva, M.L.T., Sousa, S.D., Santos, R.V., Silva, A.C., Souza, M.C., Santos, R.D., Macambira, M.J.B., 2010. Aspectos geológicos e geocronológicos das rochas magmáticas e metamórficas da região entre os municípios de Água Azul do Norte e Canaã dos Carajás – Província Mineral de Carajás. Congresso Brasileiro de Geologia 45. CDrom, Belém. (in Portuguese).

Oliveira, E.C., Lafon, J.M., Gioia, S.M.C.L., Pimentel, M.M. 2008. Datação Sm-Nd em rocha total e granada do metamorfismo granulítico da região de Tartarugal Grande, Amapá Central. Revista Brasileira Geociências 38,116–129 (in Portuguese).

Oliveira, M.A., Dall'Agnol, R., Althoff, F.J., Leite, A.A.S., 2009. Mesoarchean sanukitoid rocks of the Rio Maria Granite-Greenstone Terrane, Amazonian craton, Brazil. Journal of South American Earth Sciences 27, 146–160.

Oliveira, M.A., Dall'Agnol, R., Almeida, J.A.C., 2011. Petrology of the Mesoarchean Rio Maria suite: implications for the genesis of sanukitoid rocks. Journal of Petrology 51 (10), 2121- 2148.

Paiva Júnior, A.L., 2009. Geologia, petrografia, geocronologia e geoquímica do Granito anorogênico Seringa, Província Mineral de Carajás, SSE do Pará. Federal University of Pará. Dissertation. Graduated Program on Geology and Geochemistry, Institute of Geosciences, 158 pp. (in Portuguese).

Paiva Júnior, A.L., Lamarão, C.N., Lima, P.H.A., 2011. Geologia, Petrografia e Geoquímica do Batólito Seringa, Província Carajás, SSE do Pará. Revista Brasileira de Geociências 41(2), 185-202 (in Portuguese).

Patiño-Douce, A., 1997. Generation of metaluminous A-type granites by low pressure melting of calc-alkaline granitoids. Geology 25, 743–7.

Pidgeon, R.T., Bosch, D., Bruguier, O., 1996. Inherited zircon and titanite U-Pb systems in an Archaean syenite from southwestern Australia: implications for U-Pb stability of titanite. Earth and Planetary Science Letters 141, 187-198.

Pinho, S., Fernandes, C., Teixeira, N., Paiva Jr., A., Cruz, V., Lamarão, C., Moura, C., 2006. O magmatismo paleoproterozóico da região de São Félix do Xingu, Província Estanífera do sul do Pará: Petrografia e Geocronologia. Revista Brasileira de Geociencias 36, 724–732.

Rämö, O.T., 1991. Petrogenesis of the Proterozoic rapakivi granites and related basic rocks of southeastern Fennoscandia: Nd and Pb isotopic and general geochemical constraints. Geological Survey of Finland, Bulletin 355, 161 p.

Rämö, O.T., Dall'Agnol, R., Macambira, M.J.B., Leite, A.A.S., Oliveira, D.C., 2002. 1.88 Ga oxidized A-type granites of the Rio Maria region, eastern Amazonian craton, Brazil: positively anorogenic! Journal of Geology 110, 603-610.

Rämö, O.T.,, Haapala, I., 1995. One hundred years of rapakivi granite. Mineral Petrol 52, 129–185.

Rämö, O.T., Mänttäri, I., 2015. Geochronology of the Suomenniemi rapakivi granite complex revisited: Implications of point-specific errors on zircon U-Pb and refined λ_{87} on whole-rock Rb-Sr. Bulletin of the Geological Society of Finland 87, 25-45 http://dx.doi.org/10.17741/bgsf/87.1.002.

Rios, F.J., Villas, R.N., Fuzikawa, K., 2003. Fluid evolution in the Pedra Preta wolframite ore deposit, Paleoproterozoic Musa granite, eastern Amazon craton, Brazil. Journal of South American Earth Sciences 15, 787–802.

Rodrigues, E.S., Lafon, J.M., Scheller, T. 1992. Geocronologia Pb-Pb da Província Mineral de Carajás: primeiros resultados. In: SBG, Congresso Brasileiro de Geologia, 37, São Paulo, Brazil, Boletim de resumos expandidos 2, 183-184.

Rodrigues, D.S., Oliveira, D.C., Macambira, M.J.B., 2014. Geologia, geoquímica e geocronologia do Granito Mesoarqueano Boa Sorte, município de Água Azul do Norte, Pará – Província Carajás. Boletim do Museu Paraense Emílio Goeldi. Série Ciências da Terra 9, 597–633 (in Portuguese).

Roverato, M., Juliani, C., Marcelo Dias-Fernandes, C., Capra, L., 2017. Paleoproterozoic andesitic volcanism in the southern Amazonian craton, the Sobreiro Formation: new insights from lithofacies analysis of the volcaniclastic sequences. Precambrian Research 289, 18–30.

Santos, J.O.S., Hartmann, L.A., Gaudette, H.E., Groves, D.I., McNaugthon, N.J.,Fletcher, I.R., 2000. New understanting of the Provinces of Amazon Craton based on Integration of Field Mapping and U-Pb and Sm-Nd geochronology. Gondwana Research 3 (4), 453-488.

Santos, J.O.S., Groves, D.I., Hartmann L.A., Moura, M.A., Mcnaughton, N.J. 2001. Gold deposits of the Tapajós and Alta Floresta Domains, Tapajós-Parima orogenic belt, Amazon Craton, Brazil. Mineralium Deposita 36(3), 278-299.

Santos, J.O.S., 2003. Geotectonics of the Guyana and Central Brazil Schields. In: Bizzi, L.A., Schobbenhaus, C., Vidotti, R.M., Gonçalves, J.H. (eds.), Geology, Tectonics and Mineral Resources of Brazil, Companhia de Pesquisa de Recursos Minerais, Brasília, ISBN 85-230-0790-3, pp. 169-226.

Santos, J.O.S., Silva, L.C., Faria, M.S.G., Macambira, M.J.B., 1997. Pb-Pb single crystal evaporation isotopic study on the post-tectonic, subalkalic, A-type Moderna granite (Mapuera Intrusive Suite), State of Roraima, northern Brazil. Symposium of Granites and Symposium of Granites and Associated Mineralizations, 2. Extended Abstract and Program. Sociedade Brasileira de Geologia, pp. 273–275.

Santos, J.O.S., Van Breemen, O.B., Groves, D.I., Hartmann L.A., Almeida M.E., Mcnaughton N.J., Fletcher I.R., 2004. Timing and evolution of multiple paleoproterozoic magmatic arcs in the Tapajós Domain, Amazon Craton: constraints from SHRIMP and TIMS zircon, baddeleyite and titanite U-Pb geochronology. Precambrian Research 131, 73-109.

Santos, N.S., Oliveira, D.C., 2016. Rio Maria granodiorite and associated rocks of Ourilandia do Norte Carajás Province: Petrography, geochemistry and implications for sanukitoid petrogenesis. Journal of South American Earth Sciences 72, 279-301.

Santos, P.A., Teixeira, M.F.B., Dall'Agnol, R., Guimarães, F.V., 2013. Geologia, petrografia e geoquímica da associação Tonalito-Trondhjemito-Granodiorito (TTG) do extremo leste do Subdomínio de Transição, Província Carajás, Pará. Boletim do Museu Paraense Emílio Goeldi. Ciências Naturais. 8 (3), 257- 290 (in Portuguese).

Santos, R.D., Galarza, M.A., Oliveira, D.C., 2013. Geologia, geoquímica e geocronologia do Diopsídio-Norito Pium, Província Carajás. Boletim do Museu Paraense Emílio Goeldi, Série Ciências da Terra 8, 355–382 (in Portuguese).

Sardinha, A.S., Barros, C.E.M., Krymsky, R., 2006. Geology, geochemistry, and U-Pb geochronology of the Archean (2.74 Ga) Serra do Rabo granite stocks, Carajás Province, northern Brazil. Journal of South American Earth Sciences 20, 327–339.

Schaltegger, U., Brack, P., Ovtcharova, M., Peytcheva, I., Schoene, B., Stracke A., Marocchi, M., Bargossi, G.M., 2009. Zircon and titanite recording 1.5 million years of magma accretion, crystallization and initial cooling in a composite pluton (southern Adamello batholith, northern Italy). Earth and Planetary Science Letters 286, 208-218.

Semblano, F.R.D., Macambira, M.J.B., Vasquez, M.L., 2016. Petrography, geochemistry and Sm-Nd isotopes of the granites from eastern of the Tapajós Domain, Pará state. Brazilian Journal of Geology 46(4), 509-529.

Shellnutt, J.G., Hari, K.R., Liao, A.C.Y., Denyszyn, S.W., Vishwakarma, N., (in press). A 1.88 Ga giant radiating mafic dyke swarm across Southern India and Western Australia. Precambrian Research. https://doi.org/10.1016/j.precamres.2018.01.021.

Sidder, G.B., Mendoza, S.V. 1991. Geology of the Venezuelan Guayana Shield and its relation to the entire Guayana Shield. U.S. Geol. Surv. Open-File Rep. 91-141, Denver, 59 p.

Siégel, C., Bryan, S.E., Allen, C.M., Gust, D.A., 2018. Use and abuse of zircon-based thermometers: A critical review and a recommended approach to identify antecrystic zircons. Earth-Science Reviews 176, 87-116.

Silva, A.C., Dall'Agnol, R., Guimarães, F.V., Oliveira, D.C., 2014. Geologia, petrografia e geoquímica de Associações Tonalíticas e Trondhjemíticas Arqueanas de Vila

Jussara, Província Carajás, Pará. Boletim do Museu Paraense Emílio Goeldi. Série Ciências Naturais 9, 13 - 45 (in Portuguese).

Silva, F.S., Oliveira, D.C., Antonio, P.Y., D'Agrella-Filho, M., Lamarão, C.N., 2016. Bimodal magmatism of the Tucuma area, Carajás Province: U-Pb geochronology, classification and processes. Journal of South American Earth Sciences 72, 95-114.

Silva Jr, C.A.S., Klein, E.L., Galarza, M.A., Borges, R.M.K., Queiroz, J.D.S., Assunção, R.F.S., Araújo, A.C.S, Moore, D.J., 2015. Zircon geochronology and Pb isotope systematics in sulfides: implications for the genesis of gold mineralization in the Cuiú-Cuiú Goldfeld, Tapajós Gold Province, Amazonian Craton, Brazil. Contribuições a Geologia da Amazônia 9, 453-465.

Sylvester, P. J., 1989. Post-collisional alkaline granites. *Journal of Geology* **97**:261-280.

Spencer, K.J., Hacker, B.R., Kylander-Clark, A.R.C., Andersen T.B., Cottle, J.M., Stearns, M.A., Poletti, J.E., Seward, G.G.E., 2013. Campaign-style titanite U–Pb dating by laser-ablation ICP: Implications for crustal flow, phase transformations and titanite closure. Chemical Geology 341, 84-101.

Stern, R.A., 2001. A new isotopic and trace element standard for the ion microprobe: preliminary TIMS U – Pb and electron microprobe data, current research. Radiogenic Age and Isotopic Studies: Report 14. Geological Survey of Canada, Ottawa, Canada.

Souza, Z.S., Potrel, H., Lafon, J.M., Althoff, F.J., Pimentel, M.M., Dall'Agnol, R., Oliveira, C.G., 2001. Nd, Pb, and Sr isotopes of the Identidade Belt, an Archaean greenstone belt of the Rio Maria region (Carajás Province, Brazil): implications for the Archaean geodynamic evolution of the Amazonian Craton. Precambrian Research 109, 293–315.

Stearns, M.A., Hacker, B.R., Ratschbacher, L., Rutte, D., Kylander-Clark, A.R.C., 2015. Titanite petrochronology of the Pamir gneiss domes: Implications for mid–deep crust exhumation and titanite closure to Pb and Zr diffusion. Tectonics 34, 1–19. http://dx.doi.org/10.1002/2014TC003774.

Tallarico, F.H.B., Figueiredo, B.R., Groves, D.I., Kositcin, N., McNaughton, N.J., Fletcher, I.R., Rego, J.L., 2005. Geology and SHRIMP U-Pb geochronology of the Igarape Bahia deposit, Carajás copper - gold belt, Brazil: an Archean (2.57 Ga) example of iron-oxide Cu-Au-(U-REE) mineralization. Economic Geology 100, 7-28.

Tassinari, C.C.G., Macambira, M.J.B., 1999. Geochronological provinces of the Amazonian craton. Episodes 22, 174–182.

Tassinari, C.C.G., Macambira, M.J.B., 2004. A evolução tectônica do cráton Amazônico. In: Matesso-Neto, V., Bartorelli, A., Carneiro, C.D.R., Britto- Neves, B.B. (Eds.), Geologia do Continente Sul-Americano. Sao Paulo, SP, Brazil, pp. 471- 485. (in Portuguese).

Teixeira, M.F.B., Dall'Agnol, R., Silva, A.C., Santos, P.A., 2013. Geologia, petrografia e geoquímica do Leucogranodiorito Pantanal e dos leucogranitos arqueanos da área de Sapucaia, Província Carajás, PA: implicações petrogenéticas. Boletim do Museu Paraense Emílio Goeldi, Série Ciências Naturais 8, 291–323 (in Portuguese).

Teixeira, M.F.B., Dall'Agnol, R., Santos, J.O.S., Sousa, L.A.M., Lafon, J-M., 2017. Geochemistry, geochronology and Nd isotopes of the Gogó da Onça Granite: A new Paleoproterozoic A-type granite of Carajás Province, Brazil. Journal of South American Earth Sciences 80, 47-65.

Teixeira N.P., 1999. Contribuição ao estudo das rochas granitóides e mineralizações associadas da Suíte Intrusiva Velho Guilherme, Província Estanífera do Sul do Pará. São Paulo University. Dr. Thesis. Institute of Geosciences, 508 pp. (in Portuguese).

Teixeira, N.P., Bettencourt, J.S., Moura, C.A.V., Dall'Agnol, R., Macambira, E.M.B., 2002. Archean crustal sources for Paleoproterozoic tin-mineralized granites in the Carajás Province, SSE Pará, Brazil: Pb–Pb geochronology and Nd isotope geochemistry. Precambrian Research 119, 257–275.

W. Teixeira, N.J. Reis, J.S. Bettencourt, E.F. Klein, D.C. Silva Intraplate Paleo- to Mesoproterozoic magmatism in the Amazonian Craton reviewed: geochronology and crustal tectonics and barcode matches R. Srivastava, R. Ernst (Eds.), Dyke Swarms of the World - A Modern Perspective (IDC-7 Special Volume), Submitted (2018).

Teixeira, W., Tassinari, C.C.G., Cordani, U.G., Kawashita, K., 1989. A review of the geochronology of the Amazonian Craton: tectonic implication. Precambrian Research 42, 213 - 227.

Teruiya, R.K., Paradella, W.R., Santos, A.R., Dall'agnol, R., Veneziani, P., 2008. Integrating airborne SAR, Landsat TM and airborne geophysics data for improving geological mapping in the Amazon Region: the Cigano Granite, Carajás Province, Brazil. International Journal of Remote Sensing, 29 (13), 3957-3974.

Valério, C.S., 2006. Magmatismo Paleoproterozóico do extremo sul do Escudo das Guianas, município de Presidente Figueiredo (AM): Geologia, geoquímica e geocronologia Pb-Pb em zircão. Federal University of Amazonas. Dissertation. Manaus, Brazil. 112 pp. (In Portuguese).

Valério, C.S., Souza, V.S., Macambira, M.J.B., 2009. The 1.90–1.87 Ga magmatism in the centersouthernmost Guyana Shield, Brazil: geology, geochemistry, zircon geochronology, and tectonic implications. Journal of South America Earth Sciences 28 (3), 304–320.

Valério, C.S., Macambira, M.J.B., Souza, V.S., Dantas, E.L., Nardi, L.V.S., 2018. 1.88 Ga São Gabriel AMCG association in the southernmost Uatumã-Anauá Domain: Petrological implications for post-collisional A-type magmatism in the Amazonian Craton. Lithos (300-301), 291-313.

Vasquez M.L., Klein E.L., Quadros M.L.E.S., Bahia R.B.C., Santos A., Ricci P.S.F., Sachett C.R., Silva C.M.G., Macambira M.J.B. 1999. Magmatismo Uatumã na Província Tapajós – novos dados geocronológicos. *In*: Simpósio de Geologia da Amazônia, 6., Manaus. Resumos expandidos... Manaus: SBG-Núcleo Norte. p.471-474. (In Portuguese).

Vasquez M.L., Klein E.L., Ricci P.S.F. 2002. Granitóides pós-colisionais da porção leste da Província Tapajós. *In*: Klein E.L., Vasquez M.L., Rosa-Costa L.T. (Eds.). Contribuições à Geologia da Amazônia. SBGNúcleo Norte, Belém. 3:67-84. (In Portuguese).

Vasquez, M.L., Macambira M.J.B., Armstrong R.A. 2008b. Zircon geochronology of granitoids from the western Bacajá domain, southeastern Amazonian craton, Brazil: Neoarchean to Orosirian evolution. Precambrian Research 161, 279-302.

Windley, B.F., 1993. Proterozoic anorogenic magmatism and its orogenic connections. Journal of the Geological Society (London) 150, 39–50.

Whalen, J.B., Currie, K.L., Chappell, B.W., 1987. A-type granite: geochemical characteristics, discrimination and petrogenesis. Contributions to Mineralogy and Petrology 95, 407–419.

Whitney, D. L., Evans, B.W., 2010. Abbreviations for names of rock-forming minerals. American Mineralogist 95 (1), 185-187.

Xiong,Q., Zheng, J., Yu, C., Su, Y., Tang, H., Zhang, Z., 2008. Zircon U-Pb age and Hf isotope of Quanyishang A-type granite in Yichang: Signification for the Yangtze continental cratonization in Paleoproterozoic. Chinese Science Bulletin 54, 436-446.

Zhao, G., Cawood, P.A., Wilde, S.A., Sun, M., 2002. Review of global 2.1–1.8 Ga orogens: implications for a pre-Rodinia supercontinent. Earth-Science Reviews 59, 125–162.

Zhao, T.P., Zhou, M.F., 2009. Geochemical constraints on the tectonic setting of Paleoproterozoic A-type granites in the southern margin of the North China Craton. J. Asian Earth Sci. 36, 183-195.

Zhang, L.S., Scharer, U., 1996. Inherited Pb components in magmatic titanite and their consequence for the interpretation of U-Pb ages. Earth and Planetary Science Letters 138, 57-65.

Supplementary Table 1. U-Pb-Th SHRIMP data on zircon of the granites of the Serra dos Carajás Suite

						isotopic ratios								Ages (Ma)				
	U	Th	Th	^{206}Pb	4f^{206}	^{207}Pb		^{207}Pb		^{206}Pb	error	^{208}Pb		^{206}Pb		^{207}Pb		Disc.
spot	ppm	ppm	U	ppm	%	^{206}Pb		^{235}U		^{238}U	correl.	^{232}Th		^{238}U		^{206}Pb		%
ECR-SC-01. Serra dos Carajás Granite. zircon																		
N1619D.1-1	378	125	0.34	105	0.009	0.11527	± 0.50	5.1627	± 1.27	0.3248	± 1.16	0.918	0.0905	± 1.49	1813	± 18	1884	± 9	+4.0
N1619D.1-2	189	77	0.42	53	0.019	0.11447	± 0.73	5.1863	± 2.30	0.3286	± 2.18	0.948	0.0928	± 2.59	1832	± 35	1871	± 13	+2.0
N1619D.2-1	1315	395	0.31	111	0.279	0.06883	± 0.99	0.9296	± 1.60	0.0980	± 1.26	0.784	0.0308	± 2.04	602	± 7	893	± 21	+34.0
N1619D.6-2	242	110	0.47	68	0.012	0.11588	± 0.59	5.2479	± 1.38	0.3285	± 1.25	0.904	0.0947	± 2.97	1831	± 20	1893	± 11	+4.0
N1619D.7-1	687	321	0.48	116	0.055	0.10202	± 0.54	2.7637	± 1.22	0.1965	± 1.09	0.895	0.0584	± 1.4	1156	± 12	1873	± 10	+33.0
N1619D.7-2	285	101	0.36	81	0.000	0.11572	± 0.91	5.2829	± 1.55	0.3311	± 1.26	0.809	0.0956	± 1.67	1844	± 20	1874	± 16	+3.0
N1619D.8-1	373	76	0.21	104	0.000	0.11455	± 0.51	5.1001	± 1.27	0.3229	± 1.16	0.915	0.0881	± 3.14	1804	± 18	1869	± 9	+4.0
N1619D.9-1	395	243	0.64	112	0.000	0.11620	± 0.93	5.2899	± 1.49	0.3302	± 1.16	0.778	0.0922	± 2.59	1839	± 19	1898	± 17	3
ECR-CG-14A. Cigano granite. zircon																		
N1619E.3-1	799	81	0.11	202	0.036	0.11395	± 0.42	4.6178	± 1.14	0.2939	± 1.06	0.931	0.0917	± 2.01	1661	± 16	1863	± 8	+12.0
N1619E.7-1	387	250	0.67	111	0.000	0.11459	± 0.47	5.2840	± 1.24	0.3344	± 1.15	0.925	0.0937	± 1.32	1860	± 19	1873	± 9	+1.0
N1619E.7-2	518	387	0.77	145	0.111	0.11464	± 0.47	5.1453	± 1.20	0.3255	± 1.11	0.920	0.0877	± 1.49	1817	± 18	1874	± 9	+3.0
N1619E.8-1	596	181	0.31	175	0.014	0.11580	± 0.43	5.4658	± 1.17	0.3423	± 1.09	0.930	0.0964	± 1.38	1898	± 18	1892	± 8	0.0
N1619E.9-1	757	500	0.68	204	0.000	0.11399	± 0.71	4.9302	± 1.55	0.3137	± 1.37	0.887	0.0883	± 1.92	1759	± 21	1863	± 13	+6.0
N1619E.11-1	242	157	0.67	69	0.100	0.11536	± 0.73	5.2713	± 1.48	0.3314	± 1.28	0.868	0.0910	± 1.66	1845	± 21	1885	± 13	+2.0
CIG-1 Cigano granite. zircon																		
N1620D.1-1	467	346	0.77	131	0.000	0.11494	± 1.08	5.1901	1.51	0.3275	± 1.05	0.697	0.0912	± 1.30	1826	± 17	1879	± 19	+3.2
N1620D.2-1-4	663	473	0.74	189	0.000	0.11550	± 0.51	5.2740	± 2.02	0.3312	± 1.96	0.967	0.0909	± 2.10	1844	± 31	1888	± 9	+2.7
N1620D.2-2	430	308	0.74	121	0.000	0.11491	± 0.58	5.1707	± 1.22	0.3263	± 1.07	0.880	0.0920	± 1.35	1821	± 17	1879	± 10	+3.5
N1620D.3-1	1092	600	0.57	308	0.019	0.11544	± 0.38	5.2265	± 1.00	0.3284	± 0.92	0.923	0.0921	± 1.29	1830	± 15	1887	± 7	+3.4
N1620D.7-1	759	490	0.67	215	0.000	0.11485	± 0.43	5.2141	± 1.07	0.3293	± 0.97	0.913	0.0908	± 1.18	1835	± 16	1878	± 8	+2.6

Supplementary Table 2. U-Pb-Th SHRIMP data on zircon of the granites of the Velho Guilherme Suite

						isotopic ratios													Ages (Ma)				
	U	Th	Th	^{206}Pb	4f^{206}	^{207}Pb		^{207}Pb		^{206}Pb		error	^{208}Pb		^{206}Pb		^{207}Pb		Disc.
spot	ppm	ppm	U	ppm	%	^{206}Pb		^{235}U		^{238}U		correl.	^{232}Th		^{238}U		^{206}Pb		%
L-42 - Velho Guilherme Granite. zircon																							
N1635G.7-1 (core)	93	55	0.61	27	0.000	0.11517	± 0.89	5.2977	± 1.67	0.3336	± 1.42	0.848	0.0967	± 1.89	1856	± 23	1883	± 16	1.6
N1635G.7-2 (rim)	294	202	0.71	80	0.032	0.11500	± 0.49	5.0104	± 1.43	0.3160	± 1.35	0.940	0.0874	± 1.68	1770	± 21	1880	± 9	6.7
N1635G.7-3	110	59	0.56	31	0.113	0.11419	± 0.89	5.1621	± 1.83	0.3279	± 1.60	0.875	0.0903	± 2.35	1828	±25	1867	± 16	2.4
N1635G.8-1	334	197	0.61	95	0.022	0.11486	± 0.46	5.2328	± 1.41	0.3304	± 1.33	0.945	0.0921	± 1.85	1840	± 21	1878	± 8	2.3
N1635G.2-1	199	126	0.65	55	0.034	0.11509	± 0.58	5.0815	± 1.98	0.3202	± 1.89	0.956	0.0894	± 2.07	1791	± 30	1881	± 11	5.5
N1635G.2-2	193	135	0.73	53	0.201	0.11442	± 0.73	5.0879	± 1.66	0.3225	± 1.49	0.898	0.0923	± 4.56	1802	± 23	1871	± 13	4.2
N1635G.5-1	387	283	0.76	108	0.023	0.11569	± 0.42	5.2052	± 1.70	0.3263	± 1.65	0.970	0.0900	± 2.10	1820	±26	1891	± 7	4.3
N1635G.5-2	196	139	0.74	57	0.077	0.11559	± 0.69	5.4135	± 1.49	0.3397	± 1.32	0.884	0.0978	± 2.34	1885	± 22	1889	± 13	0.2
N1635G.7-5	136	69	0.52	39	0.000	0.11574	± 0.73	5.2981	± 1.48	0.3320	± 1.29	0.871	0.0970	± 1.87	1848	± 21	1891	± 13	2.6
R-10 - Antônio Vicente Granite. zircon																							
N1634A.6-1	781	563	0.74	219	0.037	0.11483	± 0.45	5.1775	± 1.43	0.3270	± 1.35	0.949	0.0924	± 1.50	1824	± 21	1877	± 8	3.3
N1634A.6-2	64	80	1.30	18	0.000	0.11628	± 1.49	5.2950	± 2.89	0.3303	± 2.48	0.857	0.0971	± 3.25	1840	± 40	1900	± 27	3.6
N1634A.6-3	665	189	0.29	184	0.041	0.11435	± 0.50	5.0764	± 1.46	0.3220	± 1.37	0.939	0.0905	± 2.44	1799	± 21	1870	± 9	4.3
N1634A.6-4	409	232	0.59	111	0.161	0.11634	± 1.53	5.0749	± 2.58	0.3164	± 2.08	0.806	0.0932	± 2.97	1772	± 32	1901	± 27	7.7
N1634A.4-1	683	378	0.57	122	0.265	0.11395	± 0.74	3.2641	± 3.33	0.2077	± 3.25	0.975	0.0825	± 4.24	1217	± 36	1863	± 13	38.0
N1634A.3-1	512	364	0.73	132	0.144	0.11519	± 0.84	4.7682	± 1.69	0.3002	± 1.46	0.866	0.0945	± 2.16	1692	± 22	1883	± 15	11.5
N1634A.8-1	684	516	0.78	198	0.000	0.11408	± 0.53	5.2950	± 1.84	0.3366	± 1.76	0.958	0.0942	± 1.90	1870	± 29	1865	± 10	-0.3
N1634A.6-5	114	58	0.52	33	0.085	0.11472	± 0.84	5.3866	± 2.16	0.3405	± 1.99	0.922	0.0971	± 2.39	1889	± 33	1875	± 15	-0.8
N1634A.2-1	649	471	0.75	184	0.033	0.11475	± 0.33	5.2303	± 1.65	0.3306	± 1.62	0.980	0.0966	± 1.68	1841	±26	1876	± 6	2.1
N1634A.2-2	90	46	0.53	26	0.095	0.11420	± 0.88	5.3697	± 1.67	0.3410	± 1.41	0.848	0.0943	± 2.62	1892	± 23	1867	± 16	-1.5
R-5 - Antônio Vicente Granite. zircon																							
N1635F.1-1	376	261	0.72	72	0.101	0.11360	± 0.56	3.5054	± 4.92	0.2238	± 4.89	0.993	0.066	± 5.16	1302	± 58	1858	± 10	33.0
N1635F.2-1	598	459	0.79	163	0.123	0.11436	± 0.72	5.0010	± 1.71	0.3172	± 1.56	0.908	0.091	± 1.82	1776	± 24	1870	± 13	5.7
N1635F.2-2	298	226	0.78	77	0.055	0.10541	± 0.60	4.3463	± 1.52	0.2990	± 1.40	0.920	0.085	± 1.68	1687	± 21	1721	± 11	2.3
N1635F.2-3	490	320	0.67	134	0.198	0.11520	± 0.49	5.0452	± 1.20	0.3176	± 1.10	0.913	0.097	± 1.29	1778	± 17	1883	± 9	6.4
N1635F.2-4	272	208	0.79	70	0.062	0.10558	± 0.58	4.3492	± 1.29	0.2988	± 1.15	0.892	0.087	± 1.35	1685	± 17	1724	± 11	2.6
N1635F.3-1	138	108	0.81	39	0.090	0.11501	± 0.85	5.2758	± 1.80	0.3327	± 1.58	0.880	0.093	± 2.10	1851	± 25	1880	± 15	1.7
N1635F.4-1	133	79	0.62	55	0.580	0.10833	± 1.22	7.1583	± 4.49	0.4792	± 4.32	0.962	0.095	± 6.16	2524	± 90	1772	± 22	-51.5
N1635F.6-1	2210	441	0.21	571	0.028	0.10589	± 0.22	4.3929	± 1.43	0.3009	± 1.41	0.988	0.085	± 1.57	1696	±21	1730	± 4	2.2
N1635F.6-2	1679	332	0.20	429	0.025	0.10609	± 0.22	4.3542	± 1.27	0.2977	± 1.25	0.985	0.085	± 1.35	1680	± 18	1733	±4	3.5

Supplementary Table 3. U-Pb-Th SHRIMP data on zircon and titanite of the granites of the Jamon Suite.

						isotopic ratios							Ages (Ma)				
spot	U ppm	Th ppm	Th/U	^{206}Pb ppm	$4f^{206}$ %	^{207}Pb/^{206}Pb		^{207}Pb/^{235}U		^{206}Pb/^{238}U		error correl.	^{208}Pb/^{232}Th		^{206}Pb/^{238}U		^{207}Pb/^{206}Pb		Disc. %
PROA-11. Jamon granite zircon																			
N17-26E.1-1	55	52	0.98	16	0.053	0.11259	± 1.27	5.3757	± 2.53	0.3463	± 2.19	0.866	0.0979	± 2.65	1917	± 36	1842	± 23	-4.7
N17-26E.3-1	49	30	0.63	14	0.060	0.11354	± 1.35	5.2286	± 2.62	0.3340	± 2.25	0.857	0.0916	± 2.99	1858	± 36	1857	± 24	-0.1
N17-26E.4B-1	47	33	0.72	14	0.000	0.11364	± 1.30	5.2894	± 2.62	0.3376	± 2.27	0.869	0.0963	± 2.86	1875	± 37	1858	± 23	-1.0
N17-26E.5-1	33	23	0.70	10	0.099	0.11727	± 1.79	5.6019	± 3.26	0.3465	± 2.72	0.835	0.1008	± 3.66	1918	±45	1915	± 32	-0.2
N17-26E.6-1	58	38	0.68	17	0.058	0.11401	± 1.33	5.4836	± 2.57	0.3488	± 2.19	0.855	0.0987	± 2.86	1929	± 36	1864	± 24	-4.0
N17-26E.7-1	48	38	0.83	14	0.126	0.11301	± 1.48	5.3076	± 2.73	0.3406	± 2.29	0.839	0.0946	± 3.13	1890	± 37	1848	± 27	-2.6
N17-26E.8-1	47	35	0.77	13	0.000	0.11377	± 1.34	5.2902	± 2.66	0.3372	± 2.30	0.864	0.0945	± 3.07	1873	± 37	1860	± 24	-0.8
N17-26E.3-2	335	202	0.62	94	0.761	0.11385	± 2.18	5.1474	± 3.25	0.3279	± 2.41	0.742	0.0931	± 4.74	1828	± 38	1862	± 39	2.1
KM-144. Musa granite. zircon																			
N1620B.1-1	329	229	0.72	100	0.070	0.11408	± 0.48	5.6158	± 1.48	0.3570	± 1.40	0.945	0.0965	± 2.60	1956	± 24	1865	± 9	-5.6
N1620B.1-2	256	281	1.13	75	0.019	0.11501	± 0.51	5.4202	± 1.52	0.3418	± 1.43	0.941	0.0943	± 1.55	1895	± 24	1880	± 9	-0.9
N1620B.2-1	154	110	0.74	45	0.121	0.11477	± 0.72	5.3692	± 1.70	0.3393	± 1.54	0.905	0.0936	± 1.82	1883	± 25	1876	± 13	-0.4
N1620B.2-2	417	224	0.56	118	0.000	0.11496	± 0.78	5.2081	± 3.55	0.3286	± 3.46	0.975	0.0925	± 7.63	1831	± 55	1879	± 14	+2.9
N1620B.7-1	588	418	0.73	130	0.048	0.11187	±0.44	3.9562	± 1.39	0.2565	± 1.32	0.949	0.0732	± 1.70	1472	± 17	1830	± 8	+21.9
N1620B.8-1	498	220	0.46	141	0.058	0.11397	± 0.45	5.1778	± 1.62	0.3295	± 1.56	0.961	0.0935	± 1.83	1836	± 25	1864	± 8	+1.7
N1620B.11-1	410	370	0.93	115	0.069	0.11459	± 0.45	5.1838	± 1.44	0.3281	± 1.37	0.948	0.0924	± 2.07	1829	± 22	1873	± 8	+2.7
KM-144. Musa granite. titanite																			
1620C.2-1	85	296	3.61	26	0.826	0.11260	± 1.83	5.5122	± 2.24	0.3551	± 1.30	0.580	0.1013	± 2.16	1959	± 22	1842	± 33	-7.4
N1620C.3-2	79	459	5.96	24	1.077	0.11561	± 2.03	5.5676	± 2.42	0.3493	± 1.32	0.547	0.0995	± 1.72	1931	± 22	1889	± 36	-2.6
N1620C.4-1	71	269	3.91	21	1.007	0.11469	± 1.98	5.5142	± 2.38	0.3487	± 1.32	0.554	0.0994	± 1.81	1928	± 22	1875	± 36	-3.3
N1620C.4-2	78	394	5.24	23	0.772	0.11606	± 1.69	5.6090	± 2.12	0.3505	± 1.28	0.603	0.0977	± 1.67	1937	± 21	1896	± 30	-2.5
N1620C.4-3	105	441	4.34	31	0.565	0.11470	± 1.44	5.4183	± 1.89	0.3426	± 1.23	0.650	0.0984	± 1.60	1899	± 20	1875	± 26	-1.5
CREMU-37A. Musa granite. zircon																			
N1620E.1-1	53	43	0.84	16	0.099	0.11600	± 1.27	5.7362	± 2.41	0.3586	± 2.04	0.848	0.0978	± 2.61	1976	± 35	1895	± 13	-4.9
N1620E.1-2	121	64	0.55	36	0.019	0.11614	± 0.73	5.5663	± 1.76	0.3476	± 1.60	0.909	0.0988	± 2.13	1923	± 27	1898	± 13	-1.5
N1620E.2-1	72	68	0.97	22	0.106	0.11471	± 1.09	5.5486	± 2.16	0.3508	± 1.87	0.864	0.0941	± 4.95	1939	± 31	1875	± 20	-3.9
N1620E.3-1	107	66	0.63	31	0.047	0.11438	± 0.92	5.2843	± 1.90	0.3351	± 1.65	0.873	0.0916	± 2.94	1863	± 27	1870	± 17	0.5
N1620E.4-1	263	211	0.83	75	0.050	0.11390	± 0.55	5.2378	± 1.80	0.3335	± 1.71	0.952	0.0942	± 2.23	1855	± 28	1862	± 10	0.4
N1620E.7-1	96	84	0.90	29	0.459	0.11572	± 1.16	5.6659	± 2.07	0.3551	± 1.72	0.830	0.1018	± 2.19	1959	± 29	1891	± 21	-4.2
N1620E.7-2	234	180	0.80	77	0.022	0.11235	± 0.79	5.9509	± 1.83	0.3841	± 1.65	0.901	0.1053	± 2.39	2096	± 30	1838	± 14	-16.4
N1620E.8-1	406	210	0.53	121	0.053	0.11546	± 0.42	5.5032	± 1.43	0.3457	± 1.37	0.955	0.0965	± 1.52	1914	± 23	1887	± 8	-1.7

Supplementary Table 3. (continued)

						isotopic ratios								Ages (Ma)				
	U	Th	Th	^{206}Pb	4f^{206}	^{207}Pb		^{207}Pb		^{206}Pb		error	^{208}Pb		^{206}Pb		^{207}Pb		Disc.
spot	ppm	ppm	U	ppm	%	^{206}Pb		^{235}U		^{238}U		correl.	^{232}Th		^{238}U		^{206}Pb		%
CREMU-37A. Musa granite. titanite																		
N1620F.5-1	192	453	2.44	56	0.268	0.11496	± 0.85	5.4092	± 1.99	0.3413	± 1.80	0.905	0.0964	± 2.00	1893	± 30	1879	± 15	-0.8
N1620F.3-1	164	551	3.48	50	0.381	0.11572	± 0.95	5.6671	± 2.06	0.3552	± 1.82	0.885	0.1003	± 2.00	1959	± 31	1891	± 17	-4.2
N1620F.4-1	199	716	3.72	58	0.542	0.11828	± 1.11	5.5237	± 2.12	0.3387	± 1.81	0.853	0.0961	± 1.97	1880	± 30	1930	± 20	3.0
N1620F.2-1	232	706	3.14	68	0.609	0.11416	± 1.04	5.3521	± 2.07	0.3400	± 1.79	0.864	0.0968	± 1.97	1887	± 29	1867	± 19	-1.2
N1620F.1-1	158	630	4.12	47	0.605	0.11461	± 1.12	5.4315	± 2.13	0.3437	± 1.82	0.851	0.0959	± 1.98	1905	± 30	1874	± 20	-1.9
N1620F.1-2	95	287	3.12	28	0.806	0.11750	±1.55	5.4704	± 2.44	0.3377	± 1.89	0.772	0.1031	± 2.18	1875	± 31	1919	± 28	2.6
KM-77A. Musa granite. zircon																		
1620H.5-1	357	222	0.64	101	0.000	0.11349	± 0.64	5.1499	± 2.54	0.3291	± 2.46	0.968	0.0889	± 2.63	1834	± 39	1856	± 12	1.4
1620H.5-2	234	171	0.76	51	0.027	0.11739	± 0.88	4.1362	± 1.53	0.2556	± 1.26	0.820	0.0535	± 1.84	1467	± 16	1917	± 16	26.2
1620H.5-3	230	180	0.81	67	0.067	0.11470	± 0.84	5.3310	± 1.48	0.3371	± 1.22	0.824	0.0923	± 1.65	1873	± 20	1875	± 15	0.2
1620H.5-4	352	246	0.72	92	0.306	0.11416	± 1.40	4.8068	± 1.78	0.3054	± 1.10	0.620	0.0958	± 1.95	1718	± 17	1867	±25	9.1
N1620H.3-1	461	320	0.72	62	0.000	0.11560	± 0.71	2.5055	± 2.53	0.1572	± 2.43	0.960	0.0463	± 2.61	941	± 21	1889	± 13	53.8
N1620H.3-2	197	164	0.86	55	0.000	0.11589	± 0.87	5.1744	± 1.54	0.3238	± 1.28	0.827	0.0922	± 1.69	1808	± 20	1894	± 16	5.2
N1620H.3-3	255	156	0.63	73	0.041	0.11569	± 0.78	5.2932	± 1.43	0.3318	± 1.20	0.838	0.0911	± 1.66	1847	± 19	1891	± 14	2.6
N1620H.2-1	863	824	0.99	95	0.174	0.08227	± 1.98	1.4545	± 2.89	0.1282	± 2.10	0.729	0.0366	± 2.28	778	± 15	1252	± 39	40.2
KM-77A. Musa granite. titanite																		
1620I.3-1	49	279	5.92	15	1.905	0.11248	± 3.23	5.5350	± 3.77	0.3569	± 1.94	0.516	0.0998	± 2.38	1967	± 33	1840	± 59	-8.0
1620I.3-2	57	265	4.82	18	1.189	0.11518	± 2.98	5.9941	± 3.52	0.3774	± 1.88	0.534	0.1057	± 2.30	2064	± 33	1883	± 54	-11.3
1620I.1-1	61	340	5.76	20	1.336	0.11384	± 2.47	5.9607	± 3.10	0.3798	± 1.86	0.602	0.1039	± 2.94	2075	± 33	1862	± 45	-13.4
N1620I.2-1	53	262	5.15	18	1.261	0.11331	± 2.55	6.2332	±3.19	0.3990	± 1.91	0.598	0.1094	±2.34	2164	± 35	1853	± 46	-19.8
DC-111. Redenção. zircon																		
N1619F.1-1	466	234	0.52	134	0.061	0.11447	± 0.52	5.2863	± 1.27	0.3349	± 1.16	0.912	0.0919	± 1.43	1862	± 19	1872	± 9	0.6
N1619F.2-1	553	472	0.88	156	0.031	0.11409	± 0.56	5.1711	± 1.28	0.3287	± 1.16	0.901	0.0915	± 1.35	1832	± 18	1866	± 10	2.1
N1619F.5-1	481	234	0.50	135	0.017	0.11561	± 0.49	5.2254	± 2.35	0.3278	± 2.30	0.978	0.0965	± 2.42	1828	± 37	1889	± 9	3.7
N1619F.7-1	529	243	0.47	149	-0.015	0.11564	± 0.46	5.2394	± 1.23	0.3286	± 1.14	0.928	0.0922	± 1.36	1832	± 18	1890	± 8	3.5
N1619F.8-1	449	244	0.56	130	0.116	0.11411	± 0.57	5.3169	± 1.30	0.3379	± 1.17	0.898	0.0947	± 1.47	1877	± 19	1866	± 10	-0.7
N1619F.9-1	560	551	1.02	159	0.056	0.11417	± 0.50	5.2156	± 1.89	0.3313	± 1.83	0.964	0.0905	± 2.10	1845	± 29	1867	± 9	1.4

Supplementary Table 3. (continued)

						isotopic ratios								Ages (Ma)				
	U	Th	Th	^{206}Pb	4f^{206}	^{207}Pb		^{207}Pb		^{206}Pb		error	^{208}Pb		^{206}Pb		^{207}Pb		Disc.
spot	ppm	ppm	U	ppm	%	^{206}Pb		^{235}U		^{238}U		correl.	^{232}Th		^{238}U		^{206}Pb		%
DC-111. Redenção. Titanite																			
N1619G.1-1	502	293	0.60	142	1.127	0.11897	± 2.25	5.4003	± 3.04	0.3292	± 2.04	0.671	0.8618	± 2.49	1835	± 33	1941	± 40	6.3
N1619G.1-2	130	455	3.63	36	1.359	0.11808	± 2.38	5.2852	± 3.37	0.3246	± 2.39	0.708	0.0246	± 3.89	1812	± 38	1927	± 43	6.8
N1619G.1-3	105	532	5.23	32	1.254	0.11349	± 1.36	5.5308	± 3.07	0.3534	± 2.36	0.769	0.0122	± 4.17	1951	± 40	1856	± 35	-5.9
N1619G.1-4	391	293	0.77	116	0.737	0.11860	± 1.77	5.6426	± 2.69	0.3451	± 2.02	0.752	0.5489	± 2.44	1911	± 33	1935	± 32	1.4
N1619G.2-1	47	224	4.93	14	2.281	0.11504	± 3.86	5.3742	± 4.90	0.3388	± 3.02	0.616	0.0149	± 6.43	1881	± 49	1881	± 70	0.0
N1619G.2-2	97	197	2.10	28	1.940	0.12500	± 3.15	5.7790	± 4.08	0.3353	± 2.59	0.636	0.0746	± 3.96	1864	± 42	2029	± 56	9.3
DC-120. Redenção. zircon																			
N1635E.3-1-3	504	394	0.81	146	0.000	0.11364	± 0.41	5.2815	± 1.70	0.3371	± 1.65	0.970	0.0947	± 1.77	1873	± 27	1858	± 7	-0.9
N1635E.3-2	485	392	0.83	137	0.040	0.11367	± 0.39	5.1664	± 1.35	0.3296	± 1.29	0.957	0.0906	± 1.38	1837	± 21	1859	± 7	1.4
N1635E.4-1	638	482	0.78	180	-0.004	0.11429	± 0.32	5.1660	± 1.31	0.3278	± 1.27	0.969	0.0908	± 1.39	1828	± 20	1869	± 6	2.5
1635E.2-1-5	605	367	0.63	150	0.000	0.11224	± 0.44	4.4677	± 1.43	0.2887	± 1.36	0.952	0.0875	± 1.92	1635	± 20	1836	± 8	12.4
1635E.2-2	160	85	0.55	44	0.000	0.11443	± 0.77	5.0594	± 1.75	0.3207	± 1.57	0.899	0.0902	± 2.65	1793	± 25	1871	± 14	4.8
1635E.1-1	295	260	0.91	73	0.022	0.11439	± 0.56	4.5697	± 1.51	0.2897	± 1.40	0.929	0.0889	± 1.70	1640	± 20	1870	± 10	13.9
1635E.1-2	570	262	0.48	157	0.005	0.11416	± 0.38	5.0405	± 1.69	0.3202	± 1.64	0.975	0.0918	± 1.82	1791	± 26	1867	± 7	4.7
DCR-42 - Redenção. zircon																			
N1634B.4-1	329	202	0.64	96	-0.034	0.11466	± 0.51	5.3577	± 1.27	0.3389	± 1.17	0.918	0.0968	± 1.38	1881	± 19	1875	± 9	-0.4
N1634B.6-1	324	294	0.94	97		0.114491	± 0.52	5.4889	± 1.28	0.3477	± 1.17	0.912	0.0977	± 1.33	1924	± 19	1872	± 9	-3.2
N1634B.1-1	244	166	0.70	70	0.175	0.113861	± 0.69	5.2411	± 1.90	0.3338	± 1.76	0.931	0.0966	± 2.00	1857	± 28	1862	± 12	0.3
N1634B.2-1	60	44	0.76	15	0.367	0.111273	± 1.64	4.5617	± 2.37	0.2973	± 1.71	0.723	0.0985	± 11.64	1678	± 25	1820	± 30	8.9
N1634B.5-1	115	122	1.09	28	0.563	0.114753	± 1.30	4.4646	± 2.36	0.2822	± 1.97	0.835	0.0934	± 2.83	1602	± 28	1876	± 23	16.5

Supplementary Table 3. (continued)

						isotopic ratios								Ages (Ma)				
spot	U ppm	Th ppm	Th/U	^{206}Pb ppm	$4f^{206}$ %	^{207}Pb/^{206}Pb		^{207}Pb/^{235}U		^{206}Pb/^{238}U		error correl.	^{208}Pb/^{232}Th		^{206}Pb/^{238}U		^{207}Pb/^{206}Pb		Disc. %
ADR-136I - Bannach. zircon																			
1634E.1-1	232	151	0.67	66	0.073	0.11420	± 0.62	5.2065	± 1.57	0.3307	± 1.44	0.919	0.0936	± 1.81	1842	± 23	1867	± 11	1.6
N1634E.1-2	259	132	0.53	76	0.063	0.11369	± 0.53	5.3454	± 1.64	0.3410	± 1.55	0.945	0.0972	± 1.76	1892	± 25	1859	± 10	-2.0
N1634E.4-1	132	109	0.86	38	0.175	0.11506	± 0.82	5.3822	± 1.53	0.3393	± 1.30	0.845	0.0963	± 2.12	1883	± 21	1881	± 15	-0.1
N1634E.4-2	71	67	0.98	19	0.096	0.11515	± 1.04	4.9748	± 1.81	0.3133	± 1.49	0.819	0.0828	± 2.97	1757	± 23	1882	± 19	7.6
N1634E.4-3	171	74	0.45	46	0.112	0.11502	± 0.69	4.9748	± 2.09	0.3137	± 1.97	0.943	0.0806	± 2.36	1759	± 30	1880	± 12	7.4
1634E.7-1.1	120	57	0.49	34	0.105	0.11552	± 0.84	5.3067	± 1.80	0.3332	± 1.60	0.886	0.0931	± 2.37	1854	± 26	1888	± 15	2.1
1634E.7-1	120	57	0.49	34	0.000	0.11651	± 0.75	5.3586	± 1.76	0.3336	± 1.60	0.905	0.0948	± 2.24	1856	± 26	1903	± 13	2.9
N1634E.8-1	301	194	0.67	88	0.022	0.11504	± 0.46	5.3936	± 1.81	0.3400	± 1.75	0.967	0.0985	± 2.24	1887	± 29	1881	± 8	-0.4
1634E.9-1	347	90	0.27	98	0.054	0.11467	± 0.45	5.1726	± 1.44	0.3271	± 1.37	0.950	0.0860	± 1.98	1825	± 22	1875	± 8	3.1
1634E.10-1	231	202	0.90	65	0.044	0.11699	± 0.57	5.2863	± 2.32	0.3277	± 2.25	0.970	0.0916	± 2.46	1827	± 36	1911	± 10	5.0
1634E.10-2	202	107	0.55	58	0.051	0.11511	± 0.62	5.3506	± 1.92	0.3371	± 1.82	0.946	0.0938	± 2.20	1873	± 30	1882	± 11	0.5
1634E.10-2-5	203	107	0.55	59	0.048	0.11488	± 0.68	5.4019	± 1.68	0.3410	± 1.54	0.914	0.0942	± 2.06	1892	± 25	1878	± 12	-0.8
1634E.10-3	257	141	0.57	73	0.061	0.11402	± 0.62	5.2330	± 1.54	0.3329	± 1.42	0.917	0.0920	± 1.79	1852	± 23	1864	± 11	0.8
ADR-35A - Bannach. zircon																			
1635A.1-1	24	46	2.02	7	0.000	0.11165	± 1.81	5.1321	± 4.59	0.3334	± 4.22	0.919	0.0923	± 4.72	1855	± 68	1826	± 33	-1.8
1635A.2-1	33	36	1.12	9	0.100	0.11737	± 1.79	5.1942	± 2.98	0.3210	± 2.39	0.800	0.0933	± 3.54	1795	± 37	1916	± 32	7.3
1635A.3-1	28	52	1.93	7	0.344	0.11539	± 2.36	4.4249	± 3.43	0.2781	± 2.50	0.727	0.0817	± 3.29	1582	± 35	1886	± 42	18.2
N1635A.4-2	129	139	1.12	38	0.098	0.11391	± 0.91	5.4545	± 1.67	0.3473	± 1.40	0.839	0.1004	± 1.78	1922	± 23	1863	± 16	-3.7
N1635A.4-1	268	397	1.53	77	0.048	0.11336	± 0.51	5.2501	± 1.46	0.3359	± 1.37	0.938	0.0934	± 1.46	1867	± 22	1854	± 9	-0.8
1635A.5-1	297	68	0.24	83	0.010	0.11360	± 0.52	5.0902	± 1.51	0.3250	± 1.41	0.938	0.0881	± 2.11	1814	± 22	1858	± 9	2.7
1635A.5-2	136	223	1.69	37	-0.020	0.11592	± 0.74	5.1271	± 1.75	0.3208	± 1.58	0.906	0.0878	± 1.83	1793	± 25	1894	± 13	6.1
1635A.8-1	59	74	1.30	16	0.149	0.11329	± 1.35	4.9772	± 2.36	0.3186	± 1.94	0.822	0.0889	± 2.77	1783	± 30	1853	± 24	4.3
1635A.9-1	127	94	0.77	36	0.000	0.11399	± 0.79	5.1749	± 1.79	0.3292	± 1.61	0.899	0.0896	± 2.10	1835	± 26	1864	± 14	1.8
N1635A.9-2	115	86	0.77	34	0.126	0.11367	± 0.86	5.3987	± 2.40	0.3445	± 2.24	0.934	0.0972	± 2.50	1908	± 37	1859	± 16	-3.1
N1635A.11-1	107	83	0.80	31	0.190	0.11329	± 0.97	5.2150	± 1.71	0.3339	± 1.41	0.824	0.0954	± 1.86	1857	± 23	1853	± 17	-0.3

Supplementary Table 4. U-Pb-Th SHRIMP data on zircon of the Seringa Granite

						isotopic ratios								Ages (Ma)				
	U	Th	Th	^{206}Pb	4f^{206}	^{207}Pb		^{207}Pb		^{206}Pb		error	^{208}Pb		^{206}Pb		^{207}Pb		Disc.
spot	ppm	ppm	U	ppm	%	^{206}Pb		^{235}U		^{238}U		correl.	^{232}Th		^{238}U		^{206}Pb		%
AC-45. Seringa. zircon																			
N16-26A.1-1	700	349	0.52	210	0.000	0.11497	± 0.37	5.5329	± 1.31	0.3490	± 1.25	0.959	0.09595	± 1.53	1930	± 21	1879	± 7	-3.1
N16-26A.1-2	117 6	571	0.50	336	0.000	0.11495	± 0.31	5.2696	± 1.25	0.3325	± 1.21	0.969	0.09321	± 1.32	1850	± 20	1879	± 6	1.8
N16-26A.5-1	871	259	0.31	251		0.11471	± 0.35	5.2999	± 1.29	0.3351	± 1.25	0.962	0.09385	± 1.46	1863	± 20	1875	± 6	0.8
N16-26A.5-2	58	30	0.54	17	0.388	0.11778	± 1.97	5.5406	± 2.87	0.3412	± 2.09	0.728	0.09310	± 5.32	1892	± 34	1923	± 35	1.8
N16-26A.5-3	40	20	0.51	11	0.000	0.11863	± 1.62	5.4065	± 3.21	0.3305	± 2.77	0.863	0.09031	± 3.74	1841	± 44	1936	± 29	5.6
N16-26A.6-1	700	401	0.59	200	0.000	0.11500	± 0.40	5.2704	± 1.33	0.3324	± 1.26	0.954	0.09284	± 1.40	1850	± 20	1880	± 7	1.8
N16-26A.6-2	144	96	0.69	42	0.000	0.11718	± 0.88	5.4817	± 1.80	0.3393	± 1.57	0.873	0.09583	± 2.10	1883	± 26	1914	± 16	1.8
N1626A.5-4	625	483	0.80	180	0.000	0.11556	± 0.34	5.3420	± 1.31	0.3353	± 1.27	0.967	0.09398	± 1.34	1864	± 21	1889	± 6	1.5
N1626A.8-1 (core)	225	132	0.60	65	0.081	0.11419	± 0.61	5.2643	± 1.53	0.3344	± 1.40	0.916	0.09459	± 1.71	1859	± 23	1867	± 11	0.5
N1626A.8-2 (rim)	88	43	0.51	26	0.094	0.11419	± 1.02	5.4240	± 1.98	0.3445	± 1.71	0.859	0.09606	± 2.38	1908	± 28	1867	± 18	-2.5
N1626A.10-1	261	194	0.77	78	0.000	0.11475	± 0.57	5.4754	± 1.51	0.3461	± 1.40	0.925	0.09664	± 1.60	1916	± 23	1876	± 10	-2.4
AC-59. Seringa. zircon																			
N1626H.1-1	585	242	0.43	160	0.187	0.11453	± 0.51	5.0210	± 1.51	0.3180	± 1.42	0.941	0.0913	± 1.71	1780	± 22	1872	± 9	5.7
N1626H.2-1	385	293	0.79	112	0.041	0.11587	± 0.92	5.4187	± 1.72	0.3392	± 1.46	0.846	0.0948	±1.63	1883	± 24	1893	± 16	0.7
N1626H.2-2	556	304	0.57	157	0.073	0.11435	± 0.48	5.1887	± 1.48	0.3291	± 1.40	0.946	0.0887	± 1.59	1834	± 22	1870	± 9	2.2
N1626H.3-1	452	376	0.86	130	-0.036	0.11471	± 0.51	5.2806	± 1.52	0.3339	± 1.43	0.942	0.0929	± 1.57	1857	± 23	1875	± 9	1.1
N1626H.4-1	747	621	0.86	207	0.016	0.11626	± 0.69	5.1694	± 1.53	0.3225	± 1.37	0.894	0.0893	± 1.62	1802	± 22	1900	± 12	5.9
N1626H.5-1	386	240	0.64	103	0.212	0.11625	± 0.70	4.9967	± 1.63	0.3117	± 1.47	0.902	0.0891	± 1.90	1749	± 22	1899	± 13	9.0
N1626H.6-1	128	98	0.79	37	0.065	0.11430	± 0.83	5.3854	± 1.76	0.3417	± 1.56	0.884	0.0972	± 1.88	1895	± 26	1869	± 15	-1.6
N1626H.8-1	460	218	0.49	134	0.077	0.11374	± 0.44	5.3175	± 1.37	0.3391	± 1.30	0.947	0.0941	± 1.49	1882	± 21	1860	± 8	-1.4
N1626H.8-2	687	480	0.72	198	0.000	0.11467	± 0.33	5.3084	± 1.31	0.3358	± 1.26	0.968	0.0937	± 1.38	1866	± 20	1875	± 6	0.5
N1626H.8-3	76	33	0.45	22	0.203	0.11444	± 1.16	5.3297	± 2.11	0.3378	± 1.76	0.834	0.0907	± 3.53	1876	± 29	1871	± 21	-0.3

Supplementary Table 4. (continued)

						isotopic ratios								Ages (Ma)				
spot	U ppm	Th ppm	Th/U	^{206}Pb ppm	$4f^{206}$ %	^{207}Pb/^{206}Pb		^{207}Pb/^{235}U		^{206}Pb/^{238}U		error correl.	^{208}Pb/^{232}Th		^{206}Pb/^{238}U		^{207}Pb/^{206}Pb		Disc. %
AC-85. Seringa. zircon																			
1626B5-1	34	16	0.48	10	-0.082	0.11614	± 2.56	5.3491	± 3.52	0.3340	± 2.42	0.687	0.0942	± 4.21	1858	± 39	1898	± 46	2.4
1626B5-2	57	33	0.59	16	0.000	0.11425	± 1.16	5.1757	± 2.35	0.3286	± 2.05	0.870	0.0914	± 3.01	1831	± 33	1868	± 21	2.2
1626B.4-1	37	17	0.47	10	0.153	0.11456	± 1.67	5.0388	± 2.92	0.3190	± 2.39	0.819	0.0840	± 4.38	1785	± 37	1873	± 30	5.4
1626B3-1	360	338	0.97	101	0.129	0.11473	± 0.53	5.1461	± 1.48	0.3253	± 1.39	0.935	0.0890	± 1.65	1816	± 22	1876	± 9	3.7
1626B3-2	48	26	0.56	14	0.057	0.11586	± 1.32	5.3093	± 2.50	0.3324	± 2.12	0.849	0.0906	± 3.39	1850	± 34	1893	± 24	2.6
1626B8-1	541	343	0.66	150	0.025	0.11566	± 0.60	5.1562	± 1.47	0.3233	± 1.34	0.912	0.0894	± 1.55	1806	± 21	1890	± 11	5.1
1626B11-1	589	610	1.07	161	0.161	0.11585	± 0.42	5.0831	± 1.40	0.3182	± 1.34	0.954	0.0880	± 1.46	1781	± 21	1893	± 8	6.8
1626B4-2	420	319	0.78	116	0.018	0.11613	± 0.51	5.1615	± 1.47	0.3224	± 1.38	0.939	0.0916	± 1.62	1801	± 22	1897	± 9	5.8
AC-42. Seringa. zircon																			
N1620G.2-1	992	375	0.39	162	0.000	0.10505	± 1.13	2.7481	± 1.57	0.1897	± 1.08	0.692	0.0546	± 1.78	1120	± 11	1715	± 21	37.8
N1620G.2-2	1110	487	0.45	263	0.000	0.11133	± 0.32	4.2407	± 1.10	0.2763	± 1.05	0.955	0.0803	± 1.19	1573	± 15	1821	± 6	15.4
N1620G.3-1	819	318	0.40	208	0.000	0.11201	± 0.39	4.5733	± 1.17	0.2961	± 1.11	0.945	0.0833	± 1.28	1672	± 16	1832	± 7	9.9
N1620G.6-1	638	359	0.58	176	0.255	0.11384	± 0.51	5.0332	± 2.13	0.3207	± 2.07	0.971	0.1073	± 2.36	1793	± 32	1862	± 9	4.2
N1620G.6-2	453	328	0.75	112	0.264	0.11288	± 0.64	4.4894	± 1.31	0.2884	± 1.14	0.870	0.0684	± 1.52	1634	± 16	1846	± 12	13.0
N1620G.6-3	527	208	0.41	127	0.157	0.11328	± 0.57	4.3912	± 1.59	0.2811	± 1.48	0.933	0.0490	± 2.54	1597	± 21	1853	± 10	15.6
N1620G.6-4	843	334	0.41	162	0.007	0.10735	± 2.32	3.3077	± 8.84	0.2235	± 8.53	0.965	0.0637	± 9.92	1300	100	1755	± 42	28.6
N1620G.6-5	741	351	0.49	203	0.151	0.11463	± 0.50	5.0303	± 1.20	0.3183	± 1.09	0.909	0.0925	± 1.37	1781	± 17	1874	± 9	5.7

Supplementary Table 5. U-Pb-Th SHRIMP data on zircon of the São João Granite

						isotopic ratios								Ages (Ma)				
spot	U ppm	Th ppm	Th/U	^{206}Pb ppm	$4f^{206}$ %	^{207}Pb/^{206}Pb		^{207}Pb/^{235}U		^{206}Pb/^{238}U		error correl.	^{208}Pb/^{232}Th		^{206}Pb/^{238}U		^{207}Pb/^{206}Pb		Disc. %
PC-03B. São João granite. zircon																			
N1626F.6-1	398	274	0.71	114	0.020	0.116734	± 1.32	5.3870	± 2.37	0.3347	± 1.97	0.831	0.0964	± 2.11	1861	± 32	1907	± 24	2.8
N1626F.5-1	413	173	0.43	116	0.039	0.114342	± 0.44	5.1575	± 1.47	0.3271	± 1.40	0.954	0.0905	± 2.23	1824	± 22	1870	± 8	2.8
N1626F.5-2	123	88	0.74	35	0.045	0.113683	± 0.82	5.2737	± 1.83	0.3364	± 1.64	0.895	0.0921	± 2.16	1870	± 27	1859	± 15	-0.6
N1626F.3-1	352	166	0.49	99	0.023	0.113869	± 0.48	5.1531	± 1.49	0.3282	± 1.41	0.948	0.0927	± 1.78	1830	± 22	1862	± 9	2.0
N1626F.4-1	418	220	0.54	106	0.389	0.114247	± 0.65	4.6361	± 1.54	0.2943	± 1.39	0.907	0.0746	± 2.58	1663	± 20	1868	± 12	12.4
N1626F.4-2	367	255	0.72	104	0.048	0.11428	± 0.46	5.2017	± 1.78	0.3301	± 1.72	0.967	0.0902	± 1.92	1839	± 27	1869	± 8	1.8
N1626F.9-1	188	99	0.54	52	0.143	0.116087	± 0.75	5.1392	± 1.74	0.3211	± 1.56	0.900	0.0892	± 2.16	1795	± 24	1897	± 14	6.1
N1626F1-1	658	404	0.63	187	-0.009	0.115638	± 0.35	5.2746	± 1.41	0.3308	± 1.36	0.969	0.0922	± 1.51	1842	± 22	1890	± 6	2.9
PC-21. São João granite. zircon																			
N16-26C.1-1	305	221	0.75	87	0.000	0.11533	± 0.67	5.3055	± 1.58	0.3337	± 1.44	0.907	0.0916	± 1.70	1856	± 23	1885	± 12	1.8
N16-26C.1-2	867	334	0.40	249	0.000	0.11460	± 0.42	5.2800	± 1.34	0.3342	± 1.27	0.948	0.0943	± 1.49	1859	± 20	1874	± 8	0.9
N16-26C.2-1	78	42	0.55	23	0.000	0.11410	± 1.19	5.2916	± 2.64	0.3364	± 2.36	0.894	0.0915	± 3.81	1869	± 38	1866	± 21	-0.2
N16-26C.2-2	303	215	0.73	85	0.034	0.11556	± 0.61	5.2242	± 1.57	0.3279	± 1.45	0.922	0.0950	± 2.00	1828	± 23	1889	± 11	3.7
N16-26C.2-3	395	110	0.29	109	0.064	0.11546	± 0.54	5.0921	± 1.43	0.3199	± 1.33	0.927	0.1130	± 2.11	1789	± 21	1887	± 10	6.0
N16-26C.2-4	1531	709	0.48	124	0.009	0.06328	± 0.61	0.8213	± 1.43	0.0941	± 1.29	0.903	0.0350	± 2.45	580	± 7	718	± 13	20.0
N16-26C.2-4b	1842	784	0.44	136	0.172	0.06054	± 0.94	0.7177	± 1.90	0.0860	± 1.65	0.868	0.0301	± 2.62	532	± 8	623	± 20	15.3
N16-26C.2-5	1669	842	0.52	135	0.080	0.06362	± 0.65	0.8249	± 1.39	0.0940	± 1.22	0.882	0.0304	± 1.59	579	± 7	729	± 14	21.4
N16-26C.6-1	1962	1002	0.53	174	0.137	0.07105	± 2.35	1.0095	± 2.67	0.1030	± 1.27	0.476	0.0429	± 3.02	632	± 8	959	± 48	35.8
N16-26C.6-2-1	794	350	0.46	136	0.353	0.10380	± 0.75	2.8497	± 2.15	0.1991	± 2.01	0.936	0.0700	± 2.92	1171	± 22	1693	± 14	33.7
N1626C.5-1	201	143	0.74	58	0.000	0.11484	± 0.62	5.3679	± 1.56	0.3390	± 1.44	0.919	0.0942	± 1.74	1882	± 23	1877	± 11	-0.3
N1626C.5-2	82	42	0.53	24	0.033	0.11527	± 0.97	5.4009	± 1.96	0.3398	± 1.70	0.869	0.0967	± 2.27	1886	± 28	1884	± 17	-0.1
N1626C.7-1	73	49	0.70	21	0.103	0.11466	± 1.10	5.3929	± 2.08	0.3411	± 1.77	0.849	0.0982	± 6.16	1892	± 29	1875	± 20	-1.1
N1626C.8-1	544	318	0.60	154	0.056	0.11487	± 0.40	5.2170	± 1.34	0.3294	± 1.28	0.955	0.0923	± 1.41	1835	± 20	1878	± 7	2.6

Supplementary Table. 5 (continued)

						isotopic ratios							Ages (Ma)				
	U	Th	Th	^{206}Pb	4f^{206}	^{207}Pb		^{207}Pb		^{206}Pb		error	^{208}Pb		^{206}Pb		^{207}Pb		Disc.
spot	ppm	ppm	U	ppm	%	^{206}Pb		^{235}U		^{238}U		correl.	^{232}Th		^{238}U		^{206}Pb		%
PCM-10. São João granite. zircon																			
N16-26E.3-1	605	347	0.59	167	0.040	0.11675	± 1.12	5.1616	± 1.78	0.3206	± 1.37	0.773	0.0923	± 2.52	1793	± 22	1907	± 20	6.9
N16-26E.3-2	571	467	0.84	169	0.067	0.11608	± 1.25	5.5223	± 2.75	0.3450	± 2.45	0.890	0.0952	± 2.67	1911	± 41	1897	± 23	-0.9
N16-26E.3-3	455	209	0.47	130	0.000	0.11601	± 0.54	5.3204	± 1.50	0.3326	± 1.40	0.934	0.0915	± 1.65	1851	± 22	1896	± 10	2.7
N16-26E.4-1	439	397	0.93	125	0.011	0.11382	± 1.22	5.2174	± 1.85	0.3324	± 1.40	0.753	0.0923	± 1.80	1850	± 22	1861	± 22	0.7
N16-26E.7-1	818	605	0.76	237	0.043	0.11550	± 0.72	5.3704	± 1.52	0.3372	± 1.34	0.881	0.0929	± 1.68	1873	± 22	1888	± 13	0.9
N16-26E.4-2	183	161	0.91	53	0.081	0.11605	± 0.93	5.4040	± 1.86	0.3377	± 1.61	0.865	0.0943	± 1.98	1876	± 26	1896	± 17	1.2
N16-26E.4-3	80	39	0.50	23	0.046	0.11605	± 1.18	5.3029	± 2.07	0.3314	± 1.71	0.822	0.0928	± 2.55	1845	± 27	1896	± 21	3.1
N16-26E.6-1	506	283	0.58	148	0.013	0.11548	± 0.43	5.4287	± 1.35	0.3410	± 1.28	0.948	0.0925	± 1.44	1891	± 21	1887	± 8	-0.2
PCM-13. São João granite. zircon																			
N1620A.1-1	485	295	0.63	141	0.112	0.11553	± 0.92	5.3873	± 1.47	0.3382	± 1.14	0.779	0.0936	± 1.61	1878	± 19	1888	± 17	+0.6
N1620A.1-2	645	282	0.45	189	0.000	0.11499	± 0.40	5.4128	± 1.18	0.3414	± 1.11	0.940	0.0963	± 1.28	1893	± 18	1880	± 7	-0.8
N1620A.1-3	875	672	0.79	252	0.019	0.11518	± 0.33	5.3284	± 1.12	0.3355	± 1.07	0.955	0.0923	± 1.48	1865	± 17	1883	± 6	+1.1
N1620A.3-1	928	458	0.51	268	0.027	0.11433	± 0.65	5.3066	± 1.25	0.3366	± 1.06	0.852	0.0938	± 1.19	1870	± 17	1869	± 12	-0.1
N1620A.5-1	391	264	0.70	112	0.011	0.11436	± 0.55	5.2737	± 1.32	0.3345	± 1.20	0.908	0.0923	± 1.41	1860	± 19	1870	± 10	+0.6
N1620A.11-1	1097	656	0.62	324	0.000	0.11503	± 0.32	5.4480	± 1.10	0.3435	± 1.06	0.956	0.0966	± 1.15	1903	± 17	1880	± 6	-1.4
N1620A.11-2	1088	787	0.75	319	0.019	0.11458	± 0.33	5.3890	± 1.11	0.3411	± 1.06	0.955	0.0960	± 1.16	1892	± 17	1873	± 6	-1.1
N1620A.12-1	237	156	0.68	69	0.131	0.11454	± 0.81	5.3896	± 1.57	0.3413	± 1.34	0.857	0.0955	± 1.76	1893	± 22	1873	± 15	-1.2

Notes: Isotopic ratios errors in %

All Pb in ratios are radiogenic component. all corrected for 204Pb.

disc. = discordance. as 100 - 100{t[206Pb/238U]/t[207Pb/206Pb]}

4f206 = (common ^{206}Pb) / (total measured ^{206}Pb) based on measured ^{204}Pb.

Uncertainties are 1s.

Supplementary Table 6. Geochronological data of the ~1.88 Ga old vulcano-plutonism of the Central Amazonia Province (Iriri-Xingu and Erepecuru-Trombetas domains) and Tapajós-Parima Province (Tapajós Domain and Granites of Pitinga Tin Province)

Geologic unit	Rock type		Age (Ma)	Method	References
Iriri-Xingu Domain (Central Amazonian Province)					
Rio Dourado Suite	Syenogranite	A-type magmatism	1884 ± 4	U-Pb zircon age*	Barros et al. (2006)
Rio Dourado Suite	Granite	A-type magmatism	1876 ± 39	Pb evaporation zircon age	Barros et al. (2011)
Undefined	quartz syenite	A-type magmatism	1889 ± 2	Pb evaporation zircon age	Semblano et al. (2016)
Santa Rosa Formation	Ash tuff	A-type magmatism	1884 ± 2	Pb evaporation zircon age	Fernandes et al. (2011)
Santa Rosa Formation	Rhyolite	A-type magmatism	1879 ± 2	Pb evaporation zircon age	Fernandes et al. (2011)
Santa Rosa Formation	Rhyolite lava flow	A-type magmatism	1877.4 ± 4.3	U-Pb zircon age***	Antonio et al. (2017)
Santa Rosa Formation	Felsic microgranite dike	A-type magmatism	1895 ± 11	U-Pb zircon age***	Antonio et al. (2017)
Sobreiro Formation	Dacite	calc-alkaline magmatism	1880 ± 6	Pb evaporation zircon age	Pinho et al.(2006)
Erepecuru-Trombetas Domain (Central Amazonian Province) and Anauá-Uatumã Domain including the Pitinga Tin Province (Tapajós-Parima Province)					
Iricoumé Group	Rhyolite	A-type magmatism	1888 ± 3	Pb evaporation zircon age	Costi et al. (2000)
Iricoumé Group	Dacite porphyry	A-type magmatism	1893 ± 2	Pb evaporation zircon age	Macambira et al. (2002)
Iricoumé Group	Rhyolite	A-type magmatism	1882 ± 11	U-Pb zircon age	Marques et al. (2014)
Iricoumé Group	Rhyodacite	A-type magmatism	1896 ± 7	U-Pb zircon age **	Santos (2003)
Iricoumé Group	Dacitic ignimbrite	A-type magmatism	1888 ± 2.5	Pb evaporation zircon age	Barreto et al. (2013)
Iricoumé Group	Dacitic ignimbrite	A-type magmatism	1889 ± 2	Pb evaporation zircon age	Barreto et al. (2013)
Iricoumé Group	Ignimbrite	A-type magmatism	1876 ± 10	U-Pb zircon age **	Valério et al. (2018)
Divisor Formation	porphyritic andesite	calk-alkaline magmatism	1897 ± 2	Pb evaporation zircon age	Ferron et al. (2010)
Divisor Formation	porphyritic andesite	calk-alkaline magmatism	1883 ± 2	Pb evaporation zircon age	Ferron et al. (2010)
Ouro Preto Formation	porphyritic rhyolite	A-type magmatism	1882 ± 2	Pb evaporation zircon age	Ferron et al. (2006)
Ouro Preto Formation	porphyritic rhyodacite	A-type magmatism	1885 ± 8	Pb evaporation zircon age	Ferron et al. (2006)
Ouro Preto Formation	microgranophyric rhyolite	A-type magmatism	1881 ± 2	Pb evaporation zircon age	Ferron et al. (2006)
Ouro Preto Formation	porphyritic rhyolite	A-type magmatism	1886 ± 6	Pb evaporation zircon age	Ferron et al. (2006)
Ouro Preto Formation	porphyritic rhyolite	A-type magmatism	1882 ± 2	Pb evaporation zircon age	Ferron et al. (2006)
Paraíso Formation	rhyolitic ignimbrite	A-type magmatism	1890 ± 2	Pb evaporation zircon age	Ferron et al. (2006)
São Gabriel AMCG Association	Biotite monzogranite	A-type magmatism	1889 ± 3	Pb evaporation zircon age	Valério et al. (2006)
São Gabriel AMCG Association	biotite-amphibole syenogranite	A-type magmatism	1889 ± 2	Pb evaporation zircon age	Valério et al. (2009)
São Gabriel AMCG Association	Rhyolite	A-type magmatism	1883 ± 4	Pb evaporation zircon age	Valério et al. (2009)
São Gabriel AMCG Association	hornblenda monzogranite	A-type magmatism	1888 ± 11	U-Pb zircon age***	Valério et al. (2018)

Supplementary Table 6. (continued)

Erepecuru-Trombetas Domain (Central Amazonian Province) and Anauá-Uatumã Domain including the Pitinga Tin Province (Tapajós-Parima Province)					
Geologic unit	**Rock type**		**Age (Ma)**	**Method**	**References**
Mapuera Suite/Abonari Gr.	-	A-type magmatism	1871 ± 6	Pb evaporation zircon age	Santos et al. (2001)
Mapuera S./Simão Granite	-	A-type magmatism	1875 ± 4	Pb evaporation zircon age	Ferron et al. (2006)
Mapuera S./Simão Granite	Biotite granite	A-type magmatism	1885 ± 4	Pb evaporation zircon age	Ferron et al. (2006)
Mapuera S./Simão Granite	Biotite granite	A-type magmatism	1882 ± 4	Pb evaporation zircon age	Ferron et al. (2006)
Mapuera S./Alalaú Granite	-	A-type magmatism	1876 ± 4	U-Pb zircon and titanite age **	Santos et al. (2002)
Mapuera S./Alalaú Granite	-	A-type magmatism	1879 ± 3	U-Pb zircon and titanite age **	Santos et al. (2002)
Mapuera S./Alalaú Granite	-	A-type magmatism	1880 ± 3	U-Pb zircon and titanite age **	Santos et al. (2002)
Mapuera S./Rastro Granite	Biotite granite	A-type magmatism	1882 ± 2	Pb evaporation zircon age	Ferron et al. (2006)
Mapuera S./Bom Futuro Gr.	Syenogranite	A-type magmatism	1882 ± 3	Pb evaporation zircon age	Ferron et al. (2006)
Mapuera S./Alto Pitinga Gr.	Biotite monzogranite	A-type magmatism	1885 ± 3	Pb evaporation zircon age	Ferron et al. (2006)
Mapuera S./Alto Pitinga Gr.	Biotite monzogranite	A-type magmatism	1888 ± 3	Pb evaporation zircon age	Ferron et al. (2006)
Água Branca Suite	biotite–amphibole monzogranite	calk-alkaline magmatism	1898 ± 3	Pb evaporation zircon age	Valério et al. (2009)
Água Branca Suite	biotite monzogranite	calk-alkaline magmatism	1890 ± 2	Pb evaporation zircon age	Valério et al. (2009)
Água Branca Suite?	Tonalite	calk-alkaline magmatism?	1891 ± 7	U-Pb zircon age **	Santos (2003)
Agua Branca Suite	porphyritic biotite monzogranite	calk-alkaline magmatism	1895 ± 3	Pb evaporation zircon age	Valério et al. (2009)
Pitinga Tin Province (Madeira Suite and related ganites)					
Madeira Suite	Rapakivi granite	A-type magmatism	1824 ± 2	Pb evaporation zircon age	Costi et al. (2000)
Madeira Granite	Albite-enriched granite facies	A-type magmatism	1834 ± 6	U-Pb zircon age*	Fuck et al. (1993)
Madeira Suite	Biotite granite facies	A-type magmatism	1822 ± 2	Pb evaporation zircon age	Costi et al. (2000)
Madeira Granite	Hypersolvus granite facies	A-type magmatism	1818 ± 2	Pb evaporation zircon age	Costi et al. (2000)
Madeira Granite	Hypersolvus granite facies	A-type magmatism	1794 ± 19	U-Pb zircon age **	Lenharo (1998)
Madeira Granite	Hypersolvus granite facies	A-type magmatism	1822 ± 22	U-Pb zircon age***	Bastos et al. (2014)
Água Boa Granite	Rapakivi granite facies	A-type magmatism	1798 ± 10	U-Pb zircon age **	Lenharo (1998)
Água Boa Granite	Biotite granite facies	A-type magmatism	1824 ± 24	U-Pb zircon age***	Bastos et al. (2014)
Água Boa Granite	Topaz granite facies	A-type magmatism	1815 ± 10	U-Pb zircon age **	Lenharo (1998)
Água Boa Granite	Topaz granite facies	A-type magmatism	1816 ± 20	U-Pb zircon age***	Bastos et al. (2014)
Europa Granite	Alkali-feldspar granite	A-type magmatism	1829 ± 1	Pb evaporation zircon age	Costi et al. (2000)
Europa Granite	Alkali-feldspar granite	A-type magmatism	1839 ± 6.2	U-Pb zircon age***	Bastos et al. (2014)
Europa Granite	Alkali-feldspar granite	A-type magmatism	1831 ± 11	U-Pb zircon age***	Bastos et al. (2014)
Moderna Granite	Monzogranite	A-type magmatism	1814 ± 27	Pb evaporation zircon age	Santos et al. (1997)

Supplementary Table 6. (continued)

Geologic unit	Rock type		Age (Ma)	Method	References
Tapajós Domain of the Tapajós-Parima Province					
Iriri Group	Hedembergite-fayalite rhyolite	A-type magmatism	1888 ± 2	Pb evaporation zircon age	Dall'Agnol et al. (1999d)
Iriri Group	Rhyodacite	A-type magmatism	1888 ± 2	Pb evaporation zircon age	Klein and Vasquez (2000)
Iriri Group	Rhyolite	A-type magmatism	1888 ± 7	Pb evaporation zircon age	Moura et al. (1999)
Iriri Group	-	A-type magmatism	1870 ± 8	U-Pb zircon age **	Santos et al. (2001)
Iriri Gr./Salustiano Fm.	-	A-type magmatism	1893 ±2	Pb evaporation zircon age	Vasquez et al. (1999)
Iriri Gr./Moraes Almeida Fm.	Rhyolite	A-type magmatism	1890 ± 6	Pb evaporation zircon age	Lamarão et al. (2002)
Iriri Gr./Moraes Almeida Fm.	Trachyte	A-type magmatism	1881 ± 4	Pb evaporation zircon age	Lamarão et al. (2002)
Iriri Gr./Moraes Almeida Fm.	Ignimbrite	A-type magmatism	1875 ± 4	Pb evaporation zircon age	Lamarão et al. (2002)
Maloquinha Suite	Monzogranite	A-type magmatism	1877 ± 12	U-Pb zircon age **	Santos et al. (2001)
Maloquinha Suite	Biotite-amphibole granite	A-type magmatism	1882 ± 4	Pb evaporation zircon age	Vasquez et al. (1999)
Maloquinha Suite	Monzogranite	A-type magmatism	1874 ± 7	U-Pb zircon age **	Santos et al. (2001)
Maloquinha Suite	Monzogranite	A-type magmatism	1872 ± 4	U-Pb zircon age **	Santos et al. (2001)
Maloquinha Suite	Alaskite	A-type magmatism	1899 ± 25	U-Pb zircon age **	Santos et al. (2001)
Maloquinha Suite	Leucogranite	A-type magmatism	1880 ± 9	Pb evaporation zircon age	Lamarão et al. (2002)
Jardim do Ouro granite	Hornblende-biotite monzogranite	subalkaline magmatism	1880 ± 3	Pb evaporation zircon age	Lamarão et al. (2002)
Parauari Suite	Syenogranite	calk-alkaline magmatism	1883 ± 4	U-Pb zircon age **	Santos et al. (2001)
Parauari Suite	Monzogranite	calk-alkaline magmatism	1883 ± 8	Pb evaporation zircon age	Brito et al. (1999)
Parauari Suite	Granite	calk-alkaline magmatism	1883 ± 2	Pb evaporation zircon age	Klein and Vasquez (2000)
Parauari Suite	Monzogranite	calk-alkaline magmatism	1879 ± 11	U-Pb zircon age **	Santos et al. (2000)
Parauari Suite/Central Granite	Monzogranite	calk-alkaline magmatism	1884 ± 3	Pb evaporation zircon age	Silva Jr. et al. (2015)
Parauari S./Younger São Jorge Gr.	Hornblende-biotite monzogranite	calk-alkaline magmatism	1891 ± 3	Pb evaporation zircon age	Lamarão et al. (2002)
Rosa de Maio Granite	Monzogranite	calk-alkaline magmatism	1879 ± 11	U-Pb zircon age*	Santos et al. (2000)
Caroçal Granite	-	calk-alkaline magmatism	1870 ± 3	U-Pb zircon age **	Santos et al. (2000)
Penedo Granite	-	calk-alkaline magmatism	1883 ± 4	U-Pb zircon age **	Santos et al. (2000)
Cumaru Granite	Monzogranite	calk-alkaline magmatism	1883 ± 8	Pb evaporation zircon age	Santos et al. (2000)
Tropas Suite/Ouro Roxo Ton.	Tonalite	calk-alkaline magmatism	1893 ± 3	U-Pb zircon and titanite age **	Santos et al. (2004)
Tropas Suite	Dacite	calk-alkaline magmatism	1893 ± 3	Pb evaporation zircon age	Vasquez et al. (2002)
Tropas Suite/Abacaxis Granite	Monzogranite	calk-alkaline magmatism	1892 ± 6	U-Pb zircon age*	Santos et al. (1997)
Tropas Suite	Tonalite	calk-alkaline magmatism	1897 ± 2	U-Pb zircon and titanite age **	Santos et al. (2004)
Tropas Suite	Basalt	calk-alkaline magmatism	1897 ± 2	U-Pb zircon age*	Santos et al. (1997)
Tropas Suite/Uruá Vulc.	Tuff	calk-alkaline magmatism	1896 ± 5	U-Pb zircon and titanite age **	Santos et al. (2004)
Tropas Suite	Granodiorite	calk-alkaline magmatism	1898 ± 2	U-Pb zircon age*	Santos et al. (2000)
Ingarana Suite	Gabbro	mafic magmatism	1881 ± 11	U-Pb zircon age **	Santos et al. (2004)
Ingarana Suite	Gabbro	mafic magmatism	1880 ± 2	U-Pb zircon age **	Santos et al. (2004)
Ingarana Suite	Gabbro	mafic magmatism	1881 ± 3	U-Pb zircon age **	Santos et al. (2004)

* TIMS; ** SHRIMP age; ***LA-ICP-MS

4 PETROGENESIS OF THE PALEOPROTEROZOIC (OROSIRIAN) A-TYPE GRANITES OF CARAJÁS PROVINCE, AMAZON CRATON, BRAZIL: COMBINED in situ Hf–O ISOTOPES OF ZIRCON

Mayara Fraeda Barbosa Teixeira

Roberto Dall'Agnol

João Orestes Schneider Santos

PETROGENESIS OF THE PALEOPROTEROZOIC (OROSIRIAN) A-TYPE GRANITES OF CARAJÁS PROVINCE, AMAZON CRATON, BRAZIL: COMBINED *in situ* Hf–O ISOTOPES OF ZIRCON

Mayara Fraeda Barbosa Teixeira[1]*, Roberto Dall'Agnol[1,2], João Orestes Schneider Santos[3]

[1]Graduate Course in Geology and Geochemistry, Geosciences Institute, Federal University of Pará (UFPA), Belém, PA, Brazil. E-mails: mayfraeda@gmail.com; robdal@ufpa.br; luansanmartins17@hotmail.com

[2]Instituto Tecnológico Vale (ITV), Belém, PA, Brazil. E-mail: roberto.dallagnol@itv.org.

[3]University of Western Australia, Centre for Exploration Targeting, Crawley, WA, 6009, Australia. E-mail: orestes.santos@bigpond.com

*corresponding author

Abstract

We present Lu–Hf and Oxygen isotopic analyses and complementary whole-rock Nd isotopic data for the three A-type Paleoproterozoic Suites (1880 Ma to 1857 Ma; Serra dos Carajás, Velho Guilherme and Jamon) and related granites of the Carajás Province. Zircons from all the granites have remarkably restricted initial $^{176}Hf/^{177}Hf$ and strongly negative εHf(t) values ranging from –9 to -18, and $\delta^{18}O$ fairly homogeneous varying from 5.50‰ to 7.00‰. Small differences were observed internally in the plutons or between them. These differences can result for contrasts in the crustal domains of the Carajás Province that were the source of the granites or of local contamination processes. Crustal model ages indicate a Paleoarchean source (3.3 Ga to 3.6 Ga) with a minor contribution from Mesoarchean (3.0 Ga to 3.2 Ga) melts for these granites. This model ages are older than the exposed Archean country rocks of the Orosirian granites of the Carajás Province and more investigation is needed to verify the real existence of that older Archean crust. The studied samples have Hf–O isotopic compositions that overlap within error, and evidence of contamination (crustal assimilation or mixing) of a mantle-derived magma cannot be seen. These plutons crystallized from magmas generated by melting of pre-existing igneous rocks with possibly in the Velho Guilherme Suite a minor contribution from a supracrustal (metasedimentary) component. The Nd, Hf, and O isotope compositions of the Paleoproterozoic granites of Carajás Province clearly attest to an igneous ancient crustal source in the origin of their magmas. This anorogenic granites represent a large volume of granitic magmatism generated in the late Palaeoproterozoic in the eastern of the Amazon Craton an this work shows the importance of the Archean source in the generation of the A-type Paleoproterozoic granites from Carajás province.

Keywords: A-type magmatism, Paleoproterozoic, Orosirian, Zircon Hf–O isotope, Carajás Province, Amazon Craton.

1. Introduction

A-type granite magmatism has become an important tool for modeling Precambrian intraplate crustal processes and global-scale lithospheric evolution (Dall'Agnol et al., 2012; Rämö and Haapala, 1995, 2005; Andersen et al., 2004; Johansson et al., 2016; Fraga et al., 2009; Heinonen et al., 2012). They are derived from various source rocks by a variety of processes, witch implies in some mineralogical and geochemical contrasts, thus requiring multiple petrogenetic processes. Their origin is attributed to alkaline or tholeiitic mafic magmas derived from a wide range of depleted to variably enriched mantle sources that intrude and interact with the crust (Bonin, 2007; Frost and Frost, 1997; Frost et al., 2010) or to anatexis of crustal sources affected by underplating of mafic magmas (Anderson and Bender, 1989; Rämö and Haapala, 1995; Dall'Agnol et al., 1999b, 2005) in post-collisional to post-orogenic or anorogenic settings.

This A-type magmatism is widespread in several cratons worldwide since the Neoarchaean (~2.7 Ga) until recent (Dall'Agnol et al., 2012, 2017; Cunha et al., 2016; Emslie et al., 1991; Heinonen et al., 2010; Vander Auwera et al., 2015), but they are more abundant in the late Paleoproterozoic and Mesoproterozoic (Ramo and Haapala, 1995; Dall'Agnol et al., 2012).

A larger number of Paleoproterozoic (1880-1857 Ma; Teixeira et al., submitted; Dall'Agnol et al., 2005; Teixeira et al., 2002) A-type anorogenic plutons are intruded in the Archean basement of Carajás Province, eastern Amazon Craton. These granites are grouped into three main suites according to mineralogy, geochemistry, and state of oxidation of their magmas – Jamon, Velho Guilherme, and Serra dos Carajás – and include also the Gogó da Onça, Seringa, São João, Gradaús, and Rio Branco plutons.

Contrasts in oxygen fugacity and in some geochemical features besides the mineralization associated to these suites indicate that the granite magmas were formed from different sources and degrees of melt (Dall'Agnol et al., 2005). Isotopic systems (Sr, Nd, Pb, Hf) can retain the memory of the composition and age of the source of granitic magmas in the deep crust or upper mantle and stablish constraints for their petrogenesis. Studies of isotopes and trace element indicate that most of the granites could represent mixtures of material from different sources or have been formed entirely by anatexis of older crust (Kemp and Hawkesworth, 2007). In addition, the oxygen isotope ratios of igneous rocks can reflect the $\delta^{18}O$ of their magmatic sources or be

modified by the incorporation into the melts of supracrustal materials, with distinct $\delta^{18}O$ values than the primitive magmas (Valley et al., 2005).

The Nd isotopic data on the A-type granites of the Carajás Province indicate their origin from an Archean crustal source (T_{DM} model ages of 3.35 Ga to 2.60 Ga, and ε_{Nd} values of -12 to -8 at 1880 Ma; Rämö et al., 2002; Teixeira et al., 2002; Dall'Agnol et al 2005; Teixeira et al., 2017) for different plutons of the Jamon, Serra dos Carajás, and Velho Guilherme suites and Gogó da Onça pluton. The A-type granites of Carajás Province show contrasts in oxygen fugacity and in some geochemical features that indicate origin of the magmas from different sources and degrees of melt (Dall'Agnol et al., 2005). Partial melting processes were related to the underplating of mafic magmas.

In this paper, we provide a spatially coupled *in situ* isotope zircon Hf and oxygen ($\delta^{18}O$) analyses from the anorogenic granites of Carajás Province. Precise and systematic SHRIMP U-Pb ages of the same rocks were presented by Teixeira et al. (Submitted). The isotope data presented here will allow us to evaluate previous genetic models and should assure advances on the petrogenesis of Paleoproterozoic Carajás granitic magmatism, in the understanding of the contrasts between the suites, as well as in the possible role of magma mixing and other magmatic processes in the origin of A-type granites. The aim of this paper is to contribute to the understanding of A-type granite petrogenesis and of the role of Archean sources in the origin of this magmatism.

2. Geological setting

The Carajás Province of the Amazon Craton (AC; Fig. 1a, b) contains large mineral deposits of iron, manganese, copper-gold, nickel, tin, and gold-PGE (Tallarico et al., 2005; Bettencourt et al., 2016; Moreto et al., 2015). It is an Archean nuclei surrounded by Proterozoic belts (Santos et al., 2000; Tassinari and Macambira, 2004). According to Santos et al. (2000; 2004; Fig. 1a) the Carajás Province is an Archean independent province, whereas Tassinari and Macambira (2004; Fig. 1b) insert the Carajás Province in the Central Amazonian Province. However, there is a consensus that the Carajás Province corresponds to an older Archean segment of the Amazon craton which was not affected by the Trans-Amazonian cycle.

The Amazon Craton would be part of the Supercontinent Columbia assembled ca. 1800 Ma ago (Cordani et al., 2009; Rogers and Santosh, 2002, 2009; Teixeira et al., in press) and linked by Paleo-to Mesoproterozoic mobile belts with Laurentia, North

China, and Baltica. During the Paleoproterozoic (Orosirian), mainly at the age of 1880 Ma, the Amazon craton evolution was marked by an widespread anorogenic and post-tectonic magmatism that formed hundreds of granitic batholiths and stocks concentrated in the Carajás, Central Amazonian, Tapajós-Parima, and Rondônia-Juruena provinces (Teixeira MFB et al., submitted; Dall'Agnol et al., 1999, 2005; Bettencourt et al., 2016).

The Carajás Province (3.02–2.54 Ga; Fig. 1c) comprises different domains composed mostly of diversified granitoids and greenstone sequences, and is covered, in its northern part, by a ca. 2.76 Ga volcano-sedimentary basin hosting the most important mineral deposits (Fe, Cu, Au, Mn etc.) of the craton. It was divided initially into the Carajás and Rio Maria domains (Santos, 2003) and more recently into the Mesoarchean Rio Maria Domain (2.98-2.86 Ga) and Mesoarchean to Neoarchean Sapucaia (2.95 – 2.73 Ga) and Canaã dos Carajás (3.0-2.70 Ga) domains, and the Carajás Basin (Fig. 1d; Dall'Agnol et al., 2013). These tectonic domains were stabilized at the end of the Archean and remained stable until ca. 1880 Ma when occurred the generation and emplacement of A-type granites (Dall'Agnol et al., 1994, 1999b, 2005).

2.1 The studied intrusions

The anorogenic granites of the Carajás Province (CP) were emplaced during the Orosirian (1880 to 1860 Ma; Teixeira et al., submitted) in an extensional tectonic setting. They are widespread in all three domains of CP and also in the Carajás basin (Fig. 1c). U-Pb SHRIMP ages in zircon and titanite crystals were recently obtained (Teixeira et al., submitted; Teixeira et al., 2017), and a summary of these new results are in Table 1. For a review of all geochronological data of the Paleoproterozoic granites of Carajás, see Teixeira et al. (submitted).

The oxidized A-type granites occur in the Rio Maria Domain and were grouped in the Jamon Suite (Dall'Agnol et al. 1999a), that is composed, among others, of Jamon, Musa, Redenção, and Bannach plutons, which intruded Archaean rocks (Fig. 1c). These plutons are composed of monzogranite and subordinate syenogranite with biotite or, in the less evolved facies, biotite-amphibole ± clinopyroxene. The accessory minerals are zircon, apatite, magnetite, ilmenite, allanite, and titanite (Dall'Agnol et al., 1999a, b; Oliveira, D. C. et al., 2009). Rapakivi textures are more common in Redenção and Bannach plutons (Oliveira, D.C. et al., 2009; Almeida et al., 2006).

The moderately reduced A-type granites were clustered in the Serra dos Carajás Suite constituted by Serra dos Carajás, Cigano, and Pojuca plutons (Dall'Agnol et al.,

1999a, 2005; Teixeira et al., 2002). These plutons are located in the Carajás Basin, north part of the Carajás Province. Chalcopyrite, molybdenite, and Sn mineralization are spatially associated with hydrothermally altered zones within Serra dos Carajás granite cupola (Javier-Rios et al., 1995; Bettencourt et al., 2016).

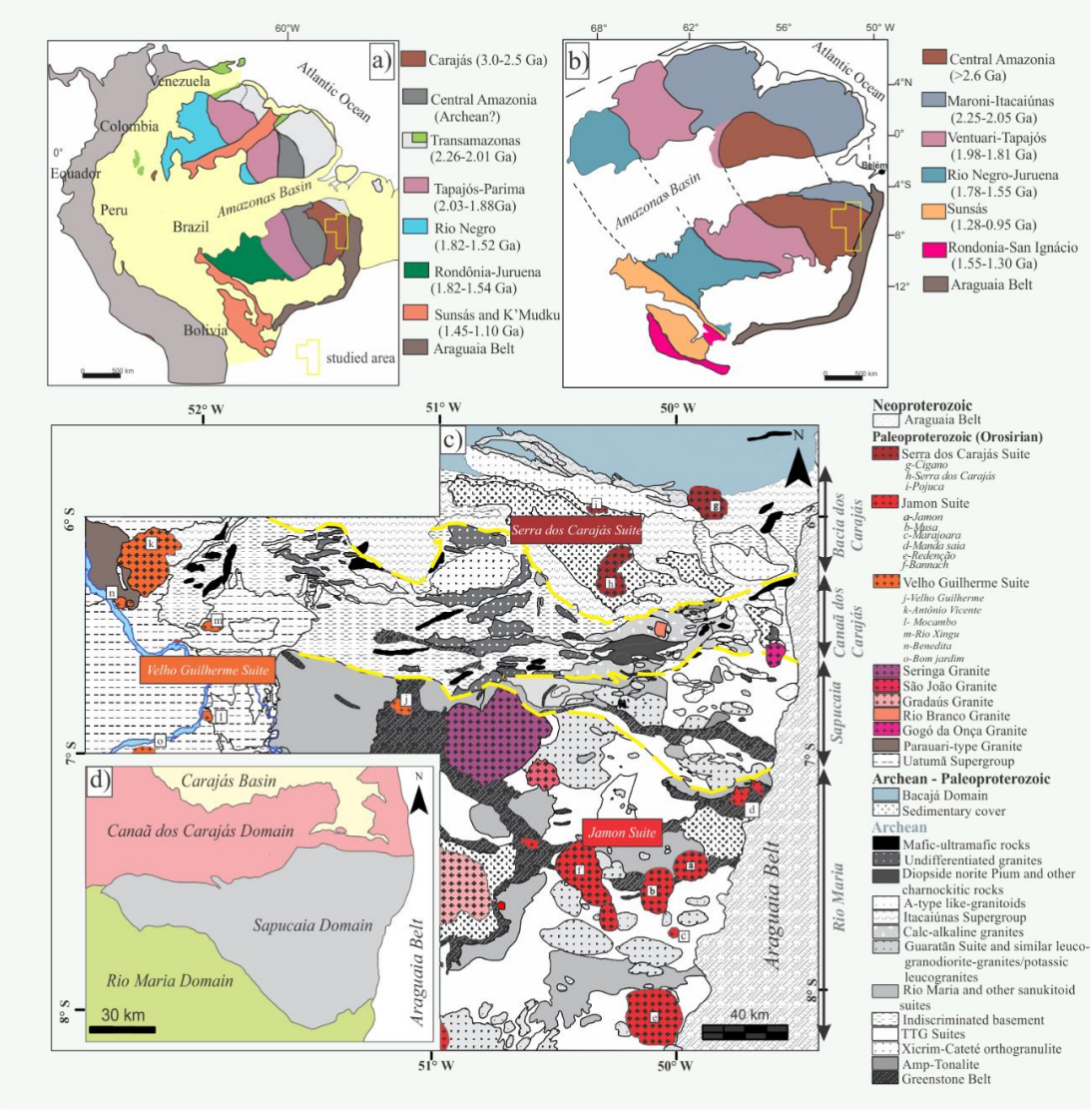

Fig. 1. Geochronological provinces of the Amazonian Craton: (a) model of Santos et al. (2004) and the study area; (b) model of Tassinari and Macambira (1999, 2004) and the study area. (c) Simplified geologic map of the Carajás Province highlighting the A-type Paleoproterozoic Granites of the Province (Dall'Agnol et al., 2005; Vasquez et al., 2008; Almeida et al., 2011; Oliveira et al., 2010; Feio et al., 2013; Silva et al., 2014; Teixeira et al., 2013; Santos et al., 2013; Gabriel and Oliveira, 2014; Rodrigues et al., 2014, modified), and the approximate limits of the tectonic Archean domains of Carajás Province (dashed yellow lines; Dall'Agnol et al., 2013). (d) Simplified map of the tectonic Archean domains of Carajás Province (Dall'Agnol et al., 2013).

The Velho Guilherme Suite outcrops in the Xingu region, and cut undifferentiated Archean rocks, intermediate to felsic volcanic rocks of the Uatumã group and the Orosirian Parauari granite. It is composed of the Velho Guilherme, Antônio Vicente, Mocambo, Rio Xingu, Benedita, and Bom Jardim granites (Teixeira 1999; Teixeira et al., 2002; Lamarão et al., 2012), that are formed of reduced

syenogranite, monzogranite, and subordinated alkali-feldspar granite. The more evolved leucogranitic facies are intensely affected by late to postmagmatic hydrothermal alteration. Primary concentrations of cassiterite are associated with greisen zones and albitized granites (Dall'Agnol et al., 1993; Teixeira, 1999).

Other studied granite plutons, including the Gogó da Onça (Teixeira et al., 2017), Seringa (Paiva Jr. et al., 2011), São João (Lima et al., 2014), Rio Branco (Santos et al., 2013), and Gradaús (Carvalho, 2017), are similar to the Serra dos Carajás or Velho Guilherme suites.

The Gogó da Onça Granite (GOG; Teixeira et al., 2017) is exposed in the border between the Sapucaia and Canaã dos Carajás domains (Fig. 1c) and it is composed of moderately reduced granodiorite, monzogranite, and syenogranite. Amphibole is the mean mafic mineral followed by biotite. Accessory minerals are zircon, titanite, allanite, apatite, magnetite, and ilmenite. Titanite is absent in the syenogranite facies. Teixeira et al. (2017) suggested that the three different facies of the GOG are related by fractional crystallization.

The Seringa and São João plutons outcrops in the northern part of the Rio Maria Domain (Fig. 1c). The Seringa is one of the largest batholiths of CP, with ~2250 km^2. Both plutons are essentially composed of moderately reduced monzogranite to reduced syenogranite, with biotite and amphibole as mean mafic minerals and zircon, apatite, magnetite, ilmenite, and allanite as the accessories phases. Primary titanite is rare or absent. The different facies of the São João pluton are probably related by fractional crystallization (Lima et al., 2014). The magmatic differentiation of the Seringa Granite is more complex and could not be explained only by fractional crystallization from a same parental magma (Paiva Jr. et al., 2011).

The Rio Branco pluton is situated in the Canaã dos Carajás Domain nearby the Sossego copper Mine and crosscuts Mesoarchean calc-alkaline granites (Santos et al., 2013; Fig 1c). It is constituted by syenogranites containing commonly chloritized biotite and fluorite, allanite, and zircon as accessory minerals. Albitization and subordinate greisenization are the main alteration processes that affected locally the granite. Albite, fluorite, topaz, chlorite, muscovite, siderophyllite, and iron oxides are the secondary phases.

3. Geochemistry

A synthesis of the whole-rock geochemical characteristics of the anorogenic granites of the Carajás Province selected for this study is presented below. The main data sources are: Jamon Suite - Gastal (1987), Dall'Agnol et al. (1999a, 2005), Oliveira, D.C. et al. (2009), Almeida et al. (2006); Velho Guilherme Suite - Dall'Agnol et al. (1993, 1994), Teixeira et al., (2002, 2005); Serra dos Carajás Suite: Barros et al. (1995), Javier-Rios et al. (1995); Gogó da Onça pluton (Teixeira et al., 2017); Seringa pluton - Paiva Jr. et al. (2011); São João pluton - Lima et al. (2014).

Major and trace element compositions of the granites of the Carajás Province are plotted in Figures 2 and 3. In Harker diagrams, the samples of all granites show SiO_2 negative correlation with Al_2O_3, FeO_t, MgO, CaO, and Na_2O (Fig. 2) and positive correlation with K_2O (Fig. 2c). For the trace elements, Ba, Sr, and Zr tend to decrease with the increase of SiO_2 (Figures 3a, b, d) behaving as compatible elements during the crystallization history of these rocks, while Rb is incompatible and shows a positive correlation with SiO_2 (Fig. 3c).

These granites show geochemical affinities with within-plate granites (Fig. 4a). In the $FeO_t/(FeO_t+MgO)$ vs SiO_2 diagram (fields of Frost et al., 2001), all these granites are classified as ferroan A-type granites (Fig. 4b). In the $FeO_t/(FeO_t+MgO)$ vs. Al_2O_3 diagram (fields from Dall'Agnol and Oliveira, 2007), the Jamon Suite granites plot in the oxidized A-type field whereas the other granites plot mostly in the reduced A-type field (Fig. 42c). According to the discrimination diagrams of Eby (1992), these granites have geochemical affinity with the A_2-subtype granites (Fig. 4d).

Table 1- U-Pb (SHRIMP) geochronology data of the Paleoproterozoic (Orosirian) A-type granites from Carajás Province

Suite	Sample	Rock	Pluton	U-Pb SHRIMP Age (Ma)	
				zircon	titanite
Serra dos Carajás	ECR-SC-01	biotite-hornblende syenogranite	*Serra dos Carajás*	1882 ± 10 (1)	
	ECR-CG-14A	biotite-hornblende monzogranite	*Cigano*	1884 ± 4 (1)	
	CIG-1	biotite monzogranite	*Cigano*	1883 ± 4 (1)	
Velho Guilherme	L-42	albitized leucogranite	*Velho Guilherme*	1882 ± 6 (1)	
	R-10	hornblende-biotite syenogranite	*Antônio Vicente*	1873 ± 3 (1)	
	R-5	leucogranite	*Antônio Vicente*	1882 ± 15 (1)	
Jamon	PROA-11	biotite-hornblende monzogranite	*Jamon*	1864 ± 8 (1)	
	KM-144B	biotite-hornblende monzogranite	*Musa*	1871 ± 4 (1)	1875 ± 14 (1)
	CREMU-37A	biotite monzogranite	*Musa*	1876 ± 13 (1)	1871 ± 22 (1)
	KM-77A	hornblende-biotite monzogranite	*Musa*	1882 ± 4 (1)	1878 ± 9 (1)
	DC-111	even-grained biotite monzogranite	*Redenção*	1867 ± 5 (1)	1888 ± 52 (1)
	DC-120	seriate leucomonzogranite	*Redenção*	1865 ± 6 (1)	
	DCR-42A	medium even-grained leucomonzogranite	*Redenção*	1871 ± 5 (1)	
	ADR-136I	cumulate granite	*Bannach*	1874 ±6 (1)	
	ADR-35A	fine-grained leucomonzogranite	*Bannach*	1857 ± 5 (1)	
Other granites	AC-45	heterogranular leucosyenogranite	*Seringa*	1879 ± 5 (1)	
	AC-59	coarse-grained biotite-hornblende monzogranite	*Seringa*	1870 ±3 (1)	
	AC-85	coarse-grained hornblende-biotite monzogranite	*Seringa*	1889 ± 8 (1)	
	AC-42	heterogranular hornblende-biotite syenogranite	*Seringa*	1879 ± 18 (1)	
	PC-03B	hornblende-biotite syenogranite	*São João*	1866 ± 4 (1)	
	PC-21	biotite monzogranite	*São João*	1880 ± 3 (1)	
	PCM-10	biotite-hornblende monzogranite	*São João*	1891 ± 5 (1)	
	PCM-13	biotite-hornblende syenogranite	*São João*	1877 ± 3(1)	
	PFR-18B	biotite-hornblende granodiorite	Gogó da Onça	1877.9 ± 9 (2)	1879 ± 15 (2)
	PFR-22	biotite-hornblende monzogranite	Gogó da Onça	1865.8 ± 10 (2)	1872 ± 13 (2)
	PFR-19B	hornblende-biotite syenogranite	Gogó da Onça	1869 ± 3 (2)	

Data sources: (1) Teixeira et al. *(submitted)*; (2) Teixeira et al. (2017).

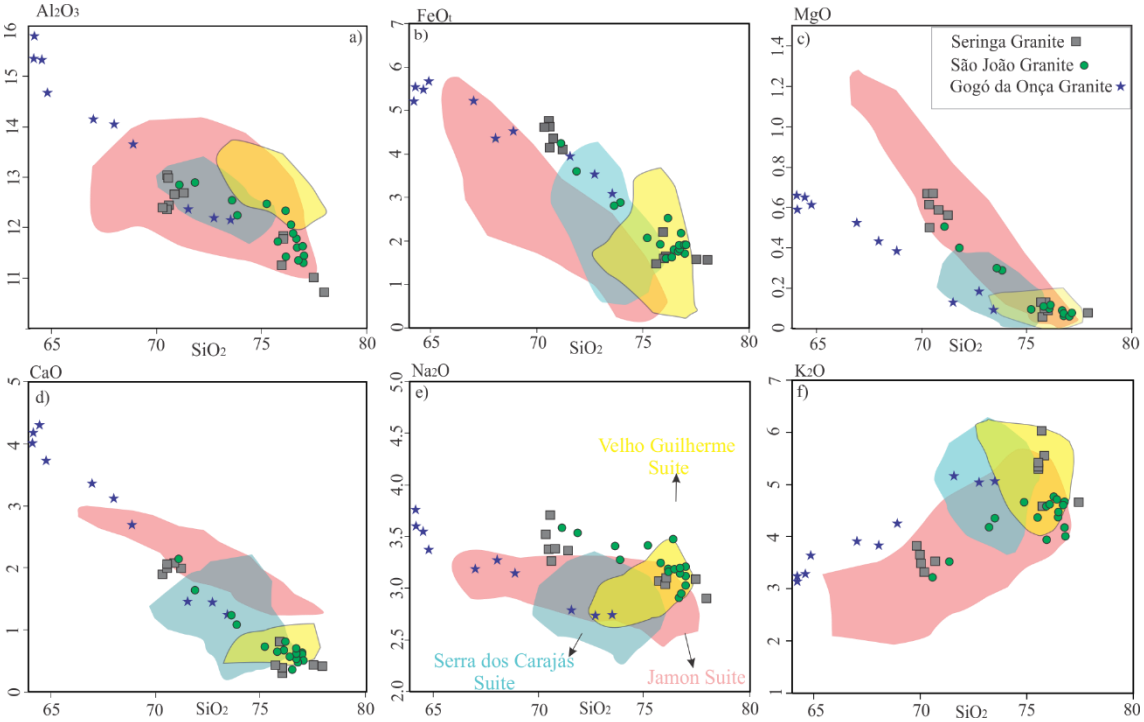

Fig. 2. Major elements Harker diagrams (oxides in wt.%) of the Orosirian granites of Carajás Province. Data sources: Jamon Suite [Dall'Agnol et al. (1999c), Dall'Agnol and Oliveira (2007); Almeida et al. (2006)]; Velho Guilherme Suite [Dall'Agnol et al. (1993); Teixeira (1999); Teixeira et al. (2005)]; Serra dos Carajás Suite [Barros et al. (1995), Javier Rios et al. (1995)]; Gogó da Onça Granite (Teixeira et al., 2017); Seringa Granite (Paiva Júnior et al., 2011); São João Granite (Lima et al., 2014).

4. Analytical techniques

4.1 Sample preparation for in situ analyses

The rock samples were crushed and milled at Federal University of Pará (UFPA) and University of Western Australia. Zircon was extracted from 1–4 kg of whole-rock of selected samples using standard crushing, sieving (60 mesh), heavy liquid (LST), and magnetic separation (Frantz) techniques. The mineral selection was made by hand picking using a binocular microscope. The selected grains were mounted on double-sided sticky tape, cast in epoxy resin together with fragments of standards, and polished to expose surfaces suitable for in situ isotopic analysis.

Back-scattered electrons (BSE) images of the grains were obtained in Tescan Vega3 at the Centre for Microscopy, Characterization, and Analysis (CMCA) of the University of Western Australia.

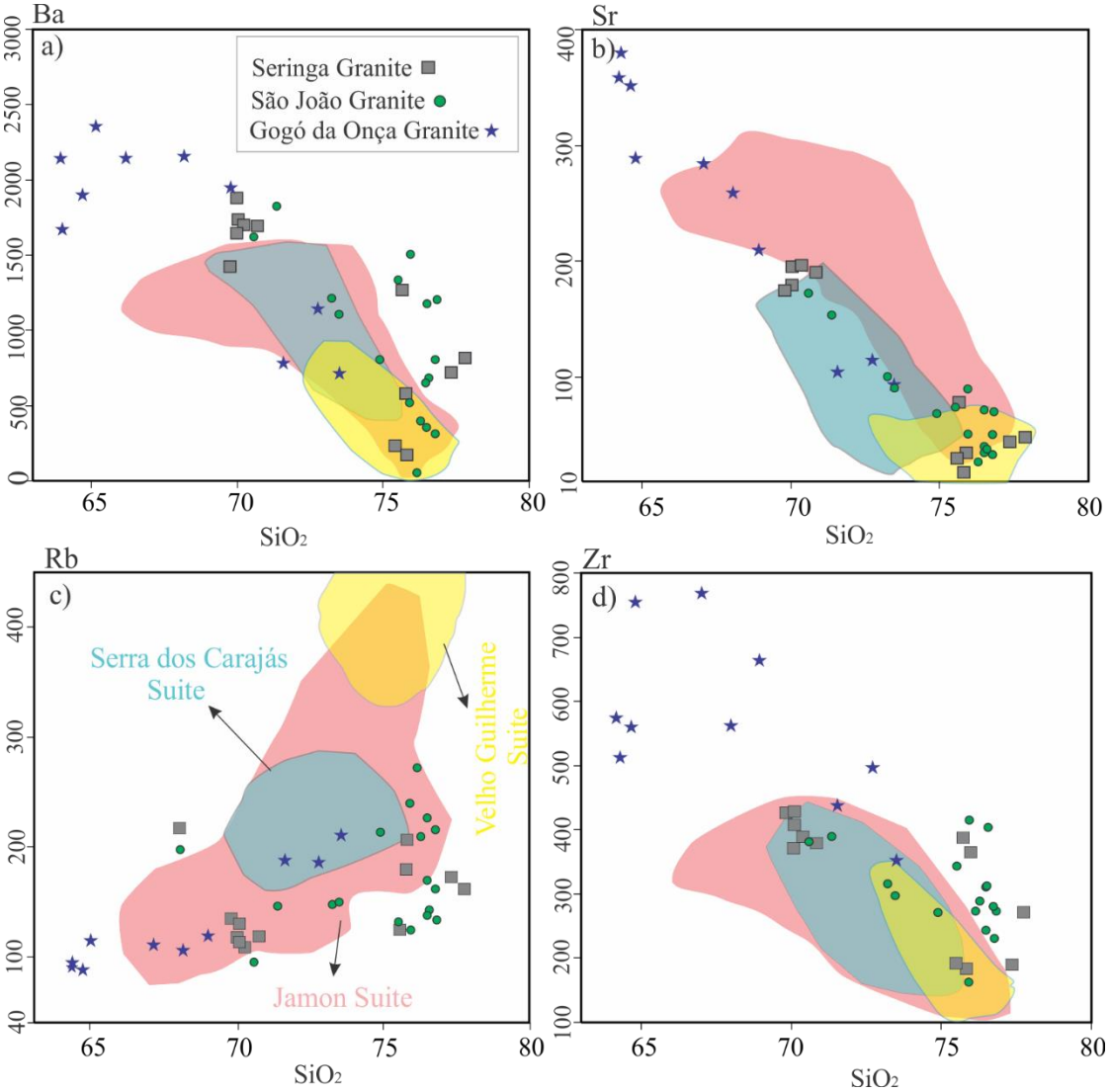

Fig. 3. Trace elements Harker diagrams (oxides in wt.%) of the Orosirian granites of Carajás Province. Data sources: Jamon Suite [Dall'Agnol et al. (1999c), Dall'Agnol and Oliveira (2007); Almeida et al. (2006)]; Velho Guilherme Suite [Dall'Agnol et al. (1993); Teixeira (1999); Teixeira et al. (2005)]; Serra dos Carajás Suite [Barros et al. (1995), Javier Rios et al. (1995)]; Gogó da Onça Granite (Teixeira et al., 2017); Seringa Granite (Paiva Júnior et al., 2011); São João Granite (Lima et al., 2014).

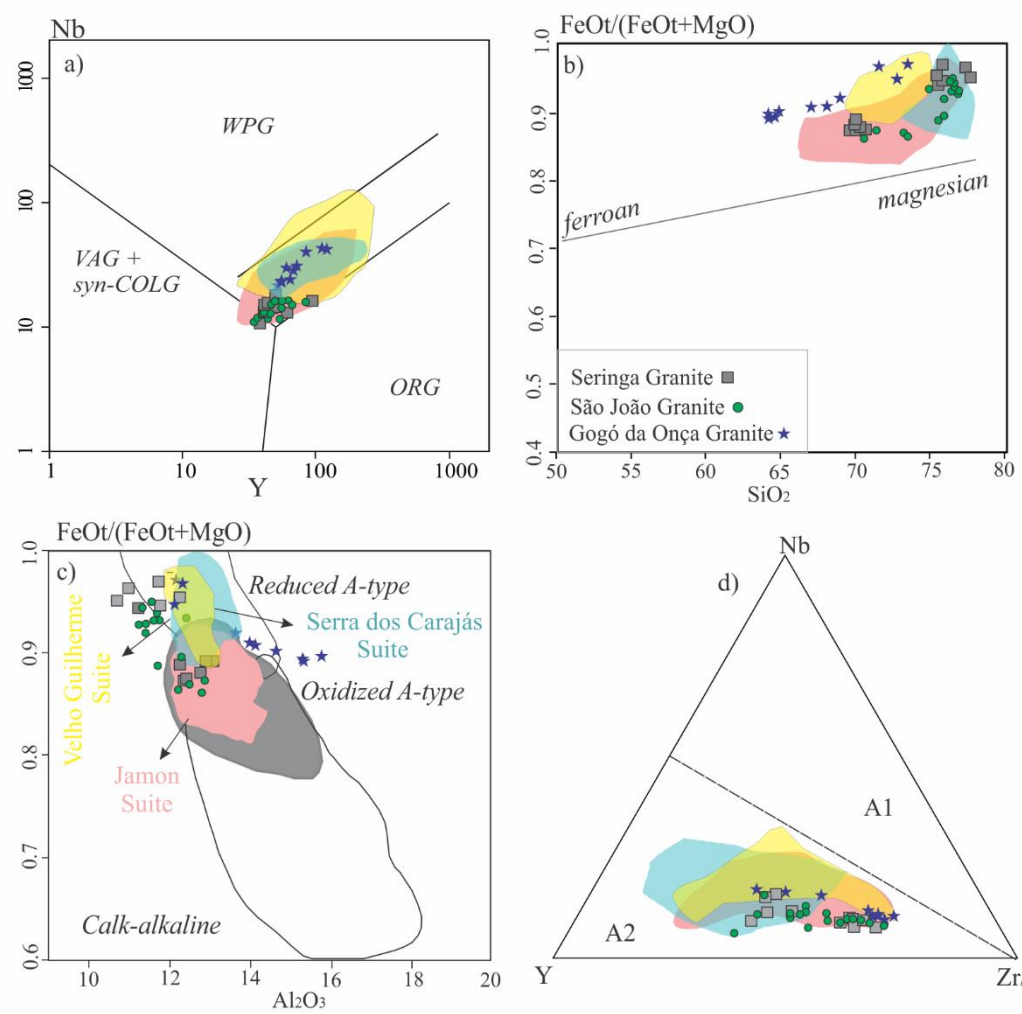

Fig.4. Geochemical classification diagrams for Paleoproterozoic granites of Carajás Province. (a) Nb-Y discrimination diagram (fields of Pearce et al., 1984); (b) (FeO_t/FeO_t+MgO) vs SiO_2 diagram (Frost et al., 2001); (c) $FeO_t/(FeO_t+MgO)$ vs. Al_2O_3 diagram (fields of calc-alkaline, reduced, and oxidized A-type granites of Dall'Agnol and Oliveira, 2007); (d) Y-Nb-Zr/4 plot (A1 and A2 fields of Eby, 1992). Data sources: Jamon Suite [Dall'Agnol et al. (1999c), Dall'Agnol and Oliveira (2007); Almeida et al. (2006)]; Velho Guilherme Suite [Dall'Agnol et al. (1993); Teixeira (1999); Teixeira et al. (2005)]; Serra dos Carajás Suite [Barros et al. (1995), Javier Rios et al. (1995)]; Gogó da Onça Granite (Teixeira et al., 2017); Seringa Granite (Paiva Júnior et al., 2011); São João Granite (Lima et al., 2014).

4.2 Zircon Oxygen isotopic analyses

Oxygen isotope ratios of zircon grains were measured using a Cameca IMS 1280 multi-collector ion microprobe at the Centre for Microscopy, Characterisation, and Analysis (CMCA), University of Western Australia (UWA). Ion-microprobe $\delta^{18}O$ was performed on 25 samples, of the A-type granites of the Carajás Province, in the same samples previously analyzed by SHRIMP for U–Pb ages (Teixeira et al., *submitted*; Teixeira et al., 2017; Table 1), in very closed proximity of the dated spot. The analytical results are presented in Supplementary Tables 1 to 6.

The sample mounts were cleaned with detergent, distilled water and ethanol in an ultrasonic bath and coated with gold (30 nm in thickness) prior to SIMS analyses. Analytical conditions were similar to those outlined in detail by Kita et al. (2009). Oxygen analyses were performed using a 3nA Gaussian Cs+ beam with an impact energy of 20 keV and was focused to a 20 mm spot. Secondary ions were sputtered using a 10 µm-raster and were introduced into the double focusing mass spectrometer within a 110 µm entrance slit and focused in the center of a 4000 µm field aperture (x 130 magnification). Secondary ions were energy filtered using a 40 eV band pass with a 5 eV gap toward the high-energy side. ^{16}O and ^{18}O were collected simultaneously in Faraday cup detectors. A normal incidence electron gun was used for charge compensation. Each analysis spot was pre-sputtered for 10 s, and analyses consisted of 20 s x 4 cycles, which gave an average internal precision of better than ± 00.2‰ (2 standard deviations or SD). Instrumental mass fractionation (IMS) was corrected using Temora 2 following the procedure described in Kita el al. (2009). Secondary standards OCG1, BR266, and Penglai were used for drift correction. Corrected $^{18}O/^{16}O$ ratios are reported in $\delta^{18}O$ notation, in per mil variations relative to Vienna standard mean ocean water (VSMOW).

Uncertainty on each $\delta\ ^{18}O$ spot has been calculated by propagating the errors on instrumental mass fractionation determination, including the error on the reference value of the standard and standard deviation of the mean oxygen isotope ratio measured on the primary standard during the session, and internal error on each sample data point.

4.3 Zircon Lu-Hf isotopic analyses

The Lu-Hf isotope compositions of zircon grains of the Carajás Province were acquired in two sessions. In the first, were analysed zircon grains of the Serra dos Carajás, Velho Guilherme and Jamon Suite and the Gogó da Onça Granite in the School of Earth Sciences at the University of Western Australia using a Thermo Neptune PLUS multi-collector ICP-MS coupled to a Cetac Analyte G2 laser ablation sampling system. Laser ablation was carried out for 60 seconds, following a 30 second on-peak baseline, at repetition rates of 4 Hz and a laser fluence of ~5 J/cm2. Spot sizes of 25 µm, 30 µm or 40 µm diameter were employed, depending on the available polished area of the zone of interest in the crystal. Ablation was conducted in a two-volume Helex sample cell, with the He carrier gas exiting the cell being combined with Ar prior to transport into the ICP-MS via nylon tubing. A small (~0.008 l/min) N2 flow was introduced into the Ar carrier gas to enhance sensitivity (Hawkesworth and Kemp, 2006; Iizuka and Hirata,

2005). The isobaric interference of Lu and Yb on ^{176}Hf was corrected by monitoring the interference-free ^{171}Yb and ^{175}Lu intensities during the analysis and then deriving ^{176}Yb and ^{176}Lu using ^{176}Yb/^{171}Yb = 0.897145 (Segal et al., 2003) and ^{176}Lu/^{175}Lu = 0.02655 (Vervoort et al., 2004). Yb isotope ratios were normalized to 173Yb/171Yb = 1.130172 (Segal et al., 2003) and Hf isotope ratios to ^{179}Hf/^{177}Hf = 0.7325 (Patchett and Tatsumoto, 1981) using an exponential law. The instrumental mass fractionation of Lu was assumed to follow that of Yb. Data were processed offline using a Microsoft Excel spreadsheet. Hf isotope data quality was monitored for each analytical session by analysis of reference zircons Temora 2 and Penglai. These yielded mean ^{176}Hf/^{177}Hf values of 0.282694 ± 17 (2 SD, n = 13) and 0.282929 ± 21 (2 SD, n = 4), identical to those determined by solution analysis (Li et al., 2010; Woodhead and Hergt, 2005). All zircon Hf isotope data are normalized to the solution ^{176}Hf/^{177}Hf value of Mud Tank zircon (0.282507 ± 6, Woodhead and Hergt, 2005, reported relative to JMC 475 ^{176}Hf/^{177}Hf = 0.282160, Vervoort et al., 1999) using the laser ablation data generated from this zircon in the same analytical session (0.282499 ± 11,2 SD, n = 15).

In the second session, Hf isotopes in zircon of the Seringa and São João plutons were measured at the GeoHistory facility in the John de Laeter Centre of the Curtin University. Previously dated zircon crystals were ablated using a Resonetics resolution M-50A excimer laser, coupled to a Nu Plasma II multi-collector inductively coupled plasma mass spectrometer (LA-MC-ICPMS). Following two cleaning pulses and a 40s period of background analysis, samples were spot ablated for 30 s at a 10Hz repetition rate using a 50 or 33 μm beam and laser energy at the sample surface of 2.2 J cm^{-2}. An additional 15s of baseline was collected after ablation. The sample cell was flushed with ultrahigh purity He (320 mL min^{-1}) and N_2 (1.2 mL min^{-1}) and high purity Ar was employed as the plasma carrier gas. All isotopes (^{180}Hf, ^{179}Hf, ^{178}Hf, ^{177}Hf, ^{176}Hf, ^{175}Lu, ^{174}Hf, ^{173}Yb, ^{172}Yb, and ^{171}Yb) were counted on the Faraday collector array. Time resolved data was baseline subtracted and reduced using Iolite (DRS after Woodhead et al., 2004), where ^{176}Yb and ^{176}Lu were removed from the 176 mass signal using ^{176}Yb/^{173}Yb = 0.7962 (Chu et al., 2002) and ^{176}Lu/^{175}Lu = 0.02655 (Chu et al., 2002) with an exponential law mass bias correction assuming ^{172}Yb/^{173}Yb = 1.35274 (Chu et al., 2002). The interference corrected ^{176}Hf/^{177}Hf was normalized to ^{179}Hf/^{177}Hf = 0.7325 (Patchett and Tatsumoto, 1980) for mass bias correction. Zircons from the Mud Tank carbonatite locality were analysed together with the samples in each session to

monitor the accuracy of the results. All Analytical ratios of $^{176}Yb/^{177}Hf$, $^{176}Lu/^{177}Hf$, and $^{176}Hf/^{177}Hf$ are reported with 2σ error.

For all analyzed grains were used the decay constant of 1.867×10^{-11} $year^{-1}$ for ^{176}Lu (Söderlund et al., 2004). The chondritic ratios of $^{176}Hf/^{177}Hf$ (0.282785) and $^{176}Lu/^{177}Hf$ (0.0336) of Bouvier et al. (2008), and the present day depleted mantle of $^{176}Lu/^{177}Hf$ (0.0388) and the $^{176}Hf/^{177}Hf$ (0.28325) of Andersen et al. (2009) were adopted in calculations. We also calculated two distinct crustal model ages t_{DM}^{C} (Supplementary Tables 1 to 6), assuming that the parental magma of the zircons was produced from an average continental crustal source with $^{176}Lu/^{177}Hf = 0.015$ (Goodge and Vervoort, 2006) or $^{176}Lu/^{177}Hf = 0.0125$ (Chauvel et al., 2014).

4.4 Sm-Nd

Nd isotopic compositions were determined in eight samples of the Seringa and São João Granite at the Laboratory of Isotope Geology (Pará-Iso) of the Federal University of Pará (UFPA), following the procedure described by Gioia and Pimentel (2000). Whole-rock samples weighing up about 100 mg, were spiked by a mixture of ^{149}Sm and ^{146}Nd for isotope dilution measurements. The Sm and Nd extraction of whole-rock samples followed conventional cation exchange techniques, using Teflon columns containing Ln Eichron® resin. The isotopic measurements of Sm and Nd were performed for part of the samples on a Thermo Neptune Multicollector mass spectrometer, and other part using an LA-ICP-MS (Laser Ablation - Inductively Coupled Plasma - Massa Spectrometer). The uncertainties calculation for the Sm/Nd and $^{143}Nd/^{144}Nd$ ratios is based on repeated analyses of BCR-1 and La Jolla reference materials, respectively (Oliveira et al., 2008). The accuracy and reproducibility of results were controlled according to the BCR-1 and La Jolla reference material (Oliveira et al., 2008). The $^{143}Nd/^{144}Nd$ ratio was normalized using $^{146}Nd/^{144}Nd = 0.7219$, and the decay constant used was the value revised by Lugmair and Marti (1978) of 6.54 ×10–12 year−1. The Nd model ages were calculated according to the DePaolo (1981) model for a depleted mantle evolution (T_{DM}). The obtained data are shown in Table 3.

5. Results

5.1 Zircon oxygen isotopes

The results of ion-microprobe $\delta^{18}O$ analyses of the studied samples from the Carajás Province are presented in Supplementary Tables 1 to 6 along with Lu-Hf isotope analyses for the same grains used for U–Pb age determination. Between eight to sixteen analyses were performed in each selected representative sample of the studied granites. Most of but not all the samples and/or grains analyzed by oxygen had been also analyzed by Lu-Hf and U-Pb SHRIMP age. It is worth noting that all these granites are preserved igneous rocks without metamorphism overprint, and their 1880 Ma to 1860 Ma zircon ages were defined in upper intercepts very close to the concordia. Only a few samples show the occurrence of older, antecryst zircon grains of 1900 Ma to 1920 Ma (Teixeira et al., *submitted*) that do not show difference in terms of $\delta^{18}O$ values with those aged of ~1880 Ma (Supplementary Table 1 to 6). Care was taken to avoid previous U–Pb analytical spots to prevent possible effects of the oxygen primary beam used in SIMS dating. All Oxygen isotopic data are presented as the $\delta^{18}O$ notation, expressed as deviations from Vienna standard mean ocean water (VSMOW, $^{18}O/^{16}O$ = 0.0020052; Baertschi, 1976) in parts per thousand.

The data of the oxygen isotopic analyses of the A-type Paleoproterozoic granites from Carajás are presented in the relative probability plots histograms of the measured $\delta^{18}O_{zrc}$ SIMS values together with the $\delta^{18}O$ range for mantle zircons (5.3 ± 0.3‰, Valley et al., 1998; Figs. 5, 6 and 7). The results are summarized below.

5.1.1 Serra dos Carajás Suite

The zircons from the Serra dos Carajás Suite have $\delta^{18}O$ values mostly ranging between 5.70‰ and 6.80‰, with few zircon grains ranging between 3.38‰ and 3.81‰ in the biotite-hornblende syenogranite and biotite monzogranite (Supplementary Table 1; Fig. 5a). They have a weighted mean $\delta^{18}O$ value of 6.30 ± 0.5‰ (2SD) for the biotite-hornblende syenogranite of the Serra dos Carajás Granite (ECR-SC-01; Fig. 5a); 6.20 ± 0.5‰ (2SD) for the biotite-hornblende monzogranite and a marginally higher 6.30 ± 0.5‰ (2SD) for the biotite monzogranite both of the Cigano pluton (ECR-CG-14A and CIG-1; Fig.5b, c).

5.1.2 Velho Guilherme Suite

The $\delta^{18}O$ values of zircons from the Velho Guilherme Suite are concentrated in the range between 5.0‰ and 7.5‰, with the highest values in the albitized leucogranite

(weighted mean of 6.78 ± 0.4‰ (2SD); Fig. 5d) and leucogranite facies (discarding the two lower anomalous values, weighted mean of 6.48 ± 0.4‰, 2SD; Fig. 5f). Zircons from the leucogranite facies of the Antônio Vicente pluton have two age populations of 1725 Ma and 1880Ma (Teixeira et al., submitted), but no $\delta^{18}O$ difference between the zircons with these two ages has been observed, except for the zircon grain (N1635F.1-1; Supplementary Table 2) that allowed a low $\delta^{18}O$ value of 2.58 ± 0.48‰ (2SD). In the hornblende-biotite syenogranite facies the $\delta^{18}O$ values vary from 6.12‰ down to mantle values (5.11‰) with a weighted mean of 5.64 ± 0.6‰ (2SD) (Fig. 5e).

5.1.3 Jamon Suite

The zircons from the Musa pluton have $\delta^{18}O$ values quite similar mostly ranging between 5.53‰ and 7.25‰, with two zircon grains of the biotite-hornblende monzogranite showing anomalous values of 3.10‰ and 3.35‰. Discarding these anomalous values, zircons from the biotite monzogranite, hornblende-biotite monzogranite and biotite-hornblende monzogranite, have, respectively, a weighted mean (2SD) of 6.26 ± 0.5‰ (Fig. 6a), 6.25 ± 0.5‰ (Fig. 6b) and 6.34 ± 0.5‰ (Fig. 6c).

In the Redenção pluton, each facies shows a variable distribution of the $\delta^{18}O$ values but dominant values are concentrated between 5.0‰ and 6.50‰. Zircons from the even-grained biotite monzogranite range from 6.22‰ down to mantle values (~5.38‰) with a weighted mean of 5.55 ± 0.5‰ (2SD; Fig. 6d). Zircons from the seriate leucomonzogranite have the highest values with a weighted mean of 6.33 ± 0.4‰ (2SD; Fig. 6e) and a maximum value of 7.03‰. Zircons from the medium even-grained leucomonzogranite have the most variable values of $\delta^{18}O$ (4.21‰ to 6.22‰; Supplementary Table 3) with a weighted mean of 5.63 ± 0.6‰ (2SD; Fig. 6g).

Zircons from the two studied facies of the Bannach pluton have values of $\delta^{18}O$ comparatively more uniform compared to the Redenção Granite ranging between 6.11‰ and 7.09‰ (Supplementary Table 3), with a weighted mean of 6.8 ± 0.5‰ for the cumulate granite (2SD; Fig. 6g) and of 6.65 ± 0.4‰ (2SD) for the fine-grained leucomonzogranite (Fig. 6h). The sample of the cumulate facies (Fig. 6g) show two distinct zircon compositional populations 1874 Ma and 1908Ma (Teixeira et al., submitted), but no $\delta^{18}O$ difference between the zircons with these two ages has been observed, (N1634E.7-1; N1634E.10-1; Supplementary Table 3).

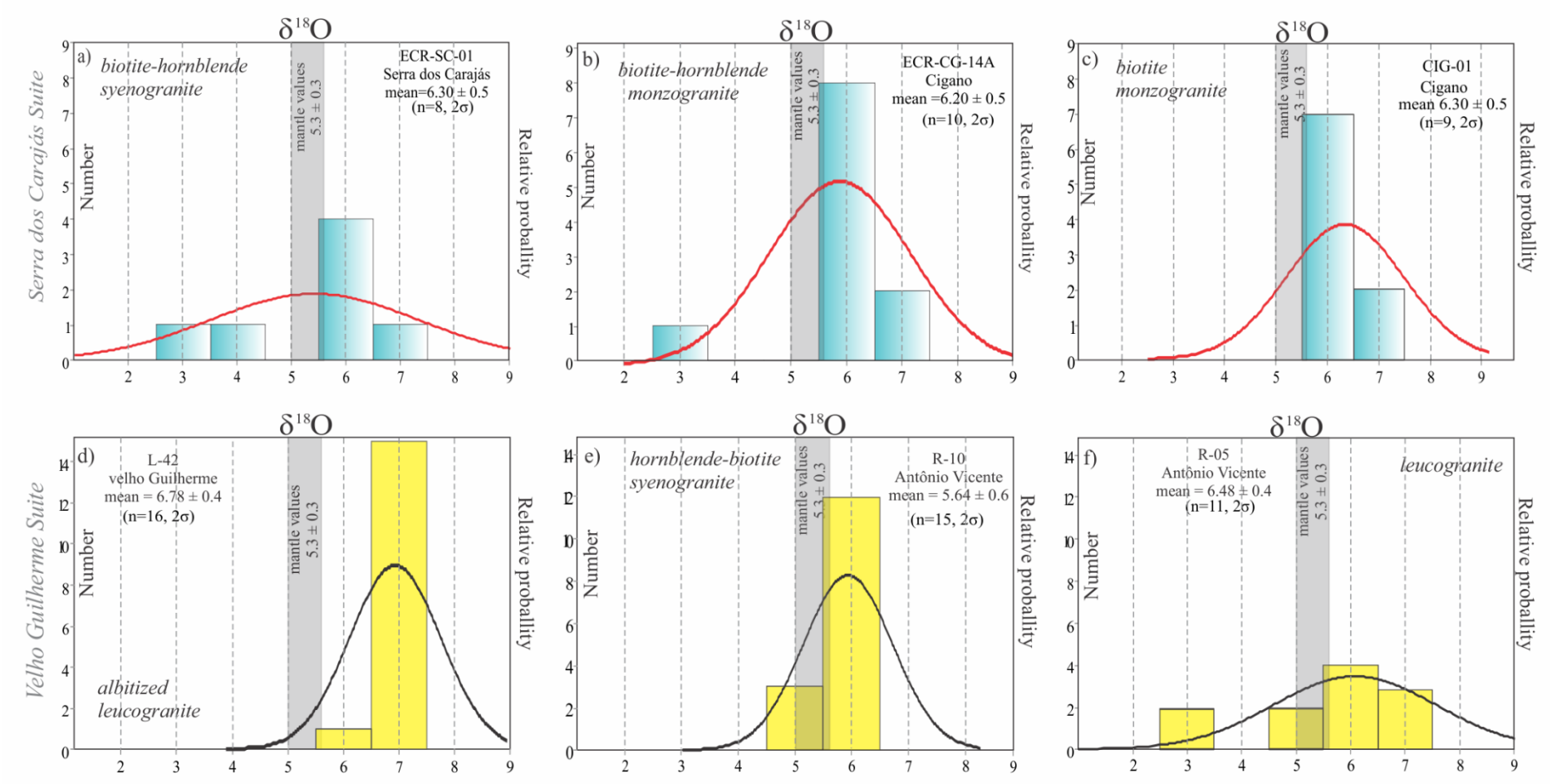

Fig. 5. Histograms and relative probability plots weighted with internal errors of the zircon oxygen isotope compositions of the samples of the Serra dos Carajás and Velho Guilherme suites of the Carajás Province relative to VSMOW(in ‰). Mean denotes the unweighted average of *n* number of in situ analysis and is given with 2SD. Mantle values from Valley et al. (1998) are also shown.

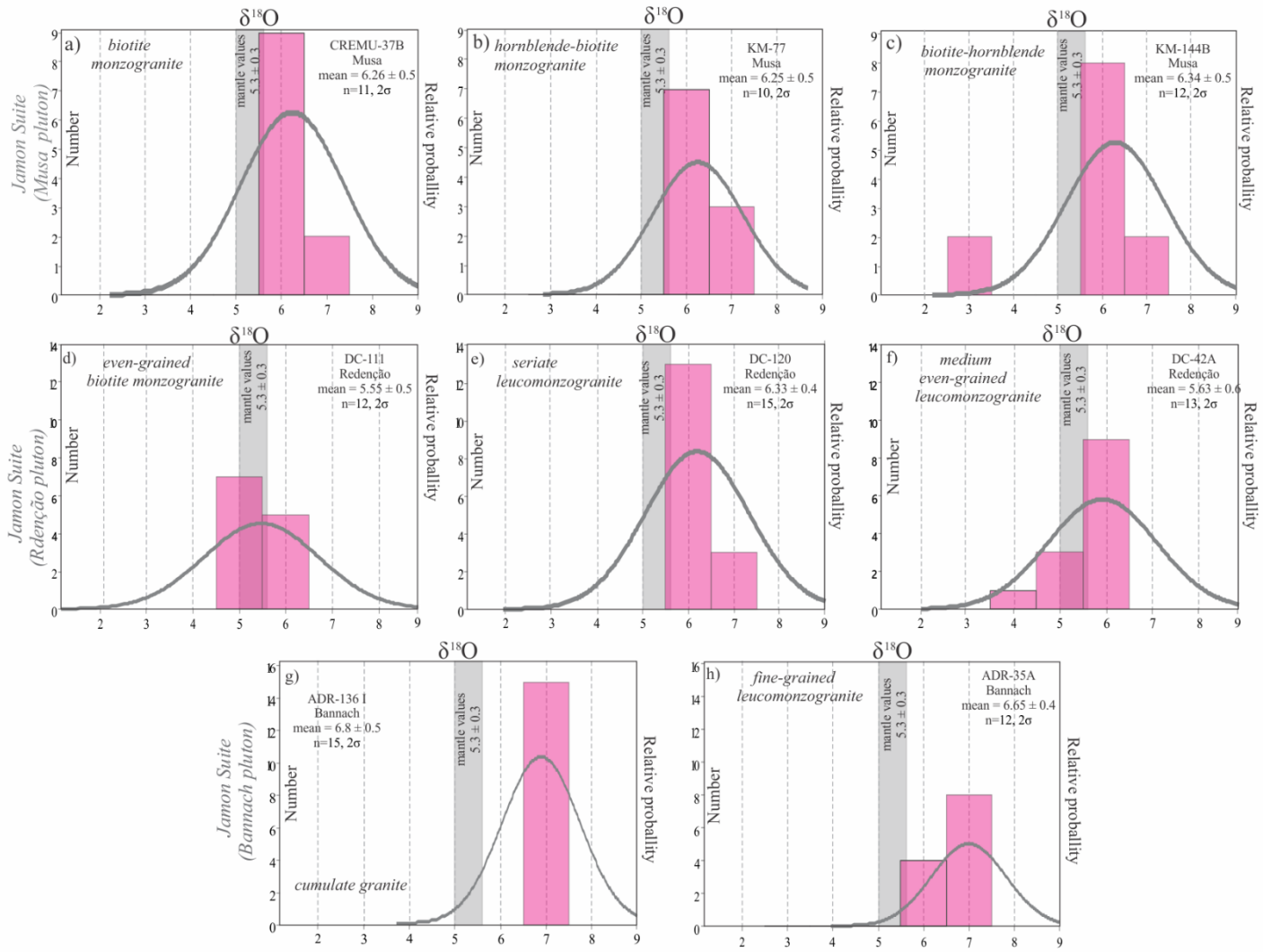

Fig. 6. Histograms and relative probability plots weighted with internal errors of the zircon oxygen isotope compositions of the samples of the Jamon Suite of the Carajás Province relative to VSMOW (in ‰). Mean denotes the unweighted average of *n* number of in situ analysis and is given with 2SD. Mantle values from Valley et al. (1998) are also shown.

5.1.4 Seringa Granite

The zircon grains of four different facies of the Seringa Batholith have similar $\delta^{18}O$ values mostly ranging between 6.00‰ and 7.00‰ (Supplementary Table 4) with a weighted mean of 6.27 ± 0.5‰ (2SD) for the heterogranular leucosyenogranite (Fig. 7a), 6.23 ± 0.5‰ (2SD) for the coarse-grained biotite-hornblende monzogranite (Fig. 7b), 6.27 ± 0.5‰ (2SD) for the coarse-grained hornblende-biotite monzogranite (Fig. 7c), and of 6.35 ± 0.5‰ (2SD) for the heterogranular hornblende-biotite syenogranite, discarding the two anomalous values that are lower than mantle average (Fig. 7d).

5.1.5 São João Granite

For the São João pluton, we have also analyzed zircon grains of four different facies. The obtained $\delta^{18}O$ values are quite homogeneous ranging between ~5.50‰ and 6.86‰ (Supplementary Table 5) except for two zircon grains of the biotite monzogranite facies (PC-21) that presented the maximum and minimum values of $\delta^{18}O$ (respectively, 14.33 ± 0.55‰, N16-26C.2-1; and 4,17 ± 0.55‰, N16-26C.2-4b; 2SD, Supplementary Table 5). Zircons from the hornblende-biotite syenogranite have a weighted mean of 6.20 ± 0.5‰ (2SD; Fig. 7e), 6.33 ± 0.5‰ (2SD) for the biotite monzogranite (Fig. 7f), 6.09 ± 0.5‰ (2SD) for the biotite-hornblende monzogranite (Fig. 7g), and 6.14 ± 0.5‰ (2SD) for the biotite-hornblende syenogranite, discarding the two anomalous values (Fig. 7h).

5.1.6 Gogó da Onça Granite

Zircon grains of three different facies of the Gogó da Onça Granite have $\delta^{18}O$ values mostly ranging between 5.64‰ and 6.99‰ (Supplementary Table 6), with a weighted mean of 6.01 ± 0.5‰ (2SD; Fig. 7i) in the biotite-hornblende monzogranite, 6.08 ± 0.5‰ (2SD; Fig. 7j) in the biotite-hornblende granodiorite, discarding an anomalous value lower than mantle average, and 6.57 ± 0.3‰ (2SD; Fig. 7k) in the hornblende-biotite syenogranite.

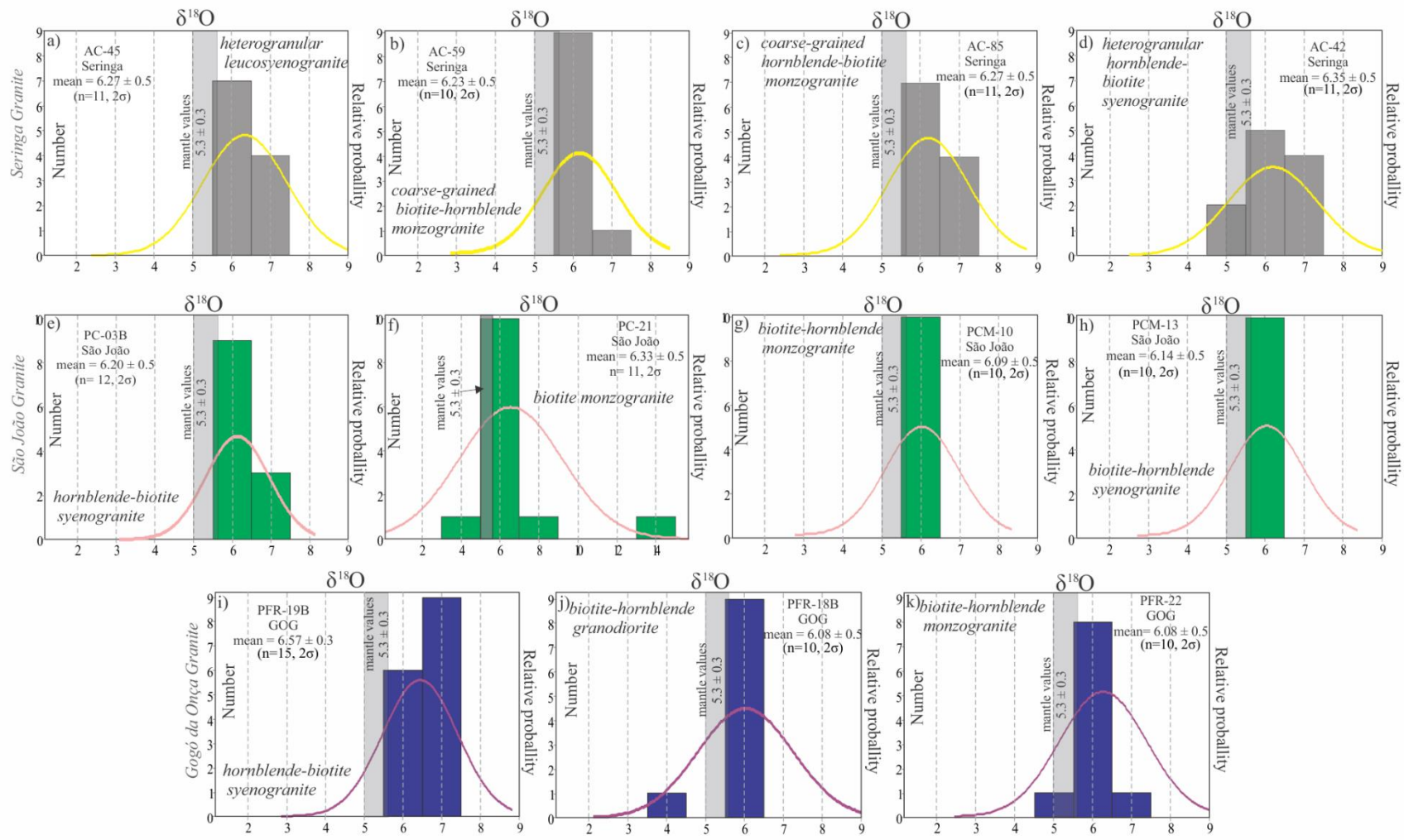

Fig. 7. Histograms and relative probability plots weighted with internal errors of the zircon oxygen isotope compositions of selected samples of the Seringa, São João, and Gogó da Onça granites of the Carajás Province relative to VSMOW (in ‰). Mean denotes the unweighted average of *n* number of in situ analysis and is given with 2SD. Mantle values from Valley et al. (1998) are also shown.

5.2 Zircon Lu-Hf isotopes

Hafnium isotope data of the studied zircons are given in Supplementary Tables 1 to 6. A total of one hundred and forty-eight zircon grains spot analyses were obtained in twenty-one samples of ten plutons of the Orosirian granites of the Carajás Province. The U-Pb SHRIMP ages used for recalculation of Lu-Hf data were obtained by Teixeira et al. (*submitted*), and are displayed in Table 1 and in Supplementary Tables 1 to 6 along with Oxygen data. From each pluton, we used the sample age or, in samples that presented two different ages populations (see Teixeira et al., submitted), we used the age of the grain (Supplementary Table 1 to 6).

Most of the zircons analyzed in this study have $^{176}Lu/^{177}Hf < 0.005$ and present day $^{176}Lu/^{177}Hf$ ratios of 0.281156 to 0.281384 (fig. 8). All analyzed granites have strongly negative ε_{Hf} values that are illustrated in relative probability plots histograms (Figs. 9 and 10). Depleted mantle model ages (T_{DM}) according to Andersen et al. (2009) are presented in Supplementary data 1 to 6, along with crustal model ages (Hf-t_{DM}^{C}).

All of the studied plutons have Mesoarchean to Paleoarchean crustal model ages, that were calculated following two different models: $t_{DM}^{C}{}_{a,}$ assuming that the source rocks of the magma had $^{176}Lu/^{177}Hf$ ratio of average crust of 0.015 (Fig. 11a,b; Goodge and Vervoort, 2006; and Supplementary Tables 1 to 6); and $t_{DM}^{C}{}_{b,}$ assuming $^{176}Lu/^{177}Hf$ ratio of 0.0125 (Fi. 11 c, d; Chauvel et al., 2014; Supplementary Tables1 to 6) and will be discussed later. The main results are summarized below.

5.2.1 Serra dos Carajás Suite

Zircons from the Serra dos Carajás Granite (biotite-hornblende syenogranite; ECR-SC-01) and Cigano pluton (biotite-hornblende monzogranite - ECR-CG-14A; biotite monzogranite - CIG-1) show a slightly larger range of $^{176}Lu/^{177}Hf$ than zircons from the Velho Guilherme and Jamon suites (Fig. 8a, b, c). The hafnium isotope composition of these plutons record initial $^{176}Hf/^{177}Hf$ ratios very homogeneous from 0.281191 to 0.281150 (Supplementary Table 1), corresponding to ε Hf values with a variation of only 3 epsilon Hf units between -13 to -16 (Fig. 9a), and $t_{DM}^{C}{}_{a}$ of 3.37 Ga to 3.46 Ga (Fig. 11 a), and $t_{DM}^{C}{}_{b}$ of 3.23 Ga to 3.31 Ga (Fig. 11 b).

5.2.2 Velho Guilherme Suite

The hafnium isotope composition of the Velho Guilherme (albitized leucogranite; L-42) and Antônio Vicente (hornblende-biotite syenogranite (R-10); and

leucogranite (R-5)) plutons show $^{176}Lu/^{177}Hf$ ratios of 0.000355 to 0.001921 (Fig. 8b). The initial $^{176}Hf/^{177}Hf$ ratios are from 0.281162 to 0.281216 (Supplementary Table 2), corresponding to ε_{Hf} values between -13.0 to -14.9 (Fig. 9a) and $t_{DM}{}^{C}{}_{a}$ of 3.32 Ga to 3.43 Ga (Fig. 11a), and $t_{DM}{}^{C}{}_{b}$ of 3.18 Ga to 3.29 Ga (Supplementary Table 2). This range excludes zircons with U-Pb age of 1724 Ma of the leucogranite sample (R-5) with initial $^{176}Hf/^{177}Hf$ ratios from 0.281300 to 0.281345 (Supplementary Table 2), corresponding to ε_{Hf} values between -12,1 to -13.7 (Fig. 9b) and $t_{DM}{}^{C}{}_{a}$ of 3.14 Ga to 3.23 Ga (Fig. 11a), and $t_{DM}{}^{C}{}_{b}$ of 3.00 Ga to 3.09 Ga (Fig. 11 b).

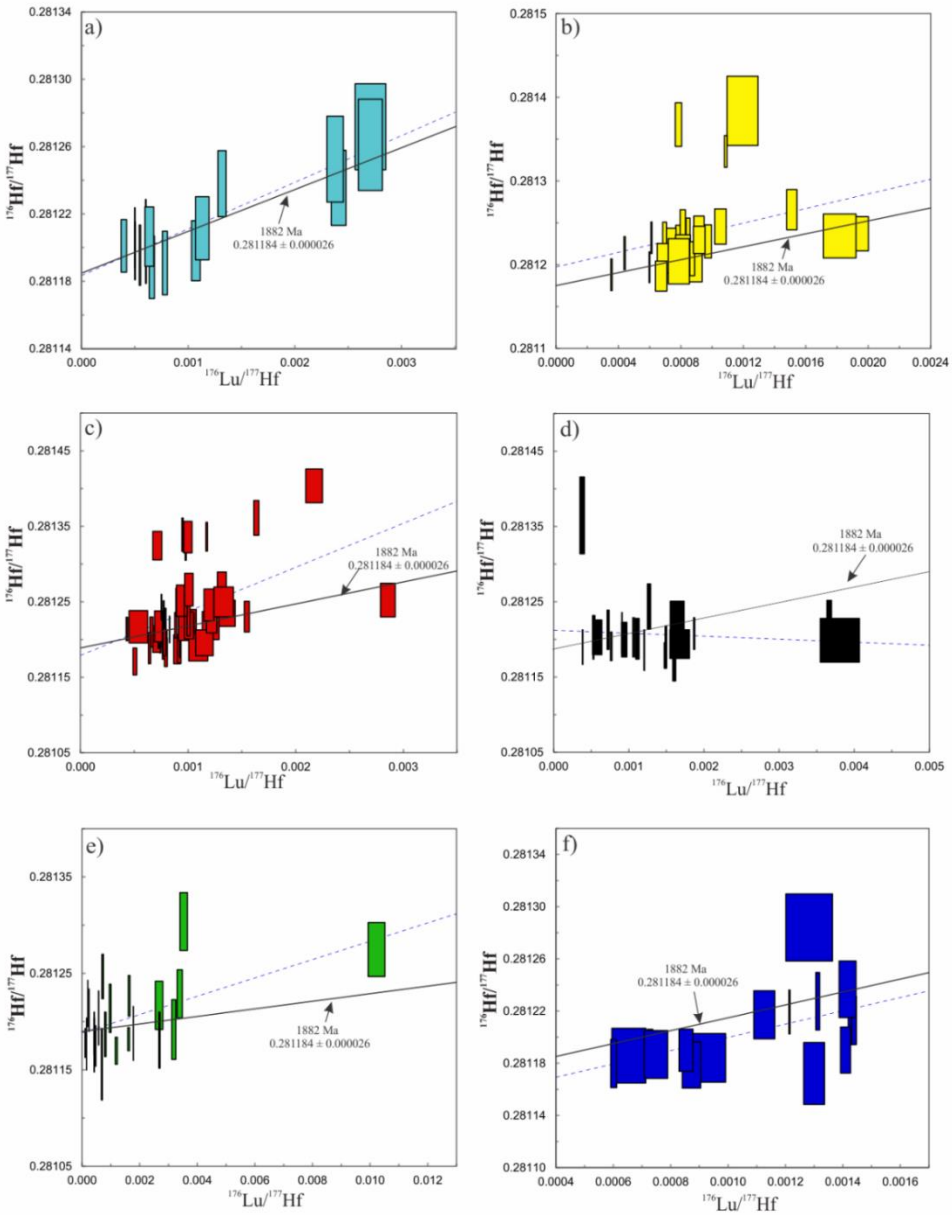

Fig. 8. Present-day $^{176}Hf/^{177}Hf$ ratio as a function of $^{176}Lu/^{177}Hf$. The straight lines in these figures are Lu– Hf reference isochrons at the preferred age of the intrusions based on U–Pb data (Teixeira et al., submitted). a) Serra dos Carajás Suite; b) Velho Guilherme Suite; c) Jamon Suite; d) Seringa Granite; e) São João Granite; f) Gogó da Onça Granite.

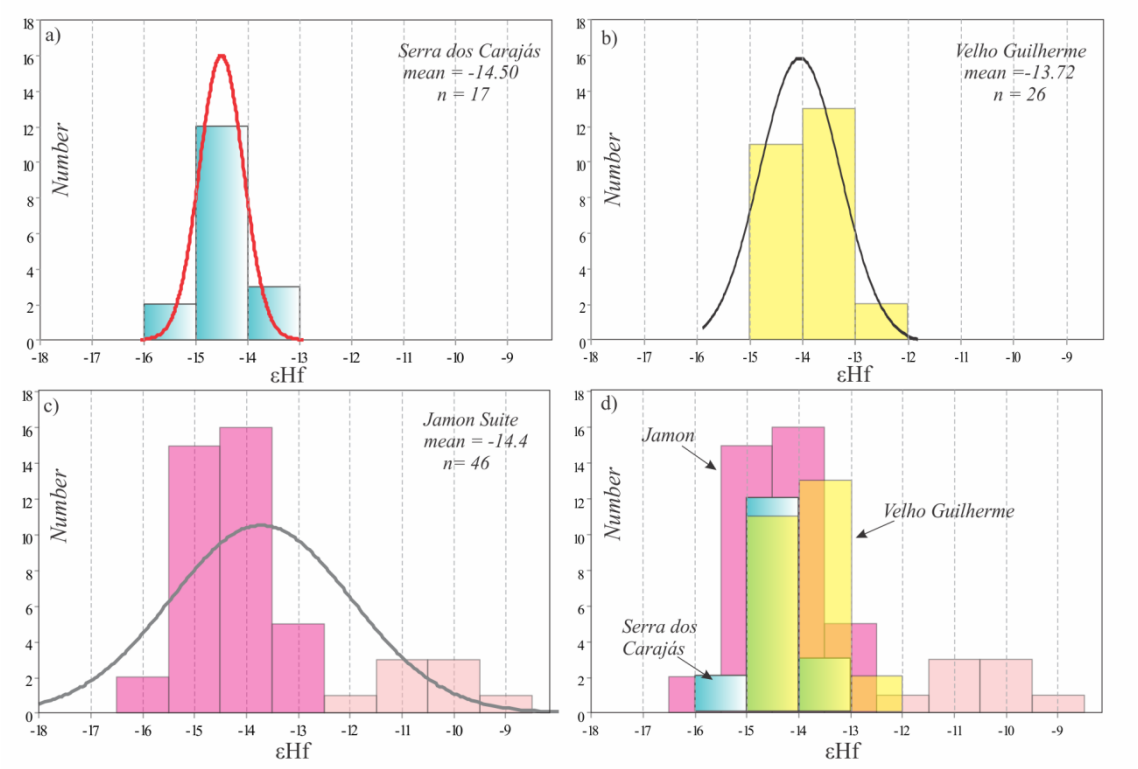

Fig. 9. Histograms and weighted relative probability plots of the initial zircon Hf isotope compositions of the samples of the Orosirian granites of the Carajás Province. (a) Serra dos Carajás Suite; (b) Velho Guilherme Suite; (c) Jamon Suite (light pink color indicates the composition of zircons from ADR-35A, fine-grained leucomonzogranite of Bannach pluton); (d) comparison between the three suites. Mean denotes the un-weighted average of n number of in situ analysis and is given with 2SD.

5.2.3 Jamon Suite

The Hf isotopic analyses for zircon grains from the seven samples of three plutons (Musa, Redenção, and Bannach) of the Jamon Suite show homogeneous Hf isotopic compositions for the Musa and Redenção plutons and for the cumulate facies (ADR-136I) of the Bannach Granite. These plutons have initial $^{176}Hf/^{177}Hf$ ratios of 0.281151–0.281230 (Supplementary Table 3), corresponding to ε_{Hf} values between -12.0 to -15.7 (Fig. 9c) and $t_{DM}{}^{C}{}_{a}$ of 3.27 Ga to 3.47 Ga (Fig. 11a), and $t_{DM}{}^{C}{}_{b}$ of 3.14 Ga to 3.32 Ga (Fig. 11 b).

Zircon crystals from the fine-grained leucomonzogranite facies (ADR-35A; U-Pb age of 1857 Ma; Supplementary Table 3) of the Bannach Granite, yield initial $^{176}Hf/^{177}Hf$ ratios of 0.281289–0.281327 (Supplementary Table 3), more radiogenic than the other plutons of this suite. ε_{Hf} values vary between -11 to -9.3 (Fig. 9c; graphically represented with light pink color), $t_{DM}{}^{C}{}_{a}$ between 3.09 Ga to 3.17 Ga (Fig. 11a), and $t_{DM}{}^{C}{}_{b}$ between 2.97 Ga to 3.05 Ga (Fig. 11b), except for one zircon grain (N1635A.11-1; See Supplementary Table 3). In general, the Jamon Suite shows also a short range of

ε_{Hf} values, except for the zircons of the ADR-35A (Fig. 9c, d), a fine-grained leucomonzogranite of the Bannach pluton. We will return to this point in the following.

5.2.4 Seringa Granite

Zircons from four studied facies (heterogranular leucosyenogranite, AC-45; coarse-grained biotite-hornblende monzogranite, AC-59; coarse-grained hornblende-biotite monzogranite, AC-85; and heterogranular hornblende-biotite syenogranite, AC-42) of the Seringa Granite have $^{176}Lu/^{177}Hf$ ratio mostly ranging between 0.0003 to 0.0018 (Fig. 8b). They record initial $^{176}Hf/^{177}Hf$ ratios mostly from 0.281119 to 0.281199 (Supplementary Table 1), corresponding to ε_{Hf} values with 6 epsilon Hf units between -12.8 to -17.3 (Fig. 10a), and $t_{DM}^{C}{}_{a}$ of 3.29 Ga to 3.58 Ga (Fig. 11b), and $t_{DM}^{C}{}_{b}$ of 3.16 Ga to 3.43 Ga (Fig.11d). The coarse-grained hornblende-biotite monzogranite (1890 Ma; Teixeira et al., *submitted*) has the more strongly negative ε_{Hf} values (Fig. 10d) and show the oldest crustal model ages (Fig. 11b,d; Supplementary Table 4) compared to the other facies.

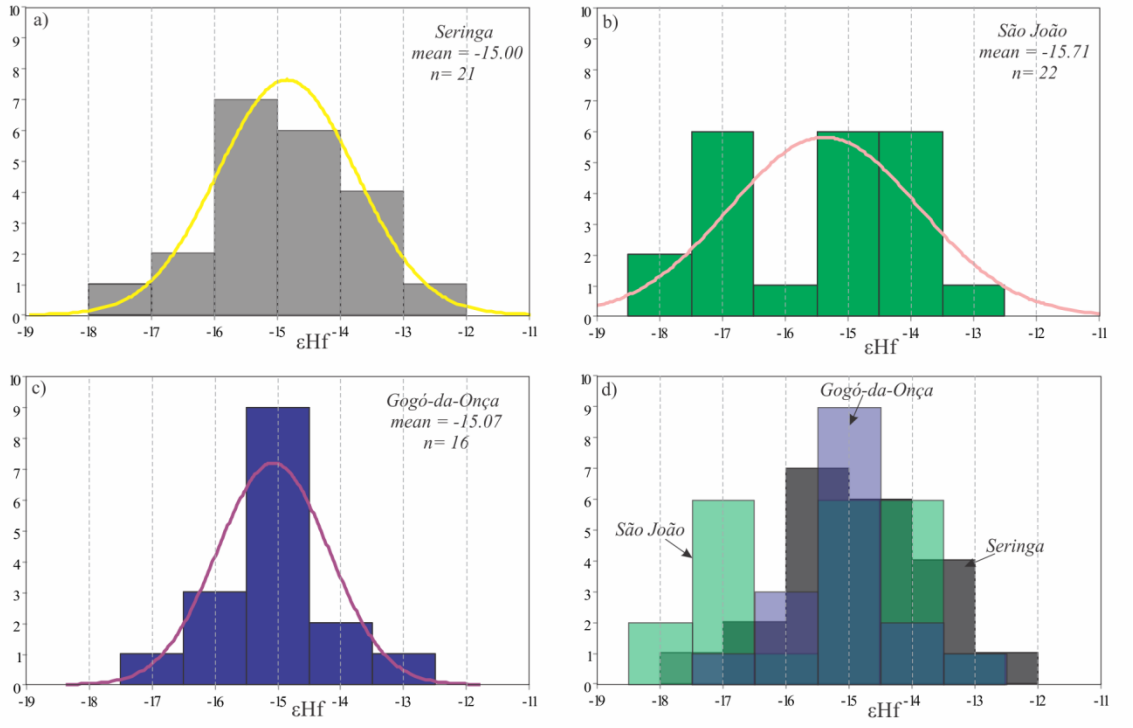

Fig. 10. Histograms and relative probability plots weighted of the initial zircon Hf isotope compositions of the samples of the Orosirian Granites of the Carajás Province. (a) Seringa Batholith; (b) São João pluton; (c) Gogó da Onça pluton; (d) comparison between them. Mean denotes the un-weighted average of n number of in situ analysis and is given with 2SD.

5.2.5 São João Granite

Except for one zircon grain (N1626F.3-1) of the hornblende-biotite syenogranite (PC-03B; 1866 Ma; Supplementary Table 5; Fig. 10b), the hafnium isotope composition of three studied facies of the São João Granite is quite homogeneous. The hornblende-biotite syenogranite (PC-03B; 1866 Ma) has initial $^{176}Hf/^{177}Hf$ ratios from 0.280913 to 0.281275, with ε_{Hf} values of -15.4 to –18.3, and $t_{DM}{}^{C}{}_{a}$ of 3.45 Ga to 3.63 Ga (Fig. 11b), and $t_{DM}{}^{C}{}_{b}$ of 3.30 Ga to 3.46 Ga (Fig. 11d); the zircon grain N1626F.3-1 show ε_{Hf} of -24.2 and $t_{DM}{}^{C}{}_{a}$ of 3.99 Ga and $t_{DM}{}^{C}{}_{b}$ of 3.79 Ga (Fig. 11d). The biotite-monzogranite (PC-21; 1880 Ma) has initial $^{176}Hf/^{177}Hf$ ratios from 0.281172 to 0.281222, with ε_{Hf} values of -12.9 to –14.7, and $t_{DM}{}^{C}{}_{a}$ of 3.31 Ga to 3.42 Ga (Fig. 11b), and $t_{DM}{}^{C}{}_{b}$ of 3.17 Ga to 3.27 Ga (Fig. 11d). The biotite-hornblende monzogranite (PCM-10; 1891 Ma) has hafnium isotope composition very homogeneous with initial $^{176}Hf/^{177}Hf$ ratios from 0.281132 to 0.281179, with ε_{Hf} values of -14.1 to –14.9 (except for one zircon grain with ε_{Hf} of -15.8; N16-26E.6-1), and $t_{DM}{}^{C}{}_{a}$ of 3.39 Ga to 3.50 Ga (Fig. 11b), and $t_{DM}{}^{C}{}_{b}$ of 3.25 Ga to 3.35 Ga (Fig. 11d). The Lu/Hf ratio of this granite is slightly higher than the Seringa pluton, ranging from 0.0007 to 0.004 (Fig. 8e).

5.2.6 Gogó da Onça Granite

The hafnium isotope composition of the Gogó da Onça hornblende-biotite syenogranite (PFR-19B) and biotite-hornblende granodiorite (PFR-18B) exhibit Lu/Hf ratio slightly lower than the Seringa and São João plutons, ranging from 0.0006 to 0.0014 (Fig. 8e), and different of the Seringa and São João plutons that show some variations between their facies, record very homogeneous initial $^{176}Hf/^{177}Hf$ ratios from 0.281140 to 0.281187 (Supplementary Table 6), corresponding to ε_{Hf} values between -14.4 to -16.5 (Fig. 10b), and $t_{DM}{}^{C}{}_{a}$ of 3.28 Ga to 3.52 Ga (Fig. 11b), and $t_{DM}{}^{C}{}_{b}$ of 3.25 Ga to 3.37 Ga (Fig. 11d).

5.3 Hf Crustal model ages

The Hf crustal modal ages calculated for the two models presented before are shown in the Fig. 11. Note that for the $^{176}Lu/^{177}Hf$ average crust of 0.015 the studied granites show $t_{DM}{}^{C}$ oldest (3.09 to 3.63 Ga; Fig 11a, b) than using the $^{176}Lu/^{177}Hf$ average crust of 0.0125 that are younger ranging between 3.0 Ga to 3.46 Ga (fig. 11c.d) but within the interval of $t_{DM}{}^{C}{}_{a}$. Independent of the $^{176}Lu/^{177}Hf$ ratio used all these plutons show considerable oldest ages than previously obtained by Nd isotopes data. In

addition, the plutons of the Seringa, São João and Gogó da Onça Granite have oldest crustal model ages than the Serra dos Carajás, Velho Guilherme and Jamon Suite (Fig. 11), this could indicate that a major late Archean crustal source was involved in the origin of this plutons.

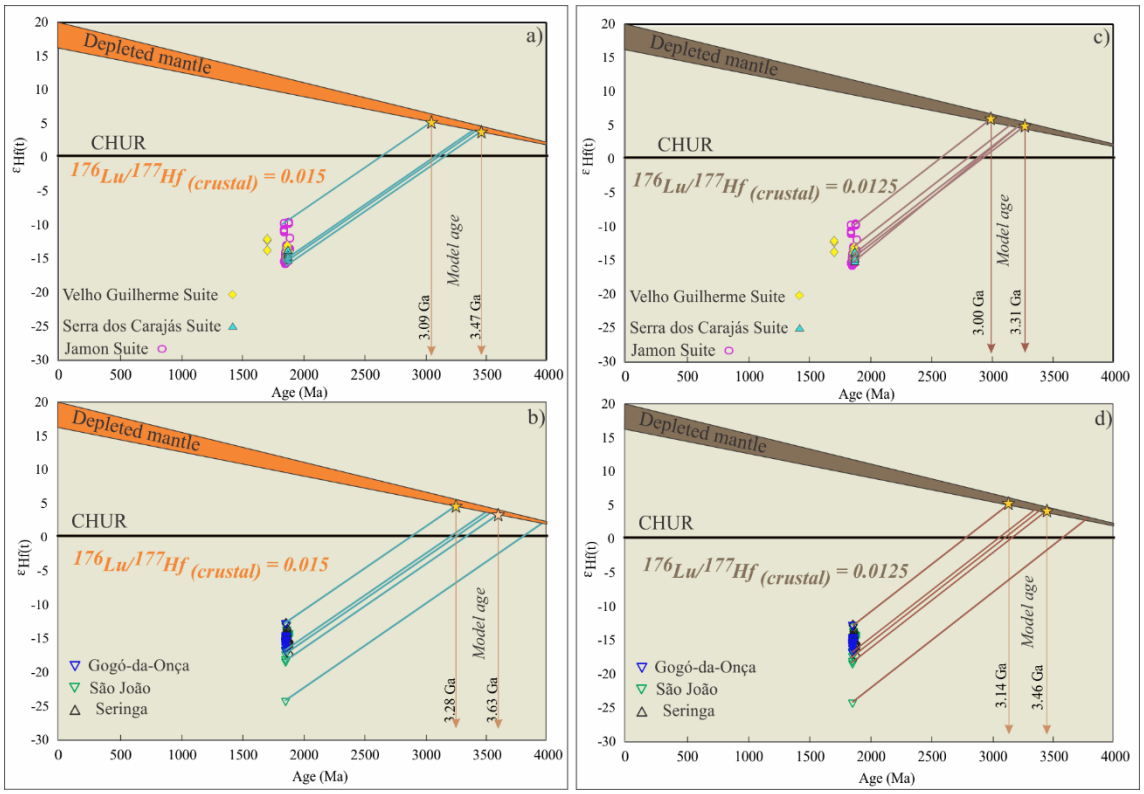

Fig. 11. Age vs Ɛ $_{Hf}$ diagram of the studied Orosirian Granites of the Carajás Province: (a , b) using the average crust of 0.015 ((a) Serra dos Carajás, Velho Guilherme and Jamon suites; (b) Seringa, São João and Gogó da Onça Granites); (c, d) using the average crust of 0.0125 ((c) Serra dos Carajás, Velho Guilherme and Jamon suites; (d) Seringa, São João and Gogó da Onça Granites).

5.4 Sm-Nd isotopes

The whole-rock Nd isotope compositions from the main facies of the Seringa and São João granites are given in Table 3 and illustrated on an age vs. εNd diagram in Fig. 12. The full data of the Nd composition of the A-type Paleoproterozoic magmatism of the Carajás Province are in Supplementary Table 7.

The Seringa batholith has Nd concentrations varying between 55.28 and 83.89 ppm, and Sm contents of 9.61 to 12.99 ppm, show little variation in $^{147}Sm/^{144}Nd$ from 0.093583 to 0.105110, with T_{DM} model ages varying from 2.86 to 2.91 Ga, and negative ε_{Nd} (at 1880 Ma) values of -10.9 to -9.9.

In the São João pluton, the Nd concentrations are of 55.28 to 83.89 ppm, and Sm contents of 9.61 to 12.99 ppm. Variation in $^{147}Sm/^{144}Nd$ from 0.099110 to 0.107698 is

also limited. The T_{DM} model ages are slightly older, between 2.89 to 2.98 Ga and ε_{Nd} (at 1880 Ma) values show a larger range (-11.3 to -9.4) compared to Seringa granite.

Table 3 – Whole-rock Sm-Nd isotopic composition of the Seringa (SG) and São João (SJ) granites

		U-Pb	Sm(ppm)	Nd(ppm)	$^{147}Sm/^{144}Nd$	2σ	$^{143}Nd/^{144}Nd$	2σ	f (Sm/Nd)	T(DM)	eNd(t)
SG	AC-42	1.87	11.18	69.03	0.09790	0.0004	0.510864	0.000007	-0.502	2.90	-10.9
	AC-59	1.87	10.25	60.09	0.10311	0.0015	0.510951	0.000019	-0.476	2.91	-10.2
	AC-66	1.88	12.99	83.89	0.09358	0.0041	0.510813	0.000018	-0.524	2.86	-10.7
	AC-85	1.88	9.61	55.28	0.10510	0.0002	0.510998	0.000006	-0.466	2.90	-9.9
SJ	PCM-10	1.91	8.96	50.27	0.10770	0.0044	0.511056	0.000044	-0.452	2.89	-9.4
	PC-21	1.88	8.91	52.36	0.10291	0.0023	0.510899	0.000038	-0.477	2.98	-11.3
	PC-03B	1.86	9.58	58.47	0.09910	0.0002	0.510914	0.000002	-0.496	2.86	-10.0
	PCM-13	1.77	14.58	88.13	0.10002	0.0003	0.510894	0.000003	-0.491	2.91	-10.8

6. Discussion

6.1 Hf-O isotope composition

Magmatic processes as assimilation or mixing might be difficult to distinguish in bulk rock isotopic analysis but can be traced by detailed isotopic analysis of zircon (Kemp et al., 2007; Andersen et al., 2004, 2009). Oxygen isotope data in zircon can provide a robust indicator of the isotopic composition of the magma from which the zircon crystallized and contaminants. According to Valley et al. (1994), $\delta^{18}O_{Zc}$ can be interpreted as the $\delta^{18}O$ in the host melt ($\delta^{18}O_{melt}$). Zircon that crystallizes from mantle derived magmas has compositions around 5.3 ± 0.3‰ (1 SD, Valley et al., 1998). Thereby, the combined Lu-Hf and Oxygen isotope in zircon allow to determine the nature of the source of the magmas, to evaluate incorporation of juvenile or evolved material, and the influence of supracrustal rocks (Hawkesworth and Kemp, 2006; Kemp et al., 2009; Wang et al., 2011).

The A-type anorogenic granites analyzed in the present study represent a large volume of granitic magmatism generated in the late Palaeoproterozoic in the eastern of the Amazon Craton. They show significant contrasts in fO_2 and occur along a considerable geographical area being distributed in the northern, western and southern parts of the Carajás Province. Most of the zircons from the intrusions analyzed in this work have a remarkably restricted initial $^{176}Hf/^{177}Hf$. The analyzed granites show within-suite maximum ranges of ca. 6 units (ε_{Hf}), and about 3 units (ε_{Hf}) for most plutons or single samples, and $\delta^{18}O$ variation is also limited (< 3‰; 2SD). They typically have negative ε_{Hf} values demonstrating a significant influence of older (Archaean) crustal sources in the origin of their magmas.

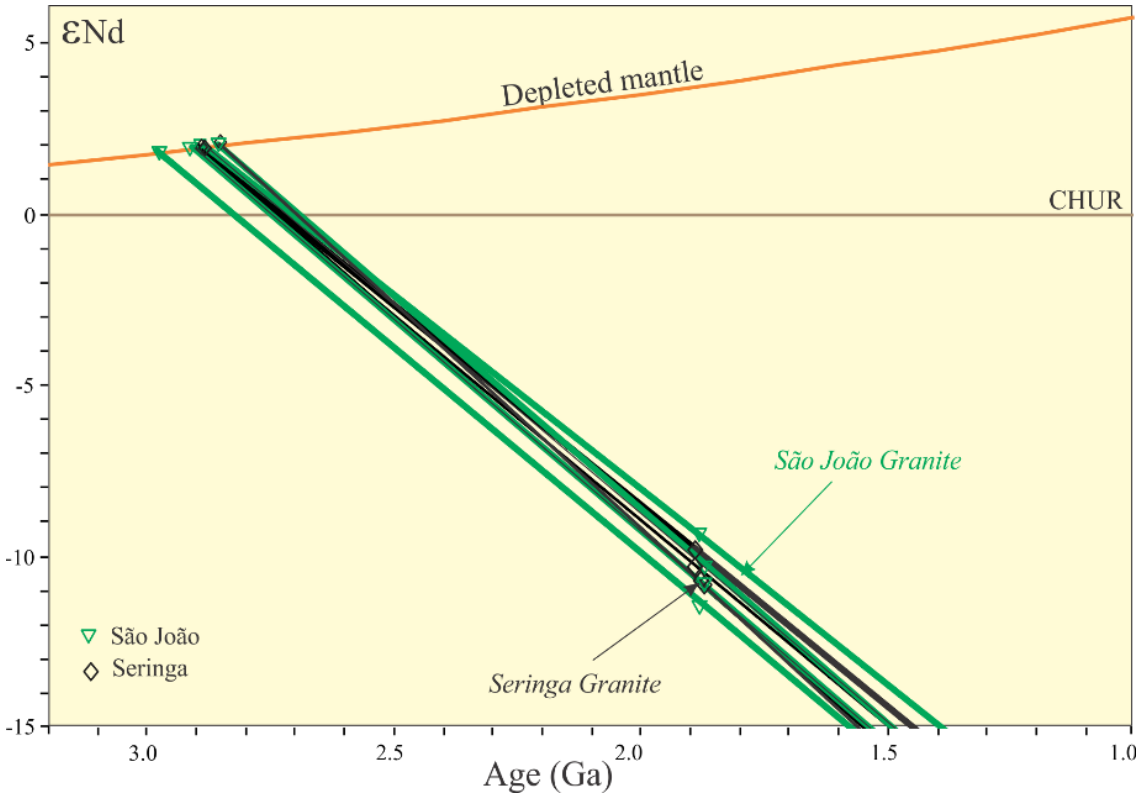

Fig. 12. Age vs. εNd diagram for the Seringa and São João plutons of the Carajás Province.

The initial Hf isotope compositions are very homogeneous (< 3 εHf units of variation) for the different plutons of the Serra dos Carajás, Velho Guilherme, and Jamon suites. Except for one zircon analysis, the fine-grained leucomonzogranite of Bannach pluton also show limited internal variation of εHf, however, it shows strong contrast in the initial Hf composition of their samples compared to the other Jamon Suite granites (Fig. 9c, d; Supplementary Table 3). Zircons that crystallized from mantle-derived magmas contaminated by crustal rocks or formed by mixing of melts from sources in the depleted mantle and the deep continental crust, usually exhibit larger within-sample Hf isotope variations compared to the Orisirian Carajás granites (Griffin et al. 2000; Hawkesworth and Kemp 2006; Andersen et al., 2009). This homogeneity may indicate that zircons in each granite sample of these three suites probably crystallized from a magma with homogeneous Hf isotope composition and that the processes and sources involved in the origin of different suites are broadly similar.

It is accepted that the different facies of the plutons that constitute the Orisirian granite suites evolved mostly by fractional crystallization (Dall'Agnol et al., 1999a, 2005; Dall'Agnol and Oliveira, 2007; Teixeira et al., 2002; Oliveira, et al., 2009), and this is particularly true for the Jamon Suite (Dall'Agnol et al., 1999a, b; Oliveira, D.C.

et al., 2009). However, the fine-grained leucogranite facies of the Bannach pluton show mineralogical, geochemical, and geochronological evidence that it was formed from an independent magma pulse, distinct genetically and younger than the less evolved facies of the same pluton (Oliveira, D.C. et al., 2009; Almeida et al., 2006; Mesquita et al., in press; Teixeira et al., submitted). The present-day $^{176}Hf/^{177}Hf$ composition of the two samples of Bannach Granite (Figure 13) and the εHf histogram demonstrate that the leucogranite facies (ADR-35A) of the Bannach pluton has a different isotopic composition and is more radiogenic compared to the cumulate granite (ADR-136I). These isotopic data summed with all independent evidences allow to conclude that a distinct and more reduced source was involved in the generation of the leucogranite facies of Bannach pluton (Fig. 13; Mesquita et al., in press).

Most facies of the Seringa, São João, and Gogó-da-Onça plutons also presented in individual samples a limited variation of inicial εHf and similar ranges to those observed in the three suites (-12.8 to -15.8; Supplementary Tables 4, 5, 6). However, the coarse-grained hornblende-biotite monzogranite of the Seringa pluton and the hornblende-biotite syenogranite of the São João pluton presented more accentuate negative ε_{Hf} values (respectively of -15.5 to -17.3 and -16.5 to -18.3; with one grain of -24.2; Fig. 15; Supplementary Table 5) compared to the other facies, which indicate significant isotopic contrasts between the different facies of each pluton. The Seringa Granite forms a large batholith (Fig. 1c) that was not studied in all its extension. On the other hand, there are geochemical contrasts between the monzogranites and syenogranites facies of the Seringa and São João granites and there is a compositional gap between those varieties (Fig. 2 and 3). This indicates that these plutons are less homogeneous than those of the three suites and deserve more detailed studies in the future. In the The Gogó da Onça Granite, the initial Hf composition is very homogeneous in the biotite-hornblende granodiorite (-14.4 to -15.2) and shows large variation and attain more negative values in the hornblende-biotite syenogranite (-12.5 to -16.5). Except for the maximum value of -12.5, εHf values are superposed to those of Seringa and São João granites (Fig. 10d).

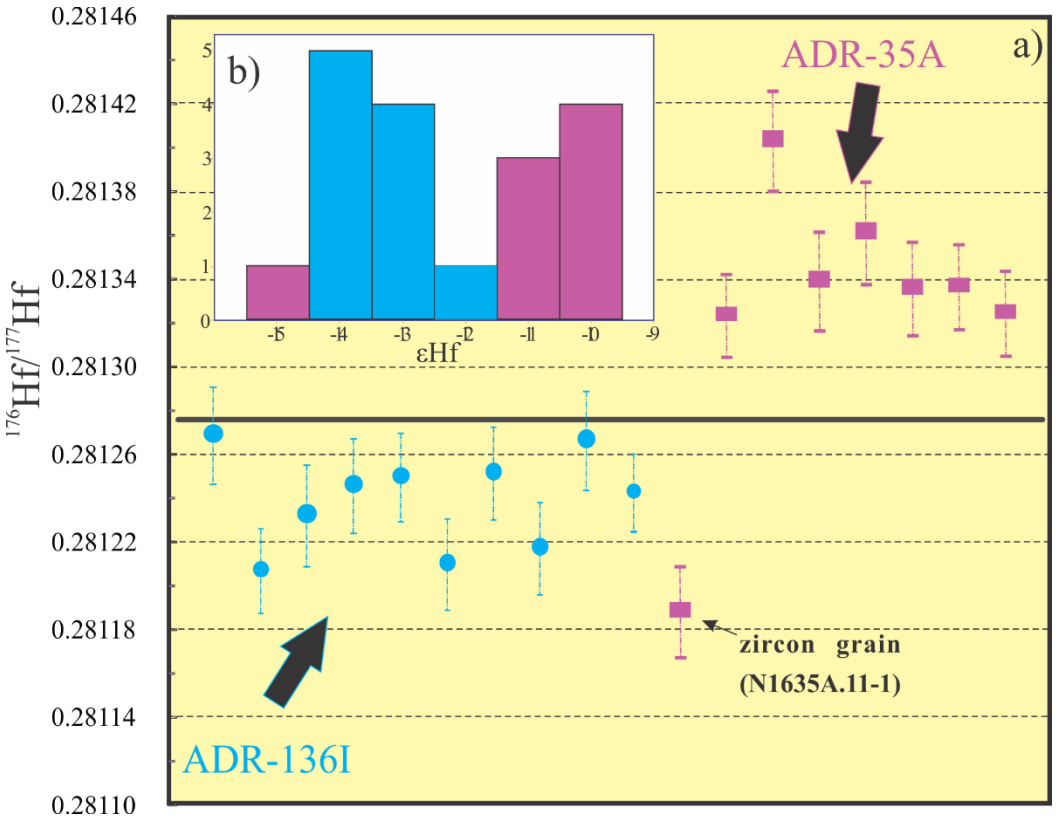

Fig. 13. a) Present-day $^{176}Hf/^{177}Hf$ composition for the Bannach Granite of the Jamon Suite; b) Histograms of the initial zircon Hf isotope compositions of the Bannach Granite. The anomalous zircon grain of the leucogranite (N1635A.11-1; See Supplementary Table 3) is indicated.

All these granites have oxygen isotopic composition generally varying from 5.50‰ to 7.00‰ but several analyzed samples display comparatively lower values between 2.50‰ and 4.87‰ with an isolated extremely higher value in a biotite monzogranite of the São João pluton (Fig. 15; Suppl. Table 5). Discarding these anomalous values, the total range in zircon $\delta^{18}O$ is of 1.1‰ in the plutons of the Serra dos Carajás Suite; 2.35‰ in the Velho Guilherme Suite; 2.20‰ in the Jamon Suite; 1.28‰ in the Seringa Granite; 1.25‰ in the São João; and 1.53‰ in the GGO. The average oxygen compositions in independent plutons vary between 5.62‰ and 6.80‰. The lower average values are found in the hornblende-biotite syenogranite (5.64‰) of the Antonio Vicente pluton and in the even-grained biotite monzogranite (5.62‰) and leucomonzogranite (5.86‰) of the Redenção pluton. The highest average values were registered in the albitized leucogranite of the Velho Guilherme pluton (6.78‰) and in the cumulate facies (6.80‰) of the Bannach pluton. The few zircon crystals that showed markedly lower $\delta^{18}O$ values do not represent the main zircon population of their respective samples and probably result of alteration processes.

It is widely accepted that magmatic zircons can preserve the igneous values of $\delta^{18}O$ even if submitted to subsequent high grade metamorphism and possibly also to magmatic assimilation or anatexis (Valley et al., 2003). On the other hand, intra-grain oxygen isotopic heterogeneities in zircon are common in granitic rocks (Kemp et al., 2007; Gagnevin et al., 2011), but we took care to not analyze areas close to microinclusions or fractures. We investigated some crystal zircons in more detail and almost all of them do not show significant $\delta^{18}O$ isotopic heterogeneities (Fig. 14 a, b, c), unless one zircon grain of the São João Granite (Fig. 14d) that presented very discordant ages and need more investigation (Teixeira et al., *submitted*). The $\delta^{18}O$ in the studied zircons exhibit a narrow range that looks consistent values retained from the magmatic stage. In addition, Dall'Agnol et al. (2005) obtained $\delta^{18}O$ values mostly ranging between 6.5 ‰ to 8.5 ‰ in whole-rock and quartz for the Serra dos Carajás, Velho Guilherme, and Jamon suites. Their results indicate higher values in whole rock than our $\delta^{18}O_{Zr}$ data, but, according to Valley et al. (2005), $\delta^{18}O$ values in whole rock tend to increase because other mineral in the rock have commonly higher $\delta^{18}O$ compared to zircon. Thus, we consider that the obtained $\delta^{18}O$ values truly reflect the composition of the magma source of these granites and are geologically meaningful.

Fractionation of O isotopes can occur during low temperature processes and, as a result, oxygen isotope data in magmatic rocks are highly sensitive to incorporation of supracrustal material and fluid alteration (Valley et al., 2005; Payne et al., 2016). In this context, the low $\delta^{18}O$ values (<5.00‰) in the Orosirian granites of Carajás may result of exchange between protoliths or magmas with contaminants or hydrothermal waters at high temperature. With regard to the leucogranite (R-05) of the Velho Guilheme Suite, zircons of that sample show zones with sieve texture indicating that the crystals were affected by intense hydrothermal processes which probably opened not only the oxygen isotopic system but also the U-Pb system (See Teixeira et al., *submitted*).

In the Redenção Granite of the Jamon Suite, the $\delta^{18}O$ values are lower in the even-grained biotite monzogranite and leucomonzogranite (average of, respectively, 5.62‰ and 5.86‰, and minimum values of 5.38‰ and 5.05‰) compared to the seriated leucomonzogranite facies (DC-120, average of 6.33‰ and range of 6.06‰ to 7.03‰). Oliveira et al. (2009) proposed that the leucogranites of the Redenção pluton should correspond to an independent intrusion of evolved magma and our oxygen results may corroborate with contrasts in the origin of different facies.

The variation in the couple Hf-O is illustrated in Figure 15, where are plotted the zircons in which both isotopes were analysed (Hf and Oxygen). It is evident that almost all studied zircon grains of the Paleoproterozoic granites have a very restrict ε_{Hf}, mostly between ca. -13.00 to -16.00, and $\delta^{18}O$ between ca. 5.50‰ and 7.00‰. The leucogranite facies (ADR-35A) of the Bannach pluton is an exception, as discussed before (Fig. 14). However, it is possible to observe subtle differences between these plutons. The plutons of the Velho Guilherme Suite are less negative in Hf and tend to have higher $\delta^{18}O$ compared to the other granites. The Seringa, São João, and Gogó da Onça granites present more variable values of Hf and lesser variation in $\delta^{18}O$ (Fig. 15). The leucogranite of the Jamon Suite (ADR-35A) has less negative ε_{Hf} and define a field distinct of all other granites.

The presence of older zircons (ca. 1900 to 1920 Ma) in the Velho Guilherme and Jamon suites, and in the Seringa pluton, was registered by Teixeira et al. (*submitted).* They interpreted these zircon grains as antecrysts from an earlier pulse of magma that were incorporated in the later 1880 Ma pulse. The Hf and oxygen isotopic compositions of these older zircons were analyzed but they do not show compositional contrasts with dominant 1880 Ma old zircons (Suppl. Tables 2, 3 and 4).

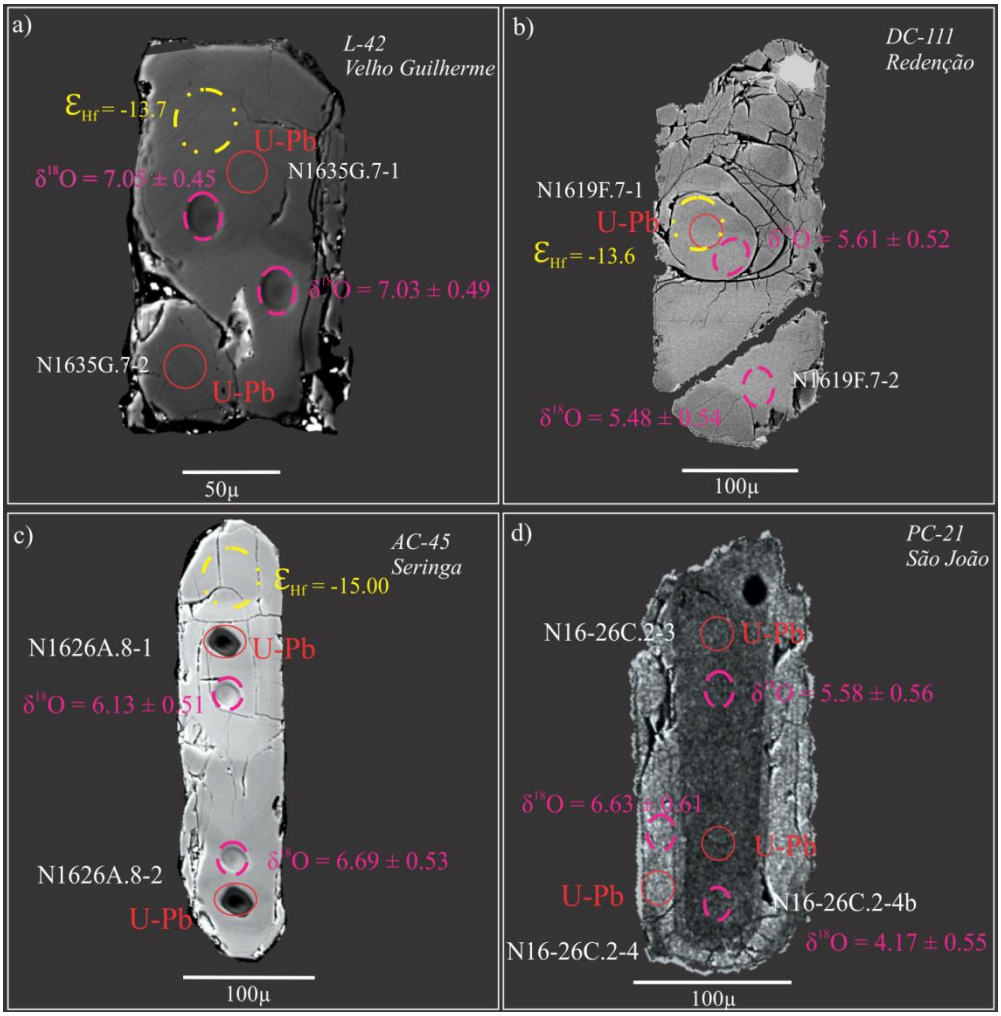

Fig. 14. Backscattered electron (BSE) images of representative zircons from the A-type Paleoproterozoic granites of the Carajás Province. Yellow circles indicate the location of LA–ICP-MS spots for Hf analysis, pink circles indicate the location of ion microprobe spots for oxygen analysis, and the red ellipse represents the location of the U–Pb SHRIMP analyses.

6.2 Model ages

The limitations of Hf model ages are discussed by several authors (Vervoort and Kemp et al., 2016; Payne et al., 2016; Nebel et al., 2007), that emphasize the fact that the $^{176}Lu/^{177}Hf$ ratio of continental crust is poorly constrained. Once the Lu/Hf ratio of zircon is not the same as the ratio in the crust from which the host melt was derived, it was proposed a two-stage Depleted Mantle (Crustal) model age T_{DM}^{c}, where in the first stage are used the measured $^{176}Hf/^{177}Hf$ (present-day), $^{176}Lu/^{177}Hf$, and U–Pb age of the zircon to calculate the $^{176}Hf/^{177}Hf$ ratio at the time of zircon crystallization. After defined the initial Hf isotope composition, in a second stage, it is needed to assume a $^{176}Lu/^{177}Hf$ value of the crustal source rock from which the zircon was derived to calculate the isotope evolution of the host rock to the point of intersection with the terrestrial reference. The main problem with this model ages is the uncertainty regarding

the appropriate value for the $^{176}Lu/^{177}Hf$ crustal composition (Payne et al., 2016; Roberts and Spencer, 2015; Chauvel et al., 2014; Dhuime et al., 2012). The calculated T_{DM}^{c} depends heavily on the choice of the $^{176}Lu/^{177}Hf$ ratio of the crust which can result in an uncertainty of a few hundred million years.

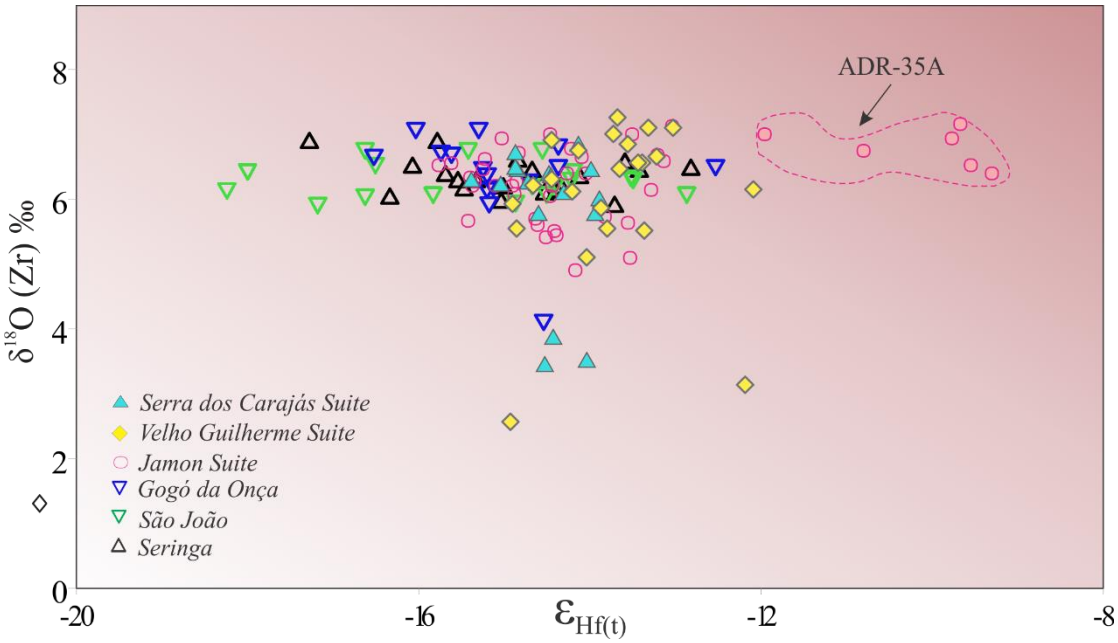

Fig. 15. ε_{Hf} vs $\delta^{18}O_{zr}$ of the A-type Paleoproterozoic granites of the Carajás Province.

In this work, the Hf-depleted mantle model age (Hf-t_{DM}) for the magmatic host rock was calculated using the measured $^{176}Lu/^{177}Hf$ referred to a model depleted mantle with a present-day $^{176}Hf/^{177}Hf = 0.28325$ (Griffin et al., 2000) and $^{176}Lu/^{177}Hf = 0.0388$ (Andersen et al., 2009). This model gives a minimum age for the source rock of the host magma (Kemp et al., 2007). However, Dall'Agnol et al. (1999a, b, 2005) presented evidence that the A-type anorogenic granite magmas of Carajás Province were derived from crustal sources. Hence, we have tried to adjust our initial model and more realistic "crustal" model ages (Hf-t_{DM}^{C}) were calculated.

Several $^{176}Lu/^{177}Hf$ ratios for the continental crust have been suggested: Goodge and Vervoort (2006) suggested a value of 0.0150 for a Proterozoic crust; Hawkesworth et al. (2010) obtained a value of 0.0159 on the basis of over 7000 measurements of granitoids; Condie et al. (2011) proposed a value of 0.020; Dhuime et al. (2011) suggested a model of a new crust (Hf-t_{NC}) based on the weighted average of modern island arcs worldwide; and, more recently, Chauvel et al. (2014) obtained a $^{176}Lu/^{177}Hf$ ratio of 0.0125 from loess deposits of several continents, assuming that Hf model ages cannot be younger than Nd model ages.

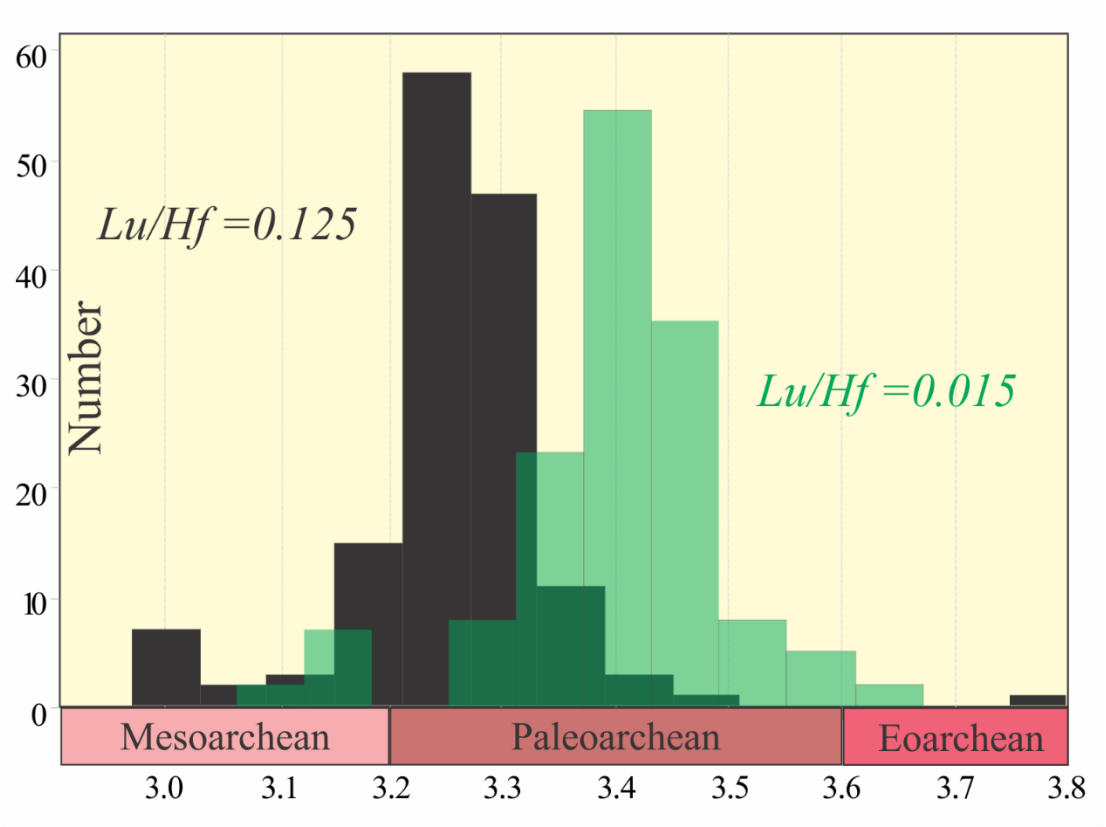

Fig. 16. Histograms of the t_{DM}^{C} of the samples of the Orisirian Granites of the Carajás Province.

Our approach in the attempt to constrain the age of the sources of the Orosirian granites of the Carajás Province was to use two different $^{176}Lu/^{177}Hf$ ratios (0.0150 of Goodge and Vervoort, 2006, and of 0.0125 of Chauvel et al., 2014) to estimate the age of the sources of the Paleoproterozoic magmatism of Carajás, and to evaluate possible differences between them.

The Hf-isotope crustal model ages adopted here are consistent with the derivation of these granites predominantly from the pre-existing crust. Independent of the values of the $^{176}Lu/^{177}Hf$ ratio, all of the studied plutons have t_{DM}^{C} that are similar and older and entirely distinct of their formation age. Adopting the $^{176}Lu/^{177}Hf$ ratio of 0.015 (Figure 16; Suppl. Tables 1 to 6), the analyzed granites have Paleoarchean sources with the mean peak between 3.4 Ga and 3.5 Ga, while, using the $^{176}Lu/^{177}Hf$ ratio of 0.0125, the crustal model ages are ca. 200 m.y younger mostly ranging between 3.2 Ga to 3.3 Ga. Independent of the adopted model, these ages are considerable older than those previously obtained by Nd isotopic data (3.0 Ga to 2.7 Ga).

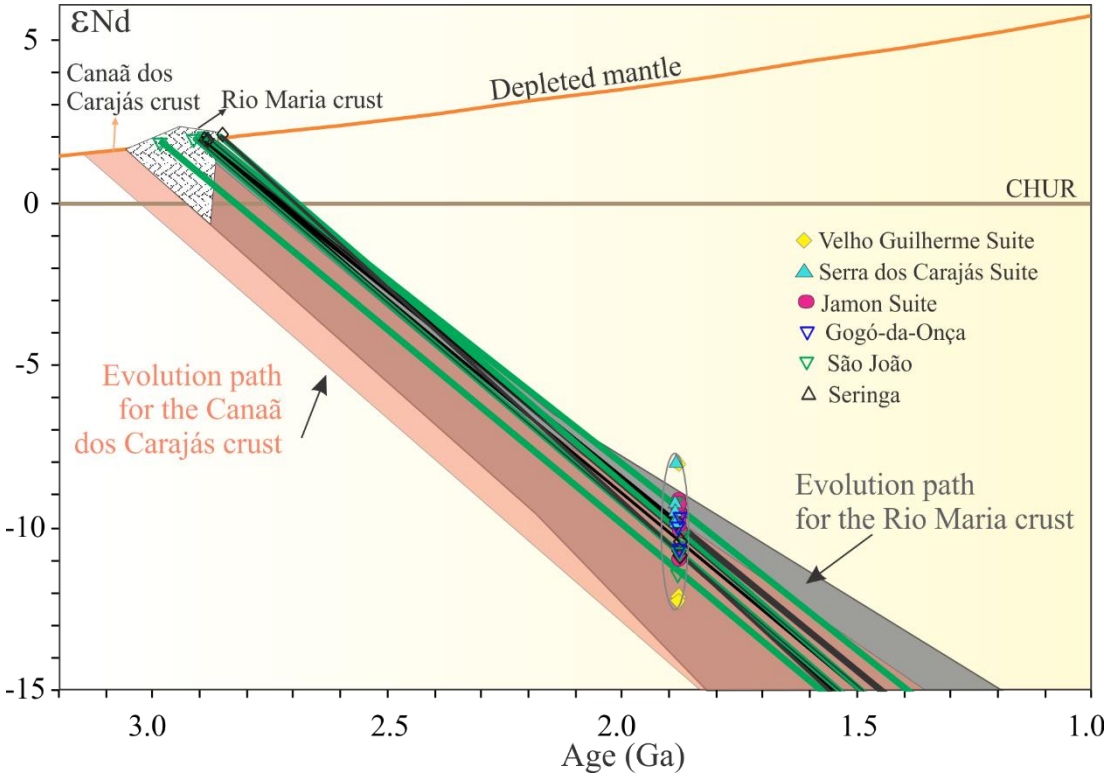

Fig. 17. εNd versus age diagram showing initial Nd isotopic composition of the Paleoproterozoic A-type granites of the Carajás Province. Fields of the Archean rocks of the Rio Maria (Rämö et al., 2002) and Canaã dos Carajás Domain (Feio et al., 2013) are also plotted for comparison. Note that the Canaã dos Carajás crust is oldest than Rio Maria crust.

Sm–Nd isotope data from whole rocks is used to calculated T_{DM} Nd ages. This is done in much the same way of Zircon Hf, but with one important difference: the T_{DM} Nd ages are calculated using a single-stage model. To illustrate this, in the Supplementary Tables 1 to 6 are given the Hf-t_{DM} ages obtained in a single-stage model for all the granites studied here, and the results are very similar to the Nd isotopic data. The εNd vs. age diagram is presented in Figure 17 and the Nd data in Supplementary Table 7.

The new data of Hf-tDMC suggests older ages than those of the Archean country rocks of these granites that vary between 2.7 Ga to 3.0 Ga. Martins et al. (2017) obtained Hf-tDMC from 3224 to 3345 Ma for the Neoarchean basalts (2745 Ma) of the Grão-Pará Group (Parauapebas Formation) of the Carajás Basin, north of the Carajás Province (Fig. 1). Those authors suggest that the basaltic rocks were derived from the subcontinental lithospheric mantle affected by upper continental crustal components. They used ratios $^{176}Lu/^{177}Hf = 0.015$ and obtained for those basalts crustal model ages that are Mesoarchean and similar to the data presented here for the sources of the

Paleoproterozoic A-type magmatism of Carajás (Fig. 18). This points to the existence of a possible older crust not exposed in the surface of the Carajás Province.

The Paleoproterozoic Era is marked by the presence of A-type rapakivi magmatism in numerous Archean cratons worldwide. Besides the Carajás Province, it is also found in the Tapajós-Parima Province of the Amazon Craton (Fig. 1a, b). In the southern part of the Guyana shield, it was described the Paleoproterozoic São Gabriel AMCG Association (1.88 Ga; Valério et al., 2018). Unlike the Carajás granites, Hf and Nd model ages indicate that the São Gabriel rocks were formed by mixing of crustal Archean (Mesoarchean to Neoarchean) and Paleoproterozoic components and small contribution of Rhyacian mantelic magmas (Valério et al., 2018).

1.7 Ga to 1.8 Ga A-type rapakivi granites derived from partial melting of crustal Archean sources (2.6–2.9 Ga) in post-orogenic extensional tectonic settings were also described in the North China Craton (NCC) (Fig. 18; Zhang et al., 2007; Zhao and Zhou 2009; Jiang et al., 2011). In the SE Tarim block, the 1.77 Ga Dunhuang A-type granites were described. They are similar to those of the NCC, occur in a similar tectonic setting, and are also derived of late Archean crustal source (Fig. 18; Sheng et al., 2014). Besides the fact that these granites were formed exclusively from Archean sources, they were formed under oxidizing conditions (Zhao and Zhou 2009) and in this aspect are similar to the plutons of the Jamon Suite (Dall'Agnol et al., 1999a, 2005).

6.3 Petrogenesis of the A-type anorogenic magmatism of the Carajás Province

A-type granites were first proposed by Loiselle and Wones (1979) to define a series of granitic rocks intruded in extensional tectonic environments such as anorogenic rift zones. Frost et al. (2001) classified the A-type granites as ferroan calc-alkaline to alkali-calcic or alkaline granitoids. However, a large number of magmatic processes including fractional crystallization of mantle-derived basaltic magmas, assimilation and fractional crystallization (AFC) processes, partial melting of mantle or crust and magma mixing between basaltic and crustal melts were proposed to explain the origin of these granites (Collins et al., 1982; Clemens et al., 1986; Whalen et al., 1987; Creaser et al., 1991; Frost and Frost, 1997; Bonin, 2007; Anderson and Bender, 1989; Dall'Agnol and Oliveira, 2007; Dall'Agnol et al., 2012).

Our data shows that all studied zircons have strongly negative epsilon Hf values (ca. -9 to -18), in agreement with strongly negative epsilon Nd values (Figure 19). Hf isotopes are generally more sensitive and produce more varying Hf isotope

compositions than Nd isotopes, though both methods demonstrate that these granites were generated from crustal sources.

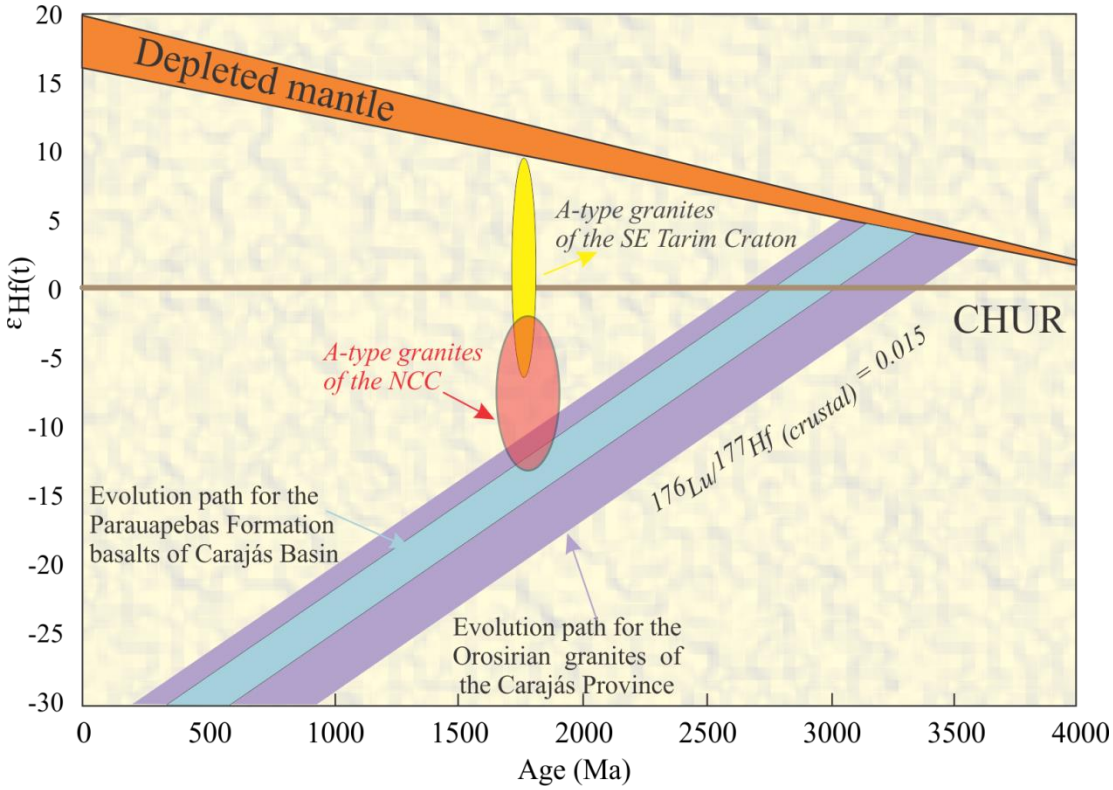

Fig. 18. εHf versus age diagram showing the evolution path of the Orosirian granites of the Carajás Province in comparison with the evolution path for the Parauapebas Formation basalts of the Carajás Basin (Martins et al., 2017), and with the Paleoproterozoic A-type granites of the North China Craton (Liu et al., 2007; Zhao and Zhou 2009; Jiang et al., 2011), and the Dunhuang A-type granite of the SE Tarim Craton (Sheng et al., 2014).

When combined, Hf and O isotope compositions indicate that the A-type Paleoproterozoic magmatism of the Carajás Province granites is derived from an ancient igneous crustal source (Fig. 20). The studied samples have Hf–O isotopic compositions that overlap within error, and evidence of contamination (crustal assimilation or mixing) of a mantle-derived magma cannot be seen.

Some samples of the Velho Guilherme and Jamon suites display oxygen isotope compositions that fall within the accepted range of mantle-like compositions (5.3 ± 0.3‰; Valley et al., 1998). However, this can be justified by the Archean source for these granites, because Archean zircons can have $\delta^{18}O$ values of 5.00‰ to 7.5‰ (Valley et al., 2005).

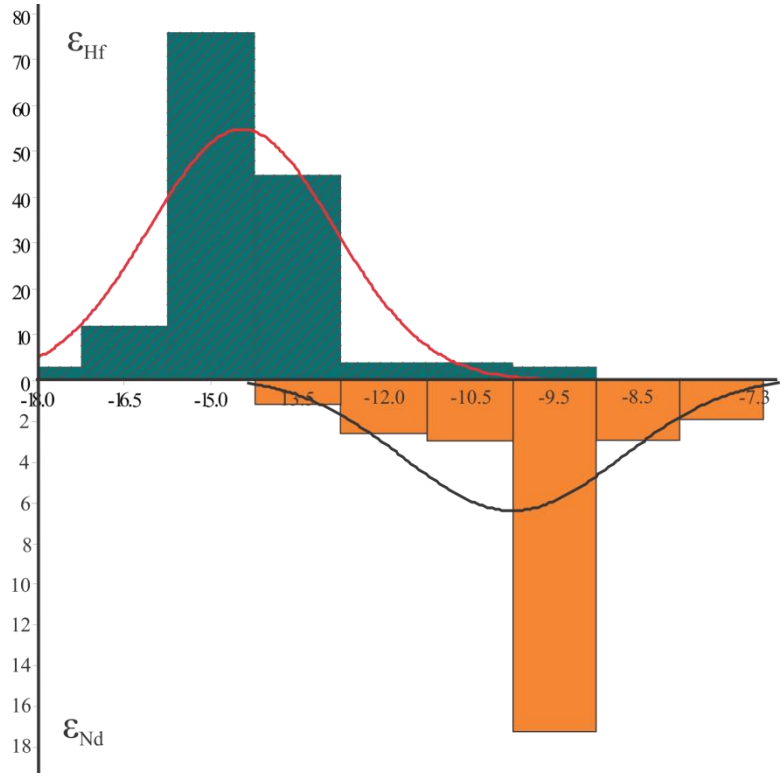

Fig. 19. Histogram of the initial εHf in zircon and whole-rock initial εNd of the Paleoproterozoic A-type granites of the Carajás Province.

The relatively homogenous and the restricted compositional range of the analyzed zircon suggests that magmatic mixing were not important in the generation of the plutons of the Orosirian granites. The Velho Guilherme Suite was derived from reduced magmas and is associated with greisen-type tin mineralization (Dall'Agnol et al., 2005; Teixeira et al., 2002). The leucogranite facies of the Antônio Vicente pluton and the albitized leucogranite of the Velho Guilherme Granite both have slightly more variable and high $\delta^{18}O$ values (up to 7.00‰) compared to the less evolved facies of the Antonio Vicente (R-10) and those of the others suites. This could imply supracrustal assimilation or influence of metasedimentary sources in the origin of that suite (Dall'Agnol et al., 2005). In the Jamon Suite, Hf composition is more variable, especially in the evolved leucogranites of Bannach and Redenção plutons, and sources with contrast in the degree of oxidation could be evolved in the generation of the mentioned leucogranites of that suite.

In spite of the general geochemical similarities between the Orosirian granites, contrasts in the oxygen fugacity and in the associated mineralization are indicative of small differences between the three anorogenic suites (Dall'Agnol et al., 2005). Some

differences are also indicated by the Hf and Oxygen data and they may result of partial melting of differing Archean crustal domains within the Carajás Province.

The Hf and O larger variation (Suppl. Table 4 and 5) shown by the biotite monzogranite of the São João pluton and the hornblende-biotite syenogranite facies of the Seringa pluton also indicates that slightly different Archean protoliths could be the sources of their magmas or that locally some supracrustal contamination has occurred. Teixeira et al. (2017) suggested that the different the facies of the Gogó da Onça Granite are possibly related by fractional crystallization. The isotope data obtained for two facies of this granite reveal a more homogenous Hf and O composition than observed in the Seringa and São João pluton and do not denote significantly heterogeneity in the source of the pluton.

Heinonen et al. (2012) proposed that small differences in Hf and Oxygen compositions observed in the Mucajaí anorthosite–monzonite–granite (AMG) complex (ca 1525 Ma) in Roraima (Brazil) northern of the Amazon Craton, may result either from a isotopically heterogeneous lower crustal source or, more likely, from contamination of the granitic magma derived from a lower crustal source during prolonged residence at upper crustal levels. This kind of contamination could also had occurred with the magmas of the Orosirian granites of Carajás because their evolution and emplacement processes are similar to those admitted for the AMCG associations, generating low pressure sheeted-like intrusions (Oliveira et al., 2008).

The Nd, Hf, and Oxygen isotope compositions of the rocks of Carajás Province clearly attest to the essential role of Archean crustal sources in the petrogenesis of the A-type magmatism of Carajás. Moreover, the new isotope data are compatible with the hypothesis that the A-type granites are derived from Archean quartz–feldspathic crustal sources with compositional variation. The Jamon Suite was considered to be derived from a sanukitoid igneous source under oxidizing conditions, whereas the reduced A-type granites of the Serra dos Carajás and Velho Guilherme suites could be derived from a quartz-feldspathic igneous source with a more reduced condition, or, possibly, with a contribution from metasedimentary rock (Dall'Agnol et al., 2005).

As discussed before, the Hf crustal model ages of the Orosirian granites are mostly Paleoarchean and suggest older sources than their Neoarchean to Mesoarchean country rocks (~2.7 Ga to 3.0 Ga). If the Hf model ages are assumed as true, this would imply that the A-type granites are derived of sources in the deep crust that are much older than the rocks exposed in surface. However, so far, there is no register of

Paleoarchean rocks in the Carajás Province and a deeper discussion and comparison about the sources evolved in the generation of these granites is limited at this point by the absence of Hf isotope composition of the A-type Paleoproterozoic granites country rocks. Nevertheless, the Hf crustal model ages of the Parauapebas Formation basalts in the Carajás Basin also attest for an older crust in the Carajás Province (Martins et al., 2017) and an inherited zircon with an age of of 3.2 Ga was identified in the Musa pluton (Machado et al., 1991).

Thus, the present data support conclusions based in previous geochemical and conventional isotope data, which suggest that the A-type Paleoproterozoic granites of Carajás Province were derived mostly from an Archaean quartz-feldspathic igneous source. The oxygen values are consistent with the interpretation that the zircons crystallized from a magma generated by melting of pre-existing igneous rocks possibly with a minor contribution from a supracrustal (metasedimentary) component.

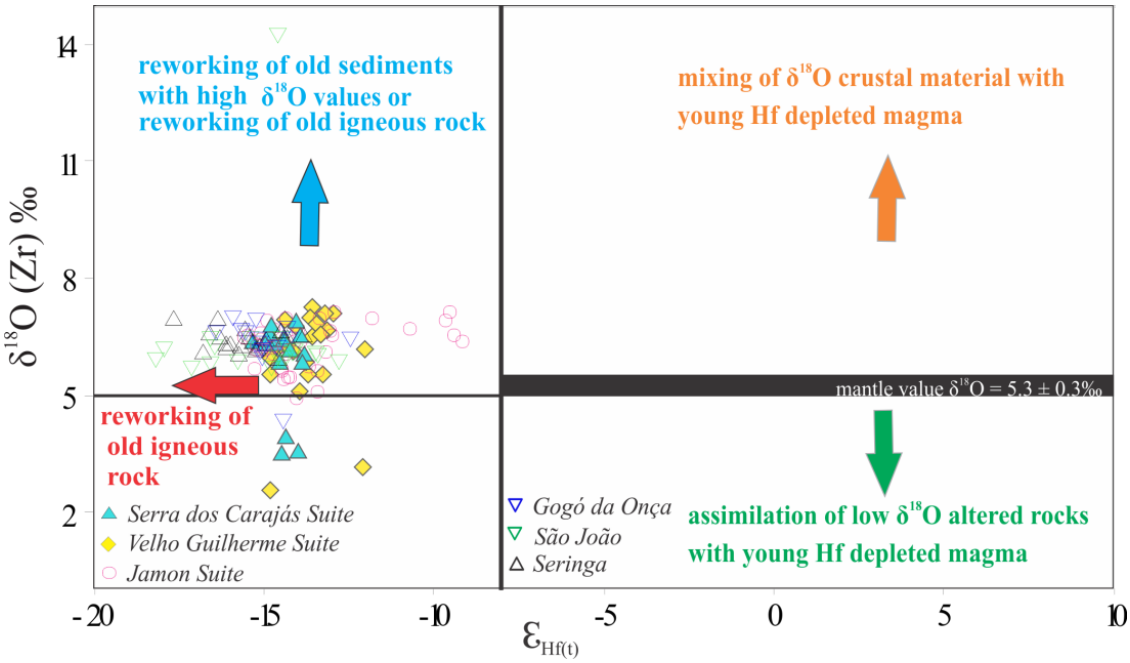

Fig. 20. Single zircons Hf(t) with $\delta^{18}O$ data from the A-type anorogenic granites of the Carajás Province.

6.4 Comparison with the Mesoproterozoic rapakivi A-type granites of Fennoscandia, Laurentia and Roraima State of Brazil

The Hf and oxygen values are consistent with the interpretation that the A-type granites of the Carajás Province were crystallized from a magma generated by melting of pre-existing igneous rocks with a minor contribution from a supracrustal (metasedimentary) component. Different from our studied granites, the Mesoproterozoic

anorthosite–mangerite–charnockite–rapakivi granite series (1650 to 1540 Ma) of Finland have initial Hf isotope compositions that vary from crustal values to depleted mantle and their origin is attributed to two distinct magma sources composed of a homogeneous Paleoproterozoic crustal component and a depleted mantle component (Heinonen et al., 2010).

In Laurentia, the Mesoproterozoic A-type granites of Central-Southwestern USA (~1.4 Ga) were emplaced within Proterozoic crust and three distinct groups of granites have been distinguished: ilmenite-series granite, magnetite-series granite, and two-mica granite (Anderson and Bender, 1989; Anderson and Morrison, 2005). The Hf isotope compositions of these granites indicate a dominantly crustal origin, although a mantle contribution is not discarded (Goodge and Vervoort, 2006). Goodge and Vervoort (2006) argue that the general similarity of their Hf isotope data suggest a high degree of uniformity in the Laurentian A-type magmas. In Carajás Province, we also observed a fair uniformity in the Hf data of the anorogenic granites which could imply a high degree of homogeneity of the Archean sources of their magmas.

The Mesoproterozoic AMG Mucajaí association of Roraima state of Brazil was derived from a Paleoproterozoic crustal source and show a more complex evolution (Fraga et al., 2009; Heinonen et al., 2012) than the Orosirian granites of Carajás Province. The AMG association is formed by anorthosite, mangerite, and different granite varieties and has a more diversified nature than the Carajás granites that have essentially granite composition. However, the behavior of Hf and O isotopes is also fairly uniform in Mucajaí (Heinonen et al., 2012).

7. Conclusions

All the A-type anorogenic granites of the Carajás Province have initial Hf and Oxygen isotope compositions fairly homogeneous, although small differences were observed internally in the plutons or between them. These differences can result for contrasts in the crustal domains of the Carajás Province that were the source of the granites or of local contamination processes.

The Hf and oxygen data are consistent with the interpretation that these plutons crystallized from magmas generated by melting of pre-existing igneous rocks with possibly in the Velho Guilherme Suite a minor contribution from a supracrustal (metasedimentary) component. The Hf crustal model ages indicate a Paleoarchean source with a minor contribution from Mesoarchean melts. The Hf model ages are older than the exposed Archean country rocks of the Orosirian granites of the Carajás Province and more investigation is needed to verify the real existence of that older Archean crust. Nevertheless, the Nd, Hf, and O isotope compositions of the Paleoproterozoic granites of Carajás Province clearly attest to an igneous ancient crustal source in the origin of their magmas.

ACKNOWLEDGEMENTS

We thank the colleagues of the Group of Granite Petrology (UFPA) for discussions. This study was conducted under a sandwich Ph.D. fellowship awarded by CAPES (Coordenação de Aperfeiçoamento de Pessoal de Nível Superior) in the context of the National Program of Strategic Areas (INCT-GEOCIAM; Bex 0201/16-2). Mineral images and compositional tests by EDS were performed at the Center for Microscopy, Characterization, and Analysis (CMCA) of the University of Western Australia. We are grateful to the CNPq (Conselho Nacional de Desenvolvimento Científico e Tecnológico) for doctoral thesis scholarship to MFBT, and research grant to R. Dall'Agnol (Proc. 306108/2014-3). This research received financial support of the INCT GEOCIAM (CNPq/FAPESPA/CAPES/PETROBRAS; Proc. 573733/2008-2) and of the Federal University of Pará (UFPA). This paper is a contribution to the Brazilian Institute of Amazonian Geosciences (INCT GEOCIAM).

REFERENCES

Almeida, J.A.C., Dall'Agnol, R., Oliveira, M.A., Macambira, M.J.B., Pimentel, M.M., Rämö, O.T., Guimarães, F.V., Leite, A.A.S., 2011. Zircon geochronology and geochemistry of the TTG suites of the Rio Maria granite-greenstone terrane: Implications for the growth of the Archean crust of Carajás Province, Brazil. Precambrian Research 187, 201-221.

Almeida, J.A.C., Dall'Agnol, R., Oliveira, D.C., 2006. Geologia, petrografia e geoquímica do granito anorogênico Bannach, Terreno granito-greenstone de Rio Maria, Pará. Revista Brasileira de Geociências 36, 282-295.

Anderson, J.L., Bender, E.E., 1989. Nature and origin of Proterozoic A-type granitic magmatism in the southwestern United States. Lithos 23, 19–52.

Anderson, J.L., Morrison, J., 2005. Ilmenite, magnetite, and peraluminous Mesoproterozoic anorogenic granites of Laurentia and Baltica. Lithos 80, 45–60.

Andersen, T., Andersson, U.B., Graham, S., Åberg, G., Simonsen, S.L., 2009. Granitic magmatism by melting of juvenile continental crust: new constraints on the source of Paleoproterozoic granitoids in Fennoscandia from Hf isotopes in zircon. Journal of the Geological Society of London 166, 233–247.

Andersen, T., Griffin, W. L., Jackson, S. E., Knudsen, T.-L., Pearson, N. J., 2004. Mid-Proterozoic magmatic arc evolution at the southwest margin of the Baltic Shield. Lithos 73, 289-318.

Barros, C.E.M., Dall'Agnol, R., Vieira, E.A.P., Magalhães, M.S., 1995. Granito Central da Serra dos Carajás: avaliação do potencial metalogenético para estanho com base em estudos da borda oeste do corpo. Boletim do Museu Paraense Emílio Goeldi. Série Ciências da Terra 7, 93–123 (in Portuguese).

Baertschi, P., 1976. Absolute ^{18}O content of standard mean ocean water. Earth Planet. Sci. Lett. 31, 341-344.

Bettencourt, J.S., Tosdal, R.M., Leite Júnior, W.B., Payolla, B.L., 1999. Mesoproterozoic rapakivi granites of the Rondonia Tin Province, southwestern border of the Amazon craton, Brazil - I. Reconnaissance U-Pb geochronology and regional implications. Precambrian Research 95, 41- 67.

Bettencourt, J.S., Juliani., Xavier, R.P., Monteiro, L.V.S., Neto, A.C.B., Klein, E.L., Assis, R.R., Leite-Jr, W.P., Moreto, C.P.N., Fernandes, C.M.D., Pereira, V.P., 2016. Metallogenetic systems associated with granitoid magmatism in the Amazon Craton: An overview of the present level of understanding and exploration significance. Journal of South American Earth Sciences 68, 22 - 49.

Bonin, B., 2007. A-type granites and related rocks: evolution of a concept, problems and prospects. Lithos 97 (1–2), 1–2.

Bouvier, A., Vervoort, J.D., and Patchett, P.J., 2008, The Lu-Hf and Sm-Nd isotopic composition of CHUR: Constraints from unequilibrated chondrites and implications for the bulk composition of terrestrial planets. Earth and Planetary Science Letters 273, 48–57. doi: 10.1016/j.epsl.2008.06.010.

Carvalho, T. A. Petrografia, Geoquímica e Suscetibilidade Magnética da Porção Leste do Granito Gradaús, Província Carajás, SE do Pará. Dissertação de Mestrado, Universidade Federal do Pará, Belém.

Chu, N.-C., Taylor, R., Chavagnac, V., Nesbitt, R., Boella, R., Milton, J., German, C., Bayon, G., Burton, K., 2002. Hf isotope ratio analysis using multi-collector inductivelycoupled plasma mass spectrometry: An evaluation of isoba-ric interference corrections. Journal of Analytic Atomic Spectrometry 17, 1567–1574.

Chauvel, C., Garçon, M., Bureau, S., Besnault, A., Jahn, B., Ding, Z., Constraints from loess on the Hf–Nd isotopic composition of the upper continental crust. Earth and Planetary Science Letters 388, 48-58.

Clemens, J.D., Holloway, J.R., White, A.J.R., 1986. Origin of an A-type granite: experimental constraints. Americqn Mineralogist 71, 317–324.

Collins, W.J., Beams, S.D., White, A.J.R., Chappell, B.W., 1982. Nature and origin of A-type granites with particular reference to southeastern Australia. Contributions to Mineralogy and Petrology 80, 189–200.

Condie, K.C., Bickford, M.E., Aster, R.C., Belousova, E., Scholl, D.W., 2011. Episodic zircon ages, Hf isotopic composition, and the preservation rate of continental crust. Geological Society of America Bulletin 123 (5–6), 951–957.

Cordani, U.G., Teixeira, W., D'Agrella-Filho, M.S., Trindade, R.I., 2009. The position of the Amazonian Craton in supercontinents. Gondwana Research 15, 396–407.

Creaser, R.A., Price, R.C., Wormald, R.J., 1991. A-type granites revisited: assessment of a residual-source model. Geology 19, 163–166.

Cunha, I.R.V., Dall'Agnol, R., Feio, G.R.L., 2016. Mineral chemistry and magnetic petrology of the Archean Planalto Suite, Carajás Province – Amazonian Craton: implications for the evolution of ferroan Archean granites. Journal of South American Earth Sciences 67, 100–121.

Dall'Agnol, R., Teixeira, N.P., Magalhães, M.S., 1993. Diagnostic features of the Tin-specialized anorogenic granites of the Eastern Amazonian region. Anais da Academia Brasileira de Ciências 65 (Suppl. 1), 33-50.

Dall'Agnol, R., Lafon, J.M., Macambira, M.J.B., 1994. Proterozoic anorogenic magmatism in the Central Amazonian Province: geochronological, petrological and geochemical aspects. Mineralogy and Petrology 50, 113–138.

Dall'Agnol, R., Rämö, O.T., Magalhães, M.S., Macambira, M.J.B., 1999a. Petrology of the anorogenic, oxidised Jamon and Musa granites, Amazonian Craton: implications for the genesis of Proterozoic A-type granites. Lithos 46, 431–462.

Dall'Agnol, R., Scaillet, B., Pichavant, M., 1999b. An experimental study of a lower Proterozoic A-type granite from the eastern Amazonian craton, Brazil. Journal of Petrology 40, 1673–1698.

Dall'Agnol, R., Teixeira, N.P., Rämö, O.T., Moura, C.A.V., Macambira, M.J.B., Oliveira, D.C., 2005. Petrogenesis of the Paleoproterozoic, rapakivi, A-Type granites of the Archean Carajás Metallogenic Province, Brazil. Lithos 80, 101–129.

Dall'Agnol, R., Oliveira, D.C., 2007. Oxidized, magnetite-series, rapakivi-type granites of Carajás, Brazil: implications for classification and petrogenesis of A-type granites. Lithos 93, 215 - 233.

Dall'Agnol, R., Frost, C.D., Rämö, O.T., 2012. IGCP Project 510 "A-type granites and related rocks through time": project vita, results, and contribution to granite research. Lithos 151, 1–16.

Dall'Agnol, R., Oliveira, D.C., Guimarães, F.V., Gabriel, E.O., Feio, G.R.L., Lamarão, C.N., Althoff, F.J., Santos, P.A., Teixeira, M.F.B., Silva, A.C., Rodrigues, D.S., Santos, M.J.P., Silva, C.R.P., Santos, R.D., Santos, P.J.L., 2013. Geologia do Subdomínio de Transição do Domínio Carajás – Implicações para a evolução arqueana da Província Carajás - Pará. SBG, Simpósio de Geologia da Amazônia 13. CD-ROM, Anais, Belém (in Portuguese).

Dall'Agnol, R., Cunha, I.R.V., Guimarães, F.V., Oliveira, D.C., Teixeira, F.B.T., Feio, G.R., Lamarão, C.N., 2017. Mineralogy, geochemistry, and petrology of Neoarchean ferroan to magnesian granites of Carajás Province, Amazonian Craton: The origin of hydrated granites associated with charnockites. Lithos 277, 3 - 32.

DePaolo, D.J., 1981. A neodymium and strontium isotopic study of the Mesozoic calc-alkaline granitic batholiths of the Sierra Nevada and Peninsular Ranges, California. Journal of Geophysical Research: Solid Earth 86, 10470–10488.

Dhuime, B., Hawkesworth, C.J., Cawood, P., 2011. When continents formed. Science 331, 154–155.

Dhuime, B., Hawkesworth, C.J., Cawood, P.A., Storey, C.D., 2012. A change in the geodynamics of continental growth 3 billion years ago. Science 335, 1334–1336.

Eby, G.N., 1992. Chemical subdivision of the A-type granitoids: petrogenesis and tectonic implications. Geology 20, 641–644.

Emslie, R. F. 1978. Anorthosite massifs, rapakivi granites, and late Proterozoic rifting in North America. Precambrian Research 7, 61-98.

Feio, G.R.L., Dall'Agnol, R., 2012. Geochemistry and petrogenesis of the Mesoarchean granites from the Canaã dos Carajás Area, Carajás Province, Brazil: implications for the origin of Archean granites. Lithos 154, 33–52.

Feio, G.R.L., Dall'Agnol, R., Dantas, E., Macambira, M.J.B., Gomes, A.C.B., Sardinha, A.S., Santos, P., 2012. Geochemistry, geochronology, and origin of the Planalto granite suite and associated rocks: implications for the Neoarchean evolution of the Carajás Province. Lithos 151, 57–73.

Feio, G.R.L., Dall'Agnol, R., Dantas, E.L., Macambira, M.J.B., Santos, J.O.S., Althoff, F.J., Soares, J.E.B., 2013. Archean granitoid magmatism in the Canaã dos Carajás area: implications for crustal evolution of the Carajás province, Amazonian craton, Brazil. Precambrian Research 227, 157–185.

Frost, B.R., Barnes, C.G., Collins, W.J., Arculus, R.J., Ellis, D.J, Frost, C.D., 2001. A geochemical classification for granitic rocks. Journal of Petrology 42, 2033–2048.

Frost, C.D., Frost, B.R., 1997. Reduced rapakivi type granites: the tholeiitic connection. Geology 25, 647–650.

Gabriel, E.O., Oliveira, D.C., 2014. Geologia, petrografia e geoquímica dos granitoides arqueanos de alto magnésio da região de Água Azul do Norte, porção sul do Domínio Carajás, Pará. Boletim do Museu Paraense Emílio Goeldi, Ciências Naturais 9 (3), 533–564 (in Portuguese).

Gastal, M.C.P., 1987. Mapeamento e petrologia do maciço granítico Musa. Rio Maria, Sudeste do Pará. Unpublished M.Sc. Thesis, Univ. Federal do Pará, Belem.

Ganevin, D., Daly, J.S., Horstwood, M.S.A., Whitehouse, M.J., 2011. In-situ zircon U–Pb, oxygen and hafnium isotopic evidence for magma mixing and mantle metasomatism in the Tuscan Magmatic Province, Italy. Earth and Planetary Science Letters 305, 45–56.

Gioia, S.M.C.L., Pimentel M.M. 2000. The Sm-Nd isotopic method in the geochronology laboratory of the University of Brasília. Anais da Academia Brasileira de Ciências 72, 220-245. doi:10.1590/S0001-37652000000200009.

Goodge, J.W., Vervoort, J.D., 2006. Origin of Mesoproterozoic A-type granites in Laurentia: Hf isotope evidence. Earth and Planetary Science Letters 243, 711-731.

Griffin, W.L., Wang, X., Jackson, S.E., Pearson, N.J., O'Reilly, S.Y., Xu, X., Zhou, X., 2002. Zircon chemistry and magma mixing, SE China: In-situ analysis of Hf isotopes, Tonglu and Pingtan igneous complexes. Lithos 61 (3–4), 237–269.

Haapala, I., Rämö,O.T. Frindt, S., 2005. Comparison of Proterozoic and Phanerozoic rift-related basaltic–granitic magmatism. Lithos 80, 1–32.

Hawkesworth, C.J., Kemp, A.I.S., 2006. Using hafnium and oxygen isotopes in zircons to unravel the record of crustal evolution. Chemical Geology 226, 144–162.

Hawkesworth, C.J., Dhuime, B., Pietranik, A.B., Cawood, P.A., Kemp, A.I.S., Storey, C.D., 2010. The generation and evolution of the continental crust. Journal of the Geological Society 167 (2), 229–248.

Heinonen, A., Andersen, T., Rämö, O.T., 2010. Re-evaluation of rapakivi petrogenesis: Source constraints from the Hf isotope composition of zircon in the rapakivi granites and associated mafic rocks of southern Finland. Journal of Petrology 51, 1687–1709.

Heinonen, A., Fraga, L., Rämö, O.T., Dall'Agnol, R., Mänttäri, I., Andersen, T. 2012. Petrogenesis of the igneous Mucajaí AMG complex, northern Amazonian craton: Geochemical, U–Pb geochronological, and Nd–Hf–O isotopic constraints. Lithos 151, 17–34

Iizuka, T., Hirata, T., 2005. Improvements of precision and accuracy in in situ Hf isotope microanalysis of zircon using the laser ablation-MC-ICPMS technique. Chemical Geology 220, 121–137.

Javier Rios, F., Villas, R.N., Dall'Agnol, R., 1995. O Granito Serra dos Carajás: fácies petrográficas e avaliação do potencial metalogenético para estanho no setor norte. Revista Brasileira de Geociências 25, 20–31 (in Portuguese).

Jiang, N., Guo, J.H., Zhai, M.G., 2011. Nature and origin of the Wenquan granite: Implications for the provenance of Proterozoic A-type granites in the North China craton. Journal of Asian Earth Sciences 42, 76–82.

Johansson, A., Waight, T., Andersen, T., Simonsen, S.L., 2016. Geochemistry and petrogenesis of Mesoproterozoic A-type granitoids from the Danish island of Bornholm, southern Fennoscandia. Lithos 244, 94-108.

Kemp, A.I.S., Hawkesworth, C.J., 2007. Magmatic and crustal differentiation history of granitic rocks from Hf–O isotopes in zircon. Science 315, 980–983.

Kemp, A.I.S., Hawkesworth, C.J., Collins, W.J., Gray, C.M., Blevin, P.L., 2009. Isotopic evidence for rapid continental growth in an extensional accretionary orogen: the Tasmanides, eastern Australia. Earth and Planetary Science Letters 284, 455–466.

Kita, N.T., Ushikubo, T., Fu, B., Valley, J.W. 2009. High precision SIMS oxygen isotope analysis and the effect of sample topography. Chemical Geology 246, 43 - 57

Lamarão, C.N., Pinho, S.C.C., Paiva Junior, A.L., Galarza-Toro, M.A., 2012. Mineralogy and geochemistry of the Paleoproterozoic, tin mineralized Bom Jardim Granite of the Velho Guilherme Suite, eastern Amazonian Craton. Journal of South American Earth Sciences, 38:159-173.

Lima, P.H.A., Lamarão, C.N., Santo, M.J.P., 2014 Petrografia, geoquímica e suscetibilidade magnética do Granito Paleoproterozóico São João, sudeste do Cráton Amazônico, Província Carajás. Boletim do Museu Paraense Emílio Goeldi 9, 47-72 (in Portuguese).

Loiselle, M.C., Wones, D.R., 1979. Characteristics and origin of anorogenic granites. Abstracts with programs-Geological Society of America 11, 468.

Lugmair, G.W., Harti, K., 1978. Lunar initial 143Nd/144Nd: differential evolution of the lunar crust and mantle. Earth and Planetary Science Letters 39, 349-357

Machado, N., Lindenmayer, Z., Krogh, T.E., Lindenmayer, D., 1991. U-Pb geochronology of Archean magmatism and basement reactivation in the Carajás area, Amazon Shield, Brazil. Precambrian Research 49, 329–354.

Martins, P.L.G., Toledo, C.L.B., Silva, A.M., Chemale Jr, F., Santos, J.O.S., Assis, L.M., 2017. Neoarchean magmatism in the southeastern Amazonian Craton, Brazil: Petrography, geochemistry and tectonic significance of basalts from the Carajás Basin. Precambrian Research 302, 340-357.

Mesquita, C.J., Dall'Agnol, R., Almeida, J.A.C., 2018. Mineral chemistry and crystallization parameters of the A-type Paleoproterozoic Bannach Granite, Carajás Province – Pará. Brazillian Journal of Geology (in press).

Moreto, C.P.N., Monteiro, L.V.S., Xavier, R.P., Creaser, R.A., DuFrane, S.A., Melo, G.H.C., Silva, M.A.D., Tassinari, C.C.G., Sato, K., 2015. Timing of multiple hydrothermal events in the iron oxide-copper-gold deposits of the Southern Copper Belt, Carajás Province, Brazil. Mineralium Deposita 50, 517-546.

Nebel, O., Nebel-Jacobsen, Y., Mezger, K., Berndt, J., 2007. Initial Hf isotope compositions in magmatic zircon from early Proterozoic rocks from the Gawler Craton, Australia: A test for zircon model ages. Chemical Geology, 23–37.

Oliveira, D.C., Dall'Agnol, R., Silva, J.B.C., Almeida, J.A.C., 2008. Gravimetric, radiometric, and magnetic susceptibility study of the Paleoproterozoic Redenção and Bannach plutons: implications for architecture and zoning of A-type granites. Journal of South American Earth Sciences 25, 100–115.

Oliveira, D.C., Dall'Agnol, R., Barros, C.E.M., Oliveira, M.A., 2009. Geology, geochemistry and magmatic evolution of the Paleoproterozoic, anorogenic oxidized A-type Redenção granite of the Jamon Suite, eastern Amazon Craton, Brazil. Canadian Mineralogist 47 (6), 1441–1468.

Oliveira, D.C., Neves, S.P., Trindade, R.I.F., Dall'Agnol, R., Mariano, G., Correia, P.B., 2010. Magnetic anisotropy of the Redenção granite, eastern Amazonian craton (Brazil): Implications for the emplacement of A-type plutons. Tectonophysics 493, 27 - 41.

Oliveira, D.C., Santos, P.J.L., Gabriel, E.O., Rodrigues, D.S., Faresin, A.C., Silva, M.L.T., Sousa, S.D., Santos, R.V., Silva, A.C., Souza, M.C., Santos, R.D.,

Macambira, M.J.B., 2010. Aspectos geológicos e geocronológicos das rochas magmáticas e metamórficas da região entre os municípios de Água Azul do Norte e Canaã dos Carajás – Província Mineral de Carajás. Congresso Brasileiro de Geologia 45. CDrom, Belém. (in Portuguese).

Oliveira, E.C., Lafon, J.M., Gioia, S.M.C.L., Pimentel, M.M. 2008. Datação Sm-Nd em rocha total e granada do metamorfismo granulítico da região de Tartarugal Grande, Amapá Central. Revista Brasileira Geociências, 38:116–129 (in Portuguese).

Paiva Júnior, A.L., Lamarão, C.N., Lima, P.H.A., 2011. Geologia, Petrografia e Geoquímica do Batólito Seringa, Província Carajás, SSE do Pará. Revista Brasileira de Geociências, 41(2):185-202 (in Portuguese).

Payne, J.L., McInerney, D.J., Barovich, K.M., Kirkland, C.L., Pearson, N.J., Hand. N., 2016. Strengths and limitations of zircon Lu-Hf and O isotopes in modelling crustal growth. Lithos 248-251: 175-192.

Patchett, J., Kouvo, O., Hedge, C., Tatsumoto, M., 1981. Evolution of continental crust and mantle heterogeneity: evidence from Hf isotopes. Contributions to Mineralogy and Petrology 78, 279–297.

Rämö, O.T., Dall'Agnol, R., Macambira, M.J.B., Leite, A.A.S., Oliveira, D.C., 2002. 1.88 Ga oxidized A-type granites of the Rio Maria region, eastern Amazonian craton, Brazil: positively anorogenic! Journal of Geology 110, 603-610.

Rämö, O.T., Haapala, I., 1995. One hundred years of rapakivi granite. Mineralalogy and Petrology 52, 129–185.

Rämö, O.T., Haapala, I., 2005. Rapakivi granites. In: Lehtinen, M., Nurmi, P. A. & Raamo, O. T. (eds) Precambrian Geology of FinlandçKey to the Evolution of the Fennoscandian Shield.Amsterdam: Elsevier, pp. 533-562.

Roberts, N.M.W., Spencer, C.J., 2015. The zircon archive of continent formation through time. Geological Society, London, Special Publications 389, 197–225

Rodrigues, D.S., Oliveira, D.C., Macambira, M.J.B., 2014. Geologia, geoquímica e geocronologia do Granito Mesoarqueano Boa Sorte, município de Água Azul do Norte, Pará – Província Carajás. Boletim do Museu Paraense Emílio Goeldi. Série Ciências da Terra 9 pp. 597–633 (in Portuguese).

Rogers, J.J.W., Santosh, M., 2002. Configuration of Columbia, a Mesoproterozoic supercontinent. Gondwana Research 5, 5–22.

Rogers, J.J.W., Santosh, M., 2009. Tectonics and surface effects of the supercontinent Columbia. Gondwana Research 15, 373–380.

Santos, J.O.S., Hartmann, L.A., Gaudette, H.E., Groves, D.I., McNaugthon, N.J., Fletcher, I.R., 2000. New understanting of the Provinces of Amazon Craton based on Integration of Field Mapping and U-Pb and Sm-Nd geochronology. Gondwana Research 3 (4), 453 - 488.

Santos, J.O.S., Van Breemen, O.B., Groves, D.I., Hartmann L.A., Almeida M.E., Mcnaughton N.J., Fletcher I.R., 2004. Timing and evolution of multiple Paleoproterozoic magmatic arcs in the Tapajós Domain, Amazon Craton: constraints from SHRIMP and TIMS zircon, baddeleyite and titanite U-Pb geochronology. Precambrian Research 131,73-109.

Santos, P.A., Teixeira, M.F.B., Dall'Agnol, R., Guimarães, F.V., 2013. Geologia, petrografia e geoquímica da associação Tonalito-Trondhjemito-Granodiorito (TTG) do extremo leste do Subdomínio de Transição, Província Carajás, Pará. Boletim do Museu Paraense Emílio Goeldi. Ciências Naturais 8 (3), 257- 290 (in Portuguese).

Santos, R.D., Galarza, M.A., Oliveira, D.C., 2013. Geologia, geoquímica e geocronologia do Diopsídio-Norito Pium, Província Carajás. Boletim do Museu Paraense Emílio Goeldi, Série Ciências da Terra 8, 355–382 (in Portuguese).

Segal, I., Halicz, L., Platzner, I.T., 2003. Accurate isotope ratio measurements of ytterbium by multi-collector inductively coupled plasma mass spectrometry applying erbium and hafnium in an improved double external normalization procedure. Journal of Analytical Atomic Spectrometry 18, 1217-1223.

Sheng, Y.Y., Zhang, J-X., Zhao, X.L., Gong, J.H., Li, Y.S., 2014. Geochronology, geochemistry and petrogenesis of the late Palaeoproterozoic A-type granites from the Dunhuang block, SE Tarim Craton, China: implications for the break-up of the Columbia supercontinent. Geol. Mag. 151, 629–648.

Silva, A.C., Dall'Agnol, R., Guimarães, F.V., Oliveira, D.C., 2014. Geologia, petrografia e geoquímica de Associações Tonalíticas e Trondhjemíticas Arqueanas de Vila Jussara, Província Carajás, Pará. Boletim do Museu Paraense Emílio Goeldi. Série Ciências Naturais 9, 13 - 45 (in Portuguese).

Söderlund, U., Patchett, P.J., Vervoort, J.D., Isachsen, C.E., 2004, The ^{176}Lu decay constant determined by Lu–Hf and U–Pb isotope systematics of Precambrian mafic intrusions: Earth and Planetary Science Letters 219, 311–324

Tallarico, F.H.B., Figueiredo, B.R., Groves, D.I., Kositcin, N., McNaughton, N.J., Fletcher, I.R., Rego, J.L., 2005. Geology and SHRIMP U-Pb geochronology of the Igarape Bahia deposit, Carajás copper - gold belt, Brazil: an Archean (2.57 Ga) example of iron-oxide Cu-Au-(U-REE) mineralization. Economic Geology 100, 7-28.

Tassinari, C.C.G., Macambira, M.J.B., 1999. Geochronological provinces of the Amazonian craton. Episodes 22, 174–182.

Tassinari, C.C.G., Macambira, M.J.B., 2004. A evolução tectônica do cráton Amazônico. In: Matesso-Neto, V., Bartorelli, A., Carneiro, C.D.R., Britto- Neves, B.B. (Eds.), Geologia do Continente Sul-Americano. São Paulo, SP, Brazil, pp. 471-485. (in Portuguese).

Teixeira, M.F.B., Dall'Agnol, R., Santos, J.O.S., Oliveira, D.C., Lamarão, C.N., McNaughton, N.J., Crystallization ages of Paleoproterozoic A-type Granite Suites and Related Granites of Carajás Province, Amazon Craton: constraints from U-Pb geochronology of zircon and titanite.

Teixeira, M.F.B., Dall'Agnol, R., Silva, A.C., Santos, P.A., 2013. Geologia, petrografia e geoquímica do Leucogranodiorito Pantanal e dos leucogranitos arqueanos da área de Sapucaia, Província Carajás, PA: implicações petrogenéticas. Boletim do Museu Paraense Emílio Goeldi, Série Ciências Naturais 8, 291–323 (in Portuguese).

Teixeira, M.F.B., Dall'Agnol, R., Santos, J.O.S., Sousa, L.A.M., Lafon, J-M., 2017. Geochemistry, geochronology and Nd isotopes of the Gogó da Onça Granite: A new Paleoproterozoic A-type granite of Carajás Province, Brazil. Journal of South American Earth Sciences 80, 47–65.

Teixeira N.P., 1999. Contribuição ao estudo das rochas granitóides e mineralizações associadas da Suíte Intrusiva Velho Guilherme, Província Estanífera do Sul do Pará. São Paulo University. Dr. Thesis. Institute of Geosciences, 508 pp. (in Portuguese).

Teixeira, N.P., Bettencourt, J.S., Moura, C.A.V., Dall'Agnol, R., Macambira, E.M.B., 2002. Archean crustal sources for Paleoproterozoic tin-mineralized granites in the Carajás Province, SSE Pará, Brazil: Pb–Pb geochronology and Nd isotope geochemistry. Precambrian Research 119, 257–275.

Teixeira, W., Hamilton, M.A., Girardi, V.A.V., Faleiros, F.M., Ernst, R.E. 2018. U-Pb baddeleyite ages of key dyke swarms in the Amazonian Craton (Carajás/ Rio Maria and Rio Apas areas): Tectoninc implications for events at 1880 Ma, 1110 Ma, 235 Ma and 200 Ma. Precambrian Research (in Press).

Valério, C.S., Macambira, M.J.B., Souza, V.S., Dantas, E.L., Nardi, L.V.S., 2018. 1.88 Ga São Gabriel AMCG association in the southernmost Uatumã-Anauá Domain: Petrological implications for post-collisional A-type magmatism in the Amazonian Craton. Lithos (300-301), 291-313.

Valley, J.W. 2003. Oxygen isotopes in zircon. In: Hanchar, J.M., Hoskin, P.W.O. (eds) Zircon. Mineralogical Society of America and Geochemical Society, Reviews in Mineralogy and Geochemistry 53, 343–385.

Valley, J.W., Lackey, J.S., Cavosie, A.J., Clechenko, C.C., Spicuzza, M.J., Basei, M.A.S., Bindeman, I.N., Ferreira, V.P., Sial, A.N., King, E.M., Peck, W.H., Sinha, A.K., Wei, C.S., 2005. 4.4 billion years of crustal maturation: oxygen isotope ratios of magmatic zircon. Contributions to Mineralogy and Petrology 150, 561–580

Valley, J.W., Chiarenzelli, J.R., McLelland, J.M. 1994. Oxygen isotope geochemistry of zircon. Earth and Planetary Science Letters 126, 187–206.

Valley, J.W., Kinny, P.D., Schulze, D.J., Spicuzza, M.J. 1998. Zircon megacrysts from kimberlite: Oxygen isotope heterogeneity among mantle melts. Contributions to Mineralogy and Petrology 133, 1–11.

Vander Auwera, J., Berza, Tudor., Gesels, J., Dupont, Alain., 2015. The Late Cretaceous igneous rocks of Romania (Apuseni Mountains and Banat): the possible role of amphibole versus plagioclase deep fractionation in two different crustal terranes. International Journal of Earth Sciences 105, 849-817.

Vasquez, M.L., Macambira M.J.B., Armstrong R.A. 2008. Zircon geochronology of granitoids from the western Bacajá domain, southeastern Amazonian craton, Brazil: Neoarchean to Orosirian evolution. Precambrian Research 161, 279-302.

Vervoort, J.D., Kemp, A.I., 2016. Clarifying the zircon Hf isotope record of crust–mantle evolution. Chemical Geology 425, 65–75.

Vervoort, J.D., Patchett, P.J., Soderlund, U., Baker, M., 2004. Isotopic composition of Yb and the determination of Lu concentrations and Lu/Hf ratios by isotope dilution using MCICPMS. Geochem. Geophys. Geosystem, 5 (11).

Wang, C.Y., Campbell, I.H., Stepanov, A.S., Allen, C.M., Burtsev, I.N., 2011. Growth rate of the preserved continental crust: II. Constraints from Hf and O isotopes in detrital zircons from Greater Russian Rivers . Geochimica et Cosmochimica Acta 75, 1308 – 1345.

Whalen, J.B., Currie, K.L., Chappell, B.W., 1987. A-type granite: geochemical characteristics, discrimination and petrogenesis. Contributions to Mineralogy and Petrology 95, 407–419.

Woodhead, J., Hergt, j., Shelley, M., Eggins, S., Kemp, R., 2004. Zircon Hf-isotope analysis with an excimer laser, depth profiling, ablation of complex geometries and concomitant age estimation. Chem Geol 209, 121–135.

Zhang, S.H., Liu, S.W., Zhao, Y., Yang, J.H., Song, B., Liu, X.M., 2007. The 1.75–1.68 Ga anorthosite– mangerite–alkali granitoid-rapakivi granite suite from the northern North China Craton: magmatism related to a Paleoproterozoic orogen. Precambrian Research 155, 287–312.

Zhao, T.P., Zhou, M.F., 2009. Geochemical constraints on the tectonic setting of Paleoproterozoic A-type granites in the southern margin of the North China Craton. Journal of Asian Earth Sciences 36, 183-195.

Supplementary Table 1. Hf and isotope analyses on zircon of the granites of the Serra dos Carajás Suite

	U/Pb							Sample Initial Ratios			Model Ages (Ga)				
Sample	Age (Ma)	$^{176}Yb/^{177}Hf$	± 2 σ	$^{176}Lu/^{17}7Hf$	± 2 σ	$^{176}Hf/^{177}Hf$ (t)	± 2 σ	$^{176}Hf/^{177}Hf$ (t)	Hf(t)	± 2 σ	T DM	$t_{DM\ a}^{C}$	$t_{DM\ b}^{C}$	$\delta^{18}O$	± 2 σ
ECR-SC-01. Serra dos Carajás - biotite-hornblende syenogranite															
N1619D.8-1	1882	0.035174	0.001273	0.001067	0.000040	0.281198	0.000018	0.281160	-15.0	0.6	2.84	3.44	3.29	6.21	0.52
N1619D.7-2	1882	0.018242	0.000085	0.000600	0.000004	0.281199	0.000020	0.281177	-14.4	0.1	2.80	3.40	3.26	3.81	0.48
N1619D.6-2	1882	0.019479	0.000255	0.000642	0.000005	0.281197	0.000016	0.281174	-14.5	0.1	2.81	3.41	3.27	3.38	0.54
N1619D.2-1	1882	0.016864	0.000363	0.000544	0.000007	0.281196	0.000018	0.281176	-14.5	0.2	2.80	3.40	3.26	6.32	0.51
N1619D.1-2	1882	0.014668	0.000147	0.000498	0.000003	0.281198	0.000017	0.281180	-14.3	0.1	2.79	3.40	3.25	6.06	0.49
N1619D.1-1	1882	0.020618	0.000816	0.000656	0.000024	0.281188	0.000019	0.281165	-14.9	0.5	2.82	3.43	3.28	6.68	0.54
N1619D.7-1	1882	na	na	na	na	na	na	na	na	na	na	na	na	6.38	0.52
N1619D.3-1	na	na	na	na	na	na	na	na	na	na	na	na	na	6.10	0.50
ECR-CG-14A. Cigano granite - biotite-hornblende monzogranite															
N1619E.11-1	1884	0.024766	0.000995	0.000778	0.000023	0.281191	0.000019	0.281163	-14.9	0.4	2.82	3.43	3.29	6.46	0.54
N1619E.9-1	1884	0.036388	0.002439	0.001128	0.000062	0.281212	0.000019	0.281171	-14.6	0.8	2.82	3.41	3.27	5.73	0.52
N1619E.8-1	1884	0.018616	0.000271	0.000598	0.000003	0.281211	0.000018	0.281189	-13.9	0.1	2.79	3.37	3.23	5.74	0.48
N1619E.7-3	na	0.015101	0.000062	0.000496	0.000002	0.281206	0.000018	0.281188	-14.0	0.1	2.78	3.38	3.24	6.44	0.52
N1619E.7-2	1884	0.041756	0.001063	0.001312	0.000038	0.281238	0.000020	0.281191	-13.9	0.4	2.80	3.37	3.23	5.95	0.52
N1619E.7-1	1884	0.019806	0.001577	0.000632	0.000041	0.281207	0.000018	0.281184	-14.1	0.9	2.79	3.39	3.25	6.80	0.52
N1619E.3-1	1884	0.011459	0.000869	0.000394	0.000025	0.281201	0.000016	0.281187	-14.0	0.9	2.78	3.38	3.24	3.44	0.50
N1619E.5-1	na	na	na	na	na	na	na	na	na	na	na	na	na	5.93	0.54
N1619E.5-2	na	na	na	na	na	na	na	na	na	na	na	na	na	5.98	0.53
N1619E.5-3	na	na	na	na	na	na	na	na	na	na	na	na	na	6.79	0.48
CIG-1 Cigano granite - biotite monzogranite															
N1620D.3-1	1883	0.076903	0.002900	0.002404	0.000070	0.281236	0.000022	0.281150	-15.38	0.45	2.89	3.46	3.31	6.25	0.55
N1620D.2-2	1883	0.075874	0.002361	0.002372	0.000077	0.281253	0.000026	0.281168	-14.74	0.48	2.86	3.42	3.28	6.23	0.53
N1620D.2-1-4	1883	0.090668	0.004072	0.002703	0.000143	0.281272	0.000026	0.281175	-14.47	0.77	2.86	3.41	3.26	6.35	0.53
N1620D.1-1	1883	0.086661	0.003278	0.002702	0.000112	0.281261	0.000027	0.281165	-14.85	0.62	2.87	3.43	3.28	6.41	0.52
N1620D.7-1	1883	na	na	na	na	na	na	na	na	na	na	na	na	6.10	0.54
N1620D.1-2	na	na	na	na	na	na	na	na	na	na	na	na	na	6.80	0.57
N1620D.2-3	na	na	na	na	na	na	na	na	na	na	na	na	na	6.53	0.57
N1620D.4-1	na	na	na	na	na	na	na	na	na	na	na	na	na	5.70	0.56
N1620D.4-2	na	na	na	na	na	na	na	na	na	na	na	na	na	6.32	0.56

Supplementary Table 2. Hf and Oxygen isotope analyses on zircon of the granites of the Velho Ghilherme Suite

	U/Pb							Sample Initial Ratios			Model Ages (Ga)				
Sample	Age (Ma)	$^{176}Yb/^{177}Hf$	± 2 σ	$^{176}Lu/^{17}7Hf$	± 2 σ	$^{176}Hf/^{177}Hf$ (t)	± 2 σ	$^{176}Hf/^{177}Hf$ (t)	Hf(t)	± 2 σ	T DM	$t_{DM\ a}^{C}$	$t_{DM\ b}^{C}$	$\delta^{18}O$	± 2 σ
L-42 - Velho Guilherme - albitized leucogranite															
N1635G.2-1	1882	0.030037	0.001413	0.000915	0.000033	0.281237	0.000021	0.281205	-13.5	0.5	2.77	3.34	3.21	6.58	0.45
N1635G.2-2	1882	0.026623	0.000474	0.000845	0.000013	0.281236	0.000020	0.281206	-13.4	0.2	2.77	3.34	3.20	6.58	0.47
N1635G.5-1	1882	0.024942	0.000621	0.000784	0.000017	0.281229	0.000018	0.281201	-13.6	0.3	2.77	3.35	3.21	6.86	0.49
N1635G.5-2	1882	0.023533	0.001022	0.000733	0.000035	0.281225	0.000019	0.281198	-13.7	0.7	2.78	3.36	3.22	6.50	0.45
N1635G.7-1 (core)	1882	na	na	na	na	na	na	na	na	na	na	na	na	7.05	0.48
N1635G.7-2 (rim)	1882	0.021586	0.000466	0.000695	0.000012	0.281221	0.000030	0.281196	-13.8	0.2	2.78	3.36	3.22	7.03	0.49
N1635G.7-3	1882	0.019457	0.000225	0.000611	0.000003	0.281232	0.000019	0.281211	-13.2	0.1	2.76	3.33	3.19	6.68	0.47
N1635G.7-4	na	0.033915	0.001266	0.001053	0.000037	0.281246	0.000021	0.281208	-13.3	0.5	2.77	3.33	3.20	7.14	0.48
N1635G.7-5	1882	0.026420	0.000483	0.000812	0.000017	0.281245	0.000021	0.281216	-13.0	0.3	2.75	3.32	3.18	7.13	0.47
N1635G.8-1	1882	0.026618	0.001873	0.000812	0.000047	0.281214	0.000022	0.281185	-14.2	0.8	2.80	3.39	3.24	6.77	0.48
N1635G.1-2	na	na	na	na	na	na	na	na	na	na	na	na	na	6.26	0.53
N1635G.4-1	na	na	na	na	na	na	na	na	na	na	na	na	na	6.86	0.48
N1635G.4-2	na	na	na	na	na	na	na	na	na	na	na	na	na	6.53	0.48
N1635G.5-3	na	na	na	na	na	na	na	na	na	na	na	na	na	6.76	0.49
N1635G.5-4	na	na	na	na	na	na	na	na	na	na	na	na	na	6.87	0.47
N1635G.6-1	na	na	na	na	na	na	na	na	na	na	na	na	na	6.93	0.48
R-5 - Antônio Vicente - leucogranite															
N1635F.6-1	1724	0.036013	0.002513	0.001195	0.000099	0.281384	0.000041	0.281345	-12.1	1.0	2.59	3.14	3.00	6.17	0.49
N1635F.4-2	na	0.026010	0.001931	0.000786	0.000068	0.281204	0.000027	0.281176	-14.5	1.2	2.81	3.40	3.26	6.32	0.49
N1635F.4-1	1724	0.025642	0.001295	0.000784	0.000020	0.281368	0.000026	0.281342	-12.2	0.3	2.59	3.14	3.01	3.14	0.48
N1635F.3-1	1882	0.019471	0.000308	0.000598	0.000003	0.281197	0.000018	0.281176	-14.5	0.1	2.80	3.41	3.26	6.95	0.48
N1635F.2-4	1724	0.037358	0.000270	0.001087	0.000009	0.281336	0.000019	0.281300	-13.7	0.1	2.65	3.23	3.09	7.35	0.48
N1635F.2-3	1882	0.063467	0.003505	0.001816	0.000104	0.281235	0.000026	0.281170	-14.7	0.8	2.84	3.42	3.27	6.24	0.48
N1635F.1-1	1882	0.023330	0.001532	0.000673	0.000037	0.281187	0.000018	0.281162	-14.9	0.8	2.82	3.43	3.29	2.58	0.48
N1635F.2-2	1724	na	na	na	na	na	na	na	na	na	na	na	na	7.28	0.47
N1635F.4-4	na	na	na	na	na	na	na	na	na	na	na	na	na	5.77	0.47
N1635F.6-2	1724	na	na	na	na	na	na	na	na	na	na	na	na	5.00	0.50
N1635F.4-3	na	na	na	na	na	na	na	na	na	na	na	na	na	7.20	0.47

Supplementary Table 2. (continued)

	U/Pb					Sample Initial Ratios					Model Ages (Ga)				
Sample	Age (Ma)	$^{176}Yb/^{177}Hf$	± 2 σ	$^{176}Lu/^{17}7Hf$	± 2 σ	$^{176}Hf/^{177}Hf$ (t)	± 2 σ	$^{176}Hf/^{177}Hf$ (t)	Hf(t)	± 2 σ	T DM	$t_{DM\ a}^{C}$	$t_{DM\ b}^{C}$	$\delta^{18}O$	± 2 σ
R-10 - Antônio Vicente - hornblende-biotite syenogranite															
N1634A.8-1	1873	0.029285	0.003038	0.000859	0.000077	0.281201	0.000021	0.281170	-14.9	1.3	2.82	3.42	3.28	5.57	0.66
N1634A.6-5	1873	0.013982	0.000102	0.000439	0.000004	0.281214	0.000020	0.281198	-13.9	0.1	2.77	3.36	3.22	5.89	0.62
N1634A.6-4	1900	0.027640	0.000824	0.000826	0.000022	0.281201	0.000021	0.281171	-14.2	0.4	2.81	3.40	3.26	6.15	0.61
N1634A.6-3	1873	0.066170	0.002651	0.001921	0.000080	0.281237	0.000020	0.281169	-14.9	0.6	2.85	3.43	3.28	5.96	0.63
N1634A.6-2	1900	0.024127	0.001797	0.000700	0.000052	0.281208	0.000018	0.281183	-13.8	1.0	2.80	3.38	3.24	5.57	0.62
N1634A.6-1	1873	0.051649	0.000904	0.001510	0.000033	0.281266	0.000024	0.281212	-13.4	0.3	2.78	3.33	3.19	5.54	0.71
N1634A.4-1	1873	0.033296	0.000880	0.000974	0.000022	0.281228	0.000020	0.281193	-14.1	0.3	2.79	3.37	3.23	5.11	0.69
n16_34a_3.1	1873	0.028707	0.000503	0.000872	0.000015	0.281207	0.000020	0.281176	-14.7	0.3	2.81	3.41	3.27	na	na
N1634A.2-2	1873	0.011083	0.000119	0.000355	0.000004	0.281188	0.000019	0.281176	-14.7	0.2	2.80	3.41	3.27	na	na
N1634A.2-1	1873	0.028040	0.000378	0.000917	0.000037	0.281230	0.000016	0.281197	-13.9	0.6	2.78	3.36	3.22	na	na
N1634A.5-1	na	na	na	na	na	na	na	na	na	na	na	na	na	5.74	0.67
N1634A.5-2	na	na	na	na	na	na	na	na	na	na	na	na	na	5.83	0.66
N1634A.5-3	na	na	na	na	na	na	na	na	na	na	na	na	na	5.52	0.65
N1634A.6-6	na	na	na	na	na	na	na	na	na	na	na	na	na	5.49	0.66
N1634A.8-2	na	na	na	na	na	na	na	na	na	na	na	na	na	5.34	0.66
N1634A.8-3	na	na	na	na	na	na	na	na	na	na	na	na	na	5.54	0.71
N1634A.9-1	na	na	na	na	na	na	na	na	na	na	na	na	na	5.72	0.64
N1634A.9-2	na	na	na	na	na	na	na	na	na	na	na	na	na	5.55	0.62

Supplementary Table 3. Hf and Oxygen isotope analyses on zircon of the granites of the Jamon Suite

	U/Pb					Sample Initial Ratios					Model Ages (Ga)				
Sample	Age (Ma)	$^{176}Yb/^{177}Hf$	± 2 σ	$^{176}Lu/^{177}Hf$	± 2 σ	$^{176}Hf/^{177}Hf$ (t)	± 2 σ	$^{176}Hf/^{177}Hf$ (t)	Hf(t)	± 2 σ	T DM	$t_{DM\ a}^{C}$	$t_{DM\ b}^{C}$	$\delta^{18}O$	± 2 σ
CREMU-37A. Musa granite - biotite monzogranite															
N1620E.7-1	1876	0.015905	0.003162	0.000535	0.000086	0.281217	0.000021	0.281198	-13.8	2.2	2.77	3.36	3.22	5.71	0.59
N1620E.4-1	1876	0.013331	0.000553	0.000502	0.000017	0.281171	0.000018	0.281153	-15.4	0.5	2.83	3.46	3.31	5.64	0.57
N1620E.3-1	1876	0.027283	0.001301	0.000895	0.000032	0.281187	0.000019	0.281156	-15.3	0.6	2.84	3.45	3.31	6.24	0.53
N1620E.2-1	1876	0.022099	0.001243	0.000748	0.000033	0.281207	0.000017	0.281181	-14.4	0.6	2.80	3.40	3.26	6.16	0.54
N1620E.1-2	1876	0.029967	0.002291	0.000998	0.000073	0.281222	0.000018	0.281186	-14.3	1.0	2.80	3.39	3.25	6.37	0.56
N1620E.1-1	1876	na	na	na	na	na	na	na	na	na	na	na	na	6.42	0.59
N1620E.7-2	na	na	na	na	na	na	na	na	na	na	na	na	na	6.42	0.60
N1620E.1-3	na	na	na	na	na	na	na	na	na	na	na	na	na	6.57	0.55
N1620E.4-1	na	na	na	na	na	na	na	na	na	na	na	na	na	5.64	0.57
N1620E.7-1	na	na	na	na	na	na	na	na	na	na	na	na	na	5.71	0.59
N1620E.8-1	na	na	na	na	na	na	na	na	na	na	na	na	na	6.81	0.52
KM-77A. Musa granite - hornblende-biotite monzogranite															
N1620H.7-1	na	0.090804	0.002396	0.002850	0.000068	0.281252	0.000022	0.281151	-15.4	0.4	2.90	3.46	3.31	6.16	0.58
1620H.5-4	1882	0.025992	0.000366	0.000914	0.000016	0.281187	0.000018	0.281155	-15.2	0.3	2.84	3.45	3.30	6.44	0.56
1620H.5-3	1882	0.022254	0.000837	0.000779	0.000022	0.281194	0.000019	0.281166	-14.8	0.4	2.82	3.43	3.28	6.67	0.54
1620H.5-1	1882	0.025676	0.000175	0.000920	0.000002	0.281193	0.000017	0.281160	-15.0	0.0	2.83	3.44	3.29	6.90	0.57
N1620H.3-3	1882	0.021243	0.000218	0.000737	0.000007	0.281198	0.000015	0.281172	-14.6	0.1	2.81	3.41	3.27	5.67	0.60
N1620H.3-2	1882	0.021984	0.000581	0.000790	0.000013	0.281183	0.000019	0.281155	-15.2	0.3	2.84	3.45	3.30	6.57	0.56
N1620H.3-1	1882	na	na	na	na	na	na	na	na	na	na	na	na	5.88	0.63
1620H.5-2	1882	na	na	na	na	na	na	na	na	na	na	na	na	6.31	0.52
N1620H.2-1	1882	na	na	na	na	na	na	na	na	na	na	na	na	5.67	0.53
N1620H.1-1	na	na	na	na	na	na	na	na	na	na	na	na	na	6.26	0.52
KM-144. Musa granite - biotite-hornblende monzogranite															
N1620B.1-1	1871	na	na	na	na	na	na	na	na	na	na	na	na	6.50	0.57
N1620B.1-2	1871	na	na	na	na	na	na	na	na	na	na	na	na	5.78	0.53
N1620B.2-1	1871	na	na	na	na	na	na	na	na	na	na	na	na	6.88	0.58
N1620B.2-2	1871	na	na	na	na	na	na	na	na	na	na	na	na	3.10	0.57
N1620B.7-1	1871	na	na	na	na	na	na	na	na	na	na	na	na	5.53	0.55
N1620B.8-1	1871	na	na	na	na	na	na	na	na	na	na	na	na	6.13	0.55
N1620B.11-1	1871	na	na	na	na	na	na	na	na	na	na	na	na	7.25	0.54
N1620B.5-1	na	na	na	na	na	na	na	na	na	na	na	na	na	6.46	0.63
N1620B.5-2	na	na	na	na	na	na	na	na	na	na	na	na	na	6.29	0.55
N1620B.7-2	na	na	na	na	na	na	na	na	na	na	na	na	na	6.07	0.56
N1620B.9-1	na	na	na	na	na	na	na	na	na	na	na	na	na	3.35	0.56
N1620B.10-1	na	na	na	na	na	na	na	na	na	na	na	na	na	6.49	0.63

Supplementary Table 3. (continued)

	U/Pb							Sample Initial Ratios			Model Ages (Ga)				
Sample	Age (Ma)	$^{176}Yb/^{177}Hf$	± 2 σ	$^{176}Lu/^{17}7Hf$	± 2 σ	$^{176}Hf/^{177}Hf$ (t)	± 2 σ	$^{176}Hf/^{177}Hf$ (t)	Hf(t)	±2SE	T DM	$t_{DM\ a}^{C}$	$t_{DM\ b}^{C}$	$\delta^{18}O$	± 2 σ
DC-111. Redenção - even-grained biotite monzogranite															
N1619F.8-1	1867	0.024390	0.000180	0.000824	0.000002	0.281214	0.000018	0.281184	-14.5	0.0	2.80	3.40	3.25	5.38	0.52
N1619F.7-1 (core)	1890	0.023212	0.000294	0.000785	0.000005	0.281225	0.000017	0.281197	-13.6	0.1	2.78	3.35	3.22	5.61	0.52
N1619F.7-2 (rim)	1890													5.48	0.54
N1619F.6-1	na	0.030322	0.002575	0.000979	0.000073	0.281217	0.000018	0.281182	-14.6	1.1	2.80	3.40	3.26	5.57	0.51
N1619F.5-1	1890	0.023004	0.000335	0.000771	0.000006	0.281208	0.000017	0.281180	-14.1	0.1	2.80	3.39	3.25	4.87	0.60
N1619F.2-1	1867	0.041286	0.003438	0.001335	0.000098	0.281235	0.000017	0.281188	-14.4	1.1	2.81	3.39	3.25	5.46	0.52
N1619F.1-1	1867	0.026665	0.000241	0.000882	0.000010	0.281219	0.000017	0.281188	-14.4	0.2	2.79	3.39	3.25	5.41	0.49
N1619F.9-1	1867	na	na	na	na	na	na	na	na	na	na	na	na	5.80	0.52
N1619F.1-2	na	na	na	na	na	na	na	na	na	na	na	na	na	5.48	0.54
N1619F.5-2	na	na	na	na	na	na	na	na	na	na	na	na	na	5.45	0.54
N1619F.6-2	na	na	na	na	na	na	na	na	na	na	na	na	na	6.22	0.55
N1619F.7-3	na	na	na	na	na	na	na	na	na	na	na	na	na	5.90	0.52
DC-120. Redenção - seriate leucomonzogranite															
N1635E.4-1	1865	0.052907	0.000684	0.001541	0.000023	0.281231	0.000020	0.281176	-14.9	0.2	2.83	3.42	3.27	6.06	0.49
N1635E.3-2	1865	0.042316	0.002953	0.001205	0.000077	0.281219	0.000019	0.281176	-14.9	1.0	2.82	3.42	3.27	6.23	0.47
N1635E.3-1-3	1865	0.024014	0.001576	0.000704	0.000036	0.281200	0.000017	0.281175	-14.9	0.8	2.81	3.42	3.27	6.18	0.48
1635E.2-2	1865	0.014598	0.000148	0.000428	0.000008	0.281214	0.000015	0.281199	-14.0	0.2	2.77	3.37	3.22	6.34	0.48
1635E.2-1-5	1865	0.037314	0.003574	0.001090	0.000088	0.281190	0.000018	0.281151	-15.7	1.3	2.85	3.47	3.32	6.48	0.47
1635E.1-2	1865	0.025863	0.000632	0.000777	0.000012	0.281197	0.000018	0.281169	-15.1	0.2	2.82	3.43	3.28	6.17	0.49
1635E.1-1	1865	0.039748	0.003256	0.001148	0.000081	0.281196	0.000017	0.281155	-15.6	1.1	2.85	3.46	3.31	6.51	0.47
N1635E.1-3	na	na	na	na	na	na	na	na	na	na	na	na	na	6.31	0.45
N1635E.1-4	na	na	na	na	na	na	na	na	na	na	na	na	na	6.31	0.48
N1635E.1-5	na	na	na	na	na	na	na	na	na	na	na	na	na	6.47	0.48
N1635E.1-6	na	na	na	na	na	na	na	na	na	na	na	na	na	6.16	0.45
N1635E.3-3	na	na	na	na	na	na	na	na	na	na	na	na	na	6.58	0.47
N1635E.2-3	na	na	na	na	na	na	na	na	na	na	na	na	na	6.20	0.49
N1635E.5-1	na	na	na	na	na	na	na	na	na	na	na	na	na	6.16	0.46
N1635E.5-2	na	na	na	na	na	na	na	na	na	na	na	na	na	7.03	0.46
N1635E.5-3	na	na	na	na	na	na	na	na	na	na	na	na	na	6.34	0.48

Supplementary Table 3. (continued)

	U/Pb					Sample Initial Ratios					Model Ages (Ga)				
Sample	Age (Ma)	$^{176}Yb/^{177}Hf$	± 2 σ	$^{176}Lu/^{17}7Hf$	± 2 σ	$^{176}Hf/^{177}Hf$ (t)	± 2 σ	$^{176}Hf/^{177}Hf$ (t)	Hf(t)	± 2 σ	T DM	$t_{DM\ a}^{C}$	$t_{DM\ b}^{C}$	$\delta^{18}O$	± 2 σ
DCR-42A - Redenção - medium even-grained leucomonzogranite															
N1634B.6-1	1871	0.032997	0.001660	0.001004	0.000042	0.281219	0.000018	0.281183	-14.5	0.6	2.80	3.40	3.25	6.02	0.64
N1634B.5-1	1871	0.031957	0.000652	0.001000	0.000014	0.281226	0.000021	0.281190	-14.2	0.2	2.79	3.38	3.24	6.07	0.65
N1634B.4-1	1871	0.024216	0.000234	0.000769	0.000004	0.281237	0.000015	0.281210	-13.5	0.1	2.76	3.34	3.20	5.05	0.63
N1634B.2-1	1871	0.031483	0.001691	0.000935	0.000052	0.281250	0.000019	0.281216	-13.3	0.7	2.76	3.32	3.19	6.11	0.65
N1634B.1-1	1871	na	na	na	na	na	na	na	na	na	na	na	na	4.21	0.66
N1634B.6-3	1871	na	na	na	na	na	na	na	na	na	na	na	na	5.25	0.65
N1634B.3-1	na	na	na	na	na	na	na	na	na	na	na	na	na	5.59	0.61
N1634B.5-2	na	na	na	na	na	na	na	na	na	na	na	na	na	6.22	0.62
N1634B.5-3	na	na	na	na	na	na	na	na	na	na	na	na	na	4.54	0.63
N1634B.5-4	na	na	na	na	na	na	na	na	na	na	na	na	na	6.17	0.63
N1634B.7-1	na	na	na	na	na	na	na	na	na	na	na	na	na	6.00	0.64
N1634B.7-2	na	na	na	na	na	na	na	na	na	na	na	na	na	5.73	0.65
N1634B.7-3	na	na	na	na	na	na	na	na	na	na	na	na	na	6.28	0.65
ADR-136I - Bannach - cumulate granite															
N1634E.1-1	1874	0.044946	0.001574	0.001309	0.000041	0.281268	0.000022	0.281222	-13.0	0.4	2.76	3.31	3.18	7.09	0.36
N1634E.1-2	1874	0.023379	0.000435	0.000723	0.000006	0.281207	0.000019	0.281182	-14.5	0.1	2.80	3.40	3.25	6.98	0.43
N1634E.4-1	1874	0.043349	0.002033	0.001214	0.000048	0.281232	0.000023	0.281189	-14.2	0.6	2.80	3.38	3.24	6.75	0.38
N1634E.4-2	1874	0.041218	0.001350	0.001190	0.000045	0.281246	0.000021	0.281204	-13.7	0.5	2.78	3.35	3.21	na	na
N1634E.4-3	1874	0.044972	0.002980	0.001326	0.000090	0.281250	0.000020	0.281203	-13.7	0.9	2.78	3.35	3.21	na	na
N1634E.7-1	1908	0.021047	0.000539	0.000656	0.000014	0.281210	0.000020	0.281186	-13.5	0.3	2.79	3.37	3.23	6.97	0.34
N1634E.8-1	1874	0.031235	0.001677	0.000925	0.000037	0.281252	0.000021	0.281219	-13.1	0.5	2.75	3.32	3.18	6.54	0.38
N1634E.9-1	1874	0.025192	0.001397	0.000721	0.000036	0.281218	0.000020	0.281192	-14.1	0.7	2.78	3.38	3.23	6.60	0.36
N1634E.10-1	1908	0.033587	0.001207	0.001003	0.000039	0.281266	0.000022	0.281230	-12.0	0.5	2.74	3.27	3.14	6.96	0.37
N1634E.10-3	1874	0.024529	0.000304	0.000748	0.000003	0.281243	0.000017	0.281217	-13.2	0.1	2.75	3.32	3.19	6.65	0.37
N1634E.10-2	1874	na	na	na	na	na	na	na	na	na	na	na	na	6.63	0.39
N1634E.2-2	na	na	na	na	na	na	na	na	na	na	na	na	na	6.82	0.33
N1634E.6-1	na	na	na	na	na	na	na	na	na	na	na	na	na	6.52	0.37
N1634E.1-3	na	na	na	na	na	na	na	na	na	na	na	na	na	6.98	0.42
N1634E.2-1	na	na	na	na	na	na	na	na	na	na	na	na	na	7.00	0.47
N1634E.8-2	na	na	na	na	na	na	na	na	na	na	na	na	na	6.70	0.35
N1634E.9-2	na	na	na	na	na	na	na	na	na	na	na	na	na	7.06	0.39

Supplementary Table 3. (continued)

	U/Pb							Sample Initial Ratios			Model Ages (Ga)				
Sample	Age (Ma)	$^{176}Yb/^{177}Hf$	± 2 σ	$^{176}Lu/^{17}7Hf$	± 2 σ	$^{176}Hf/^{177}Hf$ (t)	± 2 σ	$^{176}Hf/^{177}Hf$ (t)	Hf(t)	± 2 σ	T DM	$t_{DM\ a}^{C}$	$t_{DM\ b}^{C}$	$\delta^{18}O$	± 2 σ
ADR-35A - Bannach - fine-grained leucomonzogranite															
N1635A.11-1	1857	0.019700	0.000133	0.000638	0.000010	0.281189	0.000021	0.281166	-15.4	0.2	2.82	3.44	3.29	6.31	0.52
N1635A.9-2	1857	0.029453	0.000090	0.000974	0.000005	0.281324	0.000018	0.281289	-11.0	0.1	2.66	3.17	3.05	na	na
N1635A.4-1	1857	0.070346	0.002122	0.002165	0.000078	0.281404	0.000022	0.281327	-9.7	0.3	2.63	3.09	2.97	7.11	0.45
N1635A.3-1	1857	0.030224	0.000464	0.000944	0.000006	0.281339	0.000022	0.281305	-9.5	0.1	2.64	3.11	3.00	6.50	0.51
N1635A.4-2	1857	0.053261	0.001119	0.001629	0.000023	0.281361	0.000023	0.281303	-9.8	0.1	2.65	3.12	3.01	6.91	0.47
N1635A.2-1	1916	0.030795	0.000930	0.000994	0.000039	0.281336	0.000021	0.281300	-9.3	0.4	2.65	3.12	3.01	6.36	0.53
1635A.1-1	1857	0.038732	0.000854	0.001168	0.000007	0.281337	0.000019	0.281295	-10.8	0.1	2.66	3.16	3.04	6.70	0.48
N1635A.9-1	1857	0.021901	0.001334	0.000710	0.000042	0.281325	0.000019	0.281300	-10.7	0.6	2.64	3.15	3.03	na	na
N16-35.A5-2	1857	na	na	na	na	na	na	na	na	na	na	na	na	6.11	0.47
N16-35.A5-1	1857	na	na	na	na	na	na	na	na	na	na	na	na	6.54	0.47
N16-35.A8-1	1857	na	na	na	na	na	na	na	na	na	na	na	na	6.90	0.46
N16-35.A1-2	na	na	na	na	na	na	na	na	na	na	na	na	na	6.75	0.49
N16-35.A1-3	na	na	na	na	na	na	na	na	na	na	na	na	na	6.76	0.48
N16-35.A1-5	na	na	na	na	na	na	na	na	na	na	na	na	na	6.84	0.48

Supplementary Table 4. Hf and Oxygen isotope analyses on zircon of the Seringa Granite

	U/Pb							Sample Initial Ratios			Model Ages (Ga)				
Sample	Age (Ma)	$^{176}Yb/^{177}Hf$	± 2 σ	$^{176}Lu/^{17}7Hf$	± 2 σ	$^{176}Hf/^{177}Hf$ (t)	± 2 σ	$^{176}Hf/^{177}Hf$ (t)	Hf(t)	± 2 σ	T DM	$t_{DM\ a}^{C}$	$t_{DM\ b}^{C}$	$\delta^{18}O$	± 2 σ
AC-45 - Seringa - heterogranular hornblende-biotite syenogranite															
N1626A.8-1 (core)	1879	0.075500	0.003900	0.001637	0.000092	0.281221	0.000030	0.281163	-15.0	0.8	2.85	3.44	3.29	6.13	0.51
N1626A.8-2 (rim)	1879													6.69	0.53
N16-26A.5-1	1879	0.033810	0.000920	0.000719	0.000013	0.281213	0.000026	0.281187	-14.1	0.3	2.79	3.38	3.24	6.29	0.60
N1626A.5-4	1879	0.052670	0.000950	0.001059	0.000012	0.281203	0.000026	0.281165	-13.6	0.2	2.80	3.38	3.24	6.52	0.52
N1626A.5- 3	1919	0.018610	0.000390	0.000380	0.000004	0.281190	0.000023	0.281176	-13.6	0.1	2.80	3.38	3.24	6.53	0.54
N16-26A.6-1	1879	0.059900	0.002800	0.000933	0.000035	0.281200	0.000023	0.281167	-14.9	0.6	2.82	3.43	3.28	6.57	0.52
N16-26A.6-2	1919	0.039500	0.003300	0.000597	0.000038	0.281203	0.000023	0.281181	-13.4	0.9	2.80	3.37	3.23	6.38	0.52
N16-26A.1-1	1879	0.072900	0.001100	0.001109	0.000022	0.281201	0.000027	0.281161	-15.1	0.3	2.84	3.44	3.29	5.91	0.53
N16-26A.1-2	1879	0.084600	0.001900	0.001263	0.000021	0.281244	0.000030	0.281199	-13.7	0.2	2.79	3.36	3.22	5.84	0.54
N16-26A.5-2	1919	na	na	na	na	na	na	na	na	na	na	na	na	5.71	0.52
N1626A.10-1	1879	na	na	na	na	na	na	na	na	na	na	na	na	6.35	0.55
AC-59 - Seringa - coarse-grained biotite-hornblende monzogranite															
N16-26-H.1-1	1870	0.059430	0.000380	0.000760	0.000010	0.281191	0.000019	0.281182	-14.5	0.2	2.80	3.40	3.26	6.04	0.53
N16-26-H.2-1	1870	0.031930	0.000820	0.000523	0.000006	0.281196	0.000022	0.281177	-14.7	0.2	2.80	3.41	3.27	6.38	0.59
N16-26-H.3-1	1870	0.050020	0.000570	0.000903	0.000003	0.281209	0.000027	0.281159	-15.4	0.1	2.83	3.45	3.30	6.22	0.57
N16-26-H.4-1	1870	0.249000	0.019000	0.000374	0.000030	0.281365	0.000051	0.281186	-14.4	1.2	2.79	3.39	3.25	6.06	0.53
N16-26-H.5-1	1870	0.032600	0.001300	0.000528	0.000016	0.281206	0.000026	0.281187	-14.3	0.4	2.79	3.39	3.25	6.14	0.55
N16-26-H.6-1	1870	0.023000	0.002200	0.003800	0.000260	0.281199	0.000029	0.281230	-12.8	0.9	2.81	3.29	3.16	6.43	0.60
N16-26-H.2-2	1870	na	na	na	na	na	na	na	na	na	na	na	na	6.40	0.50
N16-26-H.8-1	1870	na	na	na	na	na	na	na	na	na	na	na	na	5.88	0.53
N16-26-H.8-2	1870	na	na	na	na	na	na	na	na	na	na	na	na	6.88	0.55
N16-26-H.8-3	1870	na	na	na	na	na	na	na	na	na	na	na	na	5.88	0.54

Supplementary Table 4. (Continued)

	U/Pb							Sample Initial Ratios			Model Ages (Ga)				
Sample	Age (Ma)	$^{176}Yb/^{177}Hf$	± 2 σ	$^{176}Lu/^{17}7Hf$	± 2 σ	$^{176}Hf/^{177}Hf$ (t)	± 2 σ	$^{176}Hf/^{177}Hf$ (t)	Hf(t)	± 2 σ	T DM	$t_{DM\ a}^{C}$	$t_{DM\ b}^{C}$	$\delta^{18}O$	± 2 σ
AC-85 - Seringa - coarse-grained hornblende-biotite monzogranite															
1626B11-1	1889	0.051180	0.000420	0.003658	0.000031	0.281223	0.000029	0.281092	-17.3	0.1	3.00	3.58	3.43	6.82	0.58
1626B3-2	1889	0.014760	0.000150	0.001200	0.000004	0.281186	0.000027	0.281143	-15.5	0.1	2.86	3.47	3.32	6.11	0.52
1626B3-1	1889	0.022691	0.000087	0.001863	0.000007	0.281208	0.000021	0.281141	-15.5	0.1	2.88	3.48	3.33	6.22	0.56
1626B.4-1	1889	0.016800	0.000260	0.001475	0.000010	0.281179	0.000017	0.281126	-16.1	0.1	2.89	3.51	3.36	6.44	0.56
1626B5-1	1889	0.016590	0.000210	0.001487	0.000009	0.281190	0.000028	0.281137	-15.7	0.1	2.88	3.49	3.34	6.34	0.53
1626B5-2	1889	0.017420	0.000190	0.001598	0.000019	0.281176	0.000031	0.281119	-16.3	0.2	2.91	3.53	3.37	5.98	0.51
1626B4-2	1889	0.018200	0.001900	0.001670	0.000130	0.281194	0.000019	0.281134	-15.8	1.2	2.89	3.49	3.34	6.83	0.52
1626B8-1	1889	na	na	na	na	na	na	na	na	na	na	na	na	6.55	0.57
1626B11-2	na	na	na	na	na	na	na	na	na	na	na	na	na	6.27	0.53
1626B3-3	na	na	na	na	na	na	na	na	na	na	na	na	na	6.16	0.51
1626B3-4	na	na	na	na	na	na	na	na	na	na	na	na	na	6.99	0.58
AC-42 - Seringa - heterogranular hornblende-biotite syenogranite															
N1620G.2-2	1879	na	na	na	na	na	na	na	na	na	na	na	na	6.20	0.55
N1620G.3-1	1879	na	na	na	na	na	na	na	na	na	na	na	na	5.95	0.56
N1620G.6-1	1879	na	na	na	na	na	na	na	na	na	na	na	na	6.63	0.56
N1620G.6-2	1879	na	na	na	na	na	na	na	na	na	na	na	na	6.02	0.59
N1620G.6-3	1879	na	na	na	na	na	na	na	na	na	na	na	na	4.55	0.56
N1620G.6-5	1879	na	na	na	na	na	na	na	na	na	na	na	na	5.83	0.53
N1620G.2-1	1879	na	na	na	na	na	na	na	na	na	na	na	na	4.77	0.59
N1620G.6-4	1879	na	na	na	na	na	na	na	na	na	na	na	na	6.73	0.55
N1620G.1-7	na	na	na	na	na	na	na	na	na	na	na	na	na	6.99	0.52
N1620G.4-1	na	na	na	na	na	na	na	na	na	na	na	na	na	6.12	0.58
N1620G.1-1	na	na	na	na	na	na	na	na	na	na	na	na	na	6.64	0.57

Supplementary Table 5. Hf and Oxygen isotope analyses on zircon of the São João Granite

	U/Pb							Sample Initial Ratios			Model Ages (Ga)				
Sample	Age (Ma)	$^{176}Yb/^{177}Hf$	± 2 σ	$^{176}Lu/^{17}7Hf$	± 2 σ	$^{176}Hf/^{177}Hf$ (t)	± 2 σ	$^{176}Hf/^{177}Hf$ (t)	Hf(t)	± 2 σ	T DM	$t_{DM\ a}^{C}$	$t_{DM\ b}^{C}$	$\delta^{18}O$	± 2 σ
PC-03B - São João - hornblende-biotite syenogranite															
N16-26-F - 8	na	0.064800	0.003700	0.002660	0.000130	0.281217	0.000025	0.281123	-16.7	0.8	2.93	3.53	3.38	na	na
N1626F.9-1	1866	0.019140	0.000780	0.000793	0.000025	0.281187	0.000023	0.281159	-15.4	0.5	2.83	3.45	3.30	6.53	0.58
N1626F.5-1	1866	0.062600	0.002000	0.003378	0.000089	0.281229	0.000025	0.281109	-17.2	0.5	2.97	3.56	3.40	5.76	0.50
N1626F1-1	1866	0.036600	0.001000	0.003170	0.000071	0.281192	0.000031	0.281080	-18.3	0.4	3.01	3.63	3.46	5.98	0.52
N1626F.4-1	1866	0.030310	0.000350	0.002671	0.000021	0.281181	0.000029	0.281086	-18.0	0.1	2.98	3.61	3.45	6.24	0.52
N1626F.4-2	1866	0.018630	0.000120	0.001768	0.000004	0.281188	0.000028	0.281125	-16.6	0.0	2.90	3.53	3.37	5.89	0.51
N1626F.3-1	1866	0.120800	0.003500	0.010200	0.000290	0.281275	0.000028	0.280913	-24.2	0.7	3.58	3.99	3.79	6.05	0.60
N1626F.6-1	1866	0.031750	0.000530	0.001604	0.000030	0.281182	0.000012	0.281125	-16.6	0.3	2.90	3.53	3.37	6.52	0.53
N1626F.5-2	1866	0.024160	0.000580	0.001175	0.000035	0.281170	0.000014	0.281128	-16.5	0.5	2.88	3.52	3.36	6.31	0.50
N1626F.5-3	na	na	na	na	na	na	na	na	na	na	na	na	na	6.55	0.60
N1626F.5-4	na	na	na	na	na	na	na	na	na	na	na	na	na	6.15	0.56
N1626F.6-1	na	na	na	na	na	na	na	na	na	na	na	na	na	6.26	0.53
N1626F.6-2	na	na	na	na	na	na	na	na	na	na	na	na	na	6.20	0.51
PC-21 - Seringa - biotite monzogranite															
N16-26C.2-1	1880	0.021640	0.000350	0.000143	0.000001	0.281177	0.000027	0.281172	-14.7	0.1	2.80	3.42	3.27	14.33	0.55
N16-26C.2-2	1880	0.083630	0.000630	0.000562	0.000005	0.281204	0.000028	0.281184	-14.2	0.1	2.79	3.39	3.25	6.86	0.5
N1626C.5-2	1880	0.025190	0.000330	0.000411	0.000010	0.281185	0.000019	0.281204	-13.5	0.3	2.76	3.34	3.21	6.11	0.59
N1626C.5-1	1880	0.055600	0.001500	0.000186	0.000001	0.281219	0.000024	0.281178	-14.4	0.1	2.79	3.40	3.26	6.04	0.59
N16-26C.6-1	1880	0.139600	0.005700	0.000703	0.000025	0.281247	0.000023	0.281222	-12.9	0.5	2.74	3.31	3.17	5.92	0.52
N1626C.7-1	1880	0.015820	0.000850	0.000095	0.000004	0.281178	0.000015	0.281175	-14.6	0.6	2.79	3.41	3.27	6.54	0.53
N1626C.8-1	1880	0.038940	0.000960	0.000228	0.000006	0.281212	0.000022	0.281204	-13.5	0.4	2.76	3.35	3.21	6.15	0.51
N16-26C.1-1	1880	na	na	na	na	na	na	na	na	na	na	na	na	na	na
N16-26C.1-2	1880	na	na	na	na	na	na	na	na	na	na	na	na	na	na
N16-26C.2-3	1880	na	na	na	na	na	na	na	na	na	na	na	na	5.68	0.56
N16-26C.2-4	1880	na	na	na	na	na	na	na	na	na	na	na	na	6.63	0.61
N16-26C.2-4b	1880	na	na	na	na	na	na	na	na	na	na	na	na	4.17	0.55
N16-26C.2-5	1880	na	na	na	na	na	na	na	na	na	na	na	na	6.86	0.50
N16-26C.6-2-1	1880	na	na	na	na	na	na	na	na	na	na	na	na	6.54	0.53

Supplementary Table 5. (Continued)

	U/Pb							Sample Initial Ratios			Model Ages (Ga)				
Sample	Age (Ma)	$^{176}Yb/^{177}Hf$	± 2 σ	$^{176}Lu/^{17}7Hf$	± 2 σ	$^{176}Hf/^{177}Hf$ (t)	± 2 σ	$^{176}Hf/^{177}Hf$ (t)	Hf(t)	± 2 σ	T DM	$t_{DM\ a}^{C}$	$t_{DM\ b}^{C}$	$\delta^{18}O$	± 2 σ
PCM-10 - São João - biotite-hornblende monzogranite															
N16-26E.4-1	1891	0.158300	0.005400	0.003510	0.000130	0.281304	0.000030	0.281178	-14.2	0.5	2.88	3.40	3.25	6.22	0.54
N16-26E.4-3	1891	0.016780	0.000300	0.000459	0.000006	0.281175	0.000021	0.281159	-14.9	0.2	2.82	3.44	3.29	5.79	0.50
N16-26E.4-2	1891	0.015714	0.000065	0.000410	0.000005	0.281179	0.000031	0.281164	-14.7	0.2	2.81	3.42	3.28	6.03	0.58
N16-26E.6-1	1891	0.023850	0.000700	0.000677	0.000017	0.281156	0.000037	0.281132	-15.8	0.4	2.86	3.50	3.35	5.93	0.54
N16-26-E - 2	na	0.031900	0.001300	0.000964	0.000030	0.281214	0.000025	0.281179	-14.1	0.4	2.81	3.39	3.25	na	na
N16-26E.7-1	1891	0.052100	0.000750	0.001622	0.000029	0.281227	0.000021	0.281169	-14.5	0.3	2.84	3.42	3.27	5.91	0.51
N16-26E.3-1	1891	na	na	na	na	na	na	na	na	na	na	na	na	6.28	0.55
N16-26E.3-2	1891	na	na	na	na	na	na	na	na	na	na	na	na	6.39	0.52
N16-26E.3-3	1891	na	na	na	na	na	na	na	na	na	na	na	na	6.28	0.57
N16-26E.6-2	na	na	na	na	na	na	na	na	na	na	na	na	na	5.61	0.52
N16-26E.1-1	na	na	na	na	na	na	na	na	na	na	na	na	na	6.47	0.55
PCM-13 - São João - biotite-hornblende syenogranite															
N1620A.1-1	1877	na	na	na	na	na	na	na	na	na	na	na	na	6.27	0.56
N1620A.1-2	1877	na	na	na	na	na	na	na	na	na	na	na	na	6.45	0.56
N1620A.1-3	1877	na	na	na	na	na	na	na	na	na	na	na	na	5.96	0.59
N1620A.3-1	1877	na	na	na	na	na	na	na	na	na	na	na	na	6.12	0.57
N1620A.5-1	1877	na	na	na	na	na	na	na	na	na	na	na	na	6.10	0.55
N1620A.11-1	1877	na	na	na	na	na	na	na	na	na	na	na	na	6.13	0.52
N1620A.11-2	1877	na	na	na	na	na	na	na	na	na	na	na	na	6.35	0.54
N1620A.12-1	1877	na	na	na	na	na	na	na	na	na	na	na	na	6.30	0.55
N1620A.16-1	na	na	na	na	na	na	na	na	na	na	na	na	na	5.87	0.55
N1620A.16-2	na	na	na	na	na	na	na	na	na	na	na	na	na	5.89	0.58

Supplementary Table 6. Hf and Oxygen isotope analyses on zircon of the Gogó da Onça Granite

	U/Pb							Sample Initial Ratios			Model Ages (Ga)				
Sample	Age (Ma)	$^{176}Yb/^{177}Hf$	± 2 σ	$^{176}Lu/^{177}Hf$	± 2 σ	$^{176}Hf/^{177}Hf$ (t)	± 2 σ	$^{176}Hf/^{177}Hf$ (t)	Hf(t)	± 2 σ	T DM	$t_{DM\ a}^{C}$	$t_{DM\ b}^{C}$	$\delta^{18}O$	± 2 σ
PFR-19B. Gogó-da-Onça - hornblende-biotite syenogranite															
N1634C.3-1	1869	0.047803	0.000768	0.001430	0.000011	0.281214	0.000019	0.281163	-15.2	0.1	2.84	3.44	3.29	6.35	0.36
n16_34c_3.2	na	0.024108	0.000634	0.000727	0.000010	0.281190	0.000017	0.281164	-15.2	0.2	2.82	3.44	3.29	6.15	0.38
n16_34c_3.3	na	0.031531	0.002653	0.000925	0.000066	0.281184	0.000019	0.281151	-15.6	1.1	2.84	3.47	3.32	6.63	0.34
N1634C.3-4	1869	0.048056	0.000673	0.001409	0.000017	0.281190	0.000018	0.281140	-16.0	0.2	2.87	3.49	3.34	6.99	0.38
N1634C.3-5	1869	0.047771	0.000556	0.001438	0.000008	0.281213	0.000018	0.281162	-15.3	0.1	2.84	3.44	3.30	6.45	0.35
N1634C.4-1	na	0.029293	0.000976	0.000871	0.000032	0.281179	0.000018	0.281148	-15.8	0.6	2.85	3.47	3.32	6.67	0.33
N1634C.4-2	1869	0.047928	0.000693	0.001416	0.000030	0.281237	0.000022	0.281187	-14.4	0.3	2.81	3.39	3.25	6.76	0.35
N1634C.4-3	na	0.047201	0.003273	0.001282	0.000081	0.281284	0.000026	0.281239	-12.5	0.8	2.74	3.28	3.14	6.48	0.33
N1634C.4-4	1869	0.044100	0.001464	0.001299	0.000036	0.281172	0.000024	0.281126	-16.5	0.5	2.89	3.52	3.37	6.62	0.34
N1634C.4-5	1869	0.022078	0.002327	0.000653	0.000059	0.281186	0.000021	0.281163	-15.2	1.4	2.82	3.44	3.29	na	na
1634C.5-1	1869	0.038170	0.001161	0.001125	0.000037	0.281217	0.000018	0.281177	-14.7	0.5	2.81	3.41	3.27	6.27	0.37
N1634C.5-2	1869	0.025085	0.001812	0.000748	0.000040	0.281187	0.000018	0.281160	-15.3	0.8	2.83	3.45	3.30	6.97	0.36
N1634C.5-3	1869	na	na	na	na	na	na	na	na	na	na	na	na	6.63	0.35
N1634C.5-4	1869	na	na	na	na	na	na	na	na	na	na	na	na	6.72	0.39
N1634C.8-1	1869	na	na	na	na	na	na	na	na	na	na	na	na	6.78	0.42
N1634C.8-2	1869	na	na	na	na	na	na	na	na	na	na	na	na	6.11	0.41
PFR-18B. Gogó-da-Onça - biotite-hornblende granodiorite															
N1619I.8-1	1878	0.026759	0.001177	0.000853	0.000024	0.281190	0.000016	0.281160	-15.1	0.4	2.83	3.44	3.30	6.20	0.52
N1619I.7-1	1878	0.041115	0.000113	0.001312	0.000007	0.281228	0.000022	0.281181	-14.4	0.1	2.81	3.40	3.25	6.46	0.50
N1619I.9-2	1878	0.018061	0.000532	0.000600	0.000011	0.281180	0.000018	0.281159	-15.2	0.3	2.83	3.45	3.30	5.96	0.49
N1619I.5-1	1878	0.038475	0.000259	0.001213	0.000002	0.281219	0.000017	0.281176	-14.6	0.0	2.82	3.41	3.26	4.35	0.52
N1619I.9-1	1878	na	na	na	na	na	na	na	na	na	na	na	na	5.86	0.51
N1619I.1-1-1	1878	na	na	na	na	na	na	na	na	na	na	na	na	5.92	0.49
N1619I.2-1	1878	na	na	na	na	na	na	na	na	na	na	na	na	5.90	0.53
N1619I.7-2	1878	na	na	na	na	na	na	na	na	na	na	na	na	6.00	0.57
N1619I.1-2	na	na	na	na	na	na	na	na	na	na	na	na	na	6.46	0.57
N1619I.5-2	na	na	na	na	na	na	na	na	na	na	na	na	na	5.97	0.58

Supplementary Table 6. (continued)

	U/Pb							Sample Initial Ratios			Model Ages (Ga)				
Sample	Age (Ma)	$^{176}Yb/^{177}Hf$	± 2 σ	$^{176}Lu/^{17}7Hf$	± 2 σ	$^{176}Hf/^{177}Hf$ (t)	± 2 σ	$^{176}Hf/^{177}Hf$ (t)	Hf(t)	± 2 σ	T DM	$t_{DM\ a}^{C}$	$t_{DM\ b}^{C}$	$\delta^{18}O$	± 2 σ
PFR-22. Gogó-da-Onça - biotite-hornblende monzogranite															
N1619B.5-1	1865	na	na	na	na	na	na	na	na	na	na	na	na	6.27	0.53
N1619B.5-2	1865	na	na	na	na	na	na	na	na	na	na	na	na	6.55	0.54
N1619B.5-3	1865	na	na	na	na	na	na	na	na	na	na	na	na	5.92	0.51
N1619B.5-4	1865	na	na	na	na	na	na	na	na	na	na	na	na	6.03	0.48
N1619B.9-1	1865	na	na	na	na	na	na	na	na	na	na	na	na	5.46	0.54
N1619B.4-1	1865	na	na	na	na	na	na	na	na	na	na	na	na	5.90	0.50
N1619B.4-2	1865	na	na	na	na	na	na	na	na	na	na	na	na	6.03	0.50
N1619B.2-1	na	na	na	na	na	na	na	na	na	na	na	na	na	5.64	0.55
N1619B.6-1	na	na	na	na	na	na	na	na	na	na	na	na	na	6.19	0.54
N1619B.8-1	na	na	na	na	na	na	na	na	na	na	na	na	na	6.11	0.53

Values for $(^{176}Hf/^{177}Hf)_{CHUR}$ (0.282785) and $(^{176}Lu/^{177}Hf)_{CHUR}$ (0.0336) are from (Bouvier et al., 2008).

εHf(t) calculated using a Lu decay constant of $1.867 \cdot 10^{-11} a^{-1}$ (Soderlund et al., 2004).

Two-stage model ages (tDM c) were calculated assuming a mean $^{176}Lu/^{177}Hf$ value of 0.015 (Goodge and Vervoort, 2006) and of 0.0125 (Chauvel et al., 2014).

Present-day $^{176}Hf/^{177}Hf$ ratio of the depleted mantle = 0.28325; Anderson et al., 2009)

na = not analysed

Supplementary Table 7 – Nd data for the A-type granites of the Carajás Province.

Pluton	Sm-Nd (whole-rock)		Reference
	t_{DM}	εNd	
SERRA DOS CARAJÁS SUITE			
Cigano	2939	-9.7	Dall'Agnol et al. (2005)
	2668	-9.5	Dall'Agnol et al. (2005)
Serra dos Carajás	2611	-7.9	Dall'Agnol et al. (2005)
	2727	-9.2	Dall'Agnol et al. (2005)
Pojuca	3353	-9.7	Dall'Agnol et al. (2005)
VELHO GUILHERME SUITE			
Antônio Vicente	3254	-12.1	Teixeira et al. (2002)
Mocambo	2976	-7.9	Teixeira et al. (2002)
	3023	-12.2	Teixeira et al. (2002)
JAMON SUITE			
Musa	2821	-9.4	Dall'Agnol et al. (2005)
	2793	-9.3	Dall'Agnol et al. (2005)
	2596	-9.6	Dall'Agnol et al. (2005)
Jamon	3024	-9.7	Dall'Agnol et al. (2005)
	2874	-9.5	Dall'Agnol et al. (2005)
Redenção	2785	-8.8	Ramo et al. (2002)
	2807	-10.5	Ramo et al. (2002)
	2789	-9.7	Ramo et al. (2002)
	2727	-9.6	Ramo et al. (2002)
Bannach	2844	-9.6	Ramo et al. (2002)
Felsic dikes	2830	-10	Dall'Agnol et al. (2005)
	2884	-9.4	Dall'Agnol et al. (2005)
OTHER GRANITES RELATED			
Gogó da Onça Granite	2817	-9.48	Teixeira et al. (2017)
	2781	-9.18	Teixeira et al. (2017)
	2806	-9.07	Teixeira et al. (2017)

5 CONCLUSÕES E CONSIDERAÇÕES FINAIS

- O Granito Gogó da Onça Granite (GGO) é composto por biotita-anfibólio granodiorios, biotita-anfibólio monzogranitos e anfibólio-biotita sienogranito. É um granito metaluminoso, enriquecido em HFSE, com altas razões K_2O/Na_2O e Y/Nb. O comportamento dos elementos traços sugere que suas diferentes fácies são relacionadas por cristalização fracionada. Os dados U-Pb SHRIMP em zircão e titanita mostraram que o GGO cristalizou entre ~ 1880 e 1870 Ma. Dados isotópicos de Nd e Hf indicaram fontes crustais arqueanas para esse granito. Apresenta comportamento geoquímico similar aos granitos anorogênicos de Carajás se assemelhando mais com a Suite Serra dos Carajás e com os granitos Seringa e São João, e aos granitos Sherman (mesoproterozóico) dos EUA e o Batólito Suomenniemi (paleoproterozóico) da Finlândia.
- Os granitos do tipo-A paleoproterozóicos da Província Carajás foram colocados entre 1880 e 1860 Ma, com o pico principal do magmatismo em 1880 Ma. Idades mais antigas (1900-1920 Ma) forma obtidas em cristais de zircão e titanita e podem representar *antecryst* de um pulso magmático precoce que foram incorporados no pulso de 1880 Ma.
- As facies de leucograniticas dos plutos Redenção e Bannach da Suíte Jamon são mais jovens (1857 a 1865 Ma) do que as fácies menos evoluídas dos mesmos plutos (1880 Ma) e representam pulsos magmáticos independentes que foram tardios na evolução magmática do pluton.
- Idades de 1732 ± 6 Ma obtidas nas facies leucogranitica do Granito Antônio Vicente poderia representar um evento magmático na região do Xingu ainda não relatado ou um evento hidrotermal isolado que permitiu o crescimento de zircões**.**
- Os dados geocronológicos mais precisos e detalhados obtidos nessa Tese adicionados às informações disponíveis na literatura, demonstram a relevância do evento magmático de 1880 Ma e indicam que a colocação desses granitos foi feita em aproximadamente 20 milhões de anos, em um tempo geológico relativamente curto.
- Todos os granitos anorogênicos de tipo-A da Província de Carajás estudados nesta Tese de Doutorado, possuem composições isotópicas de Hf e Oxigênio bastante homogêneas, embora pequenas diferenças tenham sido observadas internamente nos plutons ou entre estes. Essas diferenças podem resultar em contrastes nos domínios crustais da Província de Carajás que foram a fonte dos granitos ou de processos de contaminação local.
- Os dados de Hf e Oxigênio são consistentes com a interpretação de que esses plutons cristalizaram a partir de magmas gerados pela fusão de rochas ígneas pré-existentes com uma pequena contribuição de um componente supracrustal (metasedimentar) na Suíte Velho

Guilherme. As idades modelo crustais de Hf indicaram fontes paleoarqueana com uma menor contribuição mesoarqueana.

- As idades modelo de Hf são mais antigas do que as rochas arqueanas encaixantes desses granitos expostas na Província Carajás sendo necessário investigar a existência de crosta Aqueana mais antiga na Província Carajás. Assim, as composições de Nd, Hf e O dos granitos paleoperozoicos da Província de Carajás atestam fontes crustais ígneas arqueanas na origem de seus magmas.
- O episódio de 1880 Ma que gerou esses granitos também foi desenvolvido em outras Províncias do Cráton Amazônico, onde está ligado principalmente na formação da SLIP Uatumã. Este evento foi amplamente extensivo e também está registrado em vários cratons em todo o mundo demonstrando sua relevância na evolução tectônica dos continentes do Proterozóico. Os dados apresentados nesta Tese, portanto atestam a importância de crosta arqueana para origem desses granitos.

REFERÊNCIAS

Aleinikoff, J.N., Wintsch, R.P., Fanning, C.M., Dorais, M.J., 2002. U–Pb geochronology of zircon and polygenetic titanite from the Glastonbury Complex, Connecticut, USA an integrated SEM, EMPA, TIMS, and SHRIMP study. *Chemical Geology*, **188**: 125-147.

Ali, K.M., Kroner, A., Hegner, E., Wong, J., Li, S.Q., Gahlan, H.A., Abu El Ela, F.F. 2015. U–Pb zircon geochronology and Hf–Nd isotopic systematics of Wadi Beitan granitoid gneisses, South Eastern Desert, Egypt. *Gondwana Research*, **27**: 811-824.

Almeida F.F.M. de, Hasui Y, Poncano W.L., Dantas A.S.L., Carneiro C.D.R., Melo M.S. de, Bistrichi C.A. 1981. Mapa Geológico do Estado de São Paulo, escala 1:500.000 - Nota Explicativa. Institute de Pesquisas Tecnológicas do Estado de São Paulo, 126p.

Almeida, J.A.C., Dall'Agnol, R., Rocha, M.C., 2017. Tonalite–Trondhjemite and Leucogranodiorite–Granite Suites from the Rio Maria Domain, Carajás Province, Brazil: implications for discrimination and origin of the Archean Na-granitoids. *The Canadian Mineralogist*, **55:** 437-456.

Almeida, J.A.C., Dall'Agnol, R., Oliveira, D.C., 2006. Geologia, petrografia e geoquímica do granito anorogênico Bannach, Terreno granito-greenstone de Rio Maria, Pará. *Revista Brasileira de Geociências*, **36**: 282-295

Almeida, J.A.C., Dall'Agnol, R., Oliveira, M.A., Macambira, M.J.B., Pimentel, M.M., Rämö, O.T., Guimarães, F.V., Leite, A.A.S., 2011. Zircon geochronology and geochemistry of the TTG suites of the Rio Maria granite-greenstone terrane: Implications for the growth of the Archean crust of Carajás Province, Brazil. *Precambrian Research*, **187**: 201-221.

Almeida, J.A.C, Dall'Agnol R., Leite A.A.S., 2013. Geochemistry and zircon geochronology of the Archean granite suites of the Rio Maria granite-greenstone terrane, Carajás Province, Brazil. *Journal of South American Earth Sciences*, **42**: 103-126.

Almeida, M.E., Macambira, M.J.B., Oliveira, E.C., 2007. Geochemistry and zircon geochronology of the I-type high-K calc-alkaline and S-type granitoid rocks from southeastern Roraima, Brazil: Orosirian collisional magmatism evidence (1.97–1.96 Ga) in central portion of Guyana Shield. *Precambrian Research*, **155**: 69–97.

Altoff F. J., Barbey P., Boullier A. M. 2000. 2.8-3.0 Ga plutonism and deformation in the SE Amazonian craton: the Archean granitoids of Marajoara (Carajás Mineral Province, Brazil). *Precambrian Research*, **104:** 187-206.

Amelin, Y., Kaltenbach, A., Iizuka, T., Stirling, C.H., Ireland, T.R., Petaev, M., Jacobsen, S.B., 2010. U–Pb chronology of the Solar System's oldest solids with variable $^{238}U/^{235}U$. *Earth and Planetary Science Letters*, **300**: 343–350.

Anderson, J.L., 1983. Proterozoic anorogenic granite plutonism of North America. *Geological Society of America, Memoir*, **161**: 133–154.

Anderson, J.L., Barth, A.P., Mazdab, J.L.W.F., 2008. Thermometers and thermobarometers in granitic systems. *Reviews in Mineralogy and Geochemistry*, **69:** 121–142.

Anderson, J.L., Morrison, J., 2005. Ilmenite, magnetite, and peraluminous Mesoproterozoic anorogenic granites of Laurentia and Baltica, *Lithos*, **80**: 45–60.

Anderson, J.L., Smith, D.R., 1995. The effects of temperature and fO_2 on the Al-in-hornblende barometer. *American Mineralogist*, **80**: 549–559.

Andersen, T., Andersson, U.B., Graham, S., Åberg, G., Simonsen, S.L., 2009. Granitic magmatism by melting of juvenile continental crust: new constraints on the source of Paleoproterozoic granitoids in Fennoscandia from Hf isotopes in zircon. *Journal of Geological Society of London,* **166**: 233–247.

Andersen, T., Griffin, W. L., Jackson, S. E., Knudsen, T.-L., Pearson, N. J.,2004. Mid-Proterozoic magmatic arc evolution at the southwest margin of the Baltic Shield. *Lithos,* **73**: 289-318.

Antonio, P.Y.J., D'Agrella-Filho, M.S., Trindade, R.I.F, Nédélec, A., Oliveira, D.C., Silva, F.F., Roverato, M., Lana, C., 2017. Turmoil before the boring billion: Paleomagnetism of the 1880–1860 Ma Uatumã event in the Amazonian craton. *Gondwana Research,* **49**: 106-129.

Avelar, V.G. 1996. Geocronologia Pb-Pb por evaporação em monocristal de zircão, do magmatismo da região de Tucumã, SE do Estado do Pará, Amazônia oriental. Federal University of Pará. Dissertation. Graduated Program on Geology and Geochemistry, Institute of Geosciences, 199 pp.

Avelar, V.G., Lafon, J.M., Correia Jr, F.C., Macambira E.M B., 1999. O Magmatismo arqueano da região de Tucumã-Província Mineral de Carajás: novos resultados geocronológicos. *Revista Brasileira de Geociências,* **29**(2): 454-460.

Baertschi, P., 1976. Absolute 18O content of standard mean ocean water. *Earth Planet. Sci. Lett*. **31**: 341-344.

Barbosa, A.A., Lafon, J.M., Neves, A.P., Vale, A.G., 1995. Geocronologia Rb–Sr e Pb–Pb do Granito Redenção, SE do Pará: implicações para a evolução do magmatismo proterozóico da região de Redenção. *Boletim do Museu Paraense Emílio Goeldi. Ciências da Terra,* **7**: 147–164.

Barreto, C.J.S., Lafon, J.M., Costa, L.T.R., Lima, E.F., 2013. Vulcanismo félsico paleoproterozoico do Grupo Iricoumé, Domínio Erepecuru-Trombetas, Província Amazônia Central: dados de campo, caracterização petrográfica e geocronologia Pb-Pb em zircão. *Geologia-USP, Série Científica,* **13:** 47-71.

Barreto, C.J.S., Lafon, J.M., Costa, L.T.R., Lima, E.F., 2014. Palaeoproterozoic (~1.89 Ga) felsic volcanism of the Iricoumé Group, Guyana Shield, South America: geochemical and Sm-Nd isotopic constraints on sources and tectonic environment. *International Geology Review*. http://dx.doi.org/10.1080/00206814.2014.930800.

Barros, C.E.M., Dall'Agnol, R., Vieira, E.A.P., Magalhães, M.S., 1995. Granito Central da Serra dos Carajás: avaliação do potencial metalogenético para estanho com base em estudos da borda oeste do corpo. *Boletim do Museu Paraense Emílio Goeldi. Série Ciências da Terra,* **7**: 93–123 .

Barros, C.E.M., Dall'Agnol, R., Barbey, P., Boullier, A.M., 1997. Geochemistry of the Estrela Granite Complex, Carajás region, Brazil: an example of an Archean A-type granitoid. *Journal of South American Earth Sciences,* **10**: 321–330.

Barros, C.E.M., Sardinha, A.S., Barbosa, J.P.O., Macambira, M.J.B., 2009. Structure, petrology, geochemistry and zircon U/Pb and Pb/Pb geochronology of the synkinematic Archean (2.7 Ga) A-type granites from the Carajás Metallogenic Province, northern Brazil. *The Canadian Mineralogist,* **47:** 1423–1440.

Barros M.A.S., Padilha R.A., Rubert R.R., Pimentel M.M., ChemaleJr. F. 2006. Iriri volcanism and Rio Dourado Granite: A-Type Paleoproterozoic Magmatism in northeastern Mato Grosso – Brazil. In: Symposium on magmatism, crustal evolution, and metallogenesis of the Amazonian Craton/workshop on A-Type granites and related rocks through time (IGCP 510), 2006, Belém. Abstract volume and Field Trips Guide… Belém: PRONEX-UFPA/ SBG-NO, p.39-39.

Barros, M.A.S., Pimentel ,M.M., Silva F.R., Dantas, E.L., 2011. A Suíte Intrusiva Rio Dourado – um granito tipo A de 1,88 Ga – sudeste do Cráton Amazônico – Mato Grosso – Brasil. *Geologia USP, Série Científica,* **11**(1): 75-93.

Bastos Neto, A.C., Ferron, J.T.M.M., Chauvet, A., Chemale Jr, F., Lima, E.F., Barbanson, L., Costa, C.F.M., 2014. U–Pb dating of the Madeira Suite and structural control of the albite-enriched granite at Pitinga (Amazonia, Brazil): Evolution of the A-type magmatism and implications for the genesis of the Madeira Sn–Ta–Nb (REE, cryolite) world-class deposit. *Precambrian Research,* **243**: 181-196.

Bettencourt, J.S., Juliani., Xavier, R.P., Monteiro, L.V.S., Bastos-Neto, A.C., Klein, E.L., Assis, R.R., Leite-Jr., W.P., Moreto, C.P.N., Fernandes, C.M.D., Pereira, V.P., 2016. Metallogenetic systems associated with granitoid magmatism in the Amazon Craton: An overview of the present level of understanding and exploration significance. *Journal of South American Earth Sciences,* **68:** 22-49.

Bettencourt, J.S., Tosdal, R.M., Leite Júnior, W.B., Payolla, B.L., 1999. Mesoproterozoic rapakivi granites of the Rondonia Tin Province, southwestern border of the Amazonian craton, Brazil - I. Reconnaissance U-Pb geochronology and regional implications. *Precambrian Research,* **95**: 41- 67.

Brito-Neves, M.F.L., Almeida, M.E., Macambira, M.J.B., 1999. $^{207}Pb/^{206}Pb$ age of calc-alkaline rapakivi granite in Tapajós Gold Province, Amazon Craton, Brazil. *In*: South American Symposium on Isotope Geology, 2. Actas, 40-43.

Bonin, B., 2007. A-type granites and related rocks: evolution of a concept, problems and prospects. *Lithos,* **97**: 1–29.

Bouvier, A., Vervoort, J.D., and Patchett, P.J., 2008, The Lu-Hf and Sm-Nd isotopic composition of CHUR: Constraints from unequilibrated chondrites and implications for the bulk composition of terrestrial planets: *Earth and Planetary Science Letters*, **273**: 48–57. doi:10.1016/j.epsl.2008.06.010.

Carvalho T. A. *Petrografia, Geoquímica e Suscetibilidade Magnética do Granito Gradaús, Província Carajás, SE do Pará*. MS Dissertation. Instituto de Geociências, Universidade Federal do pará, Belém. 58p

Chauvel, C., Garçon, M., Bureau, S., Besnault, A., Jahn, B., Ding, Z., Constraints from loess on the Hf–Nd isotopic composition of the upper continental crust. *Earth and Planetary Science Letters*, **388**: 48-58.

Chu, N.-C., Taylor, R., Chavagnac, V., Nesbitt, R., Boella, R., Milton, J., German, C., Bayon, G., Burton, K., 2002. Hf isotope ratio analysis using multi-collector inductivelycoupled plasma mass spectrometry: An evaluation of isoba-ric interference corrections. *Journal of Analytic Atomic Spectrometry*, **17**: 1567–1574.

Ciborowski, T.J.R., Minifie, M.J., Kerr, A.C., Ernst, R.E., Baragar, B., Millar, I.L., 2017. A mantle plume origin for the Palaeoproterozoic Circum-Superior Large Igneous Province. *Precambrian Research,* **249**: 189-2013.

Clemens, J.D., Holloway, J.R., White, A.J.R., 1986. Origin of an A-type granite: experimental constraints. *Am. Mineral.* **71**: 317–324.

Collins, W.J., Beams, S.D., White, A.J.R., Chappell, B.W., 1982. Nature and origin of Atype granites with particular reference to southeastern Australia. *Contrib. Miner. Petrol*. **80**: 189–200.

Compston, W., Williams, I.S., Kirschvink, J.L., Zichao, Z., Guogan, M.A., 1992. Zircon U-Pb ages for the Early Cambrian time-scale. *Journal of the Geological Society, London*. **149**: 171 - 184.

Condie, K.C., 2002. Continental growth during a 1.9-Ga superplume event. *Journal of Geodynamics,* **34:** 249–264.

Condie, K.C., Belousova, E., Griffin, W.L. and Sircombe, K.N., 2009. Granitoid events in space and time: Constraints from igneous and detrital zircon age spectra. *Gondwana Research,* **15:** 228-242.

Condie, K.C., Bickford, M.E., Aster, R.C., Belousova, E., Scholl, D.W., 2011. Episodic zircon ages, Hf isotopic composition, and the preservation rate of continental crust. *Geol. Soc. Am. Bull*. **123**(5–6): 951–957.

Cordani, U.G., Teixeira, W., D'Agrella-Filho, M.S., Trindade, R.I., 2009. The position of the Amazonian Craton in supercontinents. *Gondwana Research,* **15**: 396–407.

Corfu, F., 1996. Multistage zircon and titanite growth and inheritance in an Archean gneiss complex, Winnipeg River Subprovince, Ontario. *Earth Planet. Sci. Lett*. **141**: 175– 186.

Corfu, F., Hanchar, J.M., Hoskin, P.W.O., and Kinny, P., 2003, Atlas of zircon textures, in: Hanchar, J.M., and Hoskins, P.W.O. (eds.), Zircon: *Reviews in Mineralogy and Geochemistry,* **53:** 468–500.

Corrêa, L.W.C., Macambira, M.J.B. 2014. Evolução da região de Santana do Araguaia (PA) com base na geologia e geocronologia Pb-Pb em zircão de granitoides. *Geologia USP - Serie Científica* ,**14** (2), 45-66. .

Costi, H.T., Dall'Agnol, R., Moura, C.A.V., 2000. Geology and Pb/Pb geochronology of Paleoproterozoic volcanic and granitic rocks of the Pitinga Province, Amazonian craton, northern Brazil. *International Geology Review*, **42**, 832–849.

Costi, H.T., Dall'Agnol, R., Pichavant, M., Ramo, O.T., 2009. The peralkaline tin- mineralized Madeira cryolite albite-rich granite of Pitinga, Amazonian Craton, Brazil: petrography, mineralogy and crystallization processes. *Canadian Mineralogist,* **47**: 1301-1327.

Creaser, R.A., Price, R.C., Wormald, R.J., 1991. A-type granites revisited: assessment of a residual-source model. *Geology,* **19**: 163–166.

Cruz, D. R.S., Fernandes, C.M.D., Villas, R.N.N., Juliani, C., Monteiro, L.V.S., Lagler, B., Misas, C.M.E., 2016. Paleoproterozoic volcanic centers of the São Félix do Xingu region, Amazonian Craton, Brazil: hydrothermal alteration and metallogenetic potential. *Journal of Volcanology and Geothermal Research*, **320:** 75-87.

Cunha, I.R.V., Dall'Agnol, R., Feio, G.R.L., 2016. Mineral chemistry and magnetic petrology of the Archean Planalto Suite, Carajás Province – Amazonian Craton: implications for the evolution of ferroan Archean granites. *Journal of South American Earth Sciences,* **67**: 100–121.

Dall'Agnol, R., Teixeira, N.P., Magalhães, M.S., 1993. Diagnostic features of the Tin-specialized anorogenic granites of the Eastern Amazonian region. *Anais da Academia Brasileira de Ciências,* **65**: 33-50.

Dall'Agnol, R., Lafon, J.M., Macambira, M.J.B., 1994. Proterozoic anorogenic magmatism in the Central Amazonian Province: geochronological, petrological and geochemical aspects. *Mineralogy and Petrology*, **50**: 113–138.

Dall'Agnol, R., Rämö, O.T., Magalhães, M.S., Macambira, M.J.B., 1999a. Petrology of the anorogenic, oxidised Jamon and Musa granites, Amazonian Craton: implications for the genesis of Proterozoic A-type granites. *Lithos,* **46**: 431–462.

Dall'Agnol, R., Scaillet, B., Pichavant, M., 1999b. An experimental study of a lower Proterozoic A-type granite from the eastern Amazonian craton, Brazil. *Journal of Petrology,* **40**: 1673–1698.

Dall'Agnol, R., Costi I.T, Leite A.A. da S., Magalhaes M.S. de, Teixeira N.P. 1999c. Rapakivi granites from Brazil and adjacent areas. *Precambrian Research*, **95:** 9-39.

Dall'Agnol, R., Silva Jr, R.O., Oliveira, E. P., 1999d. Geologia, petrografia e geoquímica dos diques proterozóicos da região de Rio Maria, Sudeste do Pará. *Geochimica Brasiliensis*, **13**: 163-18.

Dall'Agnol, R., Teixeira, N.P., Rämö, O.T., Moura, C.A.V., Macambira, M.J.B., Oliveira, D.C., 2005. Petrogenesis of the Paleoproterozoic, rapakivi, A-Type granites of the Archean Carajás Metallogenic Province, Brazil. *Lithos*, **80**: 101–129.

Dall'Agnol, R., Oliveira, M.A., Almeida, J.A.C., Althoff, F.J., Leite, A.A.S., Oliveira, D.C., Barros, C.E.M., 2006. Archean and Paleoproterozoic granitoids of the Carajás Metallogenetic Province, eastern Amazonian craton. *In*: Dall'Agnol, R., Rosa-Costa, L.T., Klein, E.L. (Eds.), Symposium on Magmatism, Crustal Evolution, and Metallogenesis of the Amazon Craton. Abstracts volume and field trips guide. Belém, PRONEX-UFPA/SBG-NO, pp. 99–150.

Dall'Agnol, R., Oliveira, D.C., 2007. Oxidized, magnetite-series, rapakivi-type granites of Carajás, Brazil: implications for classification and petrogenesis of A-type granites. *Lithos*, **93**: 215 - 233.

Dall'Agnol, R., Frost, C.D., Rämö, O.T., 2012. IGCP Project 510 "A-type granites and related rocks through time": project vita, results, and contribution to granite research. *Lithos*, **151**: 1–16.

Dall'Agnol, R., Oliveira, D.C., Guimarães, F.V., Gabriel, E.O., Feio, G.R.L., Lamarão, C.N., Althoff, F.J., Santos, P.A., Teixeira, M.F.B., Silva, A.C., Rodrigues, D.S., Santos, M.J.P., Silva, C.R.P., Santos, R.D., Santos, P.J.L., 2013. Geologia do Subdomínio de Transição do Domínio Carajás – Implicações para a evolução arqueana da Província Carajás - Pará. SBG, Simpósio de Geologia da Amazônia 13. CD-ROM, Anais, Belém.

Dall'Agnol, R., Cunha, I.R.V., Guimarães, F.V., Oliveira, D.C., Teixeira, F.B.T., Feio, G.R., Lamarão, C.N., 2017. Mineralogy, geochemistry, and petrology of Neoarchean ferroan to magnesian granites of Carajás Province, Amazonian Craton: The origin of hydrated granites associated with charnockites. *Lithos*, **277**: 3 - 32.

Debon, F., Le Fort, P. 1983. A chemical–mineralogical classification of common plutonic rocks and associations. *Transactions of the Royal Society of Edinburgh, Earth Sciences*, **73:** 135–149.

Deer W.A., Howie R.A., Zussman J. 1997. Rock-forming minerals. London, Second Edition Longmans (eds.). 696 p.

DePaolo, D.J., 1981. A neodymium and strontium isotopic study of the Mesozoic calc-alkaline granitic batholiths of the Sierra Nevada and Peninsular Ranges, California. J. Geophys. Res.: *Solid Earth*, **86:** 10470–10488.

Dhuime, B., Hawkesworth, C.J., Cawood, P., 2011. When continents formed. *Science* **331**: 154–155.

Dhuime, B., Hawkesworth, C.J., Cawood, P.A., Storey, C.D., 2012. A change in the geodynamics of continental growth 3 billion years ago. *Science*, **335**: 1334–1336.

DOCEGEO, 1988. Revisão litoestratigráfica da Província Mineral de Carajás e Litoestratigrafia e principais depósitos minerais. *In*: 35th Congresso Brasileiro de Geologia, Belém.

Eby, G.N., 1992. Chemical subdivision of the A-type granitoids: petrogenesis and tectonic implications. *Geology*, **20**: 641–644.

Emslie, R.F., 1991. Granitoids of rapakivi granite–anorthosite and related associations. *Precambrian Research*, **51**: 173–192.

Feio, G.R.L., Dall'Agnol, R., 2012. Geochemistry and petrogenesis of the Mesoarchean granites from the Canaã dos Carajás Area, Carajás Province, Brazil: implications for the origin of Archean granites. *Lithos,* **154:** 33–52.

Feio, G.R.L., Dall'Agnol, R., Dantas, E., Macambira, M.J.B., Gomes, A.C.B., Sardinha, A.S., Santos, P., 2012. Geochemistry, geochronology, and origin of the Planalto granite suite and associated rocks: implications for the Neoarchean evolution of the Carajás Province. *Lithos,* **151:** 57–73.

Feio, G.R.L., Dall'Agnol, R., Dantas, E.L., Macambira, M.J.B., Santos, J.O.S., Althoff, F.J., Soares, J.E.B., 2013. Archean granitoid magmatism in the Canaã dos Carajás area: implications for crustal evolution of the Carajás province, Amazonian craton, Brazil. *Precambrian Research,* **227**: 157–185.

Fernandes C.M.D., Juliani C., Monteiro L.V.S., Lagler B., Misas C.M.E. 2011. High-K calc-alkaline to A-type fissure-controlled volcanoplutonism of the São Félix do Xingu region, Amazonian craton, Brazil: Exclusively crustal sources or only mixed Nd model ages?. *Journal of South American Earth Sciences,* **32**(4): 351-368.

Ferreira, A.T.R., Lamarão, C.N., 2013. Geologia, petrografia e geoquímica das rochas vulcânicas Uatumã na área sul de São Félix do Xingu (PA), Província Carajás. *Brazilian Journal of Geology,* **43**(1): 152-167.

Ferron, J.M.T.M., Bastos Neto, A.C., Lima, E.F., Costi, H.T., Moura, C., Prado, M., Galarza, M., 2006. Geologia e geocronologia Pb-Pb de rochas graníticas e vulcânicas ácidas a intermediárias Paleoproterozóicas da Província Pitinga, Craton Amazônico. *Revista Brasileira de Geociências,* **36** (3): 499–512.

Ferron, J.M.T.M., Bastos Neto, A.C., Lima, E.F., Nardi, L.V.S., Costi, H.T., Pierosan, R., Prado, M. 2010. Petrology, geochemistry, and geochronology of Paleoproterozoic volcanic and granitic rocks (1.89–1.88 Ga) of the Pitinga Province, Amazonian Craton, Brazil. *Journal of South American Earth Sciences,* **29**: 483-449.

Fraga, L.M.B., Dall'Agnol, R., Costa, J.B.S., Macambira, M.J.B., 2009. The Mesoproterozoic Mucajaí anorthosite–mangerite–rapakivi granite complex, Amazonian craton, Brazil. *The Canadian Mineralogist,* **47**: 1469–1492.

Fraga, L.M., Vasquez, M.L., Almeida, M., Dreher, A.M., Reis, N. 2017. A influência da orogenia eo-orosiriana na formação da SLIP Uatumã, parte central do Craton Amazônico. *In*: Anais do 15º Simpósio de Geologia da Amazônia, Belém.

Frost, B.R., Barnes, C.G., Collins, W.J., Arculus, R.J., Ellis, D.J, Frost, C.D., 2001. A geochemical classification for granitic rocks. Journal of Petrology 42, 2033–2048.

Frost, C.D., Frost, B.R., 1997. Reduced rapakivi type granites: the tholeiitic connection. *Geology,* **25**: 647–650.

Frost, C.D., Frost, B.R., Chamberlain, K.R., Edwards, B., 1999. Petrogenesis of the 1.43 Ga Sherman batholith, SE Wyoming, USA: a reduced, rapakivi-type anorogenic granite. *Journal of Petrology*, **40**: 1771–1802.

Frost, C.D., Frost, B.R., 2011. On ferroan (A-type) granitoids: their compositional variability and modes of origin. *Journal of Petrology,* **52**: 39–55.

Frost, D.C., Frost, B.R., Beard, J.S., 2016. On silica-rich granitoids and their eruptive equivalents. *American Mineralogist,* **101**: 1268 – 1284.

Frost, B.R., Lindsley, D.H., 1991. Occurrence of iron–titanium oxides in igneous rocks. In: Lindsley, D.H. (Ed.), Oxide Minerals: Petrologic and Magnetic Significance, Mineralogical. *Society of America Reviews in Mineralogy*, **25**: 1–9.

Fuck, H.A., Pimentel, M.M., Daoud, W.E.K., 1993. Idade U-Pb do Granito Madeira, Pitinga (AM). *In*: 4°Congresso Brasileiro de Geoquímica, Anais 246-249, Brasília.

Gabriel, E.O., Oliveira, D.C., 2014. Geologia, petrografia e geoquímica dos granitoides arqueanos de alto magnésio da região de Água Azul do Norte, porção sul do Domínio Carajás, Pará. *Boletim do Museu Paraense Emílio Goeldi, Ciências Naturais,* **9**(3): 533–564.

Gabriel, E.O., Oliveira, D.C., Santos, M.S., 2014. Sanukitoides mesoarqueanos de Água Azul do Norte, Sul do Domínio Carajás: Novos dados e perspectivas. *In*: 47 Congresso Brasileiro de Geologia. CD-ROM, Anais, Salvador.

Ganevin, D., Daly, J.S., Horstwood, M.S.A., Whitehouse, M.J., 2011. In-situ zircon U–Pb, oxygen and hafnium isotopic evidence for magma mixing and mantle metasomatism in the Tuscan Magmatic Province, Italy. *Earth and Planetary Science Letters,* **305**: 45–56.

Gastal, M.C.P., 1987. Mapeamento e petrologia do maciço granítico Musa. Rio Maria, Sudeste do Pará. Thesis, Universidade Federal do Pará, Belem.

Gibbs, A.K., Wirth, K.R., Hirata, W.K., Olszewski, W.J., 1986. Age and composition of the Grão Pará Group Volcanics, Serra dos Carajás. *Revista Brasileira de Geociências,* **16**: 201–211.

Gioia, S.M.C.L., Pimentel M.M. 2000. The Sm-Nd isotopic method in the geochronology laboratory of the University of Brasília. *Anais da Academia Brasileira de Ciências,* **72**: 220-245. doi:10.1590/S0001-37652000000200009.

Goodge, J.W., Vervoort, J.D., 2006. Origin of Mesoproterozoic A-type granites in Laurentia: Hf isotope evidence. *Earth and Planetary Science Letters*, **243:** 711-731.

Griffin, W.L., Wang, X., Jackson, S.E., Pearson, N.J., O'Reilly, S.Y., Xu, X., Zhou, X., 2002. Zircon chemistry and magma mixing, SE China: In-situ analysis of Hf isotopes, Tonglu and Pingtan igneous complexes. *Lithos,* **61**:(3–4), 237–269.

Haapala, I., Rämö, O.T. Frindt, S., 2005. Comparison of Proterozoic and Phanerozoic rift-related basaltic–granitic magmatism. *Lithos,* **80**: 1–32.

Halliday, A.N., Davidson, J.P., Hildreth, W., and Holden, P. (1991) Modelling the petrogenesis of high Rb/Sr silicic magmas. *Chemical Geology*, **92**: 107–114.

Hanson, G.N., 1978. The application of trace elements to the petrogenesis of igneous rocks of granitic composition. *Earth and Planetary Science Letters*, **38:** 26–43.

Hanson, G.N., 1989. An approach to trace element modeling using a simple igneous system as an example. In: Lipin, B.R., McKay, G.A. Eds., Geochemistry and mineralogy of rare earth elements, *Reviews in Mineralogy,* **21**: 79–97.

Hawkesworth, C.J., Kemp, A.I.S., 2006. Using hafnium and oxygen isotopes in zircons to unravel the record of crustal evolution. *Chemical Geology*, **226**: 144–162.

Hawkesworth, C.J., Dhuime, B., Pietranik, A.B., Cawood, P.A., Kemp, A.I.S., Storey, C.D., 2010. The generation and evolution of the continental crust. *J. Geol. Soc.* **167**(2): 229–248.

Heinonen, A., Andersen, T., Rämö, O.T., 2010. Re-evaluation of rapakivi petrogenesis: Source constraints from the Hf isotope composition of zircon in the rapakivi granites and associated mafic rocks of southern Finland. *Journal of Petrology,* **51**: 1687–1709.

Heinonen, A., Fraga, L., Rämö, O.T., Dall'Agnol, R., Mänttäri, I. & Andersen, T. 2012. Petrogenesis of the igneous Mucajaí AMG complex, northern Amazonian craton: Geochemical, U–Pb geochronological, and Nd–Hf–O isotopic constraints. *Lithos,* **151**: 17–34

Heaman, L. M. (2009). The application of U-Pb geochronology to mafic, ultramafic and alkaline rocks: an evolution of the three mineral standards. *Chemical Geology*, **261**: 43-52.

Heilimo, E., Halla, J., Lauri, L.S., Rämö, O.T., Huhma, H., Kurhila, M.I., Front, K., 2009. The Paleoproterozoic Nattanen-type granites in northern Finland and vicinity post-collisional oxidized A-type suite. *Bulletin of the Geological Society of Finland,* **81**: 7–38.

Heinonen, A., Fraga, L., Rämö, O.T., Dall'Agnol, R., Mänttäri, I. & Andersen, T. 2012. Petrogenesis of the igneous Mucajaí AMG complex, northern Amazonian craton: Geochemical, U–Pb geochronological, and Nd–Hf–O isotopic constraints. *Lithos*, **151**: 17–34.

Hirata, W.K., Rigon, J.C., Kadekaru, K., Cordeiro, A.A.C., Meireles, E.A., 1982. Geologia Regional da Província Mineral de Carajás. *In*: 1st Simpósio de Geologia da Amazonia, Belém.

Hoffman, P.F., 1988. United Plates of America, the birth of a craton-Early Proterozoic assembly and growth of Laurentia. *Annual Review of Earth and Planetary Sciences,* **16**: 543–603.

Huhn, S.B., Macambira, M.J.B., Dall'Agnol, R., 1999. Geologia e geocronologia Pb-Pb do granito alcalino arqueano Planalto, região da Serra do Rabo, Carajás-PA. *In*: 6 Simpósio de Geologia da Amazônia, 463–466.

Huppert, H.E., Sparks, R.S., 1988. The generation of granitic magmas by intrusion of basalt into continental crust. *Journal of Petrology,* **29**: 599–624.

Ishihara, S., 1981. The granitoid series and mineralization. Economic Geology 75, 458–484.

Iizuka, T., Hirata, T., 2005. Improvements of precision and accuracy in in situ Hf isotope microanalysis of zircon using the laser ablation-MC-ICPMS technique. *Chem. Geol*., **220:** 121–137.

Izuka, T., Yamaguchi, T., Itano, K., Hibiya, I., Suzuki, K., 2017. What Hf isotopes in zircon tell us about crust–mantle evolution. *Lithos* **(274-275)**: 304-327

Javier-Rios, F., Villas, R.N., Dall'Agnol, R., 1995. O Granito Serra dos Carajás: fácies petrográficas e avaliação do potencial metalogenético para estanho no setor norte. *Revista Brasileira de Geociências,* **25**: 20–31.

Jiang, N., Guo, J.H., Zhai, M.G., 2011. Nature and origin of the Wenquan granite: Implications for the provenance of Proterozoic A-type granites in the North China craton. *Journal of Asian Earth Sciences,* **42**: 76–82.

Johansson, A., Waight, T., Andersen, T., Simonsen, S.L., 2016. Geochemistry and petrogenesis of Mesoproterozoic A-type granitoids from the Danish island of Bornholm, southern Fennoscandia. *Lithos,* **244**: 94-108.

Juliani, C., Fernandez, C.M.D., 2010. Well-preserved Late Paleoproterozoic volcanic centers in the São Félix do Xingu region, Amazonian craton, Brazil. *J. Volcanol. Geotherm. Res*. **191**: 167–179.

Kaur, P., Zeh, A., Chaudhri, N., Eliyas, N., 2017. Two distinct sources of 1.73–1.70 Ga A-type granites from the northern Aravalli orogen, NW India: Constraints from in situ zircon U-Pb ages and Lu-Hf isotopes. *Gondwana Research,* **49**: 164-181.

Kerr P. 1959. Optical Mineralogy. McGraw-Hill Book Co., New York, Third Edition, 492 p.

Kemp, A.I.S., Hawkesworth, C.J., 2007. Magmatic and crustal differentiation history of granitic rocks from Hf–O isotopes in zircon. *Science,* **315**: 980–983.

Kemp, A.I.S., Hawkesworth, C.J., Collins, W.J., Gray, C.M., Blevin, P.L., 2009. Isotopic evidence for rapid continental growth in an extensional accretionary orogen: the Tasmanides, eastern Australia. *Earth and Planetary Science Letters,* **284**: 455–466.

Kita, N.T., Ushikubo, T., Fu, B., Valley, J.W. 2009. High precision SIMS oxygen isotope analysis and the effect of sample topography. *Chemical Geology,* **246**: 43 - 57

Klein E., Almeida M., Rosa-Costa L.T., 2012. The 1.89-1.87 Ga Uatumã Silicic Large Igneous Province, northern South America. Large Igneous Provinces Commission. (http://www.largeigneousprovinces.org), November 2012 LIP of the Month.

Klein, E.L., Vasquez, M.L. 2000. Projeto Especial Província Mineral do Tapajós. Geologia e recursos minerais da Folha Vila Riozinho (SB.21-Z-A). Estado do Pará. Escala 1:250.000. CPRM-Serviço Geológico do Brasil, (Nota explicativa CD-ROM).

Kurhila, M., Andersen, T., Ramo, O.T., 2010. Diverse sources of crustal granitic magma: Lu-Hf isotope data on zircon in three Paleoproterozoic leucogranites of southern Finland. *Lithos* **115**: 263-271.

Lamarão C.N., Dall'Agnol R., Pimentel, M.M., 2005. Nd Isotopic composition of Paleoproterozoic volcanic and granitoid rocks of Vila Riozinho: Implications for the crustal evolution of the Tapajós Gold Province, Amazon craton. *Journal of South American Earth Sciences,* **18**: 277-292.

Lamarão, C.N., Pinho, S.C.C., Paiva Junior, A.L., Galarza-Toro, M.A., 2012. Mineralogy and geochemistry of the Paleoproterozoic, tin mineralized Bom Jardim Granite of the Velho Guilherme Suite, eastern Amazonian Craton. *Journal of South American Earth Sciences,* **38**: 159-173.

Lamarão C.N., Dall'Agnol R., Lafon J.M., Lima E.F. 2002. Geology, geochemistry, and Pb-Pb zircon geochronology of the Paleoproterozoic magmatism of Vila Riozinho, Tapajós Gold Province, Amazonian craton, Brazil. *Precambrian Research,* **119** (1-4): 189-223.

Lamarão, C.N., Silva, J.S., Borges, R.M., Dall'Agnol, R., 2014. Morphological and compositional variations of zircon and their metallogenetic implications: the example of the Jamon, Serra dos Carajás and Velho Guilherme suites, Amazonian Craton. *Brazilian Journal of Geology,* **44**(1): 105-120.

Lenharo, S.L., 1998. Evolução magmática e modelo metalogenético dos granitos mineralizados da região de Pitinga, Amazonas, Brasil, São Paulo. Thesis. Universidade de São Paulo (USP), São Paulo, Brazil, 290 p.

Lenharo, S.L., Pollard, P.J., Born, H., 2003. Petrology and textural evolution of granites associated with tin and rare-metals mineralization at the Pitinga mine, Amazonas, Brazil. *Lithos,* **66**: 37–61.

Leite-Santos, P.J., Oliveira, D.C., 2014. Trondhjemitos da área de Nova Canadá: novas ocorrências de associações magmáticas tipo TTG no Domínio Carajás. *Boletim do Museu Paraense Emílio Goeldi. Serie Ciências Terra,* **9**: 635-659.

Lima, P.H.A., 2011. *Geologia, petrografia e geocronologia do Granito São João, Província Carajás, SSE do Pará*. Trabalho de Conclusão de Curso – Federal University of Pará, Belém, 1-47p.

Lima, P.H.A., Lamarão, C.N., Santo, M.J.P., 2014 Petrografia, geoquímica e suscetibilidade magnética do Granito Paleoproterozóico São João, sudeste do Cráton Amazônico, Província Carajás. *Boletim do Museu Paraense Emílio Goeldi,* **9:** 47-72.

Ludwig, K.R., 2003. Isoplot 3.00, a geochronological took-kit for Excel: Berkeley Geochronology Center Special Publication 4, 67 p.

Ludwig, K.R., 2009. SQUID 2: A User's Manual, rev. 2.50, 12 Apr, 2009. Berkeley Geochronology Centre Special Publication 5, 110 p.

Lugmair, G.W., Harti, K., 1978. Lunar initial 143Nd/144Nd: differential evolution of the lunar crust and mantle. *Earth and Planetary Science Letters,* **39**: 349–357.

Machado, N., Lindenmayer, Z., Krogh, T.E., Lindenmayer, D., 1991. U-Pb geochronology of Archean magmatism and basement reactivation in the Carajás area, Amazon Shield, Brazil. *Precambrian Research,* **49**: 329–354.

Mackenzie W.S., Donaldson C.H., Guilford C. 1982. Atlas de Igneous Rocks and Their Textures. Harlow Essex, England: Longman Group Ltd. 148p.

Macambira, M.J.B., Lafon, J.M., 1995. Geocronologia da Província Mineral de Carajás; Síntese dos dados e novos desafios. *Boletim do Museu Paraense Emílio Goeldi,* **7**: 263–287 .

Macambira, M.J.B., Almeida, M.E., Santos, L.J., 2002. Idade zircão de vulcânicas Iricoumé do sudeste de Roraima: Contribuição para a redefinição do Supergrupo Uatumã. Boletim do II Simpósio sobre Vulcanismo e Ambientes Associados. SBG/NO, Belém - PA, p. 22.

Marques, S.N.S., Souza, V.S., Dantas, E.L., Valério, C.S., Nascimento, R.S.C., 2014. Contributions to the petrography, geochemistry and geochronology (U-Pb and Sm- Nd) of the Paleoproterozoic effusive rocks from Iricoumé Group, Amazonian Craton, Brazil. *Brazilian Journal of Geology,* **44** (1): 121–138.

Manilar, P.D., Piccoli, P.M., 1989. Tectonic discrimination of granitoids. *Geological Society of* America. Bull. **101**: 635–643.

Martins, G.G., Mendes, J.C., Schimtt, R.S., Armstrong, R., Valeriano, C.M., 2016. 550–490 Ma pre-to post-collisional shoshonitic rocks in the Ribeira Belt (SE Brazil) and their tectonic significance. *Precambrian Research*, **286**: 352-369.

Martins, P.L.G., Toledo, C.L.B., Silva, A.M., Chemale Jr, F., Santos, J.O.S., Assis, L.M., 2017. Neoarchean magmatism in the southeastern Amazonian Craton, Brazil: Petrography, geochemistry and tectonic significance of basalts from the Carajás Basin. *Precambrian Research,* **302**: 340-357.

Mesquita, C.J., Dall'Agnol, R., Almeida, J.A.C., 2018. Mineral chemistry and crystallization parameters of the A-type Paleoproterozoic Bannach Granite, Carajás Province – Pará. *Brazillian Journal of Geology* (in press).

Miller, J.S., Matzel, J.E.P., Miller, C.F., Burgess, S.D., Miller, R.B., 2007. Zircon growth and recycling during the assembly of large, composite arc plutons. *Journal of Volcanology and Geothermal Research*, **167**: 282–299.

Moreto, C.P.N., Monteiro, L.V.S., Xavier, R.P., Amaral, W.S., Santos, T.J.S., Juliani, C., Souza Filho, C.R., 2011. Mesoarchean (3.0 and 2.86 Ga) host rocks of the iron oxide–Cu–Au Bacaba deposit, Carajás Mineral Province: U–Pb geochronology and metallogenetic implications. *Mineralium Deposita,* **46**: 789–811.

Moreto, C.P.N., Monteiro, L.V.S., Xavier, R.P., Creaser, R.A., DuFrane, S.A., Melo, G.H.C., Silva, M.A.D., Tassinari, C.C.G., Sato, K., 2015. Timing of multiple hydrothermal events in the iron oxide-copper-gold deposits of the Southern Copper Belt, Carajás Province, Brazil. *Mineralium Deposita,* **50**: 517-546.

Moura C.A.V., Gorayeb P.S.S., Matsuda N.S. 1999. Geocronologia Pb-Pb em zircão do riolito Vila Raiol, Formação Iriri – sudoeste do Pará. *In*: Simpósio de Geologia da Amazônia, 6. Manaus. Resumos expandidos. Manaus: SBG p.475-477.

Nardi, L.V.S., 2016. Granitoides e séries magmáticas: o estudo contextualizado dos granitoides. *Pesquisas em Geociências*, **43**(1): 85-99.

Nardi, L.V.S., Bitencourt, M.F. 2009. A-type granitic rocks in post-collisional settings in southernmost Brazil: their classification and relationship with tectonics and magmatic series. *Canadian Mineralogist*, **47**: 1493-1503.

Nardi, L.V.S., Formoso, M.L L., Jarvis, K., Oliveira, L., Bastos Neto, A.C., 2012. REE, Y, Nb, U, and Th contents and tetrad effect in zircon from a magmatic-hydrothermal F-rich system of Sn-rare metal-cryolite mineralized granites from the Pitinga Mine, Amazonia, Brazil. *Journal of South American Earth Sciences*, **33:** 34-42.

Nakamura, N., 1974. Determination of REE, Ba, Fe, Mg, Na and K in carbonaceous and ordinary chondrites. *Geochimica et Cosmochimica Acta*, **38**: 757-775.

Nash, W.P., Crecraft, H.R. (1985) Partition coefficients for trace elements in silicic magmas. *Geochimica et Cosmochimica Acta*, **49**: 2309–2322.

Nasdala, L., Hofmeister, W., Norberg, N., Valley, J.W., 2008. Zircon M257 - a Homogeneous Natural Reference Material for the Ion Microprobe U-Pb Analysis of Zircon. *Geostandards and Geoanalytical Research*, **32**(3), 247 – 265.

Nebel, O., Nebel-Jacobsen, Y., Mezger, K., Berndt, J., 2007. Initial Hf isotope compositions in magmatic zircon from early Proterozoic rocks from the Gawler Craton, Australia: A test for zircon model ages. *Chemical Geology*, 23–37.

Oliveira, D.C., Dall'Agnol, R., Silva, J.B.C., Almeida, J.A.C., 2008. Gravimetric, radiometric, and magnetic susceptibility study of the Paleoproterozoic Redenção and Bannach plutons: implications for architecture and zoning of A-type granites. *Journal of South American Earth Sciences*, **25**: 100–115.

Oliveira, D.C., Dall'Agnol, R., Barros, C.E.M., Oliveira, M.A., 2009. Geology, geochemistry and magmatic evolution of the Paleoproterozoic, anorogenic oxidized A-type Redenção granite of the Jamon Suite, eastern Amazon Craton, Brazil. *Canadian Mineralogist*, **47**(6): 1441–1468.

Oliveira, D.C., Neves, S.P., Trindade, R.I.F., Dall'Agnol, R., Mariano, G., Correia, P.B., 2010. Magnetic anisotropy of the Redenção granite, eastern Amazonian craton (Brazil): Implications for the emplacement of A-type plutons. *Tectonophysics*, **493**: 27 - 41.

Oliveira, D.C., Santos, P.J.L., Gabriel, E.O., Rodrigues, D.S., Faresin, A.C., Silva, M.L.T., Sousa, S.D., Santos, R.V., Silva, A.C., Souza, M.C., Santos, R.D., Macambira, M.J.B., 2010. Aspectos geológicos e geocronológicos das rochas magmáticas e metamórficas da região entre os municípios de Água Azul do Norte e Canaã dos Carajás – Província Mineral de Carajás. *In*: 45 Congresso Brasileiro de Geologia. CDrom, Belém.

Oliveira, E.C., Lafon, J.M., Gioia, S.M.C.L., Pimentel, M.M. 2008. Datação Sm-Nd em rocha total e granada do metamorfismo granulítico da região de Tartarugal Grande, Amapá Central. *Revista Brasileira Geociências*, **38**:116–129.

Oliveira, M.A., Dall'Agnol, R., Althoff, F.J., Leite, A.A.S., 2009. Mesoarchean sanukitoid rocks of the Rio Maria Granite-Greenstone Terrane, Amazonian craton, Brazil. *Journal of South American Earth Sciences*, **27**: 146–160.

Oliveira, M.A., Dall'Agnol, R., Almeida, J.A.C., 2011. Petrology of the Mesoarchean Rio Maria suite: implications for the genesis of sanukitoid rocks. *Journal of Petrology*, **51**(10): 2121- 2148.

Paiva Júnior, A.L., 2009. *Geologia, petrografia, geocronologia e geoquímica do Granito anorogênico Seringa, Província Mineral de Carajás, SSE do Pará*. MS Dissertation, Instituto de Geociências, Universidade Federal do Pará, 158 p.

Paiva Júnior, A.L., Lamarão, C.N., Lima, P.H.A., 2011. Geologia, Petrografia e Geoquímica do Batólito Seringa, Província Carajás, SSE do Pará. *Revista Brasileira de Geociências*, **41**(2): 185-202.

Patiño-Douce, A., 1997. Generation of metaluminous A-type granites by low pressure melting of calc-alkaline granitoids. *Geology*, **25**: 743–7.

Patchett, J., Kouvo, O., Hedge, C., Tatsumoto, M., 1981. Evolution of continental crust and mantle heterogeneity: evidence from Hf isotopes. *Contributions to Mineralogy and Petrology*, **78**: 279–297.

Payne, J.L., McInerney, D.J., Barovich, K.M., Kirkland, C.L., Pearson, N.J., Hand. N., 2016. Strengths and limitations of zircon Lu-Hf and O isotopes in modelling crustal growth. *Lithos,* **248-251**: 175-192.

Peck, W.H., Valley, J.W., Graham, C.M., 2003. Slow oxygen diffusion rates in igneous zircon from metamorphic rocks. *American Mineralogist*, **88**: 1003-1014.

Pidgeon, R.T., Bosch, D., Bruguier, O., 1996. Inherited zircon and titanite U-Pb systems in an Archaean syenite from southwestern Australia: implications for U-Pb stability of titanite. *Earth and Planetary Science Letters,* **141**: 187-198.

Pinho, S., Fernandes, C., Teixeira, N., Paiva Jr., A., Cruz, V., Lamarão, C., Moura, C., 2006. O magmatismo paleoproterozóico da região de São Félix do Xingu, Província Estanífera do sul do Pará: Petrografia e Geocronologia. *Revista Brasileira de Geociências,* **36:** 724–732.

Poitrasson, F., Duthou, J.L., Pin, C., 1995. The relationship between petrology and Nd isotopes as evidences for contrasting anorogenic granite genesis: example of the Corsican Province (SE France). *Journal of Petrology,* **36**: 1251–1274.

Rämö, O.T., 1991. Petrogenesis of the Proterozoic rapakivi granites and related basic rocks of southeastern Fennoscandia: Nd and Pb isotopic and general geochemical constraints. *Geological Survey of Finland, Bulletin,* **355**: 161 p.

Rämö, O.T., Dall'Agnol, R., Macambira, M.J.B., Leite, A.A.S., Oliveira, D.C., 2002. 1.88 Ga oxidized A-type granites of the Rio Maria region, eastern Amazonian craton, Brazil: positively anorogenic! *Journal of Geology,* **110**: 603-610.

Rämö, O.T., Haapala, I., 1995. One hundred years of rapakivi granite. *Mineral Petrol,* **52**: 129–185.

Rämö, O.T., Haapala, I., 2005. Rapakivi granites. In: Lehtinen, M., Nurmi, P. A. & Raamo, O. T. (eds) Precambrian Geology of FinlandçKey to the Evolution of the Fennoscandian Shield.Amsterdam: Elsevier, pp. 533-562.

Rämö, O.T., Mänttäri, I., 2015. Geochronology of the Suomenniemi rapakivi granite complex revisited: Implications of point-specific errors on zircon U-Pb and refined λ_{87} on whole-rock Rb-Sr. *Bulletin of the Geological Society of Finland,* **87**: 25-45. http://dx.doi.org/10.17741/bgsf/87.1.002.

Rios, F.J., Villas, R.N., Fuzikawa, K., 2003. Fluid evolution in the Pedra Preta wolframite ore deposit, Paleoproterozoic Musa granite, eastern Amazon craton, Brazil. *Journal of South American Earth Sciences,* **15**: 787–802.

Roberts, N.M.W., Spencer, C.J., 2015. The zircon archive of continent formation through time. *Geological Society, London, Special Publications,* **389**: 197–225

Rodrigues, E.S., Lafon, J.M., Scheller, T. 1992. Geocronologia Pb-Pb da Província Mineral de Carajás: primeiros resultados. *In*: SBG, Congresso Brasileiro de Geologia, 37, São Paulo, Brazil, Boletim de resumos expandidos 2, 183-184.

Rodrigues, D.S., Oliveira, D.C., Macambira, M.J.B., 2014. Geologia, geoquímica e geocronologia do Granito Mesoarqueano Boa Sorte, município de Água Azul do Norte, Pará – Província Carajás. *Boletim do Museu Paraense Emílio Goeldi. Série Ciências da Terra,* **9**: 597–633.

Rogers, J.J.W., Santosh, M., 2002. Configuration of Columbia, a Mesoproterozoic supercontinent. *Gondwana Reseach,* **5**: 5–22.

Rogers, J.J.W., Santosh, M., 2009. Tectonics and surface effects of the supercontinent Columbia. *Gondwana Research,* **15:** 373–380.

Roverato, M., Juliani, C., Marcelo Dias-Fernandes, C., Capra, L., 2017. Paleoproterozoic andesitic volcanism in the southern Amazonian craton, the Sobreiro Formation: new insights from lithofacies analysis of the volcaniclastic sequences. *Precambrian Research,* **289**: 18–30.

Santos, J.O.S., Hartmann, L.A., Gaudette, H.E., Groves, D.I., McNaugthon, N.J.,Fletcher, I.R., 2000. New understanting of the Provinces of Amazon Craton based on Integration of Field Mapping and U-Pb and Sm-Nd geochronology. *Gondwana Research,* **3**(4): 453-488.

Santos, J.O.S., Groves, D.I., Hartmann L.A., Moura, M.A., Mcnaughton, N.J. 2001. Gold deposits of the Tapajós and Alta Floresta Domains, Tapajós-Parima orogenic belt, Amazon Craton, Brazil. *Mineralium Deposita,* **36**(3): 278-299.

Santos, J.O.S., 2003. Geotectonics of the Guyana and Central Brazil Schields. In: Bizzi, L.A., Schobbenhaus, C., Vidotti, R.M., Gonçalves, J.H. (eds.), Geology, Tectonics and Mineral Resources of Brazil, Companhia de Pesquisa de Recursos Minerais, Brasília, ISBN 85-230-0790-3, p. 169-226.

Santos, J.O.S., Silva, L.C., Faria, M.S.G., Macambira, M.J.B., 1997. Pb-Pb single crystal evaporation isotopic study on the post-tectonic, subalkalic, A-type Moderna granite (Mapuera Intrusive Suite), State of Roraima, northern Brazil. Symposium of Granites and Symposium of Granites and Associated Mineralizations, 2. Extended Abstract and Program. Sociedade Brasileira de Geologia, p. 273–275.

Santos, J.O.S., Van Breemen, O.B., Groves, D.I., Hartmann L.A., Almeida M.E., Mcnaughton N.J., Fletcher I.R., 2004. Timing and evolution of multiple paleoproterozoic magmatic arcs in the Tapajós Domain, Amazon Craton: constraints from SHRIMP and TIMS zircon, baddeleyite and titanite U-Pb geochronology. *Precambrian Research,* **131:** 73-109.

Santos, N.S., Oliveira, D.C., 2016. Rio Maria granodiorite and associated rocks of Ourilandia do Norte Carajás Province: Petrography, geochemistry and implications for sanukitoid petrogenesis. *Journal of South American Earth Sciences,* **72**: 279-301.

Santos, P.A., Teixeira, M.F.B., Dall'Agnol, R., Guimarães, F.V., 2013. Geologia, petrografia e geoquímica da associação Tonalito-Trondhjemito-Granodiorito (TTG) do extremo leste do Subdomínio de Transição, Província Carajás, Pará. *Boletim do Museu Paraense Emílio Goeldi. Ciências Naturais,* **8**(3): 257- 290 .

Santos, R.D., Galarza, M.A., Oliveira, D.C., 2013. Geologia, geoquímica e geocronologia do Diopsídio-Norito Pium, Província Carajás. *Boletim do Museu Paraense Emílio Goeldi, Série Ciências da Terra,* **8**: 355–382.

Sardinha, A.S., Barros, C.E.M., Krymsky, R., 2006. Geology, geochemistry, and U-Pb geochronology of the Archean (2.74 Ga) Serra do Rabo granite stocks, Carajás Province, northern Brazil. *Journal of South American Earth Sciences,* **20**: 327–339.

Schaltegger, U., Brack, P., Ovtcharova, M., Peytcheva, I., Schoene, B., Stracke A., Marocchi, M., Bargossi, G.M., 2009. Zircon and titanite recording 1.5 million years of magma accretion, crystallization and initial cooling in a composite pluton (southern Adamello batholith, northern Italy). *Earth and Planetary Science Letters,* **286**: 208-218.

Segal, I., Halicz, L., Platzner, I.T., 2003. Accurate isotope ratio measurements of ytterbium by multi-collector inductively coupled plasma mass spectrometry applying erbium and hafnium in an improved double external normalization procedure. *Journal of Analytical Atomic Spectrometry*, **18:** 1217-1223.

Semblano, F.R.D., Macambira, M.J.B., Vasquez, M.L., 2016. Petrography, geochemistry and Sm-Nd isotopes of the granites from eastern of the Tapajós Domain, Pará state. *Brazilian Journal of Geology,* **46**(4): 509-529.

Shand, S.J., 1950. Eruptive Rocks, their Genesis, Composition, Classification and their Relation to Ore Deposit. 4th ed., *London,* 488 pp.

Sheng, Y.Y., Zhang, J-X., Zhao, X.L., Gong, J.H., Li, Y.S., 2014. Geochronology, geochemistry and petrogenesis of the late Palaeoproterozoic A-type granites from the Dunhuang block, SE Tarim Craton, China: implications for the break-up of the Columbia supercontinent. *Geol. Mag.*, **151:** 629–648.

Shellnutt, J.G., Hari, K.R., Liao, A.C.Y., Denyszyn, S.W., Vishwakarma, N., (in press). A 1.88 Ga giant radiating mafic dyke swarm across Southern India and Western Australia. *Precambrian Research.* https://doi.org/10.1016/j.precamres.2018.01.021.

Sidder, G.B., Mendoza, S.V. 1991. Geology of the Venezuelan Guayana Shield and its relation to the entire Guayana Shield. U.S. Geol. Surv. Open-File Rep. 91-141, Denver, 59 p.

Siégel, C., Bryan, S.E., Allen, C.M., Gust, D.A., 2018. Use and abuse of zircon-based thermometers: A critical review and a recommended approach to identify antecrystic zircons. *Earth-Science Reviews,* **176**: 87-116.

Silva, A.C., Dall'Agnol, R., Guimarães, F.V., Oliveira, D.C., 2014. Geologia, petrografia e geoquímica de Associações Tonalíticas e Trondhjemíticas Arqueanas de Vila Jussara, Província Carajás, Pará. *Boletim do Museu Paraense Emílio Goeldi. Série Ciências Naturais* **9**, 13 - 45.

Silva, F.S., Oliveira, D.C., Antonio, P.Y., D'Agrella-Filho, M., Lamarão, C.N., 2016. Bimodal magmatism of the Tucuma area, Carajás Province: U-Pb geochronology, classification and processes. *Journal of South American Earth Sciences,* **72**: 95-114.

Silva Jr, C.A.S., Klein, E.L., Galarza, M.A., Borges, R.M.K., Queiroz, J.D.S., Assunção, R.F.S., Araújo, A.C.S, Moore, D.J., 2015. Zircon geochronology and Pb isotope systematics in sulfides: implications for the genesis of gold mineralization in the Cuiú-Cuiú Goldfeld, Tapajós Gold Province, Amazonian Craton, Brazil. *Contribuições a Geologia da Amazônia,* **9**: 453-465.

Smith, J.V., Brown, W.L., 1988. Feldspar minerals. 2. ed., Berlin, Springer-Verlag, 828 p.

Sylvester, P. J., 1989. Post-collisional alkaline granites. *Journal of Geology* **97**:261-280.

Spencer, K.J., Hacker, B.R., Kylander-Clark, A.R.C., Andersen T.B., Cottle, J.M., Stearns, M.A., Poletti, J.E., Seward, G.G.E., 2013. Campaign-style titanite U–Pb dating by laser-ablation ICP: Implications for crustal flow, phase transformations and titanite closure. *Chemical Geology,* **341**: 84-101.

Stern, R.A., 2001. A new isotopic and trace element standard for the ion microprobe: preliminary TIMS U – Pb and electron microprobe data, current research. Radiogenic Age and Isotopic Studies: Report 14. *Geological Survey of Canada*, Ottawa, Canada.

Söderlund, U., Patchett, P.J., Vervoort, J.D., and Isachsen, C.E., 2004, The 176Lu decay constant determined by Lu–Hf and U–Pb isotope systematics of Precambrian mafic intrusions: *Earth and Planetary Science Letters,* **219**: 311–324.

Sousa, L.A.M. 2017. *Petrografia, Susceptibilidade Magnética e Química Mineral do Granito anorogênico Ggogó da Onça, Província Carajás.* Trabalho de Conclusão de Curspo (TCC), Instituto de geociências e Engenharia, Universidade do Oeste do Pará (UFOPA) 88p.

Souza, Z.S., Potrel, H., Lafon, J.M., Althoff, F.J., Pimentel, M.M., Dall'Agnol, R., Oliveira, C.G., 2001. Nd, Pb, and Sr isotopes of the Identidade Belt, an Archaean greenstone belt of the Rio Maria region (Carajás Province, Brazil): implications for the Archaean geodynamic evolution of the Amazonian Craton. *Precambrian Research,* **109**: 293–315.

Stearns, M.A., Hacker, B.R., Ratschbacher, L., Rutte, D., Kylander-Clark, A.R.C., 2015. Titanite petrochronology of the Pamir gneiss domes: Implications for mid–deep crust exhumation and titanite closure to Pb and Zr diffusion. *Tectonics,* **34**: 1–19.

Streckeisen, A., 1976. To each plutonic rock its proper name. *Earth-Sci. Rev*. **12**: 1 -33.

Sun, S.S., Mcdonough, W. F., 1989. Chemical and isotopic systematics of oceanic basalts: implications for mantle composition and processes. In: Saunders, A.D., Norry, M.J. (Eds.), Magmatism in the Ocean Basins: *Geological Society of London Special Publication,* **42**: 313-345.

Tallarico, F.H.B., Figueiredo, B.R., Groves, D.I., Kositcin, N., McNaughton, N.J., Fletcher, I.R., Rego, J.L., 2005. Geology and SHRIMP U-Pb geochronology of the Igarape Bahia deposit, Carajás copper - gold belt, Brazil: an Archean (2.57 Ga) example of iron-oxide Cu-Au-(U-REE) mineralization. *Economic Geology*, **100**: 7-28.

Tassinari, C.C.G., Macambira, M.J.B., 1999. Geochronological provinces of the Amazonian craton. *Episodes,* **22**: 174–182.

Tassinari, C.C.G., Macambira, M.J.B., 2004. A evolução tectônica do cráton Amazônico. *In*: Matesso-Neto, V., Bartorelli, A., Carneiro, C.D.R., Britto- Neves, B.B. (Eds.), Geologia do Continente Sul-Americano. Sao Paulo, SP, Brazil, p. 471- 485. .

Teixeira, M.F.B., Dall'Agnol, R., Silva, A.C., Santos, P.A., 2013. Geologia, petrografia e geoquímica do Leucogranodiorito Pantanal e dos leucogranitos arqueanos da área de Sapucaia, Província Carajás, PA: implicações petrogenéticas. *Boletim do Museu Paraense Emílio Goeldi, Série Ciências Naturais,* **8**: 291–323.

Teixeira, M.F.B., Dall'Agnol, R., Santos, J.O.S., Sousa, L.A.M., Lafon, J-M., 2017. Geochemistry, geochronology and Nd isotopes of the Gogó da Onça Granite: A new Paleoproterozoic A-type granite of Carajás Province, Brazil. *Journal of South American Earth Sciences,* **80**: 47-65.

Teixeira N.P., 1999. Contribuição ao estudo das rochas granitóides e mineralizações associadas da Suíte Intrusiva Velho Guilherme, Província Estanífera do Sul do Pará. Thesis. Instituto de geociências, Universidade de São Paulo (USP), 508 p.

Teixeira, N.P., Bettencourt, J.S., Moura, C.A.V., Dall'Agnol, R., Macambira, E.M.B., 2002. Archean crustal sources for Paleoproterozoic tin-mineralized granites in the Carajás Province, SSE Pará, Brazil: Pb–Pb geochronology and Nd isotope geochemistry. *Precambrian Research,* **119**: 257–275.

Teixeira, W., Reis, N.J., Bettencourt, J.S., Klein, E.F., Oliveira, D.C., Intraplate Paleo- to Mesoproterozoic magmatism in the Amazonian Craton reviewed: geochronology and crustal tectonics and barcode matches R. Srivastava, R. Ernst (Eds.), Dyke Swarms of the World - A Modern Perspective (IDC-7 Special Volume), Submetido (2018).

Teixeira, W., Hamilton, M.A., Girardi, V.A.V., Faleiros, F.M., Ernst, R.E. 2018. U-Pb baddeleyite ages of key dyke swarms in the Amazonian Craton (Carajás/ Rio Maria and Rio Apas areas): Tectoninc implications for events at 1880 Ma, 1110 Ma, 235 Ma and 200 Ma. *Precambrian Research* (in Press).

Teixeira, W., Tassinari, C.C.G., Cordani, U.G., Kawashita, K., 1989. A review of the geochronology of the Amazonian Craton: tectonic implication. *Precambrian Research,* **42**: 213 - 227.

Teruiya, R.K., Paradella, W.R., Santos, A.R., Dall'agnol, R., Veneziani, P., 2008. Integrating airborne SAR, Landsat TM and airborne geophysics data for improving geological mapping in the Amazon Region: the Cigano Granite, Carajás Province, Brazil. *International Journal of Remote Sensing*, **29** (13): 3957-3974.

Valério, C.S., 2006. *Magmatismo Paleoproterozóico do extremo sul do Escudo das Guianas, município de Presidente Figueiredo (AM): Geologia, geoquímica e geocronologia Pb-Pb em zircão*. MS Dissertation. Universidade Federal de Manaus, 112 p.

Valério, C.S., Souza, V.S., Macambira, M.J.B., 2009. The 1.90–1.87 Ga magmatism in the centersouthernmost Guyana Shield, Brazil: geology, geochemistry, zircon geochronology, and tectonic implications. *Journal of South America Earth Sciences*, **28**(3): 304–320.

Valério, C.S., Macambira, M.J.B., Souza, V.S., Dantas, E.L., Nardi, L.V.S., 2018. 1.88 Ga São Gabriel AMCG association in the southernmost Uatumã-Anauá Domain: Petrological implications for post-collisional A-type magmatism in the Amazonian Craton. *Lithos*, **(300-301)**: 291-313.

Valley, J.W. 2003. Oxygen isotopes in zircon. In: Hanchar, J.M., Hoskin, P.W.O. (eds) Zircon. Mineralogical Society of America and Geochemical Society, *Reviews in Mineralogy and Geochemistry,* **53**: 343–385.

Valley, J.W., Lackey, J.S., Cavosie, A.J., Clechenko, C.C., Spicuzza, M.J., Basei, M.A.S., Bindeman, I.N., Ferreira, V.P., Sial, A.N., King, E.M., Peck, W.H., Sinha, A.K., Wei, C.S., 2005. 4.4 billion years of crustal maturation: oxygen isotope ratios ofmagmatic zircon. *Contributions to Mineralogy and Petrology,* **150**: 561–580

Valley, J.W., Chiarenzelli, J.R., McLelland, J.M. 1994. Oxygen isotope geochemistry of zircon. *Earth and Planetary Science Letters*, **126**: 187–206.

Valley, J.W., Kinny, P.D., Schulze, D.J. & Spicuzza, M.J. 1998. Zircon megacrysts from kimberlite: Oxygen isotope heterogeneity among mantle melts. *Contributions to Mineralogy and Petrology*, **133**: 1–11.

Vander Auwera, J., Berza, Tudor., Gesels, J., Dupont, Alain., 2015. The Late Cretaceous igneous rocks of Romania (Apuseni Mountains and Banat): the possible role of amphibole versus plagioclase deep fractionation in two different crustal terranes. *International Journal of Earth Sciences,* **105**: 849-817.Vasquez M.L., Klein E.L., Quadros M.L.E.S., Bahia R.B.C., Santos A., Ricci
P.S.F., Sachett C.R., Silva C.M.G., Macambira M.J.B. 1999. Magmatismo Uatumã na Província Tapajós – novos dados geocronológicos. *In*: Simpósio de Geologia da Amazônia, 6., Manaus. Resumos expandidos. Manaus: SBG-Núcleo Norte. p. 471-474. .

Vasquez M.L., Klein E.L., Ricci P.S.F. 2002. Granitóides pós-colisionais da porção leste da Província Tapajós. *In*: Klein E.L., Vasquez M.L., Rosa-Costa L.T. (Eds.). Contribuições à Geologia da Amazônia. SBGNúcleo Norte, Belém. p. 67-84.

Vasquez, M.L., Macambira M.J.B., Armstrong R.A. 2008b. Zircon geochronology of granitoids from the western Bacajá domain, southeastern Amazonian craton, Brazil: Neoarchean to Orosirian evolution. *Precambrian Research,* **161**: 279-302.

Vervoort, J.D., Kemp, A.I., 2016. Clarifying the zircon Hf isotope record of crust–mantle evolution. *Chem. Geol*. **425**: 65–75.

Vervoort, J.D., Patchett, P.J., Soderlund, U., Baker, M., 2004. Isotopic composition of Yb and the determination of Lu concentrations and Lu/Hf ratios by isotope dilution using MCICPMS. *Geochem. Geophys. Geosystem,* **5** (11).

Wang, C.Y., Campbell, I.H., Stepanov, A.S., Allen, C.M., Burtsev, I.N., 2011. Growth rate of the preserved continental crust: II. Constraints from Hf and O isotopes in detrital zircons from Greater Russian Rivers . *Geochimica et Cosmochimica Acta,* **75**: 1308 – 1345.

Windley, B.F., 1993. Proterozoic anorogenic magmatism and its orogenic connections. *Journal of the Geological Society (London),* **150:** 39–50.

Whalen, J.B., Currie, K.L., Chappell, B.W., 1987. A-type granite: geochemical characteristics, discrimination and petrogenesis. *Contributions to Mineralogy and Petrology,* **95:** 407–419.

Whitney, D. L., Evans, B.W., 2010. Abbreviations for names of rock-forming minerals. *American Mineralogist,* **95**(1): 185-187.

Woodhead, J., Hergt, j., Shelley, M., Eggins, S., Kemp, R., 2004. Zircon Hf-isotope analysis with an excimer laser, depth profiling, ablation of complex geometries and concomitant age estimation. *Chem Geol,* **209** 121–135.

Xiong,Q., Zheng, J., Yu, C., Su, Y., Tang, H., Zhang, Z., 2008. Zircon U-Pb age and Hf isotope of Quanyishang A-type granite in Yichang: Signification for the Yangtze continental cratonization in Paleoproterozoic. *Chinese Science Bulletin,* **54**: 436-446.

Zhang, L.S., Scharer, U., 1996. Inherited Pb components in magmatic titanite and their consequence for the interpretation of U-Pb ages. *Earth and Planetary Science Letters,* **138**: 57-65.

Zhang, S.H., Liu, S.W., Zhao, Y., Yang, J.H., Song, B., Liu, X.M., 2007. The 1.75–1.68 Ga anorthosite– mangerite–alkali granitoid-rapakivi granite suite from the northern North China Craton: magmatism related to a Paleoproterozoic orogen. *Precambrian Research,* **155**: 287–312.

Zhao, G., Cawood, P.A., Wilde, S.A., Sun, M., 2002. Review of global 2.1–1.8 Ga orogens: implications for a pre-Rodinia supercontinent. *Earth-Science Reviews,* **59**: 125–162.

Zhao, T.P., Zhou, M.F., 2009. Geochemical constraints on the tectonic setting of Paleoproterozoic A-type granites in the southern margin of the North China Craton. *J. Asian Earth Sci*., **36**: 183-195.

UNIVERSIDADE FEDERAL DO PARÁ
INSTITUTO DE GEOCIÊNCIAS
PROGRAMA DE PÓS-GRADUAÇÃO EM GEOLOGIA E GEOQUÍMICA

PARECER

Sobre a Defesa Pública da Tese de Doutorado de MAYARA FRAEDA BARBOSA TEIXEIRA

A banca examinadora da Tese de Doutorado de **MAYARA FRAEDA BARBOSA TEIXEIRA** orientanda do Prof. Dr. Roberto Dall'Agnol (UFPA), composta pelos professores doutores Farid Chemale Junior (UNISINOS), Wilson Teixeira (USP), Moacir José Buenano Macambira (UFPA), e Davis Carvalho de Oliveira (UFPA) após apresentação da sua tese intitulada **"ESTUDOS ISOTÓPICOS DE U-Pb, Lu-Hf E $\delta^{18}O$ EM ZIRCÃO: IMPLICAÇÕES PARA A PETROGÊNESE DOS GRANITOS TIPO-A PALEOPROTEROZOICOS DA PROVÍNCIA CARAJÁS – CRÁTON AMAZÔNICO"**, emite o seguinte parecer:

A candidata realizou sua apresentação de forma clara, bem organizada e segura no tempo estipulado. Na arguição mostrou domínio da temática abordada e respondeu às perguntas formuladas pela banca. O trabalho escrito foi apresentado na forma de artigo e atende as exigências básicas para uma tese de doutorado.

Finalmente, a banca examinadora decidiu por unanimidade aprovar a tese de doutorado.

Belém, 05 de abril de 2018.

Prof. Dr. Roberto Dall'Agnol (Orientador – UFPA)

Prof. Dr. Farid Chemale Junior (UNISINOS)

Prof. Dr. Wilson Teixeira (USP)

Prof. Dr. Moacir José Buenano Macambira (UFPA)

Prof. Dr. Davis Carvalho de Oliveira (UFPA)